The Role of ATM Regulatory Proteins In DNA Damage Signalling

Kathleen Penicud

A thesis submitted for the degree of Doctor of Philosophy

University College London

August 2012

Supervisor: **Axel Behrens**
Mammalian Genetics Laboratory
Cancer Research UK London Research Institute

Declaration

I, Kathleen Penicud, confirm that the work presented in this thesis is my own. Where information has been derived from other sources, I confirm that this has been indicated in the thesis.

Abstract

The DNA damage activated checkpoint kinase ATM is mutated in ataxia telangiectasia, which is characterised by cancer predisposition and neural degeneration. After ionising radiation (IR) ATM signalling proceeds via interaction with Nijmegen breakage syndrome 1 (NBS1). Conversely, ATM INteractor (ATMIN) is required for ATM activation after hypotonic shock. Full ATM activation also requires concomitant chromatin modifications, including histone H4 acetylation at K16 (H4K16Ac) by Tip60. However, the molecular mechanisms underpinning ATM pathway choice and physiological stimuli for ATMIN dependent ATM signalling were unclear.

The aims of my PhD studies were to (a) establish physiological roles for ATMIN dependent ATM signalling, (b) investigate the mechanisms and consequences of ATM co-factor choice, and (c) identify novel ATM regulatory proteins.

I characterised ATMIN's role in preventing DNA damage accumulation in the embryo. Moreover, ATMIN suppresses DNA damage at the telomere. Loss of ATMIN from telomerase deficient cells exacerbates telomere dysfunction. Conversely, ATMIN is dispensable for oncogene induced senescence after colonic $KRas^{G12D}$ expression.

To investigate ATM pathway choice I generated $nbs1^{\Delta/\Delta}$; $atmin^{\Delta/\Delta}$ MEFs. These compound mutants exhibit reduced senescence and increased proliferation compared to $nbs1^{\Delta/\Delta}$, despite increased endogenous DNA damage. A similar phenotype was observed in the intestine. Both $nbs1^{\Delta/\Delta}$;$atmin^{\Delta/\Delta}$ MEFs and intestinally-deleted $nbs1^{\Delta G}$;$atmin^{\Delta G}$ mice were extremely radiosensitive. Furthermore, ATMIN deletion augments IR-induced ATM substrate phosphorylation. Thus, competition between ATMIN and NBS1 for ATM interaction is fundamental to ATM signalling and disrupting this balance is deleterious to cells.

An shRNA screen identified DMAP1 as a novel ATM regulator. DMAP1 deficient cells are radiosensitive, and exhibit impaired ATM signalling after both IR and hypotonic shock. DMAP1 interacts with Tip60, and is required for Tip60 acetylation of H4K16 after DNA damage. Histone deacetylase inhibitors rescued ATM substrate

phosphorylation and H4K16Ac levels after IR in DMAP1 depleted cells. Thus DMAP1 is a novel regulator of ATM function.

Acknowledgements

Firstly, I would like to thank Axel for being an excellent supervisor and giving me the opportunity to work in his lab. I have greatly benefitted from his vision and insight, willingness to offer his time, collaborative nature and his support throughout my PhD.

I'd also like to thank all past and present members of the Behrens' group. In particular, I am greatly indebted to Nnennaya Kanu for her friendship and support - from showing me how to run my very first western blot, to proof reading my thesis, and countless occasions in between. I'm grateful to Clive Da Costa for his support and keeping the Behrens Lab running so efficiently. Thank-you to Rocio Sancho, Clive Da Costa, Ralph Gruber and Atanu Chakraborty for, amongst much other help and advice, their willingness to proof-read chapters of my thesis. I'd like to thank my Thesis Committee, Simon Boulton and Vincenzo Costanzo, for their comments and suggestions throughout my PhD. My PhD would not have been possible without the excellent BRU units at both the LRI and CH; thank-you to all the technicians that have made this work possible.

Last but not least, I'd like to thank my family for a lifetime of love and support. Thank-you to all my invaluable friends - especially to my wonderful housemate Ben for his assumption every PhD setback is overcome via a well-mixed G&T; to Lizzie and Dave for keeping me so frequently well-fed and watered; to Nana for keeping our resolution to make it to the ballet or theatre more weeks than not; and to Liz, Amy, Sophie and Ami for their love of 'just one after work' at the BFI bar. And, saving the best until last, a huge thank-you to my fabulous fiancé Tim for his unwavering love, understanding and support - and for all the fun adventures that we've had during my PhD.

Table of Contents

Table of figures

List of tables

Abbreviations

5'-dRP	5'-deoxyribose-5-phosphatase
53BP1	p53 Binding Protein 1
AID	Activation-induced Cytidine Deaminase
ALT	Alternative Lengthening of Telomeres
ASCIZ	Chk2-Interacting Zn^{2+}-Finger Protein
A-T	Ataxia-Telangiectasia
A-TLD	Ataxia-Telangiectasia Like Disorder
ATM	Ataxia-Telangiectasia Mutated
ATR	ATM and Rad3-related protein
ATRIP	**A**taxia Telangiectasia Related Interacting Protein
BER	Base Excision Repair
BRCA1	Breast Cancer 1
BRCA2	Breast Cancer 2
BRCT	Brca1 C-terminal
CDC25A	Cell Division Cycle 25 Homolog A
Cdk1	Cyclin Dependent Kinase 1
Cdk2	Cyclin Dependent Kinase 2
CK2	Caesin Kinase 2
CNS	Central Nervous System
CSR	Class Switch Recombination
DAPI	4-6-diamidino-2-phenylindole
ddH_2O	Double-Distilled Water
DDR	DNA Damage Response
DMAP1	DNA Methyltransferase Associated Protein 1
DMEM	Dulbecco's Modified Eagle's Medium
DMSO	Dimethyl Sulfoxide
DNA-PKcs	Catalytic Subunit of DNA-Dependent Protein Kinase
DSB	Double Strand Break
DYNLL1	L8 Dynein light chain
EYA1	Eyes Absent Homolog 1
EYA3	Eyes Absent Homolog 3

FAT domain	FATC, ATM, TRRAP domain
FATC domain	FAT C-terminal domain
FCS	Foetal calf serum
FHA	Fork Head Associated
FISH	Fluorescent In Situ Hybridisation
GFP	Green Fluorescent Protein
H3K9me3	Histone 3 lysine 9 tri-methylated
H4K16	Histone 4 lysine 16
H4K16Ac	Histone 4 lysine 16 acetylated
HAT	Histone Acetyl Transferase
HDAC1	Histone Deacetylase 1
HDAC2	Histone Deacetylase 2
HMGN1	High Mobility Group Nucleosomal binding 1
HP1	Heterochromatin-binding Protein 1
HR	Homologous Recombination
IF	Immunofluorescence
Ig	Immunoglobulin
IP	Immunoprecipitate
IR	Ionising Radiation
ISH	In Situ Hybridisation
KAP1	KRAB-Associated Protein 1
MDC1	Mediator of DNA-damage Checkpoint 1
MOF	Males absent On the First
MMEJ	Microhomology-Mediated End Joining
Mre11	Meiotic Recombination 11
NBS	Nijmegen Breakage Syndrome
NBS1	Nijmegen Breakage Syndrome 1
NCS	Neocarzinostatin
NHEJ	Non Homologous End Joining
n.s.	not significant
NSC	Neural Stem Cell
OIS	Oncogene Induced Senescence

PAS	Periodic Acid-Schiff
PBS	Phosphate Buffered Saline
PFA	Paraformaldehyde
pH3	Phospho-Histone H3
PI	Propidium Iodide
PI3-K	Phosphoinositide-3-kinase
POT1	Protector OF TELOMERES 1
RAG1	Recombination Activating Gene 1
RAG2	Recombination Activating Gene 1
RAP1	Repressor and Activator Protein 1
ROS	Reactive Oxygen Species
RPA	Replication Protein A
s.d.	Standard Deviation
SDS	Sodium Dodecyl Sulfate
SDS-PAGE	Sodium Dodecyl Sulfate-Polyacrylamide Gel Electrophoresis
SMARD	Single Molecule Analysis of Replicated DNA
SMC1	Structural Maintenance of Chromosome protein 1
SHM	Somatic Hypermutation
SVZ	Subventricular Zone
TAE	Tris Acetate EDTA buffer
TBS-T	Tris Buffered Saline Tween-20
TIN2	TRF1-Interacting Nuclear Protein 2
TRF1	Telomere Repeat-Binding Factor 1
TRF2	Telomere Repeat-Binding Factor 2
Tris	Tris(hydroxymethyl)aminomethane
TRRAP	Transformation/transcription domain-associated protein
TSA	Trichostatin A
TTP1	POT1-and TIN2-Interacting Protein
UT	Untreated
V(D)J	Variable (Diversity) Joining
WSTF	Williams-Beuren Syndrome Transcription Factor

Chapter 1. Introduction

1.1 DNA Damage And Disease

1.1.1 The importance of DNA damage repair

Cells continually experience a great variety of insults to their genome. Endogenous DNA damage includes replication errors, the spontaneous depurination of DNA bases and double strand breaks (DSBs). A DSB occurs when both strands of the DNA double helix are severed in close proximity, and arise from a range of situations including stalled replication forks or during B and T cell maturation. DNA damage can also be exogenously induced, for example cross-linked dimers induced by the UV component of sunlight or DSBs induced by ionising radiation (IR). Continued proliferation of cells with undetected and unrepaired DNA damage leads to increasing genomic instability. This is deleterious to cellular function, and dangerous for the organism as DNA damage underlies cancer development. It is therefore unsurprising that the cell has evolved exquisite, extensive networks for the detection, repair and resolution of DNA damage.

At the hub of these networks sit three homologous phosphoinositide 3-kinase (PI3-K) related kinases - ataxia-telangiectasia mutated (ATM), ATM and Rad3-related protein (ATR) and the Catalytic Subunit of DNA-Dependent Protein Kinase (DNA-PKcs). The linchpins of the DNA damage response (DDR), each has specialised, complimentary and sometimes overlapping roles in maintaining genomic integrity. ATM and DNA-PKcs principally detect double strand breaks, whereas ATR responds to single-strand DNA damage (Figure 1).

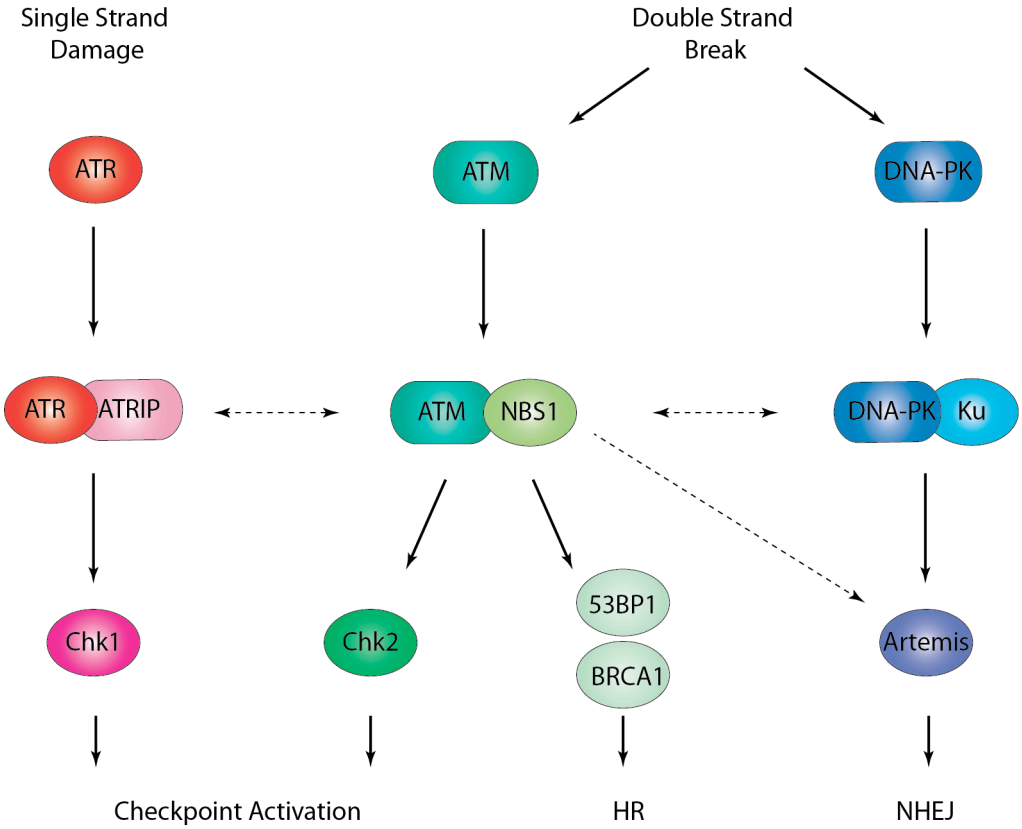

Figure 1: ATM, ATR and DNA-PKcs are activated by DNA damage

ATR, together with its co-factor ATRIP, responds to single-strand DNA damage and phosphorylates Chk1, activating cell cycle checkpoints. ATM, together with its co-factor NBS1, is activated by DNA double strand breaks and activates cell cycle checkpoints via Chk2. ATM also phosphorylates the DNA repair proteins 53BP1 and BRCA1, promoting repair by the HR pathway. Conversely, DNA-PKcs interacts with its co-factor Ku and phosphorylates Artemis, promoting repair by the NHEJ pathway. There is some cross talk between the pathways; for example ARTEMIS is an ATM substrate and ATM dependent HR repair proceeds via generation of single stranded DNA, activating ATR.
HR, Homologous Recombination; NHEJ, Non-Homologous End Joining; DSBs

It is crucial for organisms to maintain genomic integrity, as unrepaired or incorrectly repaired DNA lesions can contribute to cancer development. The majority of hereditary cancer syndromes involve mutation in DNA repair genes (Nagy et al., 2004), and genomic instability is a hallmark of tumour development (Hanahan and Weinberg, 2011). The fundamental importance of DNA repair is highlighted by several systemic human disorders all caused by mutations in a single DNA repair gene.

1.1.2 Ataxia-telangiectasia

The homozygous recessive disorder ataxia-telangiectasia (A-T) is caused by mutation in ATM. Patients are characterised by early onset progressive cerebellar ataxia, ocular telangiectasia, immunodeficiency, neurodegeneration, radiosensitivity, and cancer predisposition, especially to lymphomas. Although the first reported case of A-T was in 1926 (Syllaba and Henner, 1926), and A-T was first described as a distinct disease in 1957 (Boder and Sedgwick, 1957), it was not until 1995 the gene responsible, ATM, was identified by positional cloning (Savitsky et al., 1995).

The *atm* gene occupies 160kB of genomic DNA and encodes a 13kB transcript from across 88 exons. To date, 430 different ATM mutations have been reported for A-T (Fokkema et al., 2011). Many of these are truncation or splicing mutations, which result in shorter, unstable ATM proteins. Some correlations have been drawn between the mutation site and phenotype severity (Guo et al., 2010b). Mouse models of A-T, with truncation mutations found in A-T patients, recapitulate many of the clinical features including radiosensitivity, sterility, growth retardation and T-cell lymphoma (Barlow et al., 1996; Xu et al., 1996; Elson et al., 1996). Although a very rare disorder, characterisation of the A-T phenotype and ATM protein function has been pivotal to our understanding of the cellular DNA damage response.

1.1.3 Nijmegen Breakage Syndrome

Nijmegen Breakage Syndrome (NBS) is caused by mutation in the ATM co-factor Nijmegen Breakage Syndrome 1 (NBS1). NBS has a similar clinical presentation to A-T, including immunodeficiency and predisposition to cancer. However, in contrast to A-T patients, NBS patients exhibit microcephaly. Like A-T, it is a rare autosomal recessive syndrome. Unlike A-T, the same mutation, *nbs1*$^{657\Delta5}$, is present in approximately 90% of patients (Varon et al., 1998). Rather than a complete loss of the protein, this mutation occurs at a splice site and leads to the production of two truncated proteins (Maser et al., 2001). The N-terminal fragment, proximal to the mutation site, produces a 26kDa protein. The NBS1$^{657\Delta5}$ mutation deletes five bases and introduces a

stop codon. Remarkably, an alternative, internal start codon is present approximately 30 bases upstream of the deletion. After loss of the five bases, this start codon is in the same reading frame as the remainder of the NBS1 protein. Internal translation initiation from this methionine synthesises a 70kDa C-terminal NBS1 fragment in some cell types. Although this protein is present at much lower amounts than the wildtype protein, it is sufficient for viability (Maser et al., 2001). We know this as whilst the complete mouse knock-out for NBS1 is embryonically lethal (Zhu et al., 2001), a 'humanised NBS mouse model' containing the $NBS1^{657\Delta5}$ mutation is viable (Difilippantonio et al., 2005).

1.1.4 Ataxia-Telangiectasia Like Disorder

Ataxia-Telangiectasia Like Disorder (A-TLD) shares many of the same clinical features as A-T, including cerebellar degeneration, radiosensitivity and chromosomal instability. A-TLD was only identified as a distinct disease in 1999, when four patients previously diagnosed with A-T were shown to have truncation mutations in the *mre11* gene. Meiotic Recombination 11 (Mre11) encodes a component of the MRN complex (Mre11, Rad50, NBS1) that localises to DSBs. The *atm* locus is at 11q23 (Gatti et al., 1988), very close to *mre11* at 11q21 (Petrini et al., 1995), which may explain why A-T and A-TLD had not previously been identified as separate disorders. Although clinically very similar to A-T, A-TLD patients do not display immunodeficiency or cancer predisposition. Mice homozygous for the Mre11 truncation mutation observed in A-TLD patients ($mre11^{ATLD/ATLD}$) recapitulate the disorder, including increased genomic instability without malignancy (Theunissen et al., 2003). The difference between A-T and A-TLD symptoms suggests some distinct functions for ATM and Mre11.

1.1.5 NBS-Like Disorder

To date, a single patient with mutations in Rad50, the third component of the MRN complex, has been reported (Waltes et al., 2009). The maternally derived *rad50* allele of this patient had a truncation mutation, whereas a mutated terminal 'stop' codon in the paternally derived allele gave rise to a longer Rad50 protein. However, very low

amounts of this protein were detected, suggesting the longer isoform is more unstable than wildtype Rad50. NBS-Like Disorder shares many of the same clinical features as NBS; including radiosensitivity, microcephaly, dwarfism and a 'bird-like' face. However, no immunodeficiency or cancer predisposition was observed. As this disorder has so far only been described in one individual, it is premature to conclude NBS-Like Disorder does not predispose to cancer development. Indeed, due to the combination of two distinct mutations in the patient's two *rad50* alleles it may be a unique case.

1.1.6 Seckel Syndrome

Seckel syndrome is characterised by dwarfism, mental retardation, microexencephaly with micrognathia, a narrow face and bird-like protrusion of the nose. All known patients have almost undetectable ATR protein levels and carry an ATR^{A2101G} mutation, which results in impaired splicing and introduction of a premature stop codon . A recent mouse model, which introduced the human ATR^{A2101G} mutation and surrounding exons, recapitulated Seckel syndrome. Mutants exhibit high levels of replicative stress, especially in tissues with high proliferation rates, including the intestine (Murga et al., 2009). Murine models with a complete loss of the ATR locus are pre-gastrulation lethal (de Klein et al., 2000), so presumably the 'leaky' ATR^{A2101G} splicing mutation allows enough ATR to be synthesised for viability, albeit with a severe clinical phenotype.

1.2 ATM Orchestrates the DNA DSB Response

1.2.1 ATM activation

The DNA-damage activated checkpoint kinase ATM is a large 350kDa protein with several domains of interest (Figure 2). Towards ATM's N-terminus lies the substrate binding domain (Khanna et al., 1998). The FAT (FATC, ATM, TRRAP) and FATC (FAT C-terminal) domains are conserved amongst, and indeed may be unique to, the PI3-K related kinase family (Bosotti et al., 2000). ATM's protein kinase domain resides in the C-terminal half of the protein.

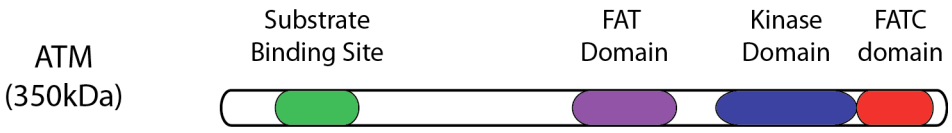

Figure 2: Overview of ATM protein domains

ATM's key domains of interest are depicted. The FAT and FATC domains are conserved amongst PI3-K related protein kinase family.

ATM's interaction with chromatin under basal conditions is dependent upon the chromatin architecture. Loss of the nucleosome binding protein High Mobility Group Nucleosomal binding 1 (HMGN1) results in global chromatin changes that increases the pool of chromatin bound ATM, and impedes ATM's activation (Kim et al., 2009). In undamaged cells ATM is present as an unphosphorylated dimer. ATM's FATC domain shields its kinase domain, preventing ATM autophosphorylation in undamaged cells (Bakkenist and Kastan, 2003).

DNA damage promotes ATM autophosphorylation and monomerisation; and activated ATM localises to the DSB site (Bakkenist and Kastan, 2003). The activated ATM kinase has a wide range of substrates and our characterisation of all ATM's substrates is far from complete. An IP-Mass Spec screen identified over 700 proteins phosphorylated upon consensus ATM and ATR phosphorylation sites (SQTQ) after DNA damage (Matsuoka et al., 2007). A positive control for this screen was the ATM co-factor and substrate NBS1.

1.2.2 The MRN Complex is a DSB sensor

The initial sensor of DSBs is believed to be the MRN complex. NBS1, Rad50 and Mre11 stably associate in a 2:2:2 ratio *in vivo* to form the MRN complex (Trujillo et al., 1998); although *in vitro* purification studies suggest a range of stoichiometries are possible (van der Linden et al., 2009). In both human and murine cells depletion of any MRN protein reduces the levels of other complex members, suggesting reciprocal

stabilisation (Lamarche et al., 2010). Mre11 is at the heart of the complex, interacting with both Rad50 and NBS1. Neither direct interaction, nor binding motifs indicative of an interaction, have been observed between Rad50 and NBS1. Real-time imaging of laser-generated DSBs showed Mre11 and NBS1 localise to the break site within seconds of induction (Lukas et al., 2004), indicating the MRN complex is an initial sensor of DSBs.

1.2.2.1 NBS1 is an essential DSB signalling scaffold

NBS1 is a 95kDa protein containing a two BRCT and one Forkhead Associated (FHA) domain, an Mre11 interaction domain, and a C-terminal ATM interaction motif (Figure 3). NBS1 has a nuclear localisation signal and localises the MRN complex to the nucleus, crucial for recruitment to DSBs. NBS1 mutants lacking the Mre11 interaction domain (*nbs1*^{tr645}) are nuclear, but $Mre11_2Rad50_2$ is retained in the cytoplasm (Desai-Mehta et al., 2001). Association of NBS1 with Mre11/Rad50 stimulates their nuclease and DNA binding activities, but NBS1 itself has no reported enzymatic activity - or indeed any putative enzymatic domains. Rather, NBS1's BRCT domains bind serine-phosphorylated Ser-X-Thr motifs, and the FHA domain binds threonine-phosphorylated Ser-X-Thr motifs (Lloyd et al., 2009; Williams et al., 2009) conferring NBS1 with the functions necessary to act as a key scaffolding and signalling protein.

NBS1 is required for ATM activation and downstream substrate phosphorylation in response to DSBs. NBS1 is an ATM substrate - activated ATM phosphorylates NBS1 after IR on consensus SQ motifs, including S278 and S343 (Gatei et al., 2000; Wu et al., 2000; Lim et al., 2000). However NBS1 is also upstream of ATM activation. The MRN complex is a key, early sensor of DSBs. Upon DSB induction NBS1 is rapidly recruited to the damage site where it remains stably bound to the chromatin. Immunofluorescence studies in irradiated A-T patient cells demonstrate ATM is not required for the localisation of Mre11 or NBS1 to DSBs (Mirzoeva and Petrini, 2001). Consequently, NBS1 can be considered to be both upstream and downstream of ATM activation.

Elucidation of which MRN complex functionalities are required for ATM activation is more intricate. Neocarzinostatin (NCS) treated NBS and A-TLD cells demonstrate markedly reduced pS1981-ATM (Uziel et al., 2003). Irradiation of NBS cells reconstituted with various NBS1 mutants indicates IR-induced pS1981-ATM phosphorylation is abolished in NBS1 deficient cells, but was recovered in a mutant lacking the ATM phosphorylation sites (S278A/S343A), but not by a mutant lacking the ATM binding domain (NB^{FR5}) (Cerosaletti and Concannon, 2004). Thus, from these studies one would conclude NBS1-ATM interaction, but not ATM phosphorylation of NBS1, is required pS1981-ATM foci formation at DSBs.

In summary, NBS1 is a key signalling scaffold effecting DNA repair, linking the DSB sensors Mre11 and Rad50 to a wide range of downstream repair and signalling proteins, and ensuring these interactions only occur at break sites.

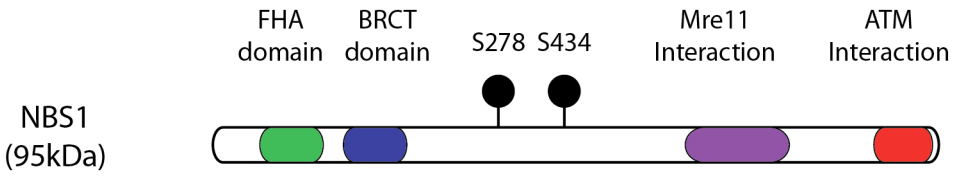

Figure 3: Schematic of domains present upon NBS1

Overview of the protein domains present upon wildtype NBS1. The ATM phosphorylation sites, S278 and S434, are indicated by black circles.

1.2.2.2 Mre11 facilitates DNA unwinding at DSBs

Mre11 is a highly conserved 85kDa protein with a phosphoesterase domain, two C-terminal DNA binding domains; and exhibits endo- and exonuclease activity against both single and double stranded DNA (Paull and Gellert, 1998; Paull and Gellert, 1999). Unwinding of DNA ends is essential for ATM activation (Lee and Paull, 2005). Mre11 readily forms homodimers, which can use their DNA binding domains to bridge DSB termini (Williams et al., 2008). Mre11's nuclease activity facilitates initial DSB resection. A mouse model for Mre11 with a mutated nuclease domain demonstrated whilst Mre11's nuclease activity is an essential function for DSB repair, it is not

required for ATM activation (Buis et al., 2008). Thus Mre11 has functions in DNA damage repair distinct from ATM activation and the MRN complex.

1.2.2.3 Rad50 synapses DSB termini

Rad50 is a 150kDa protein with both structural and sequence homology to the Structural Maintenance of Chromosomes (SMC) family. Elucidation of the Rad50 crystal structure revealed Rad50's N-terminal Walker A, and C-terminal Walker B, motifs stably associate with one another forming a globular domain capable of binding DNA DSB termini (Hopfner et al., 2000). Further structural studies demonstrated Rad50 interacts with Mre11 through an interaction motif at the apex of its globular domain (Hopfner et al., 2001). The globular domains of two Rad50 molecules can interact. This binding is ATP dependent, with two ATP molecules binding at the interface. However, the ATP hydrolysis is too weak to support motor or helicase functions (Hopfner et al., 2000). Given ATP binding induces conformation changes enhancing Rad50's affinity for dsDNA, perhaps ATP binding and hydrolysis cycles regulate the duration of MRN binding at DNA DSB termini.

Between Rad50's two Walker motifs are approximately 575 amino acids, which form a long coiled-coil domain terminating in a zinc hook (CXXC). The zinc-dependent dimerisation of two Rad50 molecules though the CXXC motifs enables Rad50/Mre11 to span the two termini of a DNA DSB (de Jager et al., 2001; Hopfner et al., 2002). The coiled-coil domains confer Rad50 with the spatial and conformation flexibility required to span DNA DSBs of differing architecture. The tethering of DSBs is only observed *in vitro* at high Rad50/Mre11 concentrations, suggesting through Rad50 oligomerisation the summation of multiple weak interactions achieves robust and specific DNA DSB tethering (de Jager et al., 2001).

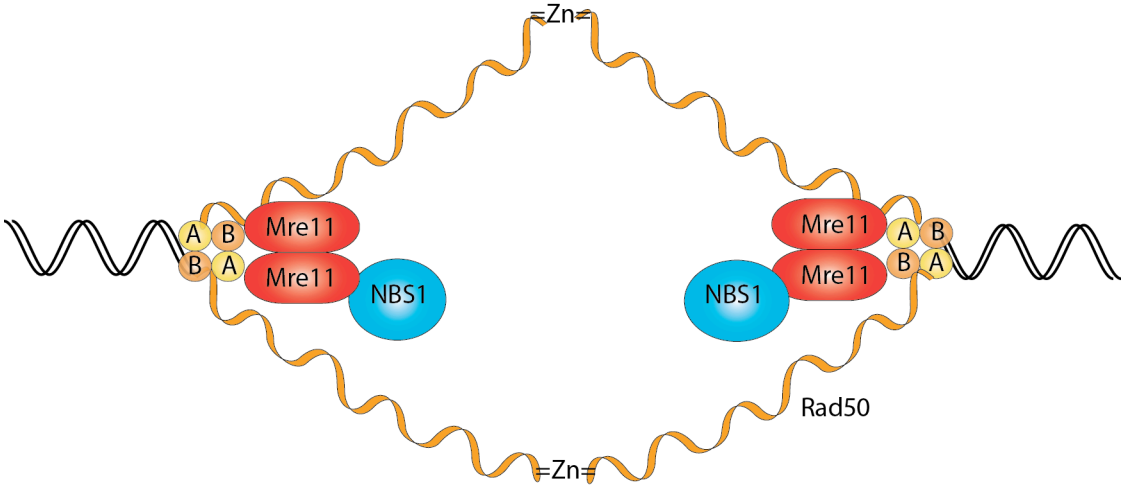

Figure 4: The MRN Complex Binds to DNA Double Strand Breaks

Schematic of the MRN complex binding to a DNA DSB. The coiled-coil domains of Rad50 (yellow) dimerise through a zinc hook, and Rad50's Walker A and Walker B domains bind the DNA DSB termini. Mre11 interacts with both NBS1 and Rad50. A = Walker A domain, B= Walker B domain.

The current molecular model of DSB termini bridging by the MRN complex encompasses two distinct modes of binding. The two DNA binding domains of an Mre11 homodimer bridge DNA ends at short range. The long flexible coiled-coil arms of Rad50 permit longer-range binding, either to tether DNA DSB ends over a longer distance or facilitate the binding of a broken chromosome with its sister chromatid (Figure 4). The MRN complex is the key immediate early sensor of DSBs, and its recruitment and retention to the damage site is essential for downstream ATM signalling. Interestingly, the tethering of either NBS1, Mre11, Mediator of DNA-damage Checkpoint 1 (MDC1) or ATM to chromatin was sufficient to elicit pH2AX foci formation (Soutoglou and Misteli, 2008), strongly suggesting the DNA damage response does not require DNA damage for signal transduction or amplification.

1.2.3 ATM phosphorylates H2AX and MDC1 at the DSB

Interaction between NBS1 and ATM facilitates ATM recruitment to the DSB, where ATM phosphorylates a wide range of DNA damage response proteins. Two crucial

ATM substrates are pT719-MDC1 (Kolas et al., 2007) and Serine-139 of histone variant H2AX, yielding pH2AX (γH2AX) (Rogakou et al., 1998). The H2A histone variant H2AX represents approximately 15% of all H2A in mammalian cells and is randomly incorporated into nucleosomes (Rogakou et al., 1998). H2AX is not an exclusive ATM target, the DNA damage kinases ATR and DNA-PKcs also phosphorylate S139-H2AX after replication stress and IR respectively (Ward and Chen, 2001; Stiff et al., 2004). Interestingly, analysis of *H2AX*$^{-/-}$ mutant mice revealed pH2AX is dispensable for the initial localisation of NBS1, Breast Cancer 1 (BRCA1) and p53 Binding Protein 1 (53BP1) to DSBs, but is required for their maintenance at the damage site. The phosphorylation of S139-H2AX creates a docking site for downstream DDR components and is a key signalling event in mediating the assembly of DNA repair foci.

Under basal conditions, tyrosine-142 of H2AX is constitutively phosphorylated by Williams-Beuren syndrome transcription factor (WSTF) (Xiao et al., 2009). After DNA damage, Tyr-142 is dephosphorylated by the phosphatases Eyes Absent Homolog 1 (EYA1) (Cook et al., 2009) and EYA3 (Krishnan et al., 2009). The importance of Tyr-142 dephosphorylation is demonstrated by the failure of WSTF deficient cells to maintain IR-induced pH2AX, pT719-MDC1 or pS1981-ATM foci (Xiao et al., 2009). Dephosphorylation of pY142-H2AX favours the recruitment of repair factors, including MDC1, over the recruitment of pro-apoptotic factors, such as JNK1, promoting DNA repair over cellular apoptosis (Cook et al., 2009). H2AX is therefore both an important binding platform for repair factors and a means to regulate the cellular outcome to DNA damage.

MCD1 contains consensus SQ/TQ phosphorylation sites, and is phosphorylated by ATM in response to DNA damage (Matsuoka et al., 2007; Kolas et al., 2007; Mailand et al., 2007). Concomitant phosphorylation of Ser-139 and dephosphorylation of Tyr-142 of H2AX creates a binding surface for MDC1 (Xiao et al., 2009). MDC1 serves as a key binding platform in DSB recognition, interacting with pH2AX through its C-terminal BRCT repeats, ATM through its FHA domain and NBS1 though its SDTD motifs. MDC1 is constitutively phosphorylated upon its SDTD repeats by Caesin Kinase 2 (CK2), enabling NBS1 to interact with MDC1 and assisting pH2AX

'spreading'. MDC1's range of interactions with ATM, NBS1 and pH2AX confer specificity for DSBs to the assembly of DNA repair foci.

Phosphorylation of H2AX spreads for up to several megabases either side of the DSB site in mammalian cells, although it is propagated less effectively on actively transcribed genes and heterochromatin (Iacovoni et al., 2010). Upon MDC1 binding to pH2AX, ATM is transiently anchored via NBS1, permitting ATM to phosphorylate adjacent H2AX motifs and achieve high density pH2AX spreading (Figure 5). Chromatin more distal from the DSB contains a lower density of pH2AX, and does not require MDC1. It is proposed a pool of soluble pS1981-ATM diffuses from the DSB site to phosphorylate more distal regions, allowing pH2AX spreading to bypass more compact heterochromatin (Savic et al., 2009) (Figure 5). As pH2AX does not propagate indefinitely, perhaps soluble ATM gradually looses its activity as it moves from the break site, capping the extent of pH2AX spreading. In yeast pH2AX also occurs, although it seems pH2AX spreading takes place over shorter distances of 50-100kB (Downs et al., 2000; Shroff et al., 2004).

The phosphorylation of the key ATM substrates H2AX and MDC1 establishes a binding platform central to DSB signalling. It is important MDC1 is only recruited to damage sites, as its stable recruitment activates an ubiquitin signalling cascade which ultimately assembles DNA repair machinery.

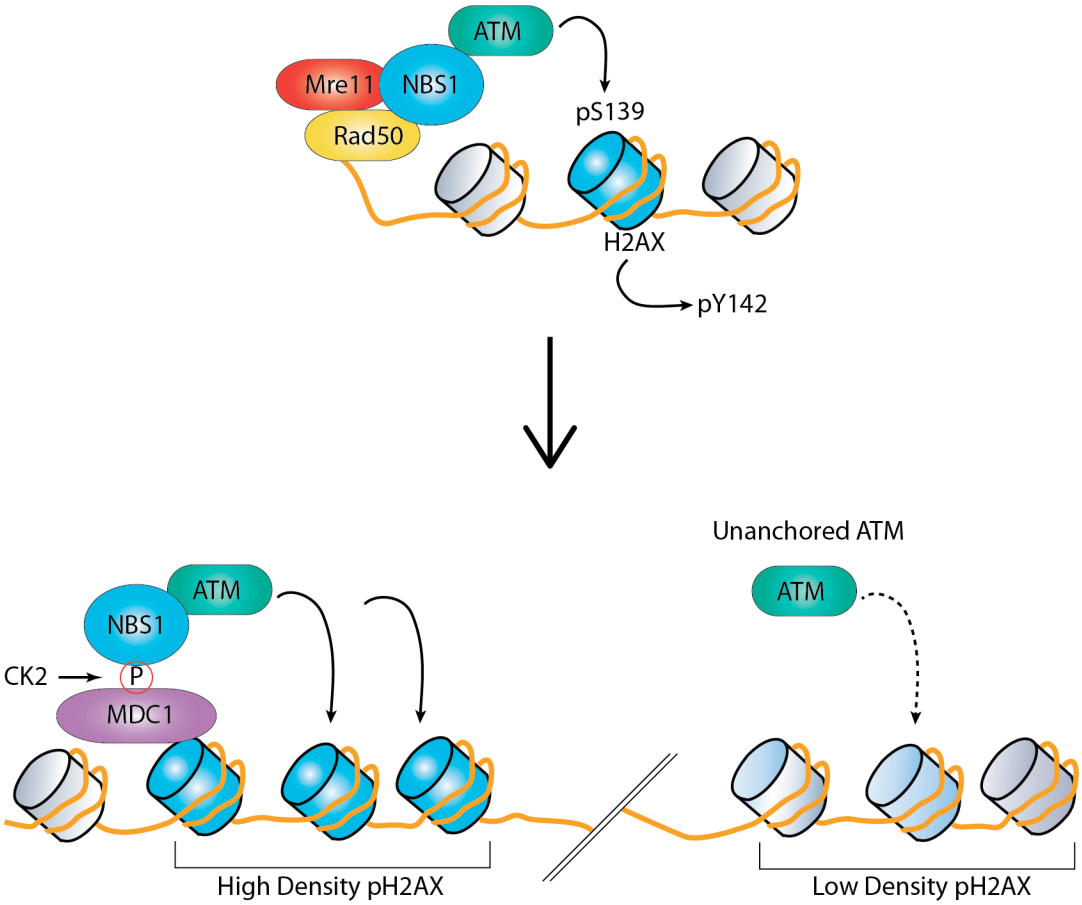

Figure 5: pH2AX spreading is propagated by ATM, NBS1 and MDC1

ATM is recruited to the DSB site by the MRN complex, and phosphorylates histone H2AX on Ser-139 in the region immediately surrounding the break. High density pH2AX spreading is achieved by MDC1 binding to pH2AX. MDC1 is constitutively phosphorylated by CK2, and NBS1 interacts with phosphorylated MCD1. This allows NBS1 to recruit ATM, which then phosphorylates the adjacent H2AX - and recruits MCD1, starting the cycle again. Unanchored ATM is prosed to phosphorylate lower density pH2AX.
MRN, Mre11 Rad50 NBS1; CK2, Caesin Kinase 2;

1.2.4 MDC1 phosphorylation activates a ubiquitination signalling cascade

The phosphorylation of MDC1 by ATM creates a binding site for the RING-domain E3 ubiquitin ligase RNF8, which binds MCD1 through an N-terminal FHA domain (Figure 6). The ubiquitin signalling cascade at a DSB can amplify the DNA damage signal to a sufficient magnitude to recruit and retain repair proteins. Once recruited, RNF8

ubiquitinates H2A and H2AX with K63-linked ubiquitin chains (Mailand et al., 2007) (Huen et al., 2007). This in turn recruits a second RING-domain E3 ubiquitin ligase, RNF168 (Doil et al., 2009; Stewart et al., 2009). RNF168 contains two Ubiquitin Interacting Motifs (MIU) and binds ubiquitinated H2A, amplifying K63 ubiquitin chains on the chromatin around the damage site (Doil et al., 2009; Stewart et al., 2009). Although not yet demonstrated, it is feasible that RNF168 has a distinct spectrum of substrates from RNF8. Nevertheless, it is evident that the key function of RNF168 is to increase the magnitude of K63-linked ubiquitinated chromatin chains initiated by RNF8 to sufficiently high concentrations for the retention of repair factors, including 53BP1 and BRCA1, at the damage site (Figure 6).

The specificity of RNF8 and RNF168 for DNA damage sites is not solely attained by MDC1. Both RNF8 and RNF168 cooperate with the same E2, UBC13. Interaction between UB13 and RNF8 is mediated by HERC2 in a DNA damage dependent manner. After DNA damage HERC2 is phosphorylated upon the consensus SQ/TQ site T4827, enabling HERC2 to bind to RNF8's FHA domain (Bekker-Jensen et al., 2010). Moreover, HERC2 is also able to bind RNF168 although the full significance of this is unknown. Knock-down of HERC2, RNF168 or RNF8 abrogates the K63-ubiqutin dependent retention of the repair proteins 53BP1 and BRCA1 at damage sites (Bekker-Jensen et al., 2010).

A recent report demonstrated DNA damage dependent SUMOylation of RNF168 and HERC2 by PIAS4 promotes their interaction with RNF8 (Rendtlew Danielsen et al., 2012). This offers the exciting possibility that SUMOylation may prove to be as crucial to DNA damage signalling as ubiquitination, phosphorylation and acetylation. Nonetheless, it is clear HERC2's ability to promote RNF8's interaction with UBC13 in a DNA damage dependent manner provides a critical regulatory loop in paring DNA damage detection and repair factor recruitment.

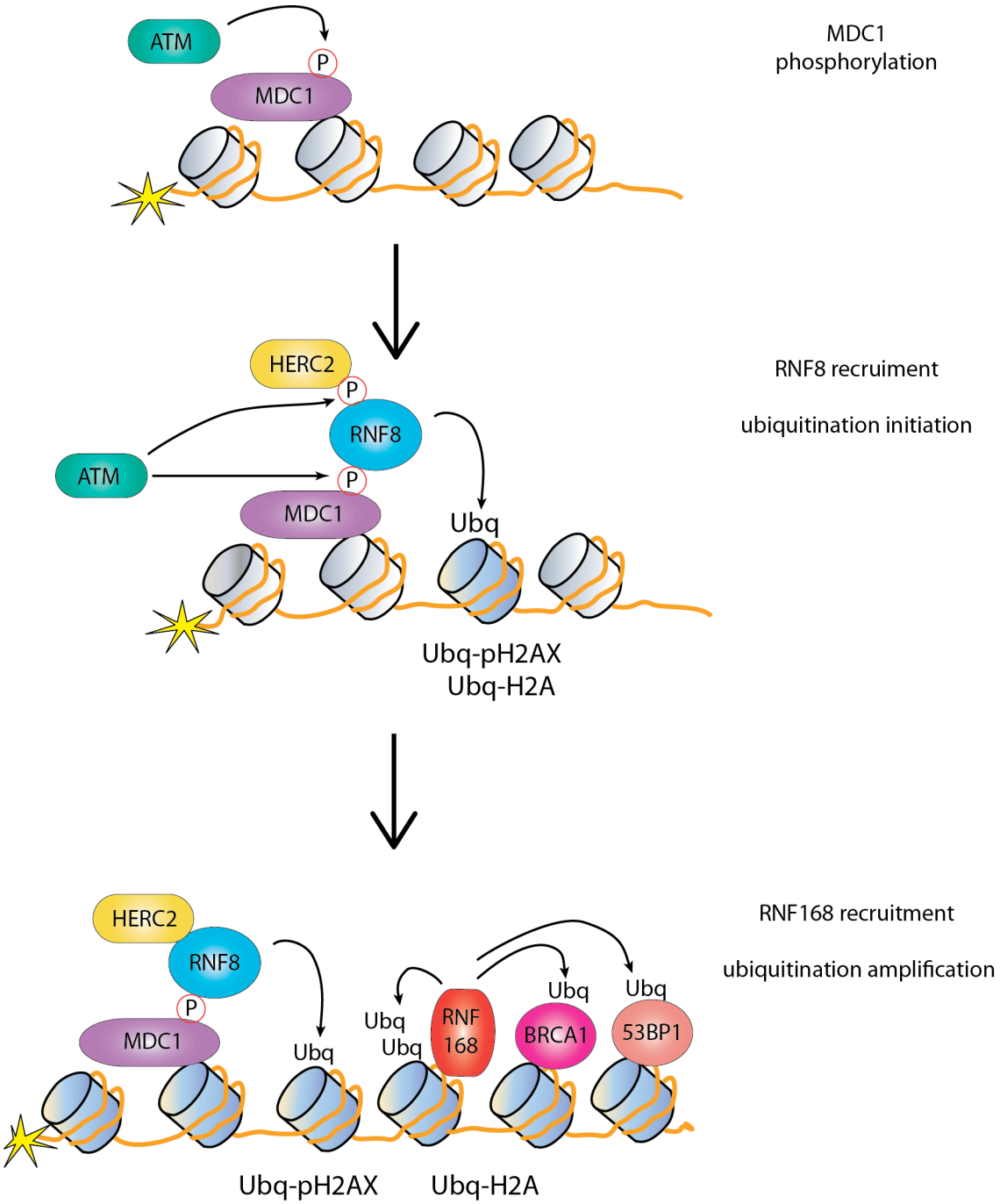

Figure 6: The Ubiquitin Signalling Cascades Amplifies The DNA Damage Response

The phosphorylation of MDC1 by ATM creates a binding site for the Ubiquitin Ligase RNF8. HERC2 dependent histone H2A and H2AX ubiquitination by RNF8 recruits RNF168, which amplifies the ubiquitin chains to a concentration able to recruit and retain the DNA repair factors 53BP1 and BRCA1.

An exciting new and expanding research area is negative regulators of ubiquitination-dependent DNA damage signalling. The deubiquitinase OTUB1 inhibits RNF168 dependent ubiquitination. In a novel mechanism, OTUB1 binds and inhibits the E2 ubiquitin ligase UBC13, preventing RNF168 activity (Nakada et al., 2010). Although little is known about the regulation of OTUB1, the observation that OTUB1 depletion increases HR-mediated DNA DSB break repair in cells treated with ATM inhibitor strongly suggests a physiological relevance for OTUB1 (Nakada et al., 2010).

1.2.5 ATM activates cell cycle checkpoints after DNA damage

Cell cycle arrest of damaged cells is critical as replication of damaged DNA and segregation of damaged chromosomes prompts escalating genomic instability. A crucial outcome of ATM activation is cell cycle-checkpoint activation. A-T patients exhibit radioresistant DNA synthesis (Houldsworth and Lavin, 1980; Painter and Young, 1980), and fail to activate the G1/S (Kastan et al., 1992) and G2/M (Beamish and Lavin, 1994) checkpoints after DNA damage. ATM phosphorylates a plethora of proteins to orchestrate cell cycle arrest, including substrates that remain bound to the damage site and those that freely diffuse in the nucleus (Figure 7).

1.2.5.1 An ATM substrate network activates cell cycle checkpoints

ATM signalling should be viewed as a network rather than discrete linear pathways; multiple activated substrates act in concert towards a common signalling outcome. For example, ATM controls S phase checkpoint activation by several complementary mechanisms. Firstly, the direct phosphorylation of Ser-957 on Structural Maintenance of Chromosome protein 1 (SMC1) is critical for S-phase checkpoint activation (Kitagawa et al., 2004). Secondly, phosphorylation of the phosphatase CDC25A by the ATM substrate Cdk2 targets CDC25A for ubiquitin mediated degradation (Falck et al., 2001). This leads to increased Thr-14 and Tyr-15 phosphorylation upon the CDC25A target Cdk2. These phosphorylations inhibit Cdk2's kinase activity and promote an S-phase arrest (Falck et al., 2001). Thirdly, ATM phosphorylates FANCD2 upon Ser-222

promoting activation of the S-phase checkpoint. Chk2 The-14 and Tyr-15 phosphorylation levels are normal in *fancd2*$^{-/-}$ cells suggesting FANCD2 signals to the checkpoint machinery in a Cdk2 and CDC25A independent mechanism (Taniguchi et al., 2002). ATM therefore activates a signalling network to effect cell cycle checkpoint activation, not just a single substrate.

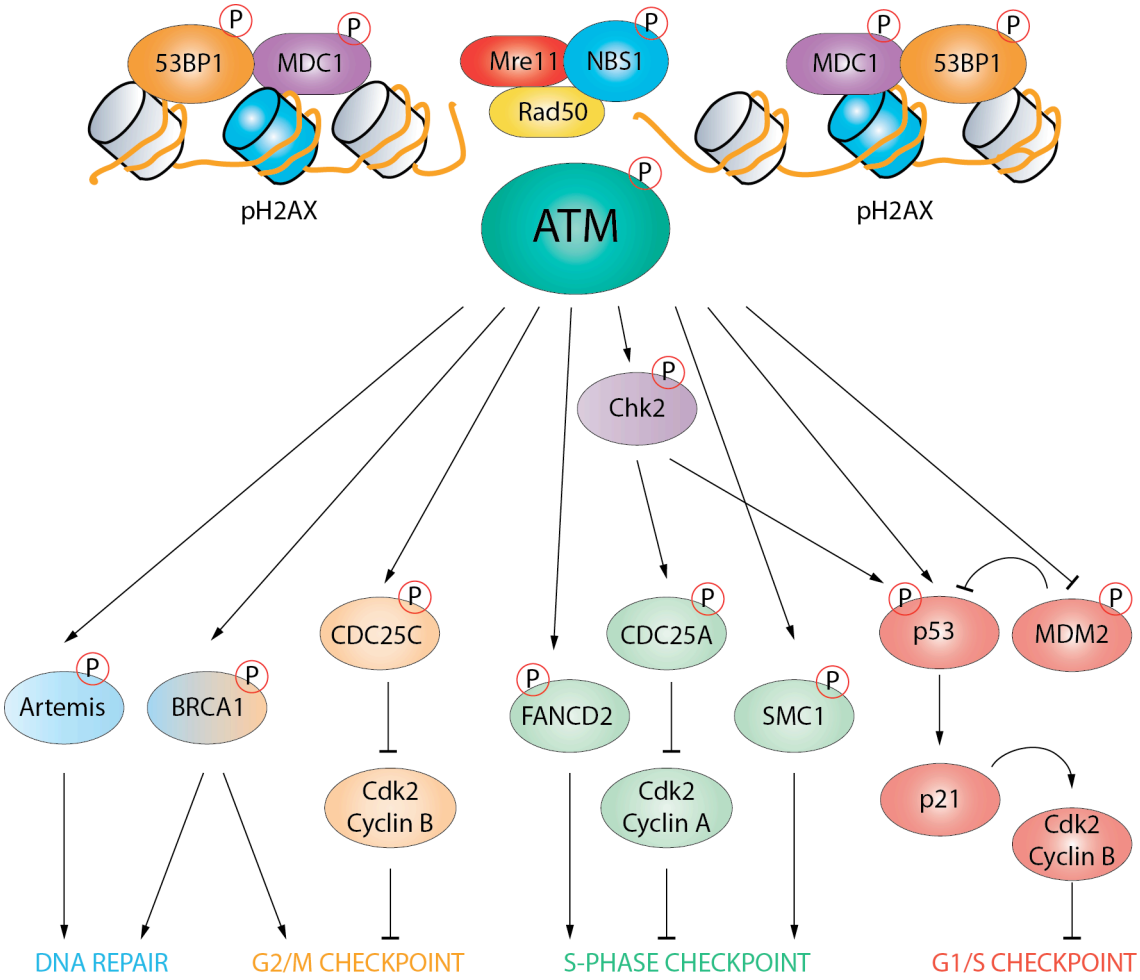

Figure 7: A network of ATM signalling activates cell cycle checkpoints and DNA repair

ATM activation in response to DNA DSBs controls a range of processes, including DNA repair and cell cycle checkpoint activation. Some ATM substrates, such as H2AX, NBS1, MDC1 and 53BP1 form part of the 'DNA Repair Foci' and remain stably bound and the DNA damage site. Others, including p53, Chk2, CDC25C and CDC25A freely diffuse through the nucleus, and bring about cell cycle checkpoint activation.

1.2.5.2 ATM and p53

The 'guardian of the genome', p53, is a key effector of G1/S checkpoint activation. p53 deficient cells fail to activate the G1/S checkpoint after irradiation. ATM phosphorylates p53 upon Ser-15, although this event is not sufficient to stabilise and activate p53 (Banin et al., 1998; Canman et al., 1998). Mice with the equivalent ATM phosphorylation site mutated, $p53^{S18A/S18A}$, exhibit a modest reduction in apoptosis after DNA damage, but have normal DNA damage checkpoint activation and a modest increase in tumourigenesis in old mice (Sluss et al., 2004). ATM activates p53 through a wider range of indirect mechanisms than just direct phosphorylation. For example, ATM phosphorylates Ser395 of MDM2, an E3 ligase that targets p53 for ubiquitin mediated degradation under basal conditions (Maya et al., 2001). Phosphorylation of MDM2 alters its oligomerisation and reduces the processivity of MDM2's ligase activity, impairing MDM2's ability to target p53 for degradation and hence increasing p53 protein levels. Moreover, pS395-MDM2 interacts with p53 mRNA in the nucleolus. This interaction promotes MDM2 sumolaytion, and sumolyated MDM2 stimulates the translation of p53 mRNA (Gajjar et al., 2012).

In addition to p53's important role in ATM signalling, p53 has a wider range of tumour suppressive activities. The Arf pathway activates p53 in response to hyperproliferation, and is thought to largely function independently of DNA damage signalling. Arf promotes p53 stabilisation by reducing MDM2's affinity for p53. p53 also has a broad range of transcriptional targets, including the pro-apoptotic genes PUMA and NOXA; the anti-oxidant protein TIGAR, and the cell-cycle inhibitor p21. Given the range of p53's tumour suppressive targets it is unsurprising $p53^{-/-}$ mice succumb to a wide range of cancers, including lymphomas, carcinomas and sarcomas (Donehower et al., 1992). The compound $atm^{-/-}$; $p53^{-/-}$ mutant developed lymphoma at an average age of two months, earlier than either of the single mutants, suggesting synergy between p53 and ATM mutations (Westphal et al., 1997; Xu et al., 1998).

1.2.6 Acetylation and the DNA damage response

Acetylation plays a crucial role in the DDR, both as a signalling moiety and by allosterically promoting the chromatin changes required for DNA repair. The histone acetyltransferase Tip60 and PI3-K-related protein TRRAP, both NuA4 complex members, are rapidly recruited to the break site (Murr et al., 2006). The yeast Tip60 homologue, Esa1, was shown to acetylate histone H4 and is required for efficient DNA repair (Bird et al., 2002). In mammalian cells, Tip60 loss is embryonically lethal and accelerated tumour onset in *Eμ-Myc*$^{+}$*; tip60*$^{+/-}$ mice demonstrated Tip60 is a haploinsufficient tumour suppressor (Gorrini et al., 2007). Indeed, multiple studies have demonstrated Tip60 deficient cells have defects in HR and DNA damage signalling. Specifically, defects in Rad51 foci formation after IR (Murr et al., 2006), reduced ATM substrate phosphorylation upon oncogenic Myc expression (Gorrini et al., 2007) and reduced IR-induced apoptosis (Ikura et al., 2000) have been reported in cells with compromised Tip60 function.

Multiple proteins associated with the NuA4 complex, including Tip60 and DNA Methyltransferase Associated Protein 1 (DMAP1), were recently identified in a genome wide shRNA screen for positive regulators of HR (Adamson et al., 2012). DMAP1 was originally characterised as an interaction partner of DNA Methyltransferase 1 (DNMT1) (Rountree et al., 2000) and subsequently shown to be part of the NuA4 complex (Cai et al., 2003), (Doyon et al., 2004). Knock-down of *dmap1* in MEFs leads to increased levels of DNA damage (Negishi et al., 2009), but the mechanistic role of DMAP1 in DNA damage signalling and repair is largely unknown.

Tip60, together with the histone acetyltransferase MOF, acetylates histone H4 tails upon K4, K8, K12 and K16. Histone H4 acetylation, in particular of H4K16, is increased after DNA damage (Li et al., 2010). Loss of H4K16 acetylation has been associated with a wide range of cancers (Fraga et al., 2005). Acetylation of H4K16 modulates both higher order chromatin structure and interaction with non-histone proteins (Shogren-Knaak et al., 2006). The impaired pH2AX and MDC1 foci formation in MOF deficient cells is largely rescued by pre-treatment with the histone deacetylase

inhibitor TSA (Sharma et al., 2010). This suggests histone acetylation is required for chromatin to adopt a state 'permissive' for DNA repair rather than as a specific post-damage signalling event. It is noteworthy that Histone Deacetylase 1 (HDAC1) and Histone Deacetylase 2 (HDAC2) are recruited to DSBs and mediate hypoacetylation of histone H3K56, promoting NHEJ repair (Miller et al., 2010). Thus, histone acetylation in DNA damage signalling is subtler that simply a crude summation of total acetylation; rather the dynamic acetylation status of specific histone residues is crucial.

A range of histone modifications, including phosphorylation, ubiquitination and methylation, have been implicated in Tip60 recruitment to DSBs. The NuA4 complex contains components capable of binding ubiquitinated and phosphorylated chromatin. Arp4 binds phosphorylated Ser129 of yeast H2A (the orthologue of human pS139-H2AX) and is essential for NuA4 recruitment to DSBs (Downs et al., 2004). MRG15, present in both MOF and Tip60 complexes, binds ubiquitinated H2B facilitating MOF and Tip60 recruitment to the damage site (Wu et al., 2011). Cells doubly deficient for RNF8 and the closely related E3 ubiquitin ligase Chfr, which ubiquitinate histone H2B, exhibit reduced H4K16Ac and impaired ATM activation. Compound mutant *Chfr*$^{-/-}$ *Rnf8*$^{-/-}$ mice develop lymphoma, illustrating the importance of histone modifications in DNA damage signalling (Wu et al., 2011).

Tip60's chromodomain binds tri-methylated histone 3 K9 (H3K9me3). It is postulated Tip60 recruitment to DSBs requires dissociation of heterochromatin-binding protein 1 (HP1) to expose the constitutive H3K9me3 (Sun et al., 2009). These results are in agreement with the finding HP1-β is phosphorylated by casein kinase 2 (CK2) upon Thr-51 after DNA damage, prompting is dissociation from chromatin and exposing the H3K9me3 mark (Ayoub et al., 2008). While these are intriguing results, the signal for CK2 localisation - which ensures Tip60 is specifically localised to damage sites - remains unclear. Neither CK2 nor HP1- β appear to be ATM, ATR or DNA-PKcs targets (Matsuoka et al., 2007). Nevertheless, the ability of NuA4 complex components to recognise phosphorylated, ubiquitinated or methylated histones underscores the extensive crosstalk between histone modifications in ATM signalling networks.

A direct role for acetylation in ATM activation is proposed by several recent papers from the Price group. It is suggested the majority of ATM molecules in an undamaged cell are constitutively associated with Tip60. Upon DNA damage ATM is acetylated by Tip60 on Lys-3016. ATM's kinase activity is dispensable for ATM acetylation, placing acetylation as a very early event of ATM activation (Sun et al., 2007). Indeed, ATM mutants with mutations in the FATC domain are unable to bind Tip60 and demonstrate defective *in vitro* kinase activity (Sun et al., 2005). It is postulated by the authors that ATM is only acetylated, and therefore activated, at the DNA damage site. However, earlier studies have demonstrated purified ATM is catalytically active *in vitro*, suggesting either ATM is constitutively acetylated or that ATM acetylation may not be crucial to its activity (Lee and Paull, 2005).

1.2.7 The repair of DNA DSBs

Cells have two main mechanisms to repair DSBs; the largely error-free homologous recombination (HR) and the error prone Non-Homologous End Joining (NHEJ) pathways (Figure 8). NHEJ enables the ligation of two DNA ends regardless of sequence, whereas HR uses the broken DNA's sister chromatid as a template to join two homologous broken ends. Thus HR is only feasible in S and G2 phase cells, and predominates during these cell cycle phases. Although NHEJ cannot discern whether two broken ends belong together, it is essential for the repair of deleterious breaks when a template chromatid is unavailable.

1.2.7.1 Non homologous end joining

The core NHEJ machinery includes the Ku heterodimer (Ku70/Ku80), recruited to the damage site within seconds of DSB induction. Ku has a toroidal structure and the central, open ring is loaded onto the DNA ends (Walker et al., 2001). Furthermore, Ku has 5'-deoxyribose-5-phosphatase (5'-dRP) lyase activity and can remove abasic sites near DSBs, helping to 'clean-up' DNA ends without extensive resection, which would favour HR over NHEJ. (Roberts et al., 2010). Ku recruits DNA-PKcs to the DSB site,

facilitating the interaction between DNA-PKcs and the DNA ends. A series of phosphorylation reactions catalysed by DNA-PKcs stabilise the DNA end, preventing resection. DNA-PKcs autophosphorylates upon a PQR cluster, inhibiting end resection; and upon an ABCDE motif, recruiting the nuclease and ATM substrate ARTEMIS. ATM also phosphorylates the DNA ligase XRCC4/LIG4 and the stimulatory factor XLF, which together ligate the broken DNA ends. ATM is estimated to be required for at least 10% of NHEJ mediated DSB repair; but the core NHEJ machinery is not required for ATM activation and recruitment. It is postulated ATM mediated cell cycle arrest is required to allow sufficient time for the NHEJ pathway to repair heterochromatic DNA breaks (Jeggo and Lobrich, 2005).

A variation on classical NHEJ is microhomology-mediated end-joining (MMEJ). The key distinction of MMEJ is the resection of approximately 4-6 nucleotides from the DNA termini to create short, complementary ends prior to ligation. MMEJ mediated DSB repair always results in the loss of some nucleotides, and it remains unclear to what extent this pathway is employed in cells with intact NHEJ components (McVey and Lee, 2008).

1.2.7.2 Homologous recombination

Entry into either the NHEJ or HR repair pathways is largely regulated at the stage of extensive DNA resection; required for HR but inhibitory to NHEJ repair. Although Mre11 is involved in the initial resection events at a DSB, it lacks the 5'-3' exonuclease activity required to generate the HR-promoting long 3'ssDNA overhangs. It is possible unidentified co-factors associate with Mre11 and switch its polarity, but Mre11's nuclease activity is likely to be limited to initial DSB resection and thus Mre11 facilitates both HR and NHEJ repair pathways (Milman et al., 2009; Zhuang et al., 2009).

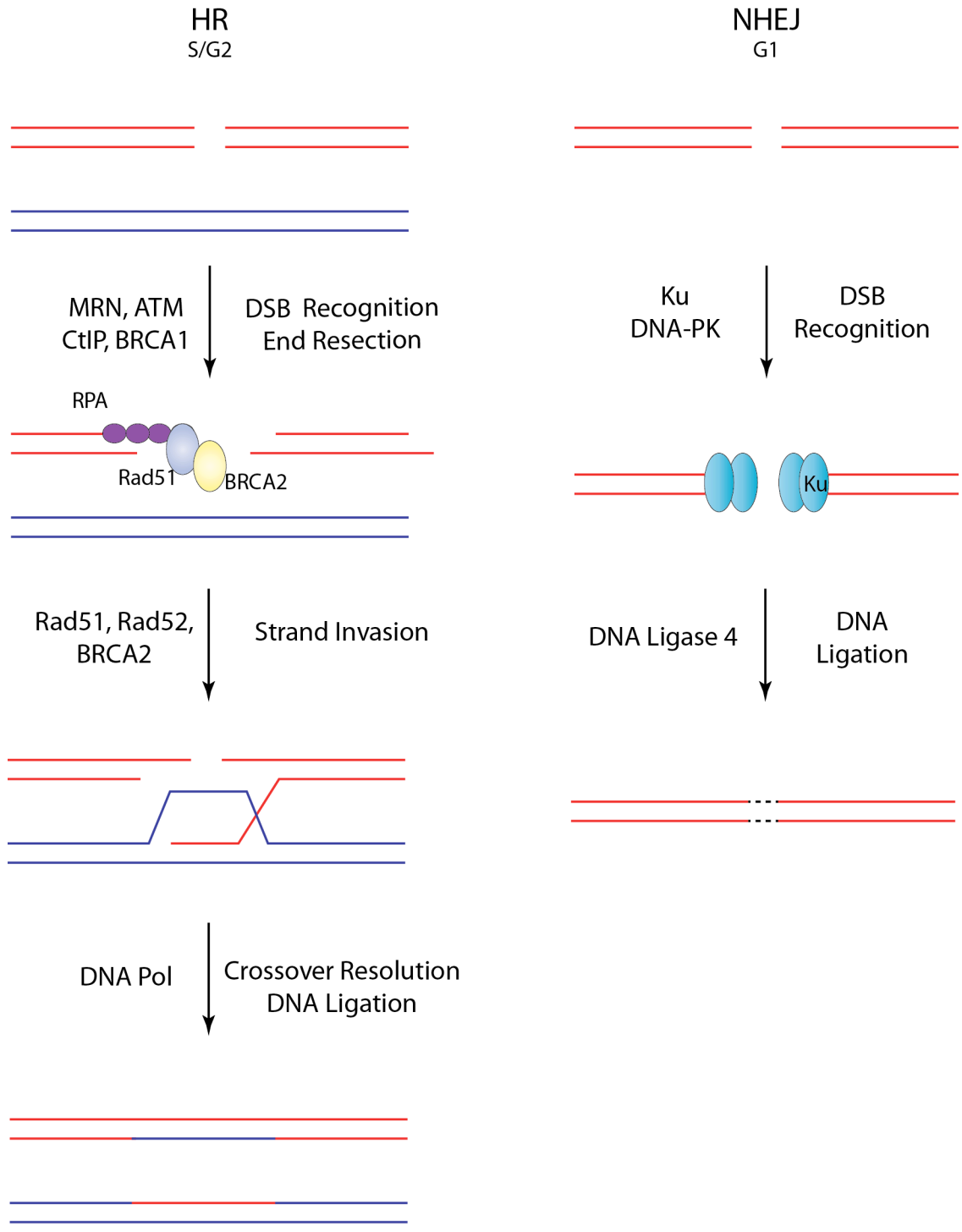

Figure 8: The Repair of DNA DBSs by HR or NHEJ

The choice of DNA DSBs repair pathway is regulated by the cell cycle; during G2/S HR predominates, and during G1 NHEJ is employed. Both pathways involve DSB detection and finish with DNA ligation, but HR also involves resection to form single stranded DNA, and homology search for a sister chromatid to use as a template for DSB repair.

End resection to form long 3'ssDNA overhangs is regulated in a cell-cycle dependent manner. During S and G2 the mammalian cell cycle dependent kinase (Cdk2) phosphorylates CtIP upon S374 (Huertas and Jackson, 2009). Phosphorylated CtIP interacts with BRCA1's C-terminal BRCT domain and the MRN complex (Yu and Chen, 2004). Thus, CtIP is only recruited to DNA damage sites when Cdk2 is active, which is when a sister chromatid would be available for HR. Upon BRCA1 binding CtIP is ubiquitinated, promoting its end-resection function (Sartori et al., 2007). Additional nucleases and helicases, such as Mre1, EXO1 and BLM also contribute to resection. ATM phosphorylates CtIP upon S664 and S745. Although the relevance of these phosphorylations for HR is unclear, they are known to upregulate transcription of the cell cycle inhibitor genes p21 and Gadd45 (Li et al., 2000b; Wu-Baer and Baer, 2001). ATM's role as a master regulator of the DNA damage response becomes evident when we consider it phosphorylates proteins at every level of the response - from detection to repair.

Resection of the DNA ends at the break site yields a single stranded DNA overhang of 100-200 nucleotides. The single-strand DNA is rapidly coated and stabilised by the single-strand DNA binding protein Replication Protein A (RPA). Rad51 filaments can then form upon the RPA-ssDNA complex, which in turn recruits Breast Cancer 2 (BRCA2). These events are also regulated by cell cycle dependent phosphorylation. Binding between BRCA2 and Rad51 is dependent upon phosphorylation of BRCA2 upon Ser-2319 by Cdk2. Phosphorylation upon Thr-309 of Rad51 by Chk1 is necessary for Rad51 recruitment to damage sites (Esashi et al., 2005; Sorensen et al., 2005). The formation of stable RAD51 filaments prompts ssDNA a homology search and strand invasion into homologous sequences. Finally, a range of DNA polymerases, ligases and resolvases promote the resolution of the crossover, yielding two repaired, intact DNA molecules (Sung and Klein, 2006).

1.2.7.3 ATM is required for repair of heterochromatin associated DSBs

ATM is required for the repair of approximately 10-25% of all DSBs (Deckbar et al., 2007; Riballo et al., 2004). Although the cell has some redundancy in its DSB repair

pathways, through DNA-PKcs dependent NHEJ repair, there is a subset of breaks critically dependent upon ATM for repair. These DBSs are not necessarily those of increasing complexity, but rather heterochromatin associated damage (Goodarzi et al., 2008). ATM's role at heterochromatin associated breaks was revealed by the observation heterochromatic breaks in KRAB-Associated Protein 1 (KAP1) deficient cells do not require ATM for repair. ATM phosphorylates KAP1 upon Ser824, reducing KAP1's affinity for heterochromatic chromatin and prompting chromatin relaxation (Goodarzi et al., 2008). A MCD1, RNF8, RNF168 and 53BP1 dependent signalling cascade promotes pS824-KAP1 localisation into repair foci at late repairing DSBs (Noon et al., 2010).

Although ATM phosphorylates pS824-KAP1 to a wildtype extent in *53bp1*$^{-/-}$ cells, pS824-KAP1 does not localise into foci at late-repairing breaks. 53BP1 is required to amplify the Mre11-NBS1 concentration at late repairing DSBs, thus increasing local ATM concentration. This achieves sufficient KAP1 phosphorylation at these breaks to promote the alteration of chromatin to a state permissive for DNA repair (Noon et al., 2010). The key NHEJ protein Artemis is dispensable for p S824-KAP1 and 53BP1 foci formation at late repairing breaks (Woodbine et al., 2011), strongly suggesting that the NHEJ pathway cannot compensate for ATM function at heterochromatic DSBs.

1.2.8 ATM and non-canonical stimuli

1.2.8.1 ATM is activated by oxidative stress

A subset of A-T symptoms, including cerebellar degeneration and ataxia, cannot readily be attributed to ATM's DSB signalling role. In cerebellar neurons ATM is equally located in the nucleus and cytoplasm, suggesting a non-DSB function for ATM (Barlow et al., 2000; Boehrs et al., 2007; Li et al., 2009). Moreover, it is well established A-T cells exhibit increased sensitivity to reactive oxygen species (ROS) (Yi et al., 1990). In parallel to this, the brains of *atm*$^{-/-}$ mutant mice display elevated levels of oxidative stress (Kamsler et al., 2001). Intriguingly, the free radical scavenger N-acetyl cysteine (NAC) rescues the haematopoietic stem cell (HSC) defect of *atm*$^{-/-}$ mice (Ito et al.,

2004). Although in that study an effect on tumour-free survival was not commented on, a subsequent paper reported feeding *atm*$^{-/-}$ mice NAC delays thymoma onset (Reliene and Schiestl, 2006). Despite the mounting evidence for ATM's involvement in oxidative stress, it was only in 2010 that the Paull lab elucidated a direct role, and defined molecular mechanism, for ATM in the oxidative stress response (Guo et al., 2010b).

In response to H_20_2 induced oxidative stress, ATM autophosphorylates upon Ser-1981 and phosphorylates a subset of its known substrates, including pS15-p53 and pT68-Chk2, but S139-H2AX phosphorylation is not observed (Guo et al., 2010b). ATM's kinase activity in response to oxidative stress is independent of interaction with the MRN complex. Indeed, it appears oxidative stress induced ATM activation slightly inhibits ATM's association with MRN (Guo et al., 2010a). This is explained by the finding ATM's active conformation after H_20_2 treatment is different from the phosphorylated monomer it adopts after DSB induction. Upon oxidative stress, ATM forms a cysteine-linked dimer, held together by an intermolecular cysteine bridge upon C2991. Mass spectrophotometry studies suggest other cysteine residues are also oxidised, but point mutation studies suggest they are dispensable for dimer formation. A subset of A-T patients carry a R3047X truncating mutation. As their symptoms differ from classical A-T, including less severe radiosensitivity and no immunodeficiency, patients with this mutation are often referred to as alterative-A-T. Zuo and colleagues demonstrated cells carrying an R3047X mutation have largely normal pS1981-ATM autophosphorylation after the DSB inducing agent camptothecin, but an impaired response to H_20_2 treatment (Guo et al., 2010b). It is postulated the region of ATM deleted in the R3047X truncation is a peroxisome targeting signal (Watters et al., 1999). It is not shown whether R3047X patients retain the ability to form cysteine linked dimers (Guo et al., 2010b), but as these patients presumably retain an intact Cys-2991, there must be additional molecular steps beyond cysteine dimer formation required for ATM activation by oxidative stress.

1.2.8.2 Non-canonical ATM stimuli alter the chromatin structure

In addition to its roles in DSB and oxidative stress signalling, ATM is activated by treatments that alter chromatin structure, including hypotonic shock and chloroquine (Bakkenist and Kastan, 2003; Kanu and Behrens, 2007). Interestingly, pH2AX foci formation is not observed under these conditions. Although ATM unequivocally plays an essential role on DSB signalling, it is evident ATM has important cellular functions beyond DSB signalling and repair.

1.2.9 ATM pSer-1981 phosphorylation

In undamaged cells, ATM is an unphosphorylated monomer. Upon DNA damage induction, such as IR-induced DSBs, ATM undergoes intermolecular phosphorylation upon Ser1981 (human) or Ser1987 (mouse) and dissociates into an active, phosphorylated monomer (Bakkenist and Kastan, 2003). Whilst pSer-1981 is a widely accepted mark of active ATM, and indeed pre-treatment with a small molecule ATM inhibitor abolishes pSer-1981 and ATM's kinase activity, pSer-1981 does not appear to be necessary for ATM activation and its function remains a controversial debate.

To address the importance of ATM phosphorylation *in vivo*, atm^{S1987A} mice were generated by reconstitution of $atm^{-/-}$ mice with an *atm* allele harbouring a Serine to Alanine (S1987A) mutation. This revealed S1987 phosphorylation is dispensable for functional ATM responses at both the cellular and organismal level (Pellegrini et al., 2006). It was postulated other serine residues could compensate for S1987A. However, generation of a mouse model revealed mutation of multiple serine residues phosphorylated upon ATM (S367, S1899, S1987) did not impair ATM activation or signalling after IR (Daniel et al., 2008). Analogously, a recombinant, *in vitro* study confirmed S1981A mutation inhibits neither ATM kinase activity nor ATM dimer dissociation (Lee and Paull, 2005). Although pS1987 correlates with active ATM, from these studies one would conclude it is neither causative nor required for ATM activation.

ATM autophosphorylation appears to be modulated by chromatin proximity. An *in vitro* study by You and colleagues elegantly demonstrated that when non-DNA bound, phosphorylated pS1981-ATM was removed from DNA damage containing Xenopus extracts and incubated in DNA-damage free extracts ATM could phosphorylate a recombinant Thr-68 containing Chk2 substrate, but not promote the autophosphorylation of inactive ATM in the extract (You et al., 2007). This suggests ATM autophosphorylation occurs in the vicinity of DNA breaks. However, their data does not exclude a model in which other factors, modified by a break, interact with ATM in the nucleolus to aid ATM activation. *In vitro* pull-down studies of ATM in Xenopus egg extracts containing DNA fragments suggested some of the ATM molecules localised to the putative break site were not phosphorylated (You et al., 2005). These reports suggest a model whereby pS1981-ATM phosphorylation is not required for ATM recruitment to the DSB, but that ATM autophosphorylation can only occur in the DSB vicinity.

A conflicting study demonstrated that only wildtype ATM, and not kinase dead or pS1981A mutants, were associated with DSBs induced by I-PpoI endonuclease (Berkovich et al., 2007). However, possible reconciliation between these reports is the difference in time after damage induction. Whereas You and colleagues assessed ATM 5-15 minutes after DNA damage, the endonuclease system employed by Berkovich and colleagues has DSB induction up to 12-15 hours before analysis of ATM recruitment. These two studies raise the intriguing possibility pS1981-ATM phosphorylation is required for ATM retention at DSBs, rather than recruitment, and mutants that cannot be activated subsequently dissociate from the surrounding chromatin. However, enhanced atm^{S1987A} retention at sites of DNA damage was observed in atm^{S1987A} animals, suggesting this is not the case (Pellegrini et al., 2006). Although ATM could be differentially regulated in murine and human cells, it seems likely that while pS1897-ATM (or pS1981) correlates with activated ATM it is not necessary for ATM activation.

1.3 ATM Has Two Co-factors - NBS1 and ATMIN

1.3.1 Murine models for NBS1 function

A range of mouse models have contributed to our understanding of NBS1 function. The first NBS1 model was the complete ablation of NBS1, by deletion of a 2kb region encompassing the promoter, exon 1 and intron 1 (Zhu et al., 2001). This approach was taken as the nature of the NBS1 mutation in NBS patients was unknown at the time. Although heterozygous *nbs1*$^{+/-}$ mice were viable, no *nbs1*$^{-/-}$ offspring were obtained. Loss of *nbs1* resulted in very early embryonic lethality at approximately E3.5. Even by this early stage the mutant blastocysts were very poorly developed. Unlike other DNA damage proteins, including BRCA1 (Xu et al., 2001), the embryonic lethality of *nbs1* deletion is not overcome by co-deletion of p53 (Yang et al., 2006).

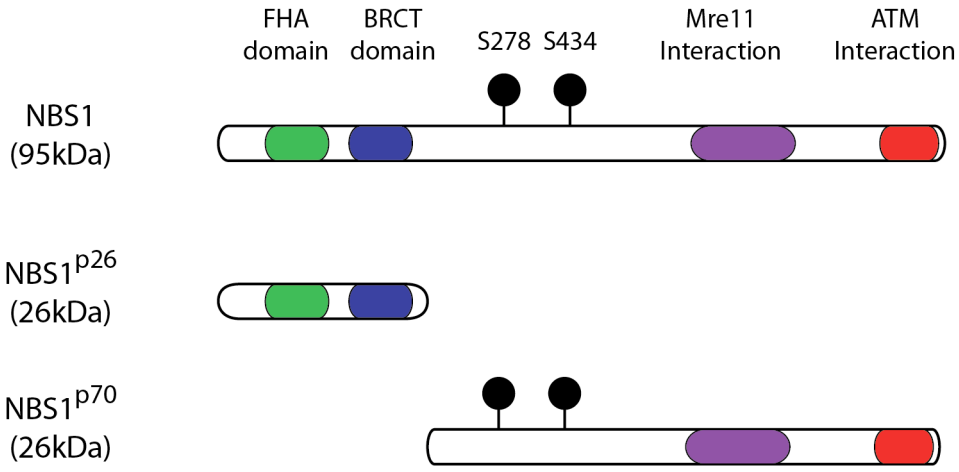

Figure 9: Overview of domains present upon NBS1, NBS1^{p26} and NBS1^{p70}

Wildtype NBS1 (top) contains FHA and BRCT domains towards its N-terminus, and Mre11 and ATM interaction domains towards the C-terminus. The ATM phosphorylation sites, S278 and S434, are indicated with black circles. The domains present on the NBS1^{p26} (middle) and NBS1^{p70} (bottom) truncations produced by *nbs1*$^{657\Delta}$ mutation are indicated

As *nbs1* loss is embryonically lethal, a revised approach was to recapitulate the mutations observed in NBS patients. Approximately 95% of NBS patients exhibit a five base pair truncation mutation, *nbs1*$^{657\Delta5}$, producing a 70kDa protein (Maser et al., 2001)

(Figure 9). Williams and colleagues deleted exons 4 and 5, encompassing the BRCT domain, to generate an 80kDa N-terminal truncated NBS1 protein (Williams et al., 2002). Mice homozygous for the mutation, $nbs1^{\Delta BRCT}$, are viable and thus the BRCT domain of NBS1 is not required for viability. $nbs1^{\Delta BRCT}$ MEFs are radiosensitive, but no cancer predisposition was observed in $nbs1^{\Delta BRCT}$ mice, in contrast to the lymphoma predisposition of NBS patients. Moreover, $nbs1^{\Delta BRCT}$ mice do not exhibit growth retardation, female sterility, immunodeficiency or spontaneous chromosomal instability (Williams et al., 2002). Although a reasonable approximation of NBS, the mutation introduced by Williams and colleagues differs from the common NBS mutation $nbs1^{657\Delta 5}$ in two key ways. Firstly, the truncated NBS1 protein in the $nbs1^{\Delta BRCT}$ model is 10kDa larger than the 70kDa protein produced in NBS cells. Secondly, internal translation initiation yields synthesis of a N-terminal, 26kDa NBS1 protein in $nbs1^{657\Delta 5}$, but not $nbs1^{\Delta BRCT}$, cells. A second model for NBS was the deletion of exon 2 and 3 to introduce a frameshift mutation (Kang et al., 2002). The subsequent $nbs1^{m/m}$ mice were viable, and produced a 75kDa N-terminal truncated NBS1. Again, this model did not fully recapitulate the NBS phenotype. Although cells were radiosensitive and displayed genomic instability; in contrast to NBS patients spermatogenesis was normal in $nbs1^{m/m}$ mice (Kang et al., 2002).

A far closer model for NBS is the 'humanised NBS1 mouse' generated by Difilippantonio and colleagues (Difilippantonio et al., 2005). The human *nbs1* locus, including the $nbs1^{657\Delta 5}$ mutation and regulatory elements, was used to generate $nbs1^{657\Delta 5}$, which were crossed to $nbs1^{+/-}$ mice, yielding $mNbs1^{-/-}$; $hNbs1^{657\Delta 5}$. These mice recapitulated NBS, including cancer predisposition, immunodeficiency and cell cycle checkpoint defects. Cells derived from $mNbs1^{-/-}$; $hNbs1^{657\Delta}$ animals exhibited diminished, but not abolished, pS1987-ATM foci formation after IR. Difilippantonio and colleagues also reconstituted $nbs1^{-/-}$ mice with various other NBS1 mutants. Interestingly, $nbs1^{tr645}$, lacking the Mre11 binding domain did not rescue the embryonic lethality of $nbs1^{-/-}$ mice (Difilippantonio et al., 2005). However, $nbs1^{H45A}$ mice mutants with a point-mutant in the FHA domain were viable. This suggests the loss of the Mre11-NBS1 interaction may be cause of the $nbs1^{-/-}$ lethal phenotype. However, FHA domain function cannot be solely attributed to Mre11 binding. Other proteins, including

CtIP, interact with NBS1 upon its FHA domain (Williams et al., 2009; Lloyd et al., 2009). Given *mdc1*$^{-/-}$ mice show a milder phenotype than the *nbs1*$^{-/-}$ lethal phenotype it seems likely the cell-lethality of *nbs1* deletion is not solely due to impaired Mre11 function.

Upon conditional *nbs1* deletion MEFs undergo premature proliferation arrest, exhibit markedly reduced Rad50 and Mre11 recruitment to DNA DSBs, and increased genomic instability (Yang et al., 2006). Interestingly, *nbs1* deletion from immortalised *nbs1*$^{f/f}$ MEFs did not lead to proliferation arrest, suggesting immortalisation enables unknown factors to compensate for NBS1's essential role in cell viability (Yang et al., 2006).

The *nbs1* conditional model (*nbs1*$^{f/f}$) enables tissue-specific *nbs1* deletion, overcoming the embryonic lethality of *nbs1*$^{-/-}$ mice and enabling elucidation of NBS1 function in adult mice. T-cell specific *nbs1* ablation, using Lck-Cre, leads to lymphopenia, reduced proliferation and aberrant V(D)J recombination (Saidi et al., 2010). Similarly, Central Nervous System (CNS)-specific deletion of *nbs1* results in cerebellar loss, proliferation arrest and apoptosis; a more severe phenotype than the *atm*$^{-/-}$ mutant (Frappart et al., 2005). This suggests NBS1 has ATM independent functions. Intriguingly, co-deletion of *atm* exacerbates the phenotype, with drastically reduced survival (Dar et al., 2011), suggesting ATM has NBS1 independent functions.

1.3.2 ATMIN defines an NBS1-independent ATM signalling pathway

NBS1 is dispensable for ATM activation in response to osmotic stress (Figure 5c of Difilippantonio et al., 2005). This observation demonstrated not all ATM signalling is NBS1 dependent. Indeed, the discrepancy between the *nbs1*$^{657\Delta5}$ and *atm*$^{-/-}$ mouse phenotypes suggests NBS1-independent functions for ATM. The mechanism of NBS1-independent ATM activation was unclear, and the existence of other ATM co-factors was unknown. NBS1 interacts with ATM through a conserved PI3-K interaction motif at its C-terminus, a motif that is shared with several other PI3-K interacting proteins including ATR interacting protein (ATRIP) and Ku80 (Falck et al., 2005). This motif

was also shown to be present on the novel protein ATM-INteractor (ATMIN) (Kanu and Behrens, 2007).

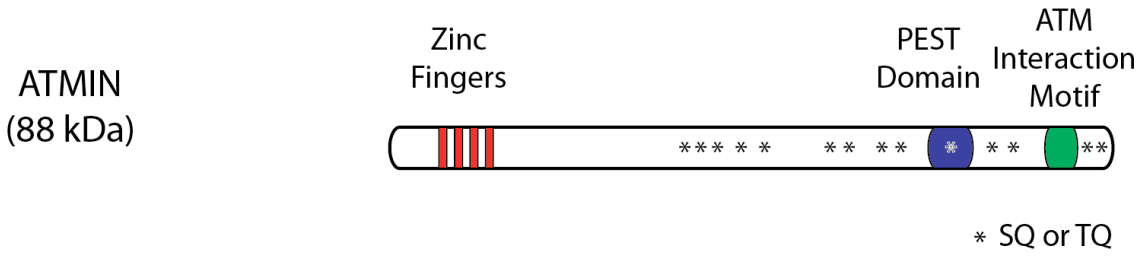

Figure 10: The novel protein ATMIN contains an ATM interaction motif

ATMIN contains four zinc fingers at its N-terminus, an extreme C-termial ATM interaction motif, and a PEST domain. Fourteen consensus ATM phosphorylation sites (SQTQ) are also present, although phosphorylation of ATMIN by ATM has not been observed.

ATMIN is a novel 823 amino acid protein located at 16q23 with a predicted molecular weight of 88.3kDa. The Behrens group were the first to identify and characterise full-length ATMIN. Previously, Heierhorst and colleagues had named ATM substrate Chk2-interacting Zn^{2+}-finger protein (ASCIZ) as a protein recruited into DNA damage foci induced by DNA methylating agents (McNees et al., 2005). ASCIZ is in fact ATMIN, but the group had not identified ATMIN's first two exons and characterised a truncated form of ATMIN lacking the first two zinc fingers. ATMIN has several domains of particular interest, including four zinc-fingers near the N-terminus, a PEST domain, several SQ consensus ATM phosphorylation motifs and a C-terminal ATM interaction motif. It is notable that despite extensive effort, and mutation of each of the SQ motifs, no phosphorylation of ATMIN by ATM has been observed (Dr Janet Cronshaw, data not shown).

The ATM interaction motif present upon ATMIN strongly suggests ATMIN and ATM interact, and indeed ATMIN co-immunoprecipitates with ATM but not the related kinase ATR. Immunofluorescence (IF) analysis demonstrated ATMIN co-localised with ATM after chloroquine and hypotonic shock treatment. Furthermore, ATMIN deficient MEFs (*atmin*$^{\Delta/\Delta}$) have normal ATM activation and substrate phosphorylation after IR, but not after hypotonic shock or replicative stress (Kanu and Behrens, 2008) .Thus, ATMIN defines an NBS1-indpedent ATM signalling pathway (Figure 11).

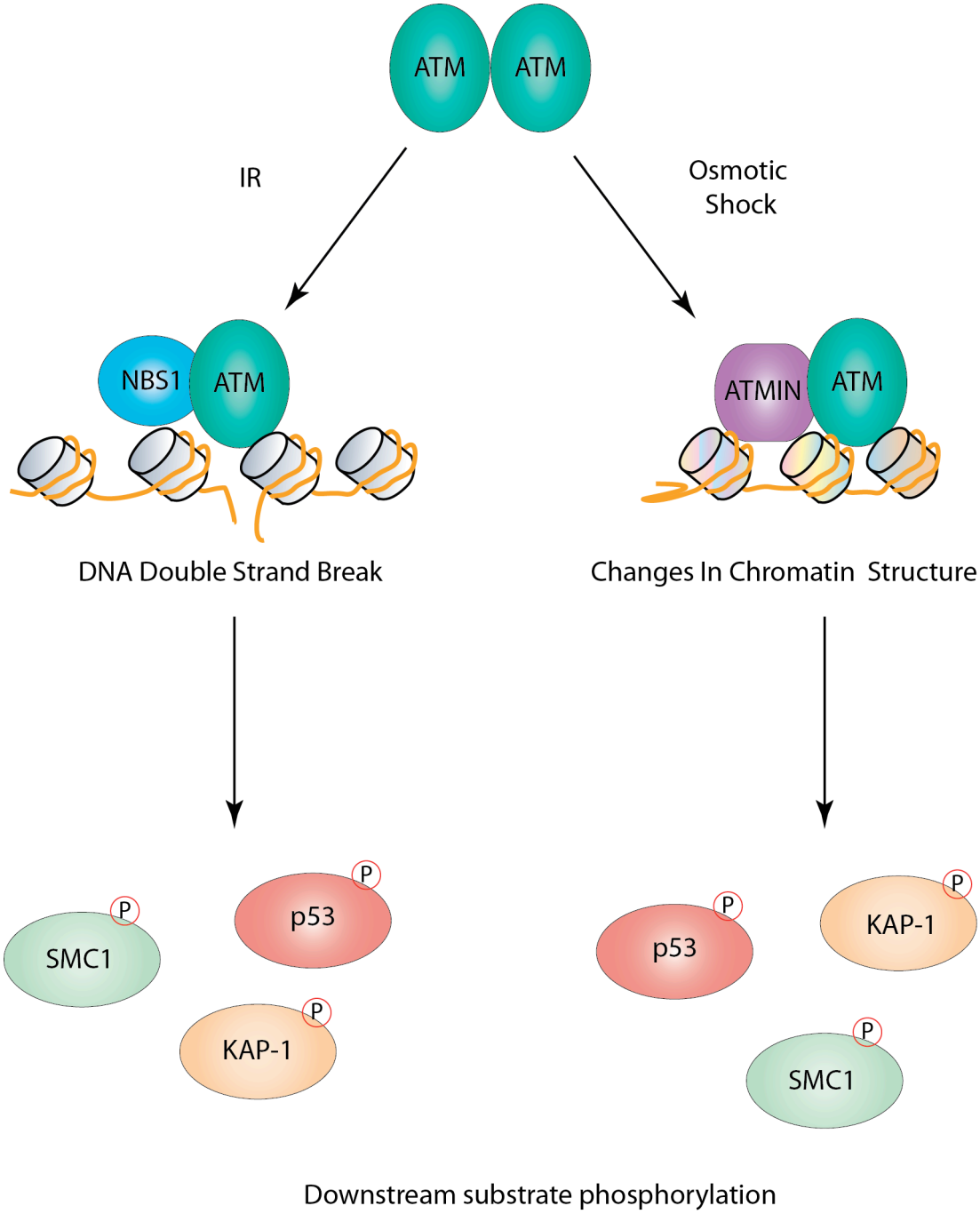

Figure 11: ATMIN defines an NBS1 independent ATM signalling pathway

In response to double strand break causing agents, such as IR, ATM associates with NBS1. However, in response to agents that cause changes in chromatin structure, such as osmotic shock, ATM interacts with its co-factor ATMIN. ATMIN is dispensable for ATM signalling after IR, and NBS1 is not required for ATM signalling after osmotic shock.

With the identification and characterisation of ATMIN, the long-standing assumption that ATM's only co-factor was NBS1 was challenged. However, the physiological relevance of ATMIN's role in ATM signalling was still unclear. Whilst the initial report of ATMIN by Kanu and Behrens clearly demonstrated a role for ATMIN in ATM activation by hypotonic shock and chloroquine, the consequences of a defective response pathway to these stimuli was unclear. To address this, a murine model for atmin loss was generated.

1.3.3 ATMIN contributes to ATM signalling in the CNS

The loss of ATMIN is embryonically lethal at approximately E16.5. Mutant embryos are characterised by exencephaly, are smaller than littermates and display organs defects, including severely impaired lung development and severe heart malformation.

Conversely, specific deletion of ATMIN in the neuronal system (*atmin*$^{\Delta N/\Delta N}$) leads to viable mice, albeit with a reduced lifespan (Kanu et al., 2010). Interestingly, the *atmin*$^{\Delta N/\Delta N}$ phenotype partially recapitulates the *atm*$^{-/-}$ mouse model, exhibiting mild neurodegeneration, and growth defects - *atmin*$^{\Delta N/\Delta N}$ mice are significantly smaller than littermate controls at birth and remain so throughout their lifespan. Moreover, ATMIN deficiency reduced the number of tyrosine positive, dopaminergic neurons, recapitulating the *atm*$^{-/-}$ phenotype. Additionally, *atmin*$^{\Delta N/\Delta N}$ mutants displayed increased levels of DNA damage in the ageing brain but reduced ATM activation. This demonstrates ATMIN dependent ATM signalling is physiologically relevant (Kanu et al., 2010).

1.3.4 ATMIN protects against B cell lymphoma

ATMIN is a tumour suppressor; B cell specific ATMIN deletion (*atmin*$^{\Delta B/\Delta B}$) results in B cell lymphoma with approximately 60% penetrance and a mean onset at 6 months (Loizou et al., 2011; see 1.5.2). As expected, the B cells from *atmin*$^{\Delta B/\Delta B}$ exhibit

severely impaired ATM signalling in response to hypotonic shock, but no reduction in IR-induced ATM signalling. SKY analysis revealed increased chromosomal translocation, including between the Myc and IgH loci (Loizou et al., 2011). Thus, it is clear that the non-canonical, ATMIN-dependent ATM signalling pathway has a physiological role in DNA damage repair and suppressing genomic instability and cancer development.

1.3.5 ATMIN is a transcriptional regulator

An intriguing twist in the ATMIN story has been the discovery that its four zinc fingers have DNA binding ability, and ATMIN is a transcriptional regulator (N. Kanu, manuscript in preparation). ATMIN is therefore a highly unusual protein in exhibiting both DNA damage response and transcriptional activity. A recent report characterised ATMIN as an activator of L8 Dynein light chain (DYNLL1) transcription (Jurado et al., 2012). Moreover, it has been shown that DYNLL1 is capable of binding ATMIN, and overexpression of Cherry-DYNLL1 impairs recruitment of ATMIN into foci in response to DNA methylating agents (Rapali et al., 2011). Although these are intriguing results, these *in vitro* studies did not address the relevance of the interaction for cell viability or DNA signalling, and it is unclear if the DYNLL1-ATMIN interaction is DNA damage dependent. Furthermore, in stark contrast to Rapali and colleagues, Jurado and colleagues do not see any impairment in ATMIN foci formation in Flag-DYNLL1 overexpressing cells upon MMS treatment. This may therefore be an artefact of protein overexpression or the tag, and not relevant at physiological ATMIN and DYNLL1 protein expression levels. More work is needed to establish if ATMIN's transcriptional activity is regulated by DNA damage.

In summary, it is clear the ATMIN dependent, non-canonical arm of ATM signalling has an important function in DNA damage signalling and cancer protection.

1.4 ATM and Oncogene-Induced-Senescence

1.4.1 Senescence is a permanent state of cell cycle arrest

Senescence was first characterised by Hayflick, who proposed non-immortalised human cells cultured *in vitro* undergo a finite number of cell divisions (Hayflick and Moorhead, 1961). When a cell exhausts its 'replicative potential' it does not enter apoptosis, but enters a long-term, stable cell cycle arrest. *In vitro*, senescent cells have a characteristic large flattened morphology. Definitive markers for senescence remain controversial, but p53, p21, Dec1, p16 and p19 are commonly upregulated in senescent cells. These markers can also be upregulated in non-senescent cells so concomitant upregulation of several markers is usually required to score a cell as senescent. One of the most widely accepted assays for senescence, despite a poor understanding of the molecular mechanism, is β-galactosidase activity at pH6.0 (Collado and Serrano, 2006). Senescence can be triggered by one of several oncogenic stimuli, including telomere shortening, DNA damage, epigenetic derepression of the INK4a/ARF locus and oncogenic stress

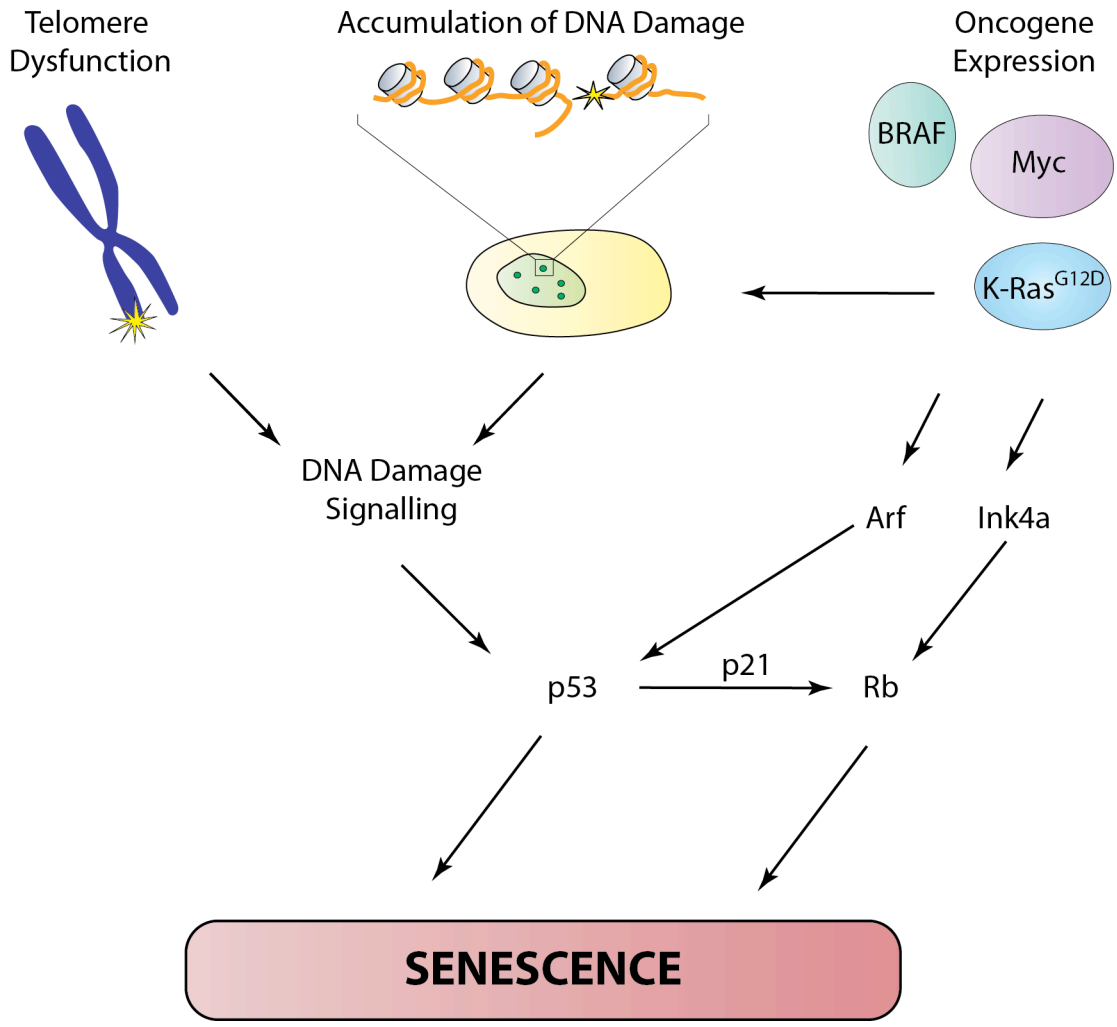

Figure 12: Multiple cellular stress signals induce senescence

Many cellular stresses activate p53 and induce senescence. There is crosstalk between senescence pathways; for example telomere dysfunction and high levels of oncogene expression promote DNA damage and can activate the ATM dependent DNA damage signalling cascade.

The tumour suppressors p53, Ink4a (p16) and Arf (p19) are key inducers of senescence. The *Ink4a/Arf* locus encodes both Ink4a and Arf (Gil and Peters, 2006). Although these two proteins share exons, their different reading frames preclude any sequence homology. Ink4a inhibits CDK4 and CDK6 promoting a G1 cell cycle arrest. Arf positively regulates p53 stability by inactivating the E3 ligase MDM2, which targets p53 for ubiquitin mediated degradation. p53 is activated by a range of stimuli, including ATM-dependent DNA damage signalling. Use of mouse models with inducible p53 expression revealed switching on p53 expression in sarcomas and liver carcinomas prompted tumour regression by senescence, involving immune cell mediated clearance

of tumour cells (Ventura et al., 2007; Xue et al., 2007). However, the regression of lymphomas following p53 expression involved widespread apoptosis rather than senescence. Thus whilst p53 is a key mediator of senescence, its activation can also lead to a variety of other outcomes.

1.4.2 Senescence is a tumour suppressive mechanism

Exciting recent advances have been made in understanding the physiological role of senescence as a stress response in ageing and cancer protection. Senescent cells can be long-lived and reside in the organism for many years, for example senescent melanocytes in moles or naevi (Michaloglou et al., 2005). Conversely, senescent cells can also be short-lived, for example phagocytes rapidly remove senescent tumour liver cells (Xue et al., 2007).

Senescence is a tumour suppressive mechanism stably blocking pre-cancerous cells in a non-proliferative state, which needs to be overcome for progression to malignancy. It was first shown by Serrano and colleagues that high levels of oncogenic $HRas^{V12}$ expression caused *in vitro* cultured cells to enter senescence (Serrano et al., 1997). Senescence as a tumour suppressive mechanism has subsequently been firmly established for a range of oncogenic stimuli and cancer types. Three seminal reports first established for a range of cancers the presence of senescent cells in pre-malignant lesions, and their absence in malignant tumours. Namely; in $KRas^{G12D}$ induced lung tumourigenesis (Collado et al., 2005); p53- dependent senescence in the early stages of a $pten^{-/-}$ prostate cancer model (Chen et al., 2005); and Su39/h1- and p53-dependent senescence in a Eμ-N-Ras lymphoma model (Braig et al., 2005). It was subsequently shown using a transgenic mouse model of doxycycline-inducible, titratable Ras expression that whilst low levels of Ras expression induced hyperplasia, high levels of Ras expression prompted Ink4a/Arf dependent senescence (Sarkisian et al., 2007). Together, these observations underpin the 'Oncogene Induced Senescence' (OIS) model - high levels of oncogenic signalling are recognised as a stress signal by the cell, prompting entry into senescence.

A pivotal role for DNA damage has since been incorporated into the OIS model. Aberrant oncogene expression causes DNA damage, for example through replication stress, in pre-malignant cells. The activated DNA damage response can signal for a cell to enter a senescence programme and acts as a barrier to tumuorigenic progression (Bartkova et al., 2005). Breaching this tumour suppressive barrier allows cells to overcome senescence and progress towards cancer. There is now much experimental evidence for OIS. Early studies used immunohistochemical staining of lung, bladder and colon cancers to demonstrate an activated DNA damage response in pre-malignant lesions, and demonstrated the presence of DNA damage by showing allelic imbalance (Bartkova et al., 2005; Gorgoulis et al., 2005). A causal link between the DNA damage response and OIS was established by the observation ablation of individual DNA damage components, such as ATM, Chk2, or p53, abrogated senescence entry and enhanced tumourigenesis in several mouse engraftment studies (Bartkova et al., 2006; Di Micco et al., 2006).

Although an important role for DNA damage signalling in OIS is well established, it does not appear to be absolutely required for senescence induction. For example, loss of the E3 ligase Skp2 in a *pten*$^{+/-}$ background resulted in p53 and Arf independent senescence and delayed tumour onset, without any observable DDR activation (Lin et al., 2010). Moreover, there is some discrepancy between the precise role ATM plays in OIS - whether it is limited to maintaining genomic stability or extends to activating senescence pathways. Bartkova and colleagues showed overexpression of mos, cdc6 or cyclin E promotes senescence in wildtype cells, but this does not occur in cells lacking functional ATM, achieved either by siATM treatment or ATM inhibitor (Bartkova et al., 2006). This suggests ATM is part of the inducible OIS barrier. Conversely, Efeyan and colleagues used *atm*$^{-/-}$ mice in a K-Ras^{G12D} model for lung adenomas, and did not observe appreciable induction of pH2AX in senescent murine lung tumours (Efeyan et al., 2009). However, as *atm*$^{-/-}$ mice succumb to T-cell lymphomas at an early age, and K-Ras^{G12D} driven lung tumours have an average onset of approximately one year, they were not able to study the effect of ATM loss on K-Ras^{G12D} driven lung adenoma. They did observed an increase in tumour grade in the lung tumours five month old of *atm*$^{-/-}$*; K-Ras*^{G12D} compared to *atm*$^{+/+}$*; K-Ras*^{G12D}. This suggests that although ATM may not

be a critical activator of p53 -mediated OIS, ATM still has a protective function in K-Ras^{G12D} driven lung adenomas.

1.4.3 Senescence and colonic serrated hyperplasia

The critical function of OIS as a tumour suppressive mechanism was recently illustrated in a model for Alternative Colorectal Tumourigenesis. This alternative 'serrated' colon cancer subtype accounts for approximately 17.5% of all proximal colonic cancers and is not thought to have APC mutations (Makinen, 2007). Although a morphologically heterogeneous group, all exhibit a serrated infolding of the neoplastic epithelium, immune cell infiltration and poor differentiation. KRas and BRAF are common activating mutations (Noffsinger, 2009). Bennecke and colleagues used intestine specific *K-Ras^{G12D}* expression as a model for serrated colonic cancers (Bennecke et al., 2010). The colons of mice expressing oncogenic *KRas^{G12D}* exhibit serrated hyperplasia, senescence and p16INK4a upregulation. However, the serrated hyperplasia did not progress to adenoma unless the senescence regulator *Ink4a/Arf* was also lost. The colons of *KRas^{G12D+};Ink4aArf$^{-/-}$* animals were characterised by invasive, metastasising carcinoma, which both molecularly and morphologically resembles human serrated tumours. Thus, the authors demonstrate the critical important of OIS in alternative colorectal tumours as a barrier to tumour progression (Bennecke et al., 2010).

1.5 ATM and B cell Maturation

1.5.1 B cell maturation requires DNA damage

In addition to ATM's role in orchestrating the cellular response to spontaneous and exogenously induced DSBs, ATM functions in the repair of programmed DSBs. Examples of programmed DBSs repaired by ATM include those induced during meiotic recombination, T and B cell maturation (Barlow et al., 1998; Xu et al., 1996). At least three different stages of B cell maturation are dependent upon DNA damage - V(D)J recombination, somatic hypermutation (SHM) and class switch recombination (CSR).

The antigen-independent somatic recombination of Variable, Diversity and Joining segments is essential for generation of antibody diversity. V(D)J recombination requires DNA DSB induction by the sequence specific Recombination Activating Gene 1 (RAG1)-2 endonuclease complex. These breaks are dependent upon the NHEJ pathway for repair; mice deficient in the NHEJ components DNA-PKcs, Ku or Ligase IV exhibit severe immunodeficiency and a block in B (and T) cell development (Bassing et al., 2002). Although not absolutely required for V(D)J recombination break repair, ATM localises to the DSB ends and facilitates repair by maintaining the DNA ends in repair complexes (Bredemeyer et al., 2006). Peripheral B cells undergo secondary V(D)J recombination, and DSBs in this process are repaired with reduced efficiency in *atm*$^{-/-}$ mice (Loizou et al., 2011).

Somatic hypermutation generates higher affinity antibodies by the induction of point mutations in the variable exons of IgH and IgL genes. Activation-induced cytidine deaminase (AID) catalyses the deamination of DNA bases in a transcription dependent mechanism introducing mutation, and hence variability, into V-region exons (Petersen-Mahrt et al., 2002). Although some initial studies suggested repair of the deaminated bases could proceed via DSB generation and repair, a plethora of more recent studies strongly suggests SHM predominantly occurs independently of the DSB repair machinery. No SHM defect is observed in *dna-pk*$^{-/-}$, *ku80*$^{-/-}$, *ku70*$^{-/-}$, *H2AX*$^{-/-}$, *53bp1*$^{-/-}$ or *atm*$^{-/-}$ mutant mice. On the contrary, the loss of the Base Excision Repair (BER) protein uracil-DNA glycosylase (UNG) or the MMR proteins mutS homologue 2 (MSH2), exonuclease I (Exo1) and mutL homologue 1 (MLH1) all lead to an impairment in SHM (Chaudhuri and Alt, 2004). Therefore whilst SHM harnesses the DNA damage machinery, it does not depend upon programmed induction and repair of DNA DSBs or ATM function.

Thirdly, AID is also involved in CSR which somatically recombines the constant regions of IgH for IgG, IgA, IgM or IgE (Figure 13). This allows specialised of a variable, antigen binding region for a range of functions (Chaudhuri and Alt, 2004). For

example, IgA is secreted in saliva and breast-milk, whereas IgM is expressed on the surface of mature B cells.

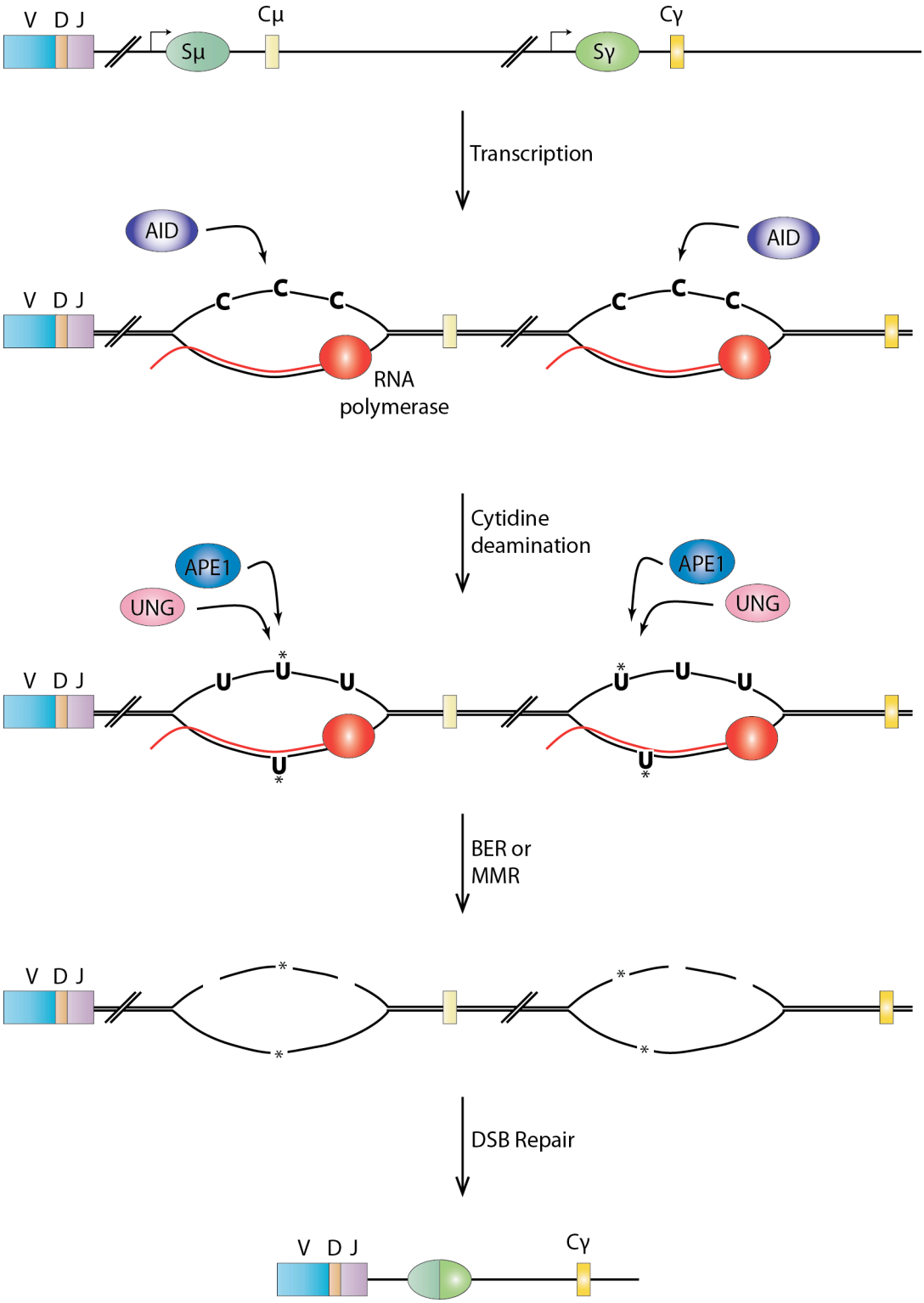

Figure 13: Class Switch Recombination of immunoglobin heavy chains

Transcription of switch regions generates single strand DNA substrates for the single-strand cytidine deaminase AID. The deoxyuridine bases created by AID are removed by

UNG1 to leave abasic sites. The endonuclease APE1 cleaves the phosphodiester backbone at abasic sites, introducing a nick into the DNA strand. The close proximity of nicks on both strands can generate a DSB. The DSB termini are synapsed by ATM and 53BP1, and the ligation of two S regions by the NHEJ pathway completes CSR. AID, activation-induced cytidine deaminase; UNG, uracil-DNA glycosylase; APE1 apurinic/apyrimidinic endonuclease 1.

1.5.2 ATM is required for efficient class switch recombination

The important role of ATM in CSR is illustrated by the observation *atm*$^{-/-}$ B cells have a 70-80% reduction in CSR efficiency (Lumsden et al., 2004). Moreover, *atm*$^{-/-}$ B cells exhibit genomic instability, including on chromosome 12 which harbours the IgH locus (Callen et al., 2007). These defects manifest as a mild impairment in progression from the pro-B to pro-B stages of B cell development, but it should be noted that *atm*$^{-/-}$ mice have normal numbers of mature, re-circulating B cells (Xu et al., 1996).

The B cell specific deletion of nbs1 (*nbs1*$^{\Delta B/\Delta B}$) leads to approximately a 50% reduction in CSR efficiency (Reina-San-Martin et al., 2005), compared to the *atm*$^{-/-}$ reduction of 70-80%. Moreover *nbs1*$^{\Delta B/\Delta B}$ do not develop B cell lymphoma, and the humanised NBS1 mouse model (*nbs1*$^{657\Delta 5}$) only develops B cell lymphoma upon co-deletion of p53 (Difilippantonio et al., 2005). Although *atm*$^{-/-}$ mice do not commonly develop B cell lymphoma, this could be because they succumb at a young age to T-cell lymphoma and therefore they do not live along enough for B cell lymphoma to develop. In a mouse knock-in model for a nine base-pair truncation mutation commonly found in A-T patients, which produces near-full length but kinase-inactive ATM (*atm*^{7636del9}), some mice developed B cell lymphoma (Spring et al., 2001). The reduced penetrance of T-cell lymphoma in *atm*^{7636del9} mice presumably permitted the necessary time for the genomic instability resulting from ATM truncation to gain the additional mutation hits required for B cell lymphoma to develop. Given the firmly established importance of the ATM co-factor NBS1 for ATM function in DSB repair, a long-standing conundrum is the discrepancy between the phenotypes of *atm* and *nbs1* deficient B cells.

In contrast to *nbs1*$^{\Delta B/\Delta B}$ mice, B cell specific deletion of ATMIN (*atmin*$^{\Delta B/\Delta B}$) leads to B cell lymphoma with approximately 60% penetrance and a mean onset age of six months

(Loizou et al., 2011). Analysis of the tumours from these mice revealed genomic instability in the B cells, including on chromosome 12, which contains the IgH locus. Loss of ATMIN also re-capitulates the reduction in the pre-B population, and normal numbers of re-circulating B cells, observed in the *atm*$^{-/-}$ mutant (Loizou et al., 2011). Akin to ATM loss, *atmin*$^{\Delta B/\Delta B}$ mice do not demonstrate an impairment in somatic hypermutation, but have a reduced efficiency in repair of the DBSs induced in peripheral B cells undergoing secondary V(D)J recombination. They have approximately a 50% reduction in CSR efficiency, and reduced co-localisation of pS1987-ATM to pH2AX sites in cells undergoing CSR (Loizou et al., 2011). ATMIN deficient chicken DT40 B lymphocytes exhibit increased rates of Ig gene conversion. Neither hypermutation nor DSB repair efficiency was affected, indicating ATMIN does not directly control the formation of abasic sites or HR (Oka et al., 2008). Taken together with observations of the *nbs1*$^{\Delta B/\Delta B}$ mutant, this suggests both canonical NBS1-dependent and non-canonical ATMIN-dependent ATM signalling is required for efficient CSR and maintenance of genomic stability in B cells.

1.6 Telomeres and the DNA Damage Response

The terminal ends of eukaryotic chromosomes pose three distinct problems to the cell. Firstly, naked chromosome ends resemble a double strand break. Left unprotected, they are recognised as HR or NHEJ substrates and deleterious chromosome fusion occurs (Figure 14). Secondly, DNA replication during S phase is unable to copy the terminal ends of a chromosome by lagging-strand synthesis, so with each round of replication terminal nucleotides are lost. Unless these are filled in, genetic information will be eroded with each successive cell division. Thirdly, the terminal ends of chromosomes are fragile sites, and as such are susceptible to replication stress. Given these facets, it is unsurprising that the eukaryotic cell has evolved highly conserved solutions to the 'chromosome end problem'.

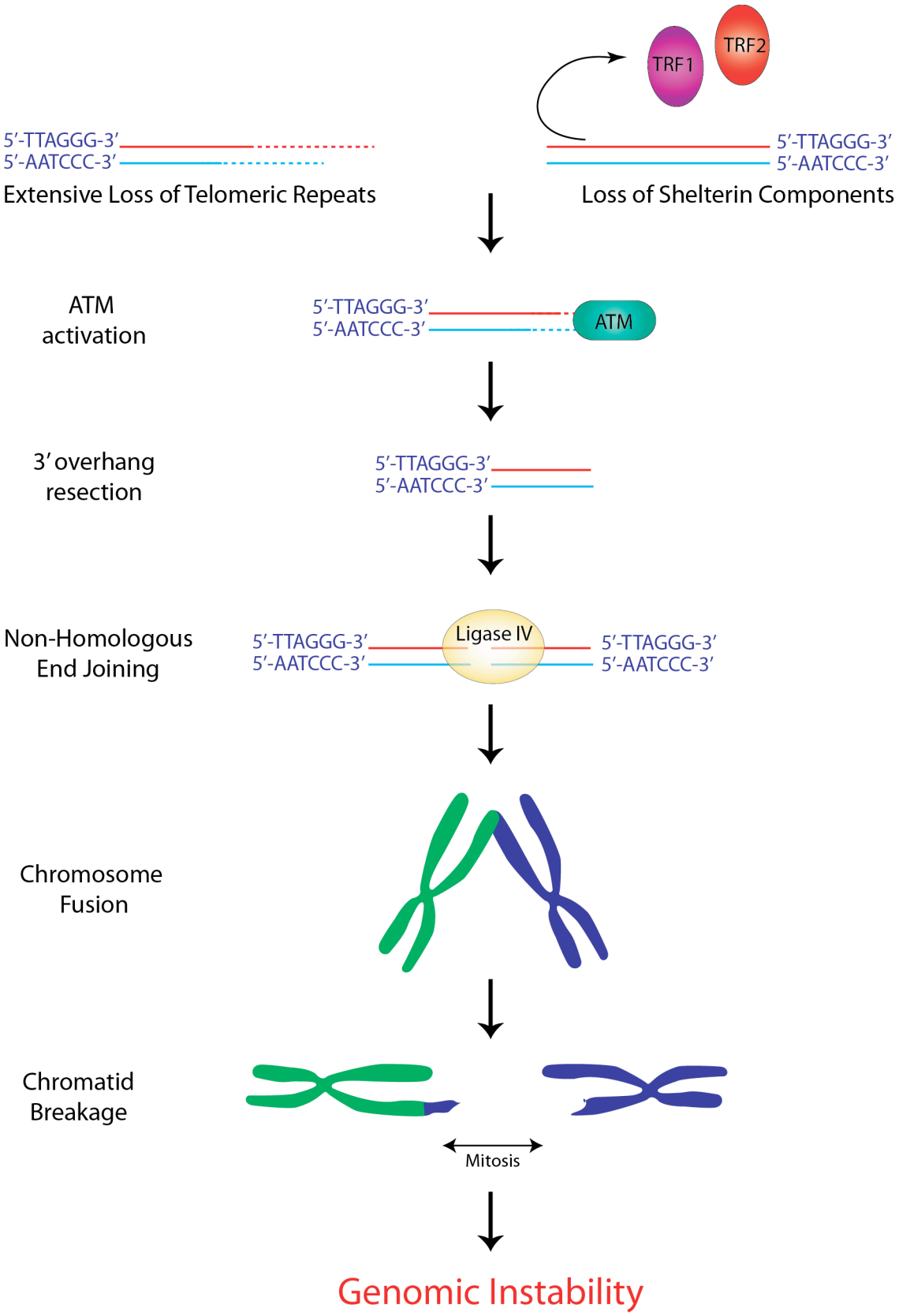

Figure 14: Telomere dysfunction can lead to genomic instability

Telomere dysfunction, arising either from critically short telomeres or loss of the shelterin complex, activates and recruits ATM. The NHEJ pathway can recruit DNA Ligase IV to join the ends of two different chromosomes, shown here in blue and green. Chromatid breakage can occur during mitosis and the unequal distribution of genetic material leads to chromosome translocations. The fusion-breakage-fusion cycle can continue though the subsequent cell divisions, leading to increasing genomic instability.

1.6.1 The end-protection problem

In human cells chromosome ends comprise of 9-15kB of the telomeric repeat TTAGGG. In mice these repeats - the telomeres - can extend as long as 100kB. Regardless of telomeres length, the distal end of an undamaged telomere is distinguished by the 'G-tail', a single stranded 3' overhang of 50-300 bases. Its name arises as it is presumed to arise by post-replicative 5'-3' exonuclease resection of the C-rich strand, leaving the G-rich 'TTAGGG' repeats of the 3' strand (Makarov et al., 1997). However, the extensive single-strand overhang, if not camouflaged in some way, is a substrate for HR. The highly repetitive sequence enables the G-tail to invade into the double-strand TTAGGG repeats and complementary base pair with bind the 3'-5' strand, forming the Telomeric Loop, or T-loop (Griffith et al., 1999)(Figure 15). This protective structure sequesters the single strand overhang so that the telomere no longer resembles a double strand break, and is therefore not recognised by ATM and the cellular DNA damage machinery.

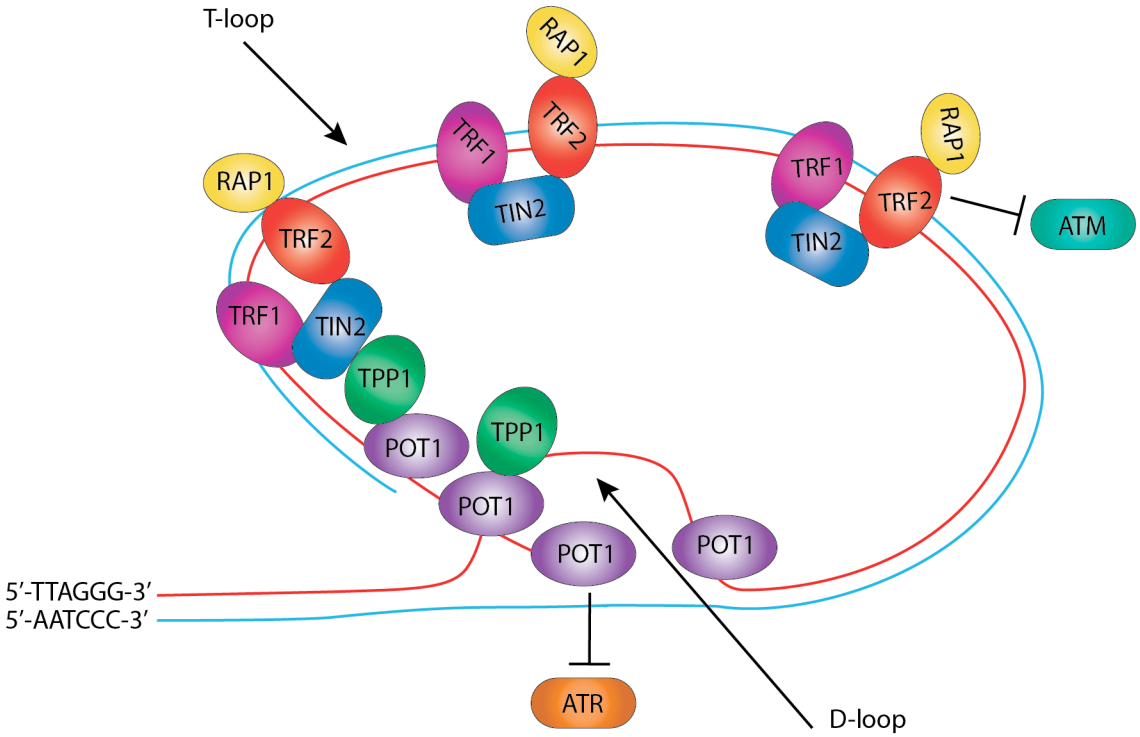

Figure 15: The Structure of Telomeres and the Shelterin Complex

Schematic representation of the T-loop and D-loop conformations adopted by telomeric DNA. The interactions of shelterin complex, consisting of TRF1, TRF2, POT1, TIN2 and TPP1, with each other and with the telomeric DNA are depicted. The inhibition of ATM and ATR by TRF2 and POT1 respectively is indicated.

As well as the T-loop, end-protection is also conferred by six proteins collectively termed the 'Shelterin Complex', which constitutively bind the telomere (Figure 15). Telomeric Repeat-Binding Factor 1 (TRF1) was identified based on its ability to bind TTAGGG repeats (Chong et al., 1995), and Telomeric Repeat Binding-Factor 2 (TRF2) as a TRF1 paralogue (Broccoli et al., 1997; Bilaud et al., 1997). Both contain SANT/Myb domains with very high specificity for the double-stranded TTAGGG telomeric repeats (Bianchi et al., 1999; Hanaoka et al., 2005). In complement to this, Protector of Telomeres 1 (POT1) binds the single stranded telomeric repeats of the G-tail overhang (Baumann and Cech, 2001). POT1-and TIN2-interacting protein (TPP1) was discovered as a POT1 interacting protein by IP-Mass Spectrometry (Liu et al., 2004). TRF1-Interacting Nuclear protein 2 (TIN2) and Repressor and Activator Protein 1 (RAP1) were first identified in yeast-two-hybrid screens for TRF1 and TRF2,

respectively (Kim et al., 1999; Li et al., 2000a). Neither TIN2 nor TPP1 directly bind DNA. TIN2 bridges TRF1 and TRF2, and TTP1 bridges POT1 and TIN2.

The affinity of some shelterin components for telomeric repeats, and others for bridging shelterin proteins, confers the shelterin complex with an exquisite selectivity for telomeres. It is critically important shelterin only localises to the telomere, as its binding to double strand breaks would inhibit DNA repair. Several independent mass spectrometry studies for shelterin interacting proteins have yielded no new members of the shelterin complex, suggesting these six factors may represent a complete picture of the shelterin complex (O'Connor et al., 2004), (Liu et al., 2004), (Ye et al., 2004). Of course, many other proteins have been identified as interacting with shelterin or the telomere, but none that are considered part of the core protective complex (Dejardin and Kingston, 2009).

Shelterin protects telomeres in part by shaping telomere structure. Firstly, shelterin aids T-loop formation, by harnessing TRF1 and TRF2's DNA remodelling activities (Griffith et al., 1998; Stansel et al., 2001). Secondly, POT1 is required for control of telomere termini. POT1 loss leads to shorter 3' overhangs and a loss of sequence specificity at the 5'end (Hockemeyer et al., 2005). Thirdly, shelterin is proposed to be a negative regulator of the enzyme telomerase, and therefore negatively regulates telomere length. POT1's single-strand DNA binding domain is required for telomerase inhibition, supporting a model whereby shelterin binding blocks telomerase from accessing the telomere (Loayza and De Lange, 2003). It is thought the binding of shelterin to telomeres is roughly proportional to telomere length. Thus shorter telomeres have fewer shelterin complexes bound, stochastically reducing inhibition of telomerase binding and increasing the propensity for telomere extension.

1.6.2 The end-replication problem

The solution to the 'end-replication problem', telomerase, was first identified by Carol Greider and Elizabeth Blackburn in *tetrahymena thermophile* (Greider and Blackburn, 1985, 1987, 1989). A unique reverse transcriptase, telomerase synthesises telomeres.

Telomerase comprises of a protein catalytic component, Tert, and an integral RNA subunit, Terc. Telomerase is a highly processive enzyme capable of adding hundreds of nucleotides to one DNA primer. The RNA Terc component recognises and binds the telomeric repeats and serves as a template for the reverse transcriptase domain of Tert. Loss of either component abolishes the enzyme's activity. Although *in vitro* reconstitution of these two subunits is sufficient for telomerase activity (Weinrich et al., 1997), several other proteins associate with the core enzyme, together termed the holoenzyme. Dyskerin binds Tert, and is believed to function as a crucial scaffold protein (Mitchell et al., 1999a). Patients with mutations in dyskerin suffer from dyskeratosis congenital and exhibit shorter telomeres and lower levels of Tert protein (Mitchell et al., 1999b). The ATPases pontin and reptin interact with Tert and dyskerin, particularly in S-phase, and their ablation impairs telomerase assembly (Venteicher et al., 2008). It is likely our picture of all proteins associated with Terc and Tert is far from complete.

In humans telomerase is normally only active in stem and progenitor cells - and is also commonly re-activated in cancer cells (Meyerson et al., 1997; Wright et al., 1996). A second, telomerase-independent, mechanism for telomere maintenance is Alternative Lengthening of Telomeres (ALT). This mechanism is observed principally in cancer cells and allows cells to maintain telomere length, and hence overcome the proliferation arrest induced by critically short telomeres, without reactivating telomerase expression. Although some mechanistic details are still to be elucidated, ALT does depend on homologous recombination. It is thought the recombination template for ALT may be either sister chromatids or C-circles - partially single stranded, circular C-rich extrachromosomal DNA comprising of telomeric repeats (Henson et al., 2009). Regardless of the precise molecular mechanism, it is clear ALT requires a range of DNA damage proteins, including Mre11, NBS1, Rad50 and FANCD2 (Jiang et al., 2005), (Fan et al., 2009). Experimental support that this mechanism only occurs in transformed cells is the observation fusion of an ATL cell with a non-transformed cells inhibits ATL activity, indicating 'normal' cells must have a molecular mechanism to suppress ATL (Perrem et al., 1999). Although many open questions remain, the

existence of a second mechanism for telomere lengthening in cancer cells underscores the fundamental importance of maintaining telomere length to every proliferative cell.

Several murine models for telomere dysfunction have been generated, including the *terc* and *tert* null strains. Terc deficient mice, *terc*$^{-/-}$, are characterised by premature ageing, shorter telomeres and genomic instability. However, as mice telomeres are up to 100kB long it takes several generations of null mice to produce mice with sufficiently short telomeres to manifest a strong phenotype. First generation *terc*$^{-/-}$ offspring are largely normal, whereas the phenotype becomes increasingly severe from the third generation onwards (Rudolph et al., 1999). Akin to this, mice lacking the reverse transcriptase component of telomerase, *mTert*$^{-/-}$, also display increasing genomic instability and shorter telomere length as homozygous null generation number increases (Erdmann et al., 2004).

Whilst it is evident from these studies in telomere deficient mice that critically short telomeres can induce proliferation arrest and senescence, it is unclear what length of telomeric repeats is considered 'critically short' by the cell. In yeast, a cell containing a telomere bereft of all telomeric repeats can still undergo several divisions before entering proliferation arrest (Abdallah et al., 2009). Thus in yeast telomere length is not a simple, immediate determinant of proliferative potential. The situation in mammals is increasingly complex. Primary cells cultured at atmospheric oxygen conditions, such as MEFs, tend to enter senescence within 6-10 population doublings; at which time their telomeres are still substantial in length. Thus telomeric length cannot be the sole determinant of replicative potential. TRF2 overexpression in human fibroblasts reduced average telomere length at senescence onset from 7 to 4kB and repressed chromosome fusions (Karlseder et al., 2002), suggesting the protected status of telomeres, and not just telomere length, affects senescence onset. A range of damage signals - such as short telomere length, DNA damage accumulation, oxidative stress and protein damage - contribute to activation of the senescence programme. The shorter the telomere the greater the damage signal, and so fewer additional stress signals are required from other components to exceed the 'critical' damage level and enter senescence. This model suggests a precise telomere length cannot be defined as 'critically short', but rather

telomere length as an indicator of proliferative potential must be viewed in the context of other cellular damage signalling.

1.6.3 Telomere dysfunction and the DNA damage response

Unprotected, damaged or critically short telomeres are recognised by the cellular DNA damage machinery. Acute deletion of *trf2* from *p53*$^{-/-}$ MEFs demonstrated the NHEJ pathway processes unprotected telomeres and widespread interchromosomal fusion ensues (Celli and de Lange, 2005). Interestingly, the concomitant deletion of DNA Ligase IV, which ablates the processing necessary for NHEJ, does not inhibit ATM activation and signalling at these deprotected telomeres - pS1987-ATM, 53BP1 and pH2AX foci all still form (Celli and de Lange, 2005). Therefore no overt processing of damaged telomeres is required for ATM signalling. Moreover, the molecular role of individual DNA damage components is starting to become clear. For example, 53BP1 binding to deprotected telomeres in *trf2*$^{-/-}$ MEFs increased chromatin motility and was required for efficient NHEJ (Dimitrova et al., 2008). The 53BP1- and ATM- dependent increase in telomere mobility presumably facilitates NHEJ between distant sites.

The 3' overhang sequestration in T-loops and masking of the telomeric repeats by shelterin binding are only part of the reason telomeres are not recognised by the DNA damage machinery. Experiments in combinations of ATM, TRF2, POT1 and ATR compound mutant cells demonstrated that TRF2 specifically inhibits ATM, whereas POT1 specifically inhibits ATR (Denchi and de Lange, 2007). TRF2 directly binds to a region of ATM encompassing the Ser1981 autophosphorylation site and inhibits ATM activation (Karlseder et al., 2004). As TRF2 is specifically localised to telomeres, this achieves the specific inhibition of ATM at telomeric repeats without compromising ATM's ability to respond to DNA damage elsewhere on the chromosome.

As one of the major functions of the telomere and shelterin complex is to prevent recognition by the DNA damage response, it was surprising and somewhat counter-intuitive to discover many DNA damage proteins localise to the telomere. The MRN complex localises to the telomere via its interaction with TRF2; and NBS1 was shown

to localise to telomeres specifically in S-phase (Zhu et al., 2000). Conversely, TRF2 does not localise to irradiation induced DNA repair foci. ATM and ATR also localise to the undamaged telomeres in G2 of the cell cycle (Verdun et al., 2005). DNA damage response proteins have been proposed to be important for telomere maintenance. The MRN complex promotes 5' end resection of newly-replicated telomeres, generating incompatible 3' overhangs which are readily bound by POT1 and hence blocking potential NHEJ mediated fusion (Deng et al., 2009).

Further support that components of the DNA damage machinery have essential roles in telomere maintenance comes from the observation cells derived from A-T or NBS patients experience accelerated telomere shortening (Vaziri et al., 1997; Ranganathan et al., 2001). Moreover, compound mutant *atm*$^{-/-}$ *terc*$^{-/-}$ late generation mice exhibit increased telomere shortening, reduced stem cell compartments and increased genomic instability compared to the single *terc*$^{-/-}$ mutant. Remarkably, intestine-specific deletion of p53 in G4 *terc*$^{-/-}$ mice reduced lifespan, despite partial restoration of the intestinal stem cell pool (Begus-Nahrmann et al., 2009). Thus accumulation of stem cells with critically short telomeres is ultimately deleterious to the organism, highlighting the importance of telomere maintenance to viability.

Together, these observations suggest a complex interplay between telomeres and the DNA damage response machinery. On the one hand, telomeres must be shielded from recognition by DNA damage factors to avoid end-to-end chromosome fusions. But, unexpectedly, telomeres also require the DNA damage machinery for efficient replication and end processing.

1.6.4 The telomere replication problem

An exciting recent discovery is telomeres are genomic fragile sites. Deletion of *trf1* from MEFs led to increased replication fork stalling upon telomeric repeats, with subsequent ATR activation and a fragile-site phenotype in metaphase. TRF1 recruits the helicases BLM and RTEL, presumably to resolve higher order DNA structures which cause DNA polymerase to stall (Sfeir et al., 2009). In agreement with this, G3 *terc*$^{-/-}$

ATR$^{S/S}$ (ATR deficient Seckel mouse) display increased telomere fusions, recombination, and shorter telomeres, suggesting ATR suppresses telomere fragility and recombination (McNees et al., 2010). Moreover, the homologous recombination protein BRCA2 localises to the telomere during G2/S, and its deletion results in telomere shortening and increased pH2AX foci at telomeres (Badie et al., 2010). Paradoxically, it appears the DNA damage response protein BRCA2 is required for efficient telomere replication, and its loss leads to DNA damage and activation of the DNA damage response. This recent trio of papers underscores the dual nature of the DNA damage machinery at the telomere - the telomere needs the specialised proteins of the DNA damage response for efficient replication, but also must be protected from recognition as a double-strand break by the DNA damage response.

Two recent papers suggest a novel role for telomeres as 'genotoxic stress sensors' (Fumagalli et al., 2012; Hewitt et al., 2012). Both papers induced DNA damage by H_20_2, NCS or IR, and observed the persistence of long-lived DNA damage foci at telomeres. Fumagalli and colleagues then demonstrated telomeric proteins confer telomeres with resistance to repair. Neither an endonuclease induced DSB next to telomeric repeats nor a DSB adjacent to tethered TRF2 was repaired. These studies demonstrate the persistence of DNA damage markers at telomeres in murine and primate cells, irrespective of telomere length. This raises the intriguing possibility telomeres act as 'genotoxic' sensors and persistent DNA damage at telomeres can instigate senescence. However, it has not yet been demonstrated that DNA damage at the telomeres of non-proliferating, terminally differentiated cells prompts entry into senescence.

1.7 Aims of the thesis

The ATM interacting protein ATMIN is required for ATM signalling in response to agents that induce changes in chromatin structure, but is dispensable for ATM signalling after double strand breaks. However, the physiological relevance of this non-canonical ATM signalling pathway was unclear. The first aim of my thesis was to characterise physiological functions for ATMIN. To this end, I analysed ATMIN function in a range of murine models; including B cell lymphoma, the developing

embryo, oncogene-induced-senescence in intestinal tumourigenesis, and telomere dysfunction in the ageing brain.

ATM signalling proceeds via ATMIN or NBS1 in a stimulus dependent manner. The mechanism of ATM co-factor choice was enigmatic. The second aim of my thesis was to investigate the mechanism and consequence of ATM co-factor choice. To achieve this I examined NBS1- and ATMIN- dependent ATM signalling in both the adult intestine and MEFs.

Moreover, we were also interested to identify novel ATM regulatory proteins. The third aim of my thesis was to identify and characterise novel regulators of ATM signalling. Thus, I performed an shRNA based screen for proteins that regulate ATM signalling, from which DMAP1 was the most interesting candidate. DMAP1's role in the DNA damage response was characterised.

Chapter 2. Materials and Methods

2.1 Materials

2.1.1 Reagents and Consumables

The consumables and reagents used in the course of this study were purchased from the companies listed or the Cancer Research-UK London Research Institute (LRI) Central Services:

0.5 ml, 1.5 ml, 2 ml tubes	Eppendorf (Cambridge, UK)
100bp DNA ladder	Life Technologies (NY, USA)
1 kb DNA ladder	Life Technologies (NY, USA)
1 ml, 5 ml, 50 ml syringes	BD Plastipak (Oxford, UK)
5 ml, 10 ml, 25 ml serological pipettes	Corning (Corning, USA)
15 ml, 50 ml tubes	Corning (Corning, USA)
18G, 19G needles	BD Microlance (Oxford, UK)
6 cm diameter dishes (adherent cells)	Corning (Corning, USA)
10 cm diameter dishes (adherent cells)	Corning (Corning, USA)
25 cm^2 flasks (adherent cells)	Corning (Corning, USA)
75 cm^2 flasks (adherent cells)	Corning (Corning, USA)
150 cm^2 flasks (adherent cells)	Corning (Corning, USA)
25 cm^2 flasks (suspension culture)	Sarstedt (Leicester, UK)
75 cm^2 flasks (suspension culture)	Greiner bio-one (Stonehouse, UK)
6-well plate (flat bottom)	BD Falcon (Oxford, UK)
24-well plate (flat bottom)	BD Falcon (Oxford, UK)
96-well plate (flat bottom)	BD Falcon (Oxford, UK)
96-well plate (non-sterile)	Nunc (Rochester, USA)
Acetic acid	Fisher Scientific (Loughborough, UK)
Adenovirus	Gene Transfer Vector Core (Iowa USA)
Agarose	Bioline (London, UK)
Ammonium chloride	LRI/CR-UK (London, UK)
Ammonium persulfate	Sigma-Aldrich (Poole, UK)

Ampicillin	Sigma-Aldrich (Poole, UK)
Aphidicolin	Sigma-Aldrich (Poole, UK)
ATM inhibitor	Calbiochem (Darmstadt, Germany)
B27 Supplement	Life Technologies (NY, USA)
Bleomycin	Sigma-Aldrich (Poole, UK)
Bovine serum albumin	Sigma-Aldrich (Poole, UK)
BrdU	Sigma-Aldrich (Poole, UK)
Calcium Phosphate Transfection Kit	Promega (Southampton, UK)
Cell strainer (45 µm Nylon)	BD Falcon (Oxford, UK)
Chromatography paper (3 mm)	Whatman (Brentford, UK)
Calf Intestinal Phosphatase (CIP)	New England Biolabs (NEB, Hitchin, UK)
Colcemid	Sigma-Aldrich (Poole, UK)
Coverslips	Menzel-Glaeser (Braunschweig, Germany)
Cuvettes	Fisher Scientific (Loughborough, UK)
DAPI	Sigma-Aldrich (Poole, UK)
ddH_2O	LRI/CR-UK (London, UK)
DirectPCR Lysis Reagent	Viagen Biotech (Los Angeles, USA)
Disodium tetraborate	AppliChem (Darmstadt, Germany)
DMEM	Life Technologies (NY, USA)
DMSO	Sigma-Aldrich (Poole, UK)
DTT	Sigma-Aldrich (Poole, UK)
DyeEx® 2.0 Spin Kit	QIAGEN (Crawley, UK)
Dynabeads M-280 Streptavidi	Life Technologies (NY, USA)
ECL Western Blotting Detection Reagents	GE Healthcare (Little Chalfont, UK)
EDTA	Sigma-Aldrich (Poole, UK)
EGF (human)	PeproTech (London, UK)
EGTA	Sigma-Aldrich (Poole, UK)
Ethanol	Fisher Scientific (Loughborough, UK)
Ethidium Bromide	Sigma-Aldrich (Poole, UK)
FACS tubes	Becton Dickinson (Oxford, UK)
FGF-basic (human)	PeproTech (London, UK)
Fluorescent Mounting Medium	DAKO (Ely, UK)

Foetal calf serum (FCS)	PAA (Yeovil, UK)
GoTaq PCR DNA Polymerase	Promega (Southampton, UK)
Glycerol	Sigma-Aldrich (Poole, UK)
Glycine	Sigma-Aldrich (Poole, UK)
Harris`s haematoxylin	LRI/CR-UK (London, UK)
HAT Assay Kit (Colourimetric)	Abcam (Cambridge, UK)
Hydrochloric acid	Fisher Scientific (Loughborough, UK)
Hydrogen peroxide	Sigma-Aldrich (Poole, UK)
Isopropanol	Fisher Scientific (Loughborough, UK)
Illustra™ GFX™ DNA Purification Kit	GE Healthcare (Little Chalfont, UK)
Industrial methylated spirit (IMS)	LRI/CR-UK (London, UK)
Kanamycin	Sigma-Aldrich (Poole, UK)
L-Glutamine	Life Technologies (NY, USA)
L-Glycine	Sigma-Aldrich (Poole, UK)
LB medium	LRI/CR-UK (London, UK)
Liopfectamine-2000	Life Technologies (NY, USA)
Marvel skimmed milk powder	A1 Laboratory Supplies Ltd (Enfield, UK)
Mayer`s haematoxylin	LRI/CR-UK (London, UK)
Magnesium Chloride	LRI/CR-UK (London, UK)
β-mercaptoethanol	Sigma-Aldrich (Poole, UK)
Methanol	Fisher Scientific (Loughborough, UK)
Microscope slides	Menzel-Glaeser (Braunschweig, Germany)
N-2 supplement	Life Technologies (NY, USA)
Neurobasal Medium	Life Technologies (NY, USA)
NeuroCult® Differentiation Supplement	StemCell Technologies (London, UK)
Neutral buffered formalin (NBF)	LRI/CR-UK (London, UK)
NEN blocking reagent	PerkinElmer (MA, USA)
Nuclear fast red	Vector Laboratories (Peterborough, UK)
Ponceau S	Sigma-Aldrich (Poole, UK)
Paraffin wax	Tissue Tek (Basingstoke, UK)
Paraformaldehyde	Sigma-Aldrich (Poole, UK)
PBS	Life Technologies (NY, USA)

Penicillin/Streptomycin	Life Technologies (NY, USA)
Phenylmethylsulfonyl fluoride (PMSF)	Sigma-Aldrich (Poole, UK)
Propium Iodide	Sigma-Aldrich (Poole, UK)
Protogel (30%)	National Diagnostics (Hessle, UK)
Poly-L-ornithine	Sigma-Aldrich (Poole, UK)
PNA probe Alexa 488–OO-$(CCCTAA)_3$	Panagene (South Korea)
Protease Inhibitor	Sigma-Aldrich (Poole, UK)
Protein A-Sepharose	Sigma-Aldrich (Poole, UK)
Protein-G Sepharose	Sigma-Aldrich (Poole, UK)
Proteinase K	Melford Laboratories (Ipswich, UK)
Protein Assay Dye Reagent	Bio-Rad (Hemel Hempstead, UK)
Opti-MEM	Life Technologies (NY, USA)
QIAGEN Plasmid Maxi Kit	QIAGEN (Crawley, UK)
QIAprep Spin Miniprep Kit	QIAGEN (Crawley, UK)
Rainbow markers	GE Healthcare (Little Chalfont, UK)
Restriction endonucleases	New England Biolabs (NEB, Hitchin, UK)
Ribonuclease	Sigma-Aldrich (Poole, UK)
RIPA buffer	New England Biolabs (NEB, Hitchin, UK)
RNase-Free DNase Set	QIAGEN (Crawley, UK
RNeasy Mini-kit	QIAGEN (Crawley, UK)
Senescence Histochemical Staining Kit	Sigma-Aldrich (Poole, UK)
Sodium Acetate	Sigma-Aldrich (Poole, UK)
Sodium Azide	Sigma-Aldrich (Poole, UK)
Sodium Chloride	LRI/CR-UK (London, UK)
Sodium Dodecyl Sulphate	Sigma-Aldrich (Poole, UK)
Sodium Fluoride	Sigma-Aldrich (Poole, UK)
Sodium Orthovanadate	New England Biolabs (NEB, Hitchin, UK)
Superscript III cDNA synthesis kit	Life Technologies (NY, USA)
SYBR Green	Life Technologies (NY, USA)
T4 DNA ligase	New England Biolabs (NEB, Hitchin, UK)
Taq PCR Core Kit	Qiagen (Crawley, UK)
TEMED	Sigma-Aldrich (Poole, UK)

Tetracycline	Sigma-Aldrich (Poole, UK)
Trichostatin A (TSA)	Sigma-Aldrich (Poole, UK)
Tris	Sigma-Aldrich (Poole, UK)
Trisodium Citrate	Sigma-Aldrich (Poole, UK)
Triton X-100	Sigma-Aldrich (Poole, UK)
Trypan Blue	Sigma-Aldrich (Poole, UK)
Trypsin	Life Technologies (NY, USA)
Vi-Cell™ sample vial	Beckman Coulter (High Wycombe, UK)
X-ray film, Fuji	Fisher Scientific (Loughborough, UK)

2.1.2 Media and Buffers

Antibody Dilution Buffer (IF-FISH)

Tris (pH 7.5)	20 mM
BSA,	2% (w/v)
Fish Gelatin	0.2% (v/v)
NaCl	150 mM
Triton X-100	0.1% (v/v)
Sodium Azide	0.1% (w/v)

ATM Lysis Buffer	final concentration.:
HEPES (pH 7.4)	20 mM
NaCl	150 mM
Tween 20	0.2%
$MgCl_2$	1.5 mM
EGTA	1 mM
supplemented with:	
DTT	2 mM
NaF	50 mM
PMSF	1 mM
Na_3VO_4	1 mM
Complete Protease Inhibitor Cocktail	1%

Base Buffer

HEPES (pH 7.4)	10 mM
NaCl	50 mM
$MgCl_2$	10 mM
supplemented with:	
DTT	1 mM
NaF	50 mM
PMSF	1 mM
Na_3VO_4	1 mM
Complete Protease Inhibitor Cocktail	1%

Blocking buffer (*in situ* hybridisation)

Blocking Reagent (Roche)	10%
Maleic Acid Buffer	90%

Blocking Buffer (Immunofluorescence)	final concentration:
FCS	10%
Triton X-100	0.1%
PBS	89.9%

Blocking Buffer (Immunohistochemistry)	final concentration
Goat Serum	10%
BSA	1%
PBS	89%

Citrate Buffer

Trisodium citrate	2.94 g
HCl (0.2 M)	22 ml
ddH_2O	up to 1 l

Detection buffer (in situ hybridisation)

5M NaCl	1 ml
1M MgCl	2 ml
0.5M Tris-HCl (pH 9.5)	10 ml
Levamisol (2 mM final conc.)	24 mg
ddH_2O	up to 50 ml

DMEM (complete Media)

DMEM	445 ml
(+ 4.5 g/l glucose, + l-glutamine, + pyruvate)	
FCS	50 ml
1% (v/v) Penicillin/Streptomycin (10000 U/ml)	5 ml

DNA Extraction Buffer

DirectPCR Lysis Reagent (mouse tail)	95 µl
Proteinase K (10 mg/ml)	5 µl

DNA Extraction Buffer (Isoproponal Method)

Tris-HCl pH 8.8	50 mM
EDTA	100 mM
NaCl	100 mM
SDS	1%
Proteinase K (10 mg/ml, Melford)	0.5 mg/ml

High Salt Buffer

Tris–HCl (pH 7.4)	100 mM
NaCl	600 mM
supplemented with:	
DTT	1 mM
NaF	50 mM
PMSF	1 mM
Na_3VO_4	1 mM
Complete Protease Inhibitor Cocktail	1 % (v/v)

Hypotonic Swelling Buffer	final concentration
NaCl	50 mM
FCS	1% (v/v)
Glucose	0.45% (v/v)
dissolved in sterile PBS	

Hybridisation Buffer	final concentration:
Deionized formamide	50% (v/v)
Dextran sulfate	10% (v/v)
Denhardt's Solution	1x
Tris-HCl pH7.5	10 mM
NaCl	600 mM
EDTA	1 mM
SDS	0.25% (w/v)
tRNA	1 mg/ml
diluted in DEPC water	

KCM buffer (IF-FISH)	
KCl	120 mM
NaCl	20 mM
Tris (pH 7.5)	10 mM
Triton X-100	0.1% (v/v)

Lysis Buffer	
Tris–HCl (pH 7.2)	80 mM
NaCl	150 mM
NP-40	0.2% (v/v)
Glycerol	10% (v/v)
supplemented with:	
NaF	50 mM
Na_3VO_4	1 mM

β-glycerophosphate	1 mM
Complete Protease Inhibitor Cocktail	1% (v/v)

NB + GF (adult neurospheres; for 500 ml)

Neurobasal Medium	474.8 ml
2% (v/v) B27 Supplement	10 ml
1% (v/v) L-Glutamine (200 mM)	5 ml
1% (v/v) Penicillin/Streptomycin (10000 U/ml)	5 ml
1% (v/v) N-2 supplement	5 ml
20 ng/ml EGF (100 µM)	100 µl
20 ng/ml FGF-basic (100 µM)	100 µl

NB + GF + laminin (adherent NSCs; for 500 ml)

Neurobasal Medium	474.8 ml
2% (v/v) B27 Supplement	10 ml
1% (v/v) L-Glutamine (200 mM)	5 ml
1% (v/v) Penicillin/Streptomycin (10000 U/ml)	5 ml
1% (v/v) N-2 supplement	5 ml
20 ng/ml EGF (100 µM)	100 µl
20 ng/ml FGF-basic (100 µM)	100 µl
Laminin	0.5 mg

Phosphate buffered saline (PBS)	final concentration:
KCl	3 mM
NaCl	136 mM
$Na_2HPO_4 \bullet 2\ H_2O$	8 mM
KH_2PO_4	15 mM

PNA hybridization solution	final concentration:
Deionized Formamide	70% (v/v)
NEN blocking reagent	0.25% (v/v) (PerkinElmer)
Tris (pH 7.5)	10 mM

Na_2HPO_4	4 mM
Citric Acid	0.5 mM
$MgCl_2$	1.25 mM

PNA Wash A	final concentration:
Formamide	70% (v/v)
Tris (pH 7.5)	10 mM

PNA Wash B	final concentration:
Tris (pH 7.5)	50 mM
NaCl	150 mM
Tween-20	0.08% (v/v)

Protein loading buffer (Laemmli buffer)	final concentration
Tris-HCl (pH 6.8)	63 mM
SDS (w/v)	2% (w/v)
Glycerol (v/v)	10% (v/v)
bromophenol blue (w/v)	0.0025% (v/v)
β-mercaptoethanol (v/v)	2.5% (v/v)

6% Resolving Gel

ddH_2O	13.2 ml
30% acrylamide mix	5.0 ml
1.5 M Tris (pH 8.8)	6.3 ml
10% SDS	250 µl
10% ammonium persulfate (APS)	250 µl
TEMED	20 µl

10% Resolving Gel

ddH_20	9.9 ml
30% acrylamide mix	8.3 ml
1.5 M Tris (pH 8.8)	6.3 ml

10% (w/v) SDS	250 µl
10% (w/v) ammonium persulfate (APS)	250 µl
TEMED	20 µl

12% Resolving Gel

ddH_2O	8.2 ml
30% acrylamide mix	10.0 ml
1.5 M Tris (pH 8.8)	6.3 ml
10% (w/v) SDS	250 µl
10% (w/v) ammonium persulfate (APS)	250 µl
TEMED	20 µl

Sodium acetate buffer

1 M sodium acetate	99 ml
1 M acetic acid	960 µl
ddH_2O	up to 1 l

10x SDS-PAGE Running buffer

Tris	300 g
Glycine	1400 g
20% SDS (v/v)	250 ml
ddH_2O	up to 10 l

1x Semi-dry transfer buffer	final concentration.:
Tris	24 mM
Glycine	192 mM
Methanol (v/v)	20%
SDS (v/v)	0.01%

20x SSC

NaCl	17.53 g
Sodium Citrate	8.82 g

DEPC water, pH 5.0	80 ml

5% Stacking gel

ddH_2O	6.8 ml
30% acrylamide mix	1.7 ml
1.0 M Tris (pH 6.8)	1.25 ml
10% (w/v) SDS	100 µl
10% (w/v) ammonium persulfate (APS)	100 µl
TEMED	10 µl

50x TAE buffer

Acetic acid	57.1 ml
$Na_2EDTA \times 2\ H_2O$	37.2 g
Tris (0.2 M)	242 g
ddH_2O	up to 1 l

20x Tris buffered saline Tween-20 (TBS-T)

NaCl (5 M)	3 l
Tris (1 M; pH 7.5)	2 l
Tween-20	200 ml
ddH2O	up to 10 l

2.1.3 Oligonucleotides

The following oligonucleotides were used for this study. All oligonucleotides were synthesised by Sigma Aldrich (Poole, U.K.)

Table 1: Genotyping Primers

Amplified DNA	Primer Sequence	Product size
atm	Mutant Forward: 5'- CTT GGG TGG AGA GGC TAT TC-3' Mutant Reverse: 5'- AGG TGA GAT GAC AGG AGA TC-3'	Wildtype: 147bp Mutant:

	Wildtype Forward: 5'-GCT GCC ATA CTT GAT CCA TG-3' Wildtype Reverse: 5'-TCC GAA TTT GCA GGA GTT G-3'	280bp
atmin	Forward: 5'-TCA GCA TCT TCT CCA GAG AGA CAG-3' Reverse: 5'-CAC ATG TGT ACA GCA CAT TCA TTG-3' Delta: 5'-CTC AGG GTA CAC ATA CTA TGC TTG C-3'	Wildtype: 430bp Floxed: 515bp Deleted: 400bp
CD19-Cre	Forward: 5'-CCA CAG AGG GAG GCA ATG TTG TGC-3' Wildtype Reverse: 5'-GTC CTT GAA AGG GGG CCT CTT CTG GC-3' Mutant Reverse: 5'-ACG ACC GGC AAA CGG ACA GAA GCA-3'	Cre: 303bp Control: 226bp
Cre	Forward: 5'-CGG TCG ATG CAA CGA GTG ATG AGG-3' Reverse: 5'-CCA GAG ACG GAA ATC CAT CGC TCG-3'	Cre: 600bp
nbs1	Forward: 5′-CAG GGC GAC ATG AAA GAA AAC-3′, Reverse: 5′- AAT ACA GTG ACT CCT GGA GG-3 Delta: 5′-ATA AGA CAG TCA CCA CTG CG-3′	Wildtype: 320bp Floxed: 380bp Delta: 590bp
p53	Forward: 5'-CAC AAA AAC AGG TTA AAC CCA G -3' Reverse: 5'-GAA GAC AGA AAA GGG GAG GG-3' Delta: 5'-AGC ACA TAG GAG GCA GAG AC-3'	Wildtype: 410bp Mutant: 490bp
LSL-K-Ras^{G12D}	Forward Wildtype: 5' GTC GAC AAG CTC ATG CGG G-3' Forward Mutant: 5' GTC GAC AAG CTC ATG CGG G-3' Reverse: 5' CCA TGG CTT GAG TAA GTC TGC-3'	Wildtype: 500bp Mutant: 550bp
LSL-ROSA26-YFP	Forward Wildtype: 5'-GGA GCG GGA GAA ATG GAT ATG-3' Forward Mutant: 5'-AAG ACC GCG AAG AGT TTG TC-3' Reverse: 5'- GGA GCG GGA GAA ATG GAT ATG-3'	Wildtype: 600bp Mutant: 320bp
terc	Forward Wildtype: 5′-CTA AGC CGG CAC TCC TTA CAA G-3′ Forward Mutant:	Wildtype: 250bp

	5′-GGG GCT GCT AAA GCG CAT-3′ Reverse: 5′-CTA AGC CGG CAC TCC TTA CAA G-3′	Mutant: 180bp

The following primers were used for qPCR analysis (see page 104).

Table 2: qPCR Primers

Gene	Primers
β-actin	Forward: 5'- ATG CTC CCC GGG CTG TAT-3' Reverse: 5′- CAT AGG AGT CCT TCT GAC CCA TTC -3′
dec1	Forward: 5'-GGC GGG GAA TAA AAC GGA GCG A-3' Reverse: 5'-CCT CAC GGG CAC AAG TCT GGA A-3'
dmap1	Forward: 5′-ACG GAG CAA TGT TCTT CCA C-3′ Reverse: 5′-CAG GCA CCT GCA CAGT CTT A-3'
gapdh	Forward: 5'-TGA AGC AGG CAT CTG AGG G-3` Reverse: 5`-CGA AGG TGG AAG AGT GGG AG-3`
tip60	Forward: 5'- CAG GAC AGC TCT GAT GGA ATA C -3' Reverse: 5'- AGA GGA CAG GCA ATG TGG TGA G-3'

The following primers were used for sequencing:

Table 3: Sequencing Primers

Vector	Sequencing Primer
pENTR	5'- TTG TAA AAC GAC GGC CAG T-3'
pSUPER	5'- AAT ACG ACT CAC TAT AG-3'
pCMV	5`-GGA CTT TCC AAA ATG TCG-3`

The following nucleotide sequences were designed to target the indicated genes for shRNA mediated knockdown.

Table 4: Target shRNA sequences

Gene	Region Targeted	Sequence (sense orientation)
ALKBH7	ORF	5'-GCA GAG GAG GAG ACG CTG A-3'
	3'-UTR	5'-ACA CCA GAT TTG TGA ATA A-3'
Ctage1	ORF	5'-CAA AGA AAG AGG AGA ATC A-3'
	3'-UTR	5'-TGA CAT TGC TTG TTT GTA A-3'
DMAP1	ORF (sequence #1)	5'-CGG AAG AAG GAG CGG GAG A-3'
	ORF (sequence #2)	5'-CGG AGG AGG GCA AGG ACT A-3'
	ORF (sequence #3)	5'-GGA CTA AGG CAG AAA CTG A-3'
	3'-UTR	5'-AAA TAG AGC TGC TGA GTT G-3'
Mycbp2	ORF	5'-GCA GAT AGG CAT AGT GAA A-3'

	3'-UTR	5'-CCA AAT ACC ATG TAC ATA A-3'
Nthl1	ORF	5'-GGA GGA GCA AGG TGA AAT A-3'
	3'-UTR	5'-TGG CTT TAC GCT TCA GGA A-3'
Rsf1	ORF (sequence #1)	5'-GAA CAG AAA GAA AGT GAA A-3'
	ORF (sequence #2)	5'-GCC AAT TGG TCG AGA CAA A-3'
	ORF (sequence #3)	5'-GCA CAA AGA TTG AGT CCA A-3'
	3'-UTR	5'-AGT AAC AGC CTT TGT GAA A-3'
Scaper	ORF	5'-GCA CAG CAG CTA AGG GAA A-3'
	3'-UTR	5'-GGG TGA AAG GAG ACA TAA A-3'
SNF2h	ORF	5'-TCC GAG GAT TAA ACT GGC T-3'
Tip60	ORF (sequence #1)	5'-GCA ATG AGA TTT ACC GCA A-3'
	ORF (sequence #2)	5'-GGA GAA AGA ATC AAC GGA A-3'
	3'-UTR	5'-GTA CAG AGG GCT GGT GAT T-3'
Znf507	ORF	5'-TGA AAG AGT TGC AGG ACA A-3'
	3'-UTR	5'-GGA AAG ATC TCT AAA TTC A-3'

2.1.4 Antibodies

Table 5: Primary Antibodies

Primary Antibody	Species	Application, Dilution	Supplier, Cat Number
53BP1	Rabbit, polyclonal	IF 1:400	Santa Cruz (CA, USA) sc22760
53BP1		IHC	
ATM	Mouse, monoclonal	WB 1:1,000 IP 5 μg	Santa Cruz (CA, USA) sc23931
pS1987-ATM	Mouse, monoclonal	WB 1:500 (mouse and human cells) IF 1:400	Cell Signalling, (Hitchin, UK), #4526
pS1981-ATM	Rabbit, monoclonal	WB 1:1,1000 (human cells)	Abcam (Cambridge, UK), ab81292
pS1981-ATM	Rabbit, monoclonal	WB 1:1,1000 (human cells)	Epitomics (California, USA), 2152-1
β-Actin	Rabbit, polyclonal	WB 1:5,000	Sigma (Poole, UK) A5060
B220-Biotin	Rat, polyclonal	IHC 1:200	BD Pharmingen (Oxford, UK), 553086
B220-APC	Rat, polyclonal	FACS 1:100	BD Pharmingen (Oxford, UK), 553092
BrdU	Rat, polyclonal	IHC 1:1000	AbD Serotec (Oxford, UK) 0BT0030CX
CD4-Biotin	Mouse, monoclonal	Negative Selection 1:100	BD Pharmingen (Oxford, UK), 553045
CD8a-Biotin	Mouse, monoclonal	Negative Selection 1:100	BD Pharmingen (Oxford, UK), 553029

CD43-FITC	Rat, polyclonal	FACS	BD Pharmingen (Oxford, UK), 561856
pS317-Chk1	Rabbit, polyclonal	WB 1:1,000	Cell Signalling, (Hitchin, UK), #2344
Chromogranin	Rabbit, polyclonal	IHC 1:200	Abcam (Cambridge, UK)
pERK (p44/42 MAPK)	Rabbit, polyclonal	WB 1:1000	Cell Signalling, (Hitchin, UK), #9201
pERK (p44/42 MAPK)	Rabbit, polyclonal	IHC 1:100	Cell Signalling, (Hitchin, UK), 4370
Dec1	Mouse, monoclonal	WB 1:1000	Santa Cruz (Calne, UK) sc101023
pS139-H2AX	Mouse, monoclonal	WB 1:1,000 IF 1:400 IHC 1:1000	Millipore (Watford, UK) 05636
pS139-H2AX	Rabbit, polyclonal	WB 1:1,000 IF 1:400	Millipore (Watford, UK) 05636
pS139-H2AX	Mouse, monoclonal	IF-FISH 1:400	Biolegend (CA, USA) 613402 clone 2F3
H4K16-Ac	Mouse, monoclonal	WB 1:500	Millipore (Watford, UK) 05-1232
HA	Rabbit, polyclonal	IP 1:200 WB1:2,000	Sigma (Poole, UK) H6908
IgM-PE	Rat	FACS	BD Pharmingen (Oxford, UK), 553409
KAP-1	Rabbit, polyclonal	WB 1:1,000	Bethyl Labs (Montgomery, USA) A300-274A
KAP-1	Rabbit, polyclonal	WB 1:1,000	Abcam (Cambridge, UK) ab10484
pS824-KAP-1	Rabbit, polyclonal	WB 1:1,000	Bethyl Labs (Montgomery, USA) A300-767A
Ki67	Rabbit, polyclonal	IHC 1:125	DAKO (Ely, UK)
Mac1-Biotin	Mouse, monoclonal	Negative Selection 1:100	BD Pharmingen (Oxford, UK), 553309
MCM6	Goat, polyclonal	IHC 1:200	Santa Cruz (CA, USA) sc-9843
MYC	Rabbit, polyclonal	IP 1:200 WB 1:2,000 IF 1:400	Sigma (Poole, UK) C3956
NK1.1-Biotin	Mouse, monoclonal	Negative Selection 1:100	BD Pharmingen (Oxford, UK), 553163
p21	Rabbit, polyclonal	WB 1:1,000	Santa Cruz (CA, USA) sc-8349
p53	Mouse,	WB 1:1,000	Santa Cruz (CA, USA) sc-

	monoclonal		126
pS15-p53	Rabbit, polyclonal	WB 1:1,000	Cell signalling (Hitchin, UK) 9284
pSer10-H3	Rabbit, polyclonal	FACS 1:200	Cell Signalling (Hitchin, UK) 06-570
SMC1	Rabbit, polyclonal	WB 1:1,000	Abcam (Cambridge, UK) ab9262
pS957-SMC1	Mouse, monoclonal	WB 1:1,000	Millipore (Watford, UK) 05-786
pS966-SMC1	Rabbit, polyclonal	WB 1:1,000	Bethyl Labs (Montgomery, USA) A300-050A
TCRβ-Biotin	Mouse, monoclonal	Negative Selection 1:100	BD Pharmingen (Oxford, UK), 553169
TCRγδ-Biotin	Mouse, monoclonal	Negative Selection 1:100	BD Pharmingen (Oxford, UK), 553176
Ter119-Biotin	Mouse, monoclonal	Negative Selection 1:100	BD Pharmingen (Oxford, UK), 553672
Tubulin (α)	Mouse, monoclonal	WB 1:5,000	Abcam (Cambridge, UK) ab7291
turbo-GFP	Mouse, monoclonal	WB: 1,1000	Origene (Maryland, USA) TA155041

Table 6: Secondary Antibodies

Secondary Antibody	Species	Application, Dilution	Supplier, Cat Number
Alexa Fluoro 488, anti Mouse	Donkey anti-Mouse IgG	IF 1:400	Life Technologies (NY, USA) A21245
Alexa Fluoro 488, anti Mouse	Goat anti-Mouse IgG	IF 1:400	Life Technologies (NY, USA) A11029
Alexa Fluoro 488, anti Rabbit	Donkey anti-Rabbit IgG	IF 1:400	Life Technologies (NY, USA) A21206
Alexa Fluoro 488, anti Rabbit	Goat anti-Rabbit IgG	IF 1:400 FACS 1:400	Life Technologies (NY, USA) A11008
Alexa Fluoro 546, anti Mouse	Goat anti-Mouse IgG	IF 1:400	Life Technologies (NY, USA) A10036
Alexa Fluoro 546, anti Rabbit	Donkey anti-Rabbit IgG	IF 1:400	Life Technologies (NY, USA) A10040
Alexa Fluoro 568 anti Mouse	Donkey anti-Mouse IgG	IF 1:400	Life Technologies (NY, USA) A10037
Alexa Fluoro 568 anti Rabbit	Donkey anti-Rabbit IgG	IF 1:400	Life Technologies (NY, USA) A11011
Alexa Fluoro 594, anti Mouse	anti Mouse IgG	IF-FISH 1:1000	Life Technologies (NY, USA) A11005
Biotin-conjugated anti-Goat	Rabbit, anti-Goat IgG	IHC 1:250	Vector Laboratories (CA, USA) BA-5000

Biotin-conjugated anti-Mouse	Donkey anti-Mouse IgG	IHC 1:250	Jackson (Newmarket, UK) 715-066-150
Biotin-conjugated anti-Rabbit	Donkey anti-Rabbit IgG	IHC 1:250	Jackson (Newmarket, UK) 711-066-152
Biotin-conjugated anti-Rat	Rabbit, anti-Rat IgG	IHC 1:500	Jackson (Newmarket, UK) 112-065-167
HRP-conjugated anti-Goat	Mouse, anti-Goat IgG	WB: 1:10,000	Jackson (Newmarket, UK) 205-032-176
HRP-conjugated anti-Mouse	Goat, anti-Mouse IgG	WB: 1:10,000	Jackson (Newmarket, UK) 115-035-174
HRP-conjugated anti-Rabbit	Mouse, anti-Rabbit IgG	WB: 1:10,000	Jackson (Newmarket, UK) 211-032-171

2.1.5 Vectors and Expression Plasmids

The Flag-ATM construct was a gift from Tanya Paull (Lee and Paull, 2005) and the HA-Tip60 a gift from Bruno Amati (Taubert et al., 2004). The Myc-DMAP1 construct was obtained from Origene (catalogue number RC222239), comprising transcript variant-1 DMAP1 cDNA with an N-terminal Myc tag, under the control of a pCMV promoter in a vector containing an Ampicillin resistance cassette. This construct was also cloned into a Green Fluorescent Protein (GFP) destination vector (Origene), yielding N-terminally GFP tagged DMAP1, under the control of a pCMV promoter, in a vector containing an Ampicillin resistance cassette.

2.2 Methods

2.2.1 Cell Culture

2.2.1.1 Cell Lines

HCT-116, 293A, 293T and Hela Ohio cells were obtained from the London Research Institute Cell Services. Cells were grown in DMEM (Life Technologies) supplemented with 10% (v/v) FCS, 20mM L-glutamine, penicillin and streptomycin (10,000 U/ml; Life Technologies). Cell lines were maintained at 37^0C, 5% $C0_2$, and at either 3% or 20% 0_2.

2.2.1.2 Murine Embryonic Fibroblast Culture

MEFs were cultured in a humidified incubator at 37°C, 5% CO_2 and 3% O_2. For some experiments, MEFs were cultured at 20% 0_2. Every three days MEFs were trypsinised and passaged 1:3 (see 'Cell Passaging', page 88). MEFs were cultured in DMEM (+4.5 g/l glucose, + glutamine, + pyruvate; Life Technologies) medium supplemented with 10% (v/v) FCS (Sigma) and 1% (v/v) penicillin and streptomycin (10,000 U/ml; Life Technologies).

2.2.1.3 Cell Passaging

Cells lines were routinely passaged twice a week at 1:5 or 1:10. Primary MEFs were passaged 1:3 every three days. For cell passaging, medium was aspirated, cells washed once with sterile PBS and incubated in 0.25% (w/v) trypsin/PBS at 37ºC for five minutes. After trypsinisation, cells were resuspended in medium pre-warmed to 37ºC.

2.2.1.4 Cell Freezing

Confluent cells were trypsinised (see Cell Passaging, page 88) then resuspended in 10 ml medium. The single cell suspension was centrifuged for five minutes at 1,500 rpm. The supernatant was aspirated, and the pellet washed once by resuspension in 10 ml medium followed by a five minute centrifugation at 1,500 rpm. The supernatant was aspirated and pellet resuspended in 1.0 ml Freezing Buffer (90% medium, 10% DMSO) and transferred to a 2.0 ml CryoVial. Aliquots were immediately stored at -70^0C overnight then transferred to a liquid nitrogen tank for long-term storage the following day. Cells were frozen at an approximate concentration of $2x10^6$ cells/ml.

2.2.1.5 Cell Thawing

Cryovials containing 1 ml cell aliquots were quickly transferred from their long-term storage in liquid nitrogen tanks to thaw in a 37ºC waterbath. Thawed cells were immediately resuspended in 10 ml pre-warmed medium and centrifuged for five

minutes at 1,500 rpm. The pellet was washed once with 10 ml medium (five minutes at 1,500 rpm), resuspended in 15 ml medium and transferred to a 75cm^2 tissue culture flask.

2.2.1.6 Lipofectamine-2000 Transfection

Cells were transfected with Lipofectamine-2000 according to manufacturer's protocol (Life Technologies). The day before transfection cells were plated in either 6 cm or 10 cm dishes at an appropriate density to achieve 60-70% confluence on the day of transfection. 6 cm and 10 cm dishes were transfected with 10 µg and 30 µg plasmid DNA respectively. Appropriate combinations of plasmid DNA for each transfection were prepared at room temperature in 15 ml falcons and diluted to 1 ml in serum-free Opti-MEM (Life Technologies). A master mix containing 20 µl (6 cm dish) or 50 µl (10 cm dish) Lipofectamine-2000 diluted to 1 ml Opti-MEM per transfection was concomitantly prepared. Both tubes were incubated at room temperature for five minutes, then combined and incubated for a further 20 minutes. After this, the transfection complex was diluted with Opti-MEM to a final volume of 3 ml (6 cm) or 8 ml (10 cm dish). Cells were washed once in PBS prior to transfection complex addition. After four to six hours the complex was aspirated from the cells. Cells were washed once with PBS and then complete media was added to the dishes.

Unless transfected cells were to be subsequently labelled with AlexaFlour488 for immunofluorescence (IF), pCMV-GFP DNA was included in the transfection mix as a transfection control, at 5% of the total DNA. Transfection efficiency was assessed 24 hours after the removal of the transfection complex by quantifying the percentage of GFP positive cells using a Zeiss HBO-100 light microscope.

When experiments required cells in 24-well plates (for example, cells adhered onto coverslips for IF) cells were transfected in 6 cm plates and split into a 24 well plate the following day.

2.2.1.7 Calcium Phosphate Transfection

Large DNA constructs, such as Flag-ATM, were transfected by calcium phosphate transfection. Transfections were carried out according to manufacturer's instructions (Promega), using 60% confluent 10 cm dishes of 293T cells. To avoid shearing the large plasmids 200 µl filter tips with the ends cut off were used to pipette DNA. Three hours before transfection, cell medium was aspirated and replaced with 8 ml of fresh medium. All transfection reagents were thawed, warmed to room temperature, and vortexed prior to use. Glass FACS tubes were used for preparation of transfection complexes. For each transfection two tubes were prepared. In tube A, 30 µg DNA was diluted in sterile H_20 to a final volume of 438 µl, then 62 µl 2.0M $CaCl_2$ was added. In tube B, 500 µl 2xHBS was slowly vortexed whilst adding the contents of tube A dropwise. The combined transfection solution was incubated at room temperature for 30 minutes. The solution was thoroughly vortexed and immediately added dropwise, with swirling, to the cells. After overnight incubation at 37ºC the medium was aspirated and replaced with new medium.

2.2.1.8 Adeno Virus Infection

Cells containing alleles flanked by loxP sites (e.g. $atmin^{f/f}$) were infected with Adeno-Cre-GFP virus to delete the floxed allele. Primary MEFs were infected at passage two. The day prior to infection, cells were passaged into 75 cm^2 adherent flasks in 15 ml medium so as to be approximately 50% confluent on the day of infection. On the day of infection, 10 µl of either Adeno-Cre-GFP or Adeno-GFP (Gene Transfer Vector Core) was added to the cells. After 48 hours, the medium was replaced and the cells left for a further 48 hours recovery before experimental use. Infection efficiency was estimated by quantifying the percentage of GFP expressing cells, and the efficiency of recombination assessed by DNA isolation and genotyping for the floxed and delta alleles. All infection steps were carried out in a Category II Containment Suite.

2.2.2 Biochemistry

2.2.2.1 Protein Extraction

Cells were washed once in ice-cold PBS and either 20 µl (6 cm dishes) or 500 µl (10 cm dishes) of ice-cold Lysis Buffer added (recipe page 77). Cells were detached using a cell scraper, and pipetted into a 1.5 ml eppendorf tube. After 15 minutes on ice, cells were sonicated with three five second pulses at an amplitude of ten microns (MSE Soniprep SANYO). The whole cell lysate was centrifuged at 4^0C for ten minutes at 13,2000 rpm (Eppendorf Centrifuge 5415 R). The supernatant was removed and either stored at -20ºC for future use or used immediately.

2.2.2.2 Bradford Assay

The protein concentration of cell lysates was determined using the colourimetric based Bradford Assay. Protein Assay Dye Reagent (Bradford Reagent, Bio-Rad) contains the dye Coomassie Brilliant Blue G-250. The unbound form of the dye has an absorption spectrum maximum of 465 nm, whereas the bound form has an absorption spectrum maximum of 595nm. The increase in absorption at 595 nm is proportional to the amount of bound dye – and therefore protein concentration. A standard curve was constructed by adding 1, 2, 4, 8, 16 and 32 µl of 1.0 mg/ml BSA to 1 ml Bradford Reagent (diluted 1:5 in ddH_20). Similarly, 2 µl of protein sample was added to cuvettes containing 1 ml diluted Bradford Reagent. Absorption was measured spectrophotometrcially (Ultrospec 3100 pro, GE Healthcare). Cell lysate protein concentration was determined by reference to the standard curve. Protein amounts across an experimental set of samples were then standardised to the same concentration and volume by dilution in appropriate volumes of lysis buffer.

2.2.2.3 Sodium Dodecyl Sulphate-Polyacrylamide Gel Electophoresis (SDS-PAGE)

Protein loading buffer (Laemmli buffer, recipe page 79) was added 1:5 to protein samples. Samples were boiled at 100^0C for ten minutes on a heat block (Techne Dri-

Block DB-2D). Meanwhile, the appropriate percentage resolving gel solution was prepared (recipe page 79). Immediately after preparation, the resolving gel solution was poured into assembled glass plates for vertical electrophoresis (C.B.S. Scientific) to fill approximately three-quarters of the gel plates. After gel polymerisation a 5% stacking gel solution (recipe page 81) was prepared, added to the top of the gel chamber and the desired size gel comb placed in the stacking gel prior to its' polymerisation (C.B.S. Scientific). Once polymerised, the gel chamber was secured to an Adjustable Slab Gel Kit (C.B.C Scientific). The tank was filled with 1xSDS-PAGE Running Buffer (recipe page 80); and Rainbow markers (GE Healthcare) and samples loaded.

2.2.2.4 Western Blot

After the SDS gel had run for an appropriate time to separate proteins to the desired resolution the gel was transferred onto a PVDF membrane (Amersham) using a semi-dry blot chamber (Hoefer Scientific Instruments). The PVDF membrane was washed once each in Methanol (Fisher scientific), ddH_20 and finally Transfer Buffer (recipe page 80). Three layers of blotting paper (Whatman) pre-soaked in Transfer Buffer were placed in the transfer chamber, followed by the membrane, gel, and a further three layers of pre-soaked blotting paper. Proteins were transferred for three hours at 120 mA. All subsequent membrane blocking, antibody incubation and washing steps were performed on a shaker. After transfer, membranes were incubated with 5% (w/v) skimmed milk [(A1 Laboratory Supplies Ltd), dissolved in TBS-T] for 20 minutes at room temperature. Following this step to block unspecific binding, membranes were incubated with primary antibody diluted 1:1000 in 5% (w/v) skimmed milk, at 4^{o}C overnight. The following day, membranes were washed with four ten minute TBS-T washes at room temperature. Secondary antibody incubation was performed for 90 minutes at room temperature with HRP-conjugated secondary antibodies (Jackson Laboratories) diluted 1:5000 in 5% (w/v) skimmed milk. Then, membranes were washed for a further four times in TBS-T. Excess liquid was removed from the membrane using blotting paper (Whatman) and the dried membrane incubated for 2 minutes with a 1:1 mix of ECL Detection Solutions 1 and 2 (GE Healthcare). Fuji X-ray

films (Fisher Scientific) were laid upon the membranes in developing cassettes for various periods of time and films developed in an X-ray developer (Jungwon).

2.2.3 DNA Damage Treatments

2.2.3.1 Irradiation

Irradiation experiments were performed using a Cs137 Gamma Irradiator at 2.1 Gy/min. Cells and mice were irradiated at the indicated doses. Mice were irradiated with lead shielding, cells without.

2.2.3.2 UV

Medium was aspirated immediately before treatment. Cells were treated with 5 J m^{-2} using a UV Stratalinker 2400 (Stratagene). After treatment, new medium was quickly added to the cells. The treated cells were harvested after a sixty minute recovery at 37ºC.

2.2.3.3 Hypotonic Shock

Cells were washed twice with sterile PBS then incubated with Hypotonic Swelling Buffer (recipe page 77) for 60 minutes.

2.2.3.4 H_20_2

Oxidative stress treatments were performed using 250 μM H_20_2 (Fisher Scientific). H_20_2 dilutions were prepared in medium from a stock solution immediately prior to treatment. Cells were washed twice with PBS then H_20_2 added for the indicated length of time.

2.2.3.5 Bleomycin

Cells were treated with 5 μM bleomycin (Sigma, B5507) diluted in complete medium. Unless indicated otherwise, cells were treated for 30 minutes.

2.2.3.6 Neocarzinostatin

Neocarzinostatin (Sigma, N9162) was added to cells at a final concentration of 200 ng/ml for the indicated length of time.

2.2.3.7 Aphidicolin

Sub-confluent cells were incubated in medium containing 5 μM aphidicolon (Sigma, A4487) for two hours.

2.2.4 Cellular Biology

2.2.4.1 Cell Culture Treatments

For some experiments, cells were incubated with small molecules prior to treatment or harvesting. ATM kinase inhibitor (Calbiochem), dissolved in DMS0, was added at a final concentration of 10 nM one hour prior to DNA damage treatment. TSA (Sigma) was added at a final concentration of 5 μM for the indicated time. DMSO containing medium was added to control cells.

2.2.4.2 BrdU Incorporation

BrdU (5-bromo-2-deoxyuridine) is a synthetic analogue of thymidine and is incorporated into newly replicated DNA during S phase. The percentage of cells incorporating BrdU in a given time period is a measure of a cell population's proliferation. Cells were grown in medium containing 10 μM BrdU (Sigma) for 30minutes, trypsinised and washed once in ice-cold PBS by centrifugation (1,500 rpm, five minutes, 4^{o}C) The resultant cell pellet was fixed, whilst vortexing, in ice-cold 70% (v/v) ethanol. Fixed cells were washed twice in PBS (1,500 rpm, five minutes, 4^{o}C) and resuspended in 2M HCl at room temperature for 30 minutes, with mixing at intervals. Cells were washed twice with PBS then incubated with 2 μl anti-BrdU antibody (Becton

Dickinson) for 20 minutes in the dark. Cells were washed once with PBS-T, and incubated with secondary antibody for 20 minutes in the dark. After one more PBS wash 50µl ribonuclease (Sigma) and 150µl propium iodide (Sigma) were added to the cell pellet for 30 minutes in the dark. The cells were analysed using a LSR II Flow Cytometer (BD) and the data analysed using Flow Jo (TreeStar).

2.2.4.3 Immunoprecipitation

Cells were harvested 48 hours after transfection (see Protein Extraction, page 91) and a Bradford Assay performed (see Bradford Assay, page 91). For each immunoprecipitation 500 µg of protein was diluted in a final volume of 500 µl Lysis Buffer (recipe page 79). From each protein lysate a 10% input control (50 µl) was removed prior to immunoprecipitation. Lysates were incubated overnight, at 4°C, on a rotating wheel with either 5 µg primary antibody or 5 µg IgG control (Life Technologies). The following morning, 40 µl of a 1:1 mix of ProteinA-Sepharose and ProteinG- Sepharose was washed three times with ice-cold Lysis Buffer. For all steps involving the pipetting of Sepharose Beads, 200 µl tips with the tips cut off were used to avoid shearing the Sepharose beads. Each wash step comprised of resuspending the beads in 1 ml Lysis Buffer by gentle inversion three to five times, then centrifugation at 2,500rpm for three minutes at 4°C. After the final wash the pellet was resuspended in 50 µl of Lysis Buffer then added to the overnight incubation of primary antibody and protein extract. The lysates were incubated for a further two hours, at 4°C, on a rotating wheel. The captured immunocomplexes were washed a further four times with 1 ml Lysis Buffer per wash. After the final wash, pelleted immunocomplexes were resuspended in Lysis Buffer, and a 1:5 dilution of Protein Loading Buffer. Samples were boiled for ten minutes at 100^0C on a heat block (Techne Dri-Block DB-2D) prior to gel loading.

2.2.4.4 ATM Co-Immunoprecipitation Assays

For experiments involving the immunoprecipitation of ATM, a modified protocol was used due to ATM's large molecular weight. The calcium phosphate method was used

for transfection (see page 90) and cells harvested in ATM lysis buffer (recipe page 74). Instead of three washes with Lysis Buffer, immunoprecipitates were instead washed three times in ATM lysis buffer (recipe page 74), once in High Salt Buffer (recipe page 76), and one wash in Base Buffer (recipe page 75).

2.2.4.5 FACS Analysis

All FACS analysis was carried out in collaboration with the LRI FACS facility. Fluorescence-activated cell sorting measurements were performed using an LSR II Flow Cytometer (BD). Analysis was carried out using FlowJo (Tree Star) software.

Cell lines were harvested for FACS by trypsin treatment (see Cell Passaging, page 88) then resuspended in medium and centrifuged at 4^{o}C for five minutes at 1,500 rpm. The pellet was resuspended in 4 ml sterile PBS and centrifuged a second time. After supernatant aspiration the pellet was resuspended in 500 µl 70% (v/v) ethanol (Fisher Scientific), pre-chilled to 4^{o}C. This cell-fixing and permeabilisation step was performed by adding 500 µl 70% (v/v) ethanol dropwise to cells, whilst vortexing the cells at a 45^{o} angle.

For both cell cycle analysis and sub-G1 cells were washed twice in PBS, by five minute centrifugation at 2,000 rpm. The cell pellet was treated with 50 µl Ribonuclease (stock 100 µl/ml) to ensure only DNA, and not RNA, is stained. Finally, 200 µl of 50 µg/ml propidium iodide (PI) was added. A FACS plot of PI staining versus cell size allows discrimination between the different cell cycle phases. Cells undergoing apoptosis have fragmented DNA, and are identified by quantifying the 'sub G1' population - those cells with PI staining below what is expected for a cell in G1.

For BrdU analysis (see BrdU Incorporation, page 94) cells were washed twice in PBS, by five minute centrifugation at 2,000 rpm then re-suspended in 2M HCl, then left at room temperature for 20 to 30 minutes with mixing at intervals. Then, the cells were washed twice more in PBS then once in PBS-T. Next, the cell pellet was incubated with 2 µl anti-BrdU antibody (Sigma) in the dark for 20 minutes. After one wash in PSB-T,

cells were stained with 50 µl secondary antibody for 20 minutes in the dark. Next, cells were washed once in PBS then incubated with 50 µl ribonuclease and 150 µl PI in the dark for 30 minutes. A FACS plot of BrdU versus PI readily identifies those cells that have incorporated BrdU, and are therefore in S-phase.

2.2.4.6 HAT Assays

Cells were transfected in 10 cm plates using Lipfectamine-2000 and harvested 48 hours later. A Bradford assay was performed, and 1 mg of protein extract was diluted to 500 µl using Lysis Buffer (see Bradford Assay, page 91). A 10% input sample (50 µl) was removed prior to immunoprecipitation. Cells were immunoprecipitated (see Immunoprecipitation, page 95) using either HA (Sigma H6908), Myc (Sigma, C3956) or IgG control (Invitrogen, 02-6102) antibodies. Washed immunocomplexes were resuspended in 50 µl of Lysis Buffer. The Histone Acetyl Transferase (HAT) activity of the immunoprecipitate was measured with a colourimetric Histone Acetyltransferase Activity Assay Kit (Abcam 65352) according to the manufacturer's protocol. Briefly, 20 µl of the immunoprecipitate was diluted to a final volume of 40 µl in ddH_20. A positive control of 10 µl nuclear extract (supplied in kit) was also diluted to a final volume of 40 µl in dd H_20. An assay mix of 50 µl of 2x HAT Assay Buffer, 5 µl HAT Substrate I, 5 µl HAT Substrate II and 5 µl NADH Generating Enzyme was prepared, and 65 µl added to the sample, and positive control, in a transparenet 96 well plate (Nunc). To account for background, 65 µl of the assay mix was added to 40 µl ddH_20. The plate was incubated at 37^oC for four hours, and the optical density at 440nm read for each well using a SpectraMax Plate Reader. All samples were normalised to the background reading. To control for equal immunoprecipitation, samples and input were resolved on a 10% SDS-PAGE electrophoresis gel and the resulting membrane probed for the protein of interest (see Western Blot).

2.2.4.7 The G2 Trap

The G2 Trap was used to assess G2/M checkpoint functionality. Cells were transfected using the Lipofectamine-2000 method then irradiated 48 hours later. Immediately after

irradiation cells were placed in medium containing 40 nM Nocodazole (Sigma, M1404) or DMSO and cultured for 18 hours. Then, the medium was carefully pipetted from the cells and placed in a FACS tube. Cells were washed once with PBS and trypsinised, and resuspended in the medium removed from the cells prior to trypsin treatment. This suspension was returned to the FACS tube, and centrifuged at room temperature for five minutes at 1,500 rpm. The pellet was resuspended in 4 ml sterile PBS and centrifuged a second time. After supernatant aspiration the pellet was resuspended in 500 µl 70% (v/v) ethanol (Fisher Scientific), pre-chilled to 4^{o}C. This cell-fixing step was performed by adding 500 µl 70% (v/v) ethanol dropwise to cells, whilst vortexing the cells at a 45^{o} angle. Fixed cells were stored at 4^{o}C then stained for FACS analysis (see page 96). Cells were stained with pSer10-H3 antibody (Cell signalling, 06-570) followed by incubation with Alexa647 secondary antibody (Life Technologies, A-31571).

2.2.4.8 Clonogenic Survival Assay

For post-irradiation survival analysis cells were irradiated at doses ranging from 0-40 Gy. Cells were immediately trypsinised and resuspended in 5 ml medium. The single cell suspension was counted using a Vi-Cell XR cell counter (Beckman Coulter). By serial dilution, solutions of 250 cells/ml and 1000 cells/ml were prepared. One ml of these solutions was added to 6 cm plates to a final volume of 3ml medium. Each cell solution was plated in triplicate. Seven days after irradiation the number of colonies per plate was counted by eye. Note that in experiments involving inhibition of ATM, the ATM inhibitor was not added to the resuspended cells after irradiation.

2.2.4.9 β-galactosidase senescence assay

Cellular senescence was assessed using the Senescent Cells Histochemical Staining Kit (Sigma, CS0030), according to manufacturer's instructions. Cells were incubated in staining mixture overnight at 37^{0}C in a non-$C0_2$ enriched environment. The following day, cells were washed three times with PBS and analysed by light microscopy (AX10 Imager.A1, Carl Zeiss). Cells with β-galactisodase activity at pH6.0 are senescent, and stain blue.

2.2.4.10 Immunofluorescence

Twenty-four hours after transfection in 6 cm plates, cells were trypsinised and passed into a 24-well plate containing coverslips. Cells were grown for a further 24 hours to adhere onto the coverslips. In some cases, cells were treated prior to fixation (for example, IR). Cells were washed once with ice-cold sterile PBS, then fixed in 500 µl 4% (w/v) paraformaldehyde (PFA) for 20 minutes at room temperature. After fixation, cells were washed three times with PBS and were either stained immediately or stored in PBS at 4^{o}C for up to a week before permeabilisation and staining. Each wash step consists of immersion in the wash solution for five minutes, on a shaker, at room temperature. Cells were permeabilised by incubation in 0.5% (v/v) Triton/PBS for three minutes at room temperatures. In some cases cells were fixed by two hours in a 1:1 pre-chilled ethanol:acetone solution at -20^{o}C. If fixed by this method, a separate permeabilisation step was unnecessary.

After three PBS washes cells were incubated in Blocking Buffer (recipe page 75) for 30 minutes at room temperature, on a shaker. Coverslips were then incubated with primary antibody diluted 1:400 in Blocking Buffer on a shaker; for either two hours at room temperature or overnight at 4^{o}C. Following primary antibody binding, coverslips were washed three times in Blocking Buffer. Secondary antibody, diluted 1:400 in Blocking Buffer, was added for one hour at room temperature, with shaking. Cells were washed with PBS and incubated with 1:10,000 DAPI (Sigma) for two minutes at room temperature, washed twice in PBS then mounted in DAKO fluorescent mounting medium (Ely).

2.2.4.11 IF-FISH

Cells were treated with 20 ng/ml colcemid (Sigma) for 30 minutes, then trypsinised (see page 88) and resuspended in hypotonic solution (0.2% (w/v) KCl, 0.2% (w/v) trisodium citrate) at room temperature, at a concentration of approximately 1x10^{5} cells/ml. After a ten minute incubation, cells were cytocentrifuged onto SuperFrost Plus slides (Menzel-

Glaser) at 450*g* for 10 minutes in a Shandon Cytospin 4. Next, cells were fixed for ten minutes in 4% (v/v) PFA, washed twice in ddH_20, then permeabalised in KCM buffer (recipe page 77) for ten minutes. Cells were then blocked for 15 minutes at 37 °C with 100 µg ml^{-1} DNase-free RNase A (Sigma) in antibody dilution buffer (recipe page 74). Slides were then incubated with primary antibody diluted in antibody dilution buffer (recipe page 74) for one hour at room temperature. After three five-minute washes in PBS-T (0.1% (v/v) Tween-20/PBS) at room temperature, slides were incubated in secondary antibody diluted in antibody dilution buffer (recipe page 74) for thirty minutes at room temperature, in the dark. All subsequent steps were performed in the dark. Slides were washed with three five-minute washes in PBS-T (0.1% (v/v) Tween-20/PBS) at room temperature then fixed for ten minutes in 4% (w/v) PFA. Fixed slides were dehydrated through the following steps; three minutes in 70% (v/v) ethanol, two minutes in 90% (v/v) ethanol and two minutes in 100% ethanol.

Air-dried slides were overlaid with 0.3 µg/ml PNA probe Alexa 488–OO-$(CCCTAA)_3$ PNA probe (Panagene) in PNA hybridisation solution (recipe page 78) and incubated at 80 °C for three minutes then overnight at room temperature. Finally, stained slides were washed with two ten minute washes in PNA Wash A (recipe page 79) then three five minute washes in PNA Wash B (recipe page 79). 50 ng/ml DAPI was added to the final wash, cells rinsed once in ddH_20 then mounted using DABCO (Sigma). Cells were imaged using a Zeiss Axio Imager M1 microscope, and an AxioCam MRm digital camera (Carl Zeiss).

2.2.5 Molecular Biology

2.2.5.1 DNA Isolation

Murine ear-snips were used for genotyping. DNA was extracted by incubation in 95 µl DirectPCR Lysis Reagent (Viagen) and 5 µl Proteinase K (10mg/ml, Melford) at 56 ºC overnight. The following day samples were heated at 85ºC for 45 minutes to inactivate Proteinase K. Samples were allowed to cool to room temperature, then centrifuged at 5,000 rpm for five minutes. Subsequently, 2 µl was used in each genotyping PCR reaction and the lysate stored at -20ºC.

For downstream applications requiring higher purity DNA preparations, such as cloning and sequencing, the isopropanol method was used for DNA isolation. 500 µl DNA Extraction Buffer (recipe page 76) was added to the tissue sample or cells. After overnight incubation at 56ºC samples were vortexed for ten seconds. Then 200 µl 5M NaCl was added and after ten seconds of vortexing samples were centrifuged at room temperature for ten minutes at 13,2000 rpm (Eppendorf Centrifuge 5415 D). The 700 µl supernatant was removed, and added to 500 µl isopropanol. The combined solution was vortexed for ten seconds and centrifuged at room temperature for ten minutes at 13,2000 rpm. Subsequently, the supernatant was discarded and pellet air-dried at room temperature for 15 minutes. The dried pellet was dissolved in 100 µl ddH_20 and incubated at 37ºC for 30 minutes on a shaker (Eppendorf Thermomixer). DNA concentration was determined using the NanoDrop Spectrophotometer (Thermo Scientific) and stored at -20ºC for future use.

2.2.5.2 Genotyping PCR

Depending on the allele to be genotyped, one of the following genotyping PCR mixes was prepared:

terc Genotyping PCR:

1 x GoTaqPCR buffer (Promega)	5 µl (5 x stock)
MgCl2	3 µl (25mM stock)
dNTPs (0.25 mM)	0.2 µl (25 mM stock)
Primer forward (1 µM)	0.2 µl (100 µM stock)
Primer reverse (1 µM)	0.2 µl (100 µM stock)
Primer delta (1 µM)	0.2 µl (100 µM stock)
GoTaq Polymerase (0.2U)	0.2 µl (5U/ µl stock)
dd H_20:	14 µl
DNA	2 µl
Total Volume:	*25* µl

All other Genotyping PCRs:

1 x CoralLoad PCR Buffer (Qiagen)	2 µl (10 x stock)
1 x Solution Q	4 µl (5 x stock)
dNTPs (0.25 mM)	0.2 µl (25 mM stock)
Primer forward (1 µM)	0.2 µl (100 µM stock)
Primer reverse (1 µM)	0.2 µl (100 µM stock)
Taq-Polymerase (0.2 U)	0.2 µl (5 U/µl stock)
ddH2O	11.2 µl
DNA	2 µl
Total Volume:	*20ul*

Depending on the genomic region to be amplified, one of the following PCR programmes was used:

Table 7: *atm* Genotyping PCR Programme

Step	Temp (^{o}C)	Time	Notes
1	94	3 min	
2	94	20 sec	
3	64	30 sec*	** minus 0.5^{o}C per cycle*
4	72	35 sec	*go to step 2 for 12 cycles*
5	94	20 sec	
6	58	30 sec	
7	72	35 sec	*go to step 5 for 25 cycles*
8	72	2 min	
9	4	*end*	

Table 8: *terc* Genotyping PCR Programme

Step	Temp (^{o}C)	Time	Notes
1	95	10 min	
2	94	1 min	
3	55	1 min	
4	72	1 min	*go to step 2 for 28 cycles*
5	72	6 min	
6	4	*end*	

Table 9: *LSL-K-Ras^{G12D}* Genotyping PCR Programme

Step	Temp (^{o}C)	Time	Notes

1	94	3 min	
2	94	30 sec	
3	60	45 sec	
4	72	1 min	*go to step 2 for 35 cycles*
5	72	10 min	
6	4	*end*	

Table 10: Genotyping PCR Programme for all other alleles:

Step	Temp (^{o}C)	Time	Notes
1	94	3 min	
2	94	30 sec	
3	60	45 sec	
4	72	45 sec	*go to step 2 for 30 cycles*
5	72	10 min	
6	4	*end*	

2.2.5.3 Agarose gel electrophoresis

PCR products were resolved on a 3.0% (w/v) agarose (Bioline) gel dissolved in 1xTAE with 1:1,000 ethidium bromide (10 mg/ml, Sigma-Aldrich). DNA separation took place at 120 V for 90 minutes. To define band size, 10 µl of a 100kB DNA ladder (Life Technologies) was also loaded. The resolved gel, and PCR product size, was visualised by UV illumination using a UV Transluminator (UVP).

2.2.5.4 RNA Isolation

The RNeasy Mini (QIAGEN) kit was used for RNA extraction, according to the manufacturers' instructions. Half a confluent 6 cm dish was used for each RNA preparation from cells. For RNA isolation from murine spleens approximately half a spleen was used for each preparation. To isolate RNA from intestinal tissue crypts and/or villi were extracted from 4 cm long intestine sections. Samples were homogenised by 8-10 passages through a 19-gauge needle (BD). The RNase-Free DNase Set (QIAGEN) was used for On-Column DNA digestion, according to the manufacturers' protocol. After extraction, RNA concentration and purity was determined using a NanoDrop Spectrophotometer (Thermo Scientific). A successful

RNA preparation should have a $OD_{260}/0D_{280}$ ration between 1.8 and 2.0. The isolated RNA was stored at -80°C.

2.2.5.5 cDNA Synthesis

The concentrations of RNA for cDNA synthesis were standardised using RNase-free water. Approximately 1 μg of RNA was used in each cDNA reaction. Superscript III First-Strand cDNA synthesis kit (Life Technologies) was used for cDNA synthesis, according to manufacturer's instructions. Random hexamer primers were used. A control reaction, not containing Reverse Transcriptase, was performed in parallel on each sample. After synthesis, cDNA was stored at -20°C.

2.2.5.6 Quantitative RT-PCR

Firstly, cDNA was diluted 1:5 in ddH_20. 1 μl of this solution was used for each qRT-PCR. Each reaction was performed in triplicate, in a 96 well plate, according to the following reaction mix:

1 x qRT-PCR Mix:

Primer 1 (10 μM Stock)	0.5 μl
Primer 2 (10 μM stock)	0.5 μl
Platinum SYBR Green	12.5 μl
ddH_20	10.5 μl
cDNA	1 μl

After preparation the plate was centrifuged at 4°C for five minutes at 2,000 rpm. The starting amount of template cDNA for each primer pair was measured by SYBR Green incorporation (Platinum Quantitative PCR SuperMix-UDG w/ROX, Life Technologies). The starting amount of cDNA in the reaction was accounted for by normalisation to either GAPDH or β-globin Ct levels according to the formula:

$$\text{Sample Expression} = 2^{-(\text{Sample Ct - Control Ct})}$$

To eliminate unspecific products, primer dimer formation and contamination a dissociation curve was performed and a 'no DNA' control reaction was included for each primer set. Data was analysed with SDS 2.3 Software (Applied Biosystems).

2.2.5.7 shRNA Cloning Strategy

For each gene to be targeted, 19 nucleotide shRNA sequences against the open reading frame (ORF) and 5'-Untranslated Region (5'-UTR) were designed using the Dharmacon Design Centre. The sense and anti-sense orientations of the target 19 nucleotide sequence were incorporated into 64 nucleotide long oligomers as indicated below:

Forward Primer: Gatcccc-*Sense*-ttcaagaga-*Antisense*-tttttggaaa
Reverse Primer: Agcttttccaaaaa- *Sense*-tctcttgaa-*Antisense*-ggg

These forward and reverse 64 nucleotide oligomers were annealed and cloned into the pSUPER vector. The terminal nucleotides at either end of this oligomer are the same as the overhangs left by BglII or HindIII restriction enzyme digestion.

Firstly, the matching forward and reverse oligomers were annealed. Briefly, 4 µl of each 100 µM primer was added to 42 µl ddH_20 and heated at 95^oC for four minutes, ten minutes at 70^oC, then slowly cooled to room temperature. Secondly, the annealed oligomers were phosphorylated for 30 minutes at 37^oC in the following reaction:

Annealed Oligomers	2 µl
1mM ATP	1 µl
10x PNK Buffer	1 µl
T4 PNK	1 µl
ddH_20	5 µl

After completion PNK was heat inactivated 70^oC for ten minutes.

The pSUPER vector was digested with HindIII and BglII (NEB) to create compatible DNA overhangs for ligation with the annealed oligomers, in the following reaction mix, at 37°C overnight:

BglII	2 µl
HindIII	2 µl
pSUPER (1µg/µl)	4 µl
10x Buffer 2 (NEB)	3 µl
ddH_20	19µl

The next day, 2 µl Antartic Phosphatase (NEB), 4 µl 10x Antartic Phosphatase Buffer (NEB) and 2 µl ddH_20 were added to the reaction, to remove the 5'-phosphate from the digested vector and prevent re-ligation. The reaction was incubated at 37°C for a further 30 minutes, then heat inactivated for five minutes at 65°C. The entire reaction was loaded onto a 1% (w/v) Agarose gel and run for one hour at 90 V. The band corresponding to digested vector was cut out and purified using the Gel Band Purification Kit (GE Healthcare), according to manufacturer's instructions.

Annealed oligomers were ligated into digested pSUPER overnight at 16°C, according to the following reaction:

T4 DNA Ligase	1 µl
10x T4 DNA Ligase buffer	1 µl
Phosphorylated, annealed oligomers	4 µl
Digested pSUPER	1 µl
ddH_20	3 µl

The next day, 2 µl ligation mix was used for transformation of XL10-Gold Bacteria (see page 107). Transformed bacteria were grown overnight on Ampicillin containing Agar plates. The following day colonies were picked, grown overnight in Ampicillin (100 µg/ml) containing LB medium, and bacteria pelleted for DNA extraction. A double digest with EcoR1 and HindIII was used to determine if the insert was present. When

separated on a 3% (w/v) Agarose gel, positive clones have a 360bp band - whereas empty vectors have a 300bp band. Positive clones were sequenced to ensure the insert contained the correct, mutation-free, sequence.

2.2.5.8 Bacterial Transformation and Plasmid Preparation

DH5α bacteria were used to amplify plasmid DNA. For each transformation, 50 µl bacteria were thawed on ice in 1.5 ml eppendorf tubes. Then, approximately 10-50 ng DNA (in a maximum 5 µl volume) was added to the bacteria. DNA and bacteria were mixed by gently tapping the eppendorf several times then left on ice for 30 minutes. Next, the bacteria were heat-shocked for 30 seconds at 42^{o}C on a heatblock (Eppendorf Thermomixer Compact). After a two minute recovery on ice 1ml pre-warmed SOC medium was added. Bacteria were grown at 37^{o}C for one hour to allow transcription and translation of the antibiotic resistance gene present on the plasmid. Bacteria were then transferred to 200 ml antibiotic containing LB and grown overnight at 37^{o}C in 500 ml flasks, with shaking. The following morning bacteria were harvested by centrifugation at 3,000 rpm for 20 minutes. Plasmid DNA was isolated from pelleted bacteria using a Plasmid Maxi Kit (QIAGEN), according to manufacturer's protocol.

For the amplification of DNA ligation reactions XL10-Gold bacteria (Aligent) were, with minor protocol adjustments. Briefly, 100 µl bacteria were used, and 2 µl β-mercaptonal was added to the bacteria ten minutes prior to DNA addition.

For the amplification of large DNA constructs, such as Flag-ATM, SURE-2 Competent cells (Aligent) and a modified protocol were used to minimise the likelihood of plasmid recombination. Transformed bacteria were grown for 48 hours in 2 l flasks, at 30^{o}C in 200ml SOC with gentle shaking. Pipette tips with the ends cut off were used for the handling of these plasmids to avoid the risk of plasmid shearing.

2.2.5.9 DNA Sequencing

DNA sequencing was performed using the Sanger method - the terminal incorporation of labelled nucleotides. Approximately 400 ng DNA was used in the following reaction mix:

BigDye Terminator Reaction Mix (BDT)	8 µl
10uM Sequencing Primer	0.32 µl
DNA	≅400 ng
ddH_20	up to 20 µl

The PCR reaction consisted of 28 cycles of the following steps:

1. 95°C for 30 seconds
2. 55 °C for 30 seconds
3. 60 °C for four minutes

Terminally labelled PCR products were purified using the DyeEx 2.0 Spin Kit (QIAGEN), according to manufacturer's instructions. Samples were sequenced by the LRI Equipment Park. Sequence reads were analysed using ApE 1.17 Plasmid Editor.

2.2.6 Animal Work

2.2.6.1 Animal Maintenance

All mice were housed in the LRI Biological Resource Units, at either Lincoln's Inn Fields or Clare Hall Laboratories. Schedule 1 Methods, as described in the Animal Scientific Procedures Act 1986, were used to cull all mice. For brain studies, mice were culled by $C0_2$ asphyxiation method. Cervical dislocation was used to cull mice for all other experiments. All murine studies were carried out according to UK Home Office guidelines and approved by the London Research Institute Animal Ethics Committee.

2.2.6.2 Mouse lines

Transgenic mice with combinations of the following mutant alleles were used in this study:

Mouse Line	Reference
atm$^{+/-}$	(Xu et al., 1996)
atmin$^{\Delta/\Delta}$	(Kanu and Behrens, 2007)
atmin$^{f/f}$	(Kanu et al., 2010)
CD19-Cre	(Rickert et al., 1997)
LSL-K-Ras^{G12D}	(Jackson et al., 2001)
nbs1$^{f/f}$	(Frappart et al., 2005)
Nestin-Cre	(Raivich et al., 2004)
p53$^{f/f}$	(Jonkers et al., 2001)
PGK-Cre	(Behrens et al., 1999)
Rosa26-LSL-YFP	(Srinivas et al., 2001)
Villin-Cre	(el Marjou et al., 2004)
Villin-CreERT	(el Marjou et al., 2004)

Starting generation (G0) *terc*$^{+/-}$ mice were obtained from Leonard Rudolph (Rudolph et al, 1999). These were intercrossed with *atmin*$^{f/f}$*; Nestin-Cre* animals to obtain starting generation (G0) *atmin*$^{f/f}$*; terc*$^{+/-}$*; Nestin-Cre* and *atmin*$^{f/f}$*; terc*$^{+/-}$ cohorts. These mice were intercrossed to obtain *atmin*$^{f/f}$*;terc*$^{-/-}$ and *atmin*$^{f/f}$*;terc*$^{-/-}$*Nestin-Cre* first generation (G1) animals, and so on for second and third generations. A cousin-mating breeding scheme was used to avoid generation of sub-strains.

2.2.6.3 BrdU injection

To determine which cells were proliferating, mice were given an intraperitoneal injection of 100 µg/g bodyweight 5-bromo-2'-deoxyuridine (BrdU; Sigma; stock: 20 mg/ml in endotoxin free-PBs). Injected animals were culled and analysed 90 minutes post injection.

2.2.6.4 Tamoxifen Injection

To express *Cre* recombinase in *Villin-CreERT* animals mice were intraperitoneally injected with tamoxifen. Three injections of 5 µl/g bodyweight (stock solution 20 mg/ml,

dissolved in peanut oil) were given at the same time each day for three consecutive days. Recombination efficiency was assessed by histological detection of *Rosa26-LSL-YFP* reporter expression, genotyping PCR and western blot of isolated tissue. The 20 mg/ml tamoxifen stock solution was prepared by dissolving 400 mg tamoxifen (Sigma) in 20 ml peanut oil (Sigma). To completely dissolve the tamoxifen, 5-6 cycles of 30 minutes on a rotating wheel then 30 minutes at 37^{o}C were followed, with vortexing.

2.2.6.5 Generation of Primary Murine Embryonic Fibroblasts

Embryos were removed at E12.5 and immediately transferred into chilled sterile PBS. Using a dissecting microscope, the placenta and yolk sac were discarded. The head and tail were removed and transferred to separate 1.5 ml eppendorfs for subsequent DNA extraction and genotyping. The heart, liver and lungs were removed and remaining embryo placed in a 6-well plate containing 4 ml DMEM (recipe page 76). The embryo was passed 8-10 times through a 1 ml syringe (BD) and an 18-gauge needle (BD) to create a single cell suspension.

2.2.6.6 Adult Neurosphere Isolation

Mice were culled by $C0_2$ asphyxiation and the brain removed, and cut coronally between the midbrain and forebrain. The forebrain was embedded with the olfactory bulb uppermost in molten 5% (w/v) low melting point agarose (dissolved in PBS; Life Technologies). Coronal 230μm brain sections were cut using a vibratome (Leica VT1000). Sections containing the sub-ventricular zone (SVZ) were retained, and transferred into PBS using a Pasteur pipet with the tip cut off. Using a dissecting microscope, the SVZ of each section was carefully dissected from both hemispheres. These were pooled in 200 μl PBS, in an 1.5 ml eppendorf tube. Tissue was dissociated by cutting with a scalpel and pipetting, and the resulting cell suspension centrifuged for five minutes at 1,000 rpm, at room temperature. The supernatant was discarded, and the pellet resuspended in 500 μl neurobasal medium (recipe page 79). The entire 500 μl single cell suspension was transferred to a 6-well plate containing 3.5 ml neural basal medium and left for at least a week to allow neurospheres to form before passaging.

2.2.6.7 Primary Neurosphere Culture

Primary adult neurospheres were cultured at 37^{o}C, 3% 0_2, 5% $C0_2$ in neurobasal medium (recipe page 79). The undifferentiated primary neurospheres were grown as suspension cultures in non-adherent plates or flasks (|BectonDickinson (BD) Falcon; Sarstedt). Every four to five days the culture was passaged by centrifugation for five minutes at 1,000 rpm, then gentle pipetting to dissociate the neurosphere. The resultant single cell suspension was passed 1:3 into fresh medium.

2.2.6.8 Neurosphere formation assay

Neurosphere cultures were centrifuged for five minutes at 1,000 rpm and the pellet resuspended in complete neurobasal medium (recipe page 79). A single cell suspension was obtained by pipetting and counted using Improved Neubauer counting chamber (Weber). The average number of viable cells in the four large quadrants multiplied by $1x10^4$ yields number of cells times 10^4/ml. In a 96-well plate (BD), 1000 and 100 cells per well were plated in triplicate, by serial dilution. After ten days the number of newly formed neurospheres were counted.

2.2.6.9 Murine B-Cell Isolation

Mice were culled by cervical dislocation and the spleen immediately placed in chilled, endotoxin-free PBS. Approximately half the spleen was processed for B-cell isolation. A cell suspension was prepared by passing the spleen, in PBS, through a 40 μM cell strainer into a 50 ml falcon. The volume was topped up to 50ml with endotoxin-free PBS and the cell solution centrifuged for four minutes at 4^{o}C, at 1,500 rpm. The supernatant was discarded and pellet resuspended in 1 ml Ammounium Chloride for 60 seconds to lyse the red blood cells. The Ammonuim Chloride was diluted by addition of 45 ml PBS and the cells centrifuged for four minutes at 4^{o}C, at 1,500 rpm. A bright red cell pellet after this centrifugation step indicated incomplete red blood cell lysis in which case the Ammounium Chloride step was repeated. Then, the pellet was resuspended in 1 ml primary antibody solution (endotoxin-free PBS/1% (v/v) FCS

containing a 1:100 dilution of the following biotin conjugated antibodies: CD4, CD8, Ter119, Mac1, NK1.1, TCRγδ and TCRβ [BD Pharmagin]). After 60 minutes at 4°C on a rotating wheel, 100 µl streptavidin-bead slurry (Life Technologies) was washed twice in endotoxin-free PBS/1% (v/v) FCS, using a magnetic strip, and added to the cells. 60 minutes later streptavidin-biotin complexes were aggregated using a magnetic strip and the supernatant - containing B cells isolated by negative selection - pipetted into a 1.5 ml eppendorf. The B cells were centrifuged at 1,500 rpm for five minutes at 4°C, and were either used immediately or stored at -80°C for future use.

2.2.6.10 Isolation of Intestinal Tissue

Mice were culled by cervical dislocation and the intestines removed. The cecum was separated from the rest of the intestine, and discarded. The colon and small intestine were flushed with ice-cold PBS to remove faecal contents. Intestines were cut longitudinally into similar size sections, placed on a gut roller and cut open. At this point, sections of approximately 4 cm were removed from the small intestine and colon for biochemistry. The remainder of the intestine was fixed overnight in 10% NBF (w/v), and then transferred to 70% (v/v) ethanol. For biochemistry, it is necessary to separate the villi and crypts from the muscle layer. Sections were incubated in 15 ml falcons, on ice, in 30 mM EDTA, for two to three hours with regular vortexing. Then, the remaining gut tissue was removed and the epithelial cells centrifuged at 1,500 rpm, for five minutes, at 4°C. Pelleted crypt and villi cells were washed once in PBS then either used immediately or stored at -80°C for future use.

2.2.7 Histology

All tissue embedding and staining was performed by the LRI Experimental Histopathology Service.

2.2.7.1 Tissue Fixation and Processing

Isolated tissues were fixed in 10% (w/v) NBF overnight, and transferred into 70% (v/v) ethanol the following day. For paraffin embedding fixed tissue was incubated at 40°C in

a series of dehydration steps - 30 minutes in 70% (v/v) ethanol, one hour in 85% (v/v) ethanol, one hour in 95% (v/v) ethanol then one hour in 100% (v/v) ethanol. Dehydrated tissue was then cleared in xylene three times at 40^{o}C for one hour then immersed in paraffin wax (Tissue Tek) at 60^{o}C for one hour. Next, samples were embedded in paraffin wax in embedding cassettes (Tissue-Tek) and cooled for 30 min at 4°C. Once cooled, embedded cassettes were either stored at room temperature for future use or cut immediately. A manual microtome (RM2235, Leica) was used to cut 4 μM thick sections. Cut sections were mounted on Superfrost Ultra Plus charged slides (Menzel-Glaeser).

2.2.7.2 Haematoxylin and eosin Staining

Haematoxylin stains basophilic structures, including nucleic acids and ribosome, blue. Conversely eosinophilic structures, including proteins, are stained pink by eosin. Therefore in haematoxylin and eosin (H&E) stained sections the nucleus appears blue and cytoplasm pink. All the following steps were performed at room temperature. Paraffin-embedded tissue sections were dewaxed by three minute incubation in xylene. Sections were hydrated by a series of three minute incubation steps - twice in 100% ethanol, twice in 70% (v/v) ethanol and finally twice in dd$H_2$0. Sections were stained in Harris's haematoxylin for five minutes then washed under running water for five minutes. Washed sections were differentiated for five seconds in 1% (v/v) acid alcohol (1% HCl/ 70% (v/v) ethanol) then washed under running water for five minutes. Afterwards, the sections were incubated in 1% (w/v) eosin Y for five minutes then washed again under running water for five minutes. Finally, sections were dehydrated by two three-minute washes in 70% (v/v) ethanol then two in 100% (v/v) ethanol. Sections were cleared with two three-minute immersions in xylene then mounted using DPX mounting medium (DAKO).

2.2.7.3 Immunohistochemistry

Paraffin embedded sections were dewaxed by immersion in xylene for 3 minutes. Next, sections were hydrated by the following series of three minute incubation steps - twice

in 100% ethanol, twice in 70% (v/v) ethanol and finally twice in water. For antigen retrieval Citrate Buffer (recipe page 75) was pre-heated at full power in a microwave for five minutes, then the sections added and heated for a further ten minutes. Sections were cooled to room temperature then incubated for ten minutes in 1.6% H_20_2/PBS (v/v) and washed in three, three minute PBS washes. Unspecific binding was blocked by 30 minutes room temperature incubation in Blocking Buffer (recipe page 75). The section was then incubated for one hour or overnight in primary antibody (see Table 5). Sections were washed for three times in PBS, for five minutes per wash. Washed sections were incubated with biotin tagged secondary antibodies, diluted in 1% (w/v) BSA/PBS for one hour at room temperature. Next, samples were washed a further three times in PBS, for five minutes each wash and subsequently incubated in diaminobenzidine/H_2O_2 (DAB solution; Biogenex) for three to five minutes. The staining reaction was terminated by washing the sections in ddH_20. If desired, sections were counterstained in Mayer's haemotoxyin for five minutes. The sections were dehydrated by washing twice in 70% (v/v) ethanol then twice in 100% ethanol. Prior to mounting, sections were cleared with two three-minute immersions in xylene then mounted using DPX mounting medium (Raymond A. Lamb).

Some staining protocols did not involve antibody-based staining. For the detection of alkaline phosphatase-positive enterocytes in the intestine, nitro blue tetrazolium (NBT; Roche)/5-bromo-4-chloro-3-indolyl phosphate (BCIP; Roche) solution was employed. The nuclei were counterstained with nuclear fast red (Vector Laboratories). Alcian blue (AB; Sigma)/periodicacid-Schiff (PAS; Sigma) staining specifically marked mucous glycoconjugate-containing goblet cells.

2.2.7.4 In-situ Hybridisation

Paraffin embedded tissue was sectioned at 8 μM then dewaxed by two five minute immersions in xylene. Dewaxed sections were hydrated through a series of five minute washes; twice in 100% ethanol, once in 95% (v/v) ethanol, once in 70% (v/v) ethanol then once in ddH_20. After a PBS wash, slides were incubated in 10 μg/ml proteinase K, diluted in 100 mM Tris-HCl pH7.5/50 mM EDTA at 37^oC for 15 minutes then washed

in 0.2% (w/v) glycine/PBS and fixed in 4% (w/v) PFA for ten minutes. Sections were then washed three times in PBS and incubated in 4xSSC buffer for two minutes (recipe page 80).

Sections were pre-hybridised, without the probes, for one hour in a 57^{o}C humidified chamber in hybridization buffer (recipe page 77). Next, 1 ng/ml probe was added and denatured at 75^{o}C for 15 minutes, then cooled on ice for five minutes before overnight hybridisation at 57^{o}C. The next day the following washes were performed; ten minutes in 60°C 5xSSC, 30 minutes in 60°C 50% (v/v) formamide/2xSSC, 30 minutes in 60^{o}C 2xSSC, twice in 60^{o}C 0.2xSSC for 30 minutes, then five minutes in room temperature maleic buffer and finally in blocking buffer at room temperature for thirty minutes (for recipes see pages 80, 75).

Sections were then incubated at 37^{o}C for two hours in sheep anti-DIG alkaline phosphatase-conjugated antibody (Roche; diluted 1:1000 in blocking buffer). Subsequently, sections were washed twice at room temperature in maleic acid buffer for fifteen minutes then incubated for five minutes in detection buffer. For development, sections were incubated in 1 ml detection buffer (recipe page 75) supplemented with 4.5 µl nitro blue tetrazolium (NBT; Roche) and 3.5 µl 5-bromo-4-chloro-3-indolyl phosphate (BCIP; Roche) in the dark. The reaction was terminated by incubation of the sections in detection buffer, and after one wash in ddH_20 sections were mounted in VectaMountAQ (Vector Laboratories).

The *atmin* in situ hybridisation (ISH) probe was designed and generated by Dr Nnennaya Kanu, and the *olfm4* ISH probe was designed and generated by Dr Markus Diefenbacher.

2.2.8 Statistical Analysis

The Student's unpaired *t*-test was used to assess statistical significance. For survival analysis, the Log Rank Mann Whitney test was used. A *p*-valve of <0.5 was considered statistically significant.

Chapter 3. Investigation of ATMIN function in oxidative stress signalling, telomere dysfunction and intestinal hyperplasia

Mutation in DNA damage repair genes can lead to systemic disorders, with different tissues exhibiting distinct phenotypes. ATM mutation in the brain causes neurodegeneration and ataxia, whereas mutation in the immune system predisposes to cancer. One aim of my PhD was to investigate physiological functions of ATMIN using a range of *in vivo* models.

3.1 ATMIN is required for endogenous DNA damage repair

3.1.1 DNA damage accumulation in ATMIN deficient cells

The *atmin*$^{f/f}$ mouse, generated by Dr Nnennaya Kanu, permits the tissue-specific deletion of ATMIN function (Kanu and Behrens, 2007). LoxP sites flank exon four, which encodes the terminal 601 amino acids of 818 amino acid ATMIN, including the ATM interaction motif, SQTQ motifs and the most C-terminal zinc finger (Figure 16a).

atmin$^{f/f}$ mice were crossed with mice expressing *Cre* recombinase under the control of the 3-phosphoglycerate kinase promoter (PGK-Cre) (Lallemand et al., 1998), achieving germline *atmin* deletion (*atmin*$^{\Delta/\Delta}$). Recombination of the *atmin* locus was confirmed by genotyping PCR of embryonic tail and brain genomic DNA (Figure 16b). Deletion of *atmin* is embryonically lethal at approximately E16.5. Histological analysis of *atmin*$^{\Delta/\Delta}$ embryos at E15.5 shows clear differences. *atmin*$^{\Delta/\Delta}$ embryos are significantly smaller than their littermates, exhibit midbrain exencephaly and craniofacial, heart, and lung defects (Figure 17).

The embryonic lethality of several DNA damage response genes, including BRCA1, is rescued by p53 co-deletion (Xu et al., 2001). I set up *p53*$^{+/-}$; *atmin*$^{\Delta/+}$ breeding pairs to

investigate if a similar rescue occurred with ATMIN. However, in contrast to the predicted frequency (n=12) no *p53*$^{+/-}$; *atmin*$^{\Delta/\Delta}$ or *p53*$^{-/-}$; *atmin*$^{\Delta/\Delta}$ offspring were obtained in over 60 pups, as assessed by genotyping at weaning age (Figure 16c). Hence, p53 deletion does not rescue the *atmin*$^{\Delta/\Delta}$ embryonic lethality. A recently published paper (Jurado et al., 2010) subsequently confirmed this observation.

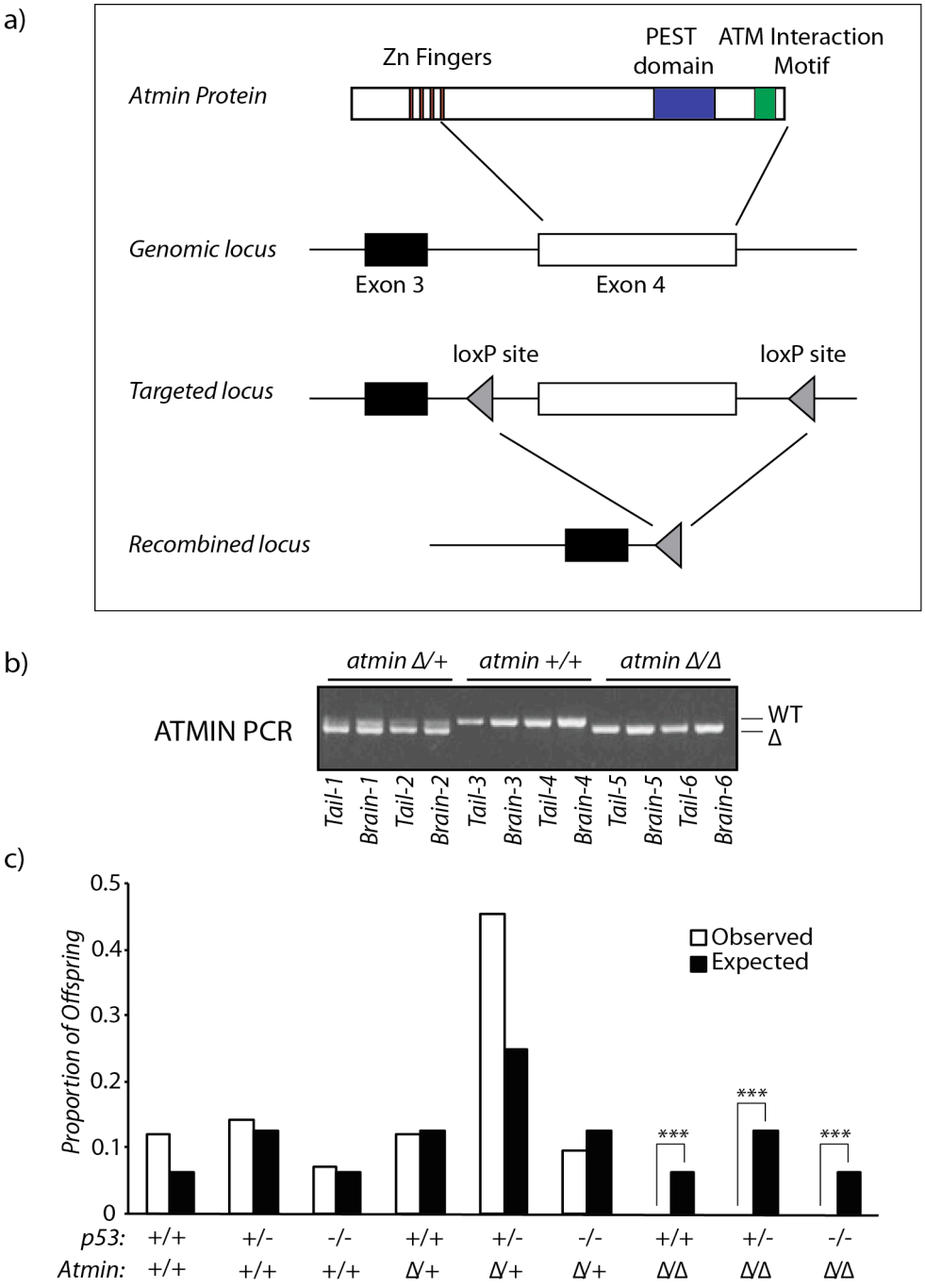

Figure 16: The embryonic lethality of *atmin*$^{\Delta/\Delta}$ is not rescued by p53 co-deletion

a) Schematic of the targeted *atmin* locus. Expression of *Cre* recombinase results in recombination between the loxP sites, i.e. deletion of exon four. b) Genotyping PCR for the *atmin* locus. DNA was extracted from the head and tail of E12.5 embryos. The lower delta (Δ) band indicates *atmin* deletion. c) The expected and observed genotypes, at weaning, of 63 offspring from *atmin*$^{\Delta/+}$*; p53* $^{+/-}$ breeding pairs. Number of offspring per genotype is represented as proportional of total offspring. Student's t-test was used for statistical analysis (****p<0.001*).

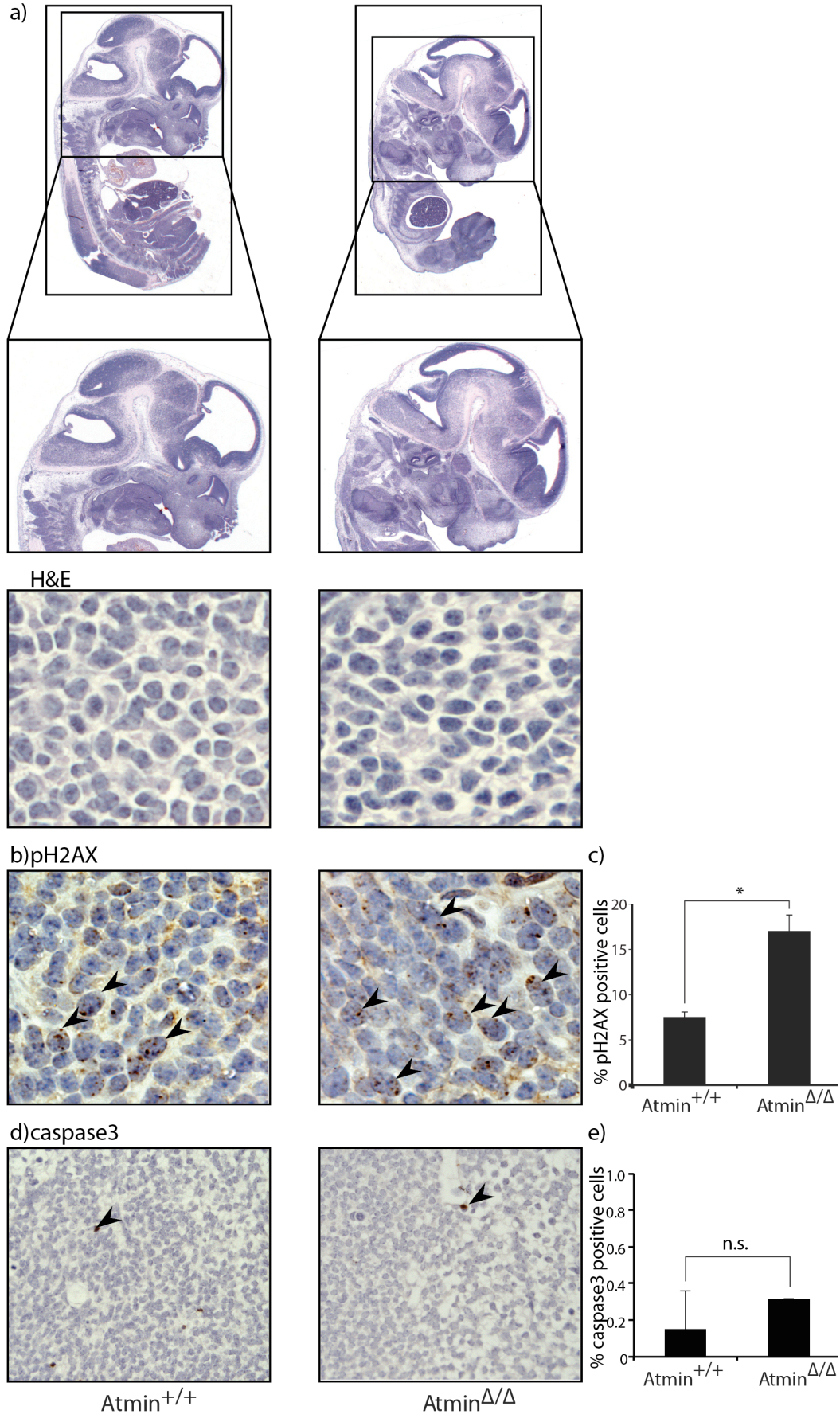
a)
H&E
b)pH2AX
c)
% pH2AX positive cells
20
15
10
5
0
*
Atmin+/+
AtminΔ/Δ
d)caspase3
e)
% caspase3 positive cells
1.0
0.8
0.6
0.4
0.2
0
n.s.
Atmin+/+
AtminΔ/Δ
Atmin+/+
AtminΔ/Δ

Figure 17: Accumulation of DNA damage in *atmin*$^{\Delta/\Delta}$ embryos

a) H&E staining of sagittal E15.5 *atmin*$^{+/+}$ and *atmin*$^{\Delta/\Delta}$ sections, and a higher-magnification image of the brain. b) Representative images of E15.5 hindbrains immunostained for pH2AX. Arrows indicate cells containing pH2AX foci. c) Quantification of (b); specifically of cells containing three or more pH2AX foci; n=3 embryos. d) Representative caspase-3 staining in the hindbrains of E15.5 embryos. Arrows indicate caspase-3 positive cells. e) Quantification of (d); n=3 embryos. Student's t-test was used for statistical analysis (*$p<0.05$).

ATMIN interacts with the DNA damage kinase ATM, so we postulated ATMIN contributes to the repair of endogenous DNA damage. I quantified pH2AX foci in the hindbrain of *atmin*$^{\Delta/\Delta}$ E15.5 embryos. At this developmental stage the smaller embryo size and neural defects of *atmin*$^{\Delta/\Delta}$ are evident, yet embryos are viable (Figure 17a). The hindbrains of E15.5 control *atmin*$^{+/+}$ embryos had an average of 7.5% cells containing pH2AX foci. Conversely, *atmin*$^{\Delta/\Delta}$ embryos had over double the wildtype level of DNA damage, with 17.0% *atmin*$^{\Delta/\Delta}$ cells positive for pH2AX (Figure 17b, c). I next examined the extent of cell death in the hindbrain of E15.5 embryos by quantifying cells positive for the apoptotic marker caspase-3. Interestingly, *atmin*$^{\Delta/\Delta}$ embryos do not have a higher proportion of apoptotic cells compared to *atmin*$^{+/+}$embryos (Figure 17d, e). Indeed, both genotypes had fewer than 0.5% caspase positive cells. Therefore, the elevated DNA damage in *atmin*$^{\Delta/\Delta}$ embryos does not correlate with increased cell death, and is thus unlikely to be the sole cause of *atmin*$^{\Delta/\Delta}$ embryonic lethality.

To further investigate the impact of ATMIN loss on endogenous DNA damage levels, I generated *atmin*$^{\Delta/\Delta}$ and littermate *atmin*$^{+/+}$ control MEFs. Primary MEFs were cultured for four passages at either physiological (3%) or atmospheric (20%) oxygen levels then stained for the DNA damage markers pS1987-ATM and pH2AX. After four passages at 20% 0_2, 62% of *atmin*$^{\Delta/\Delta}$ cells contained pH2AX foci - in contrast to just 38% of control (*atmin*$^{+/+}$) cells. There was no significant difference between pH2AX positive cells in passage two *atmin*$^{\Delta/\Delta}$ and *atmin*$^{\Delta/\Delta}$ MEFs. Thus it is evident *atmin*$^{\Delta/\Delta}$ MEFs accumulate more DNA damage over time than *atmin*$^{+/+}$ MEFs (Figure 18b, c).

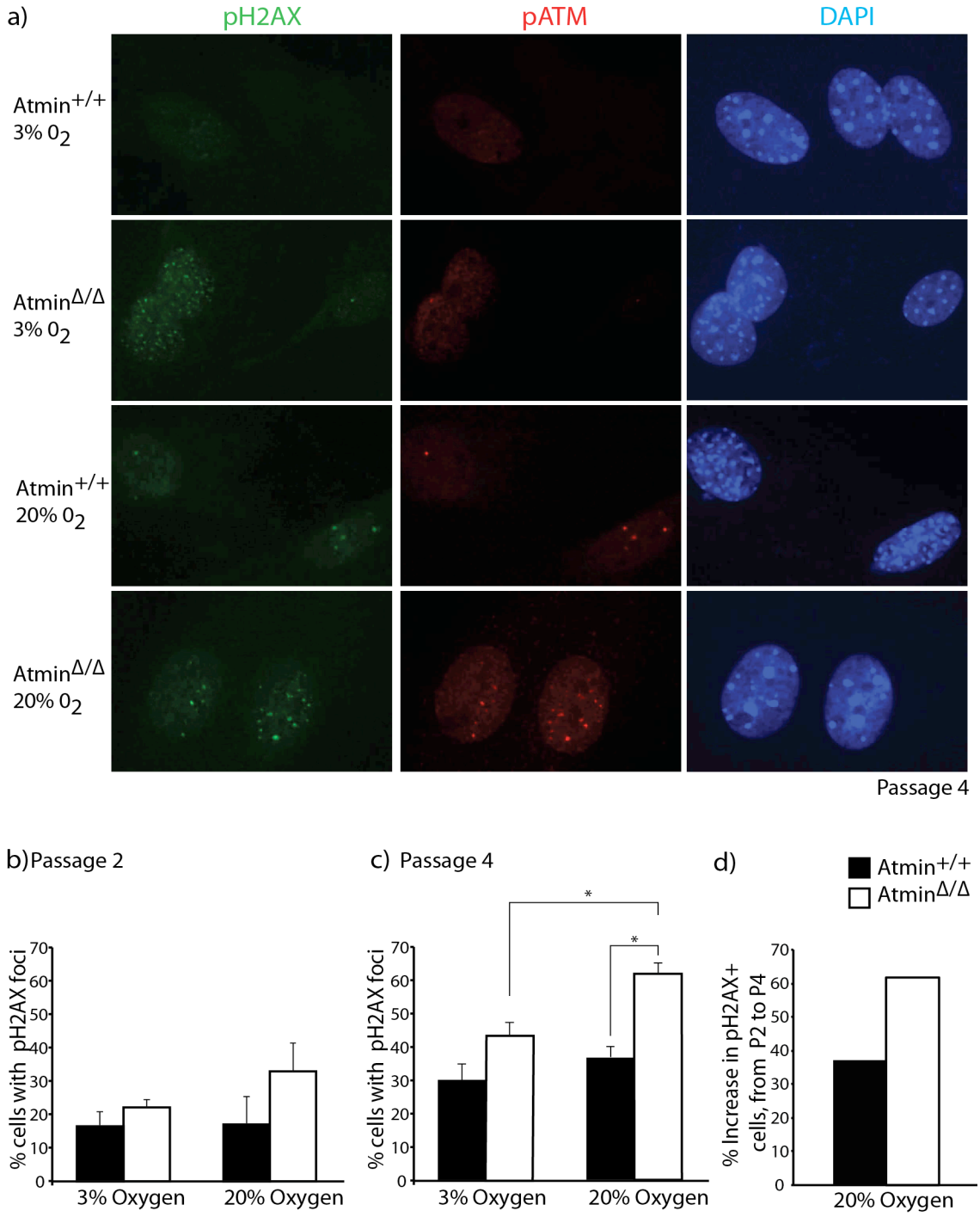

Figure 18: High levels of endogenous DNA damage in *atmin*$^{\Delta/\Delta}$ MEFs

atmin$^{+/+}$ and *atmin*$^{\Delta/\Delta}$ MEFs were cultured at either 3% or 20% oxygen for four passages, then fixed and immunofluorescently co-stained for pH2AX and pS1987-ATM. (a) Representative images of *atmin*$^{+/+}$ and *atmin*$^{\Delta/\Delta}$ cells at passage four. Quantification of *atmin*$^{+/+}$ and *atmin*$^{\Delta/\Delta}$ cells with pH2AX foci at (b) passage two and (c) passage four. (d) The percentage change in the proportion of pH2AX positive cells at passage four compared to passage two, for cells cultured at 20% oxygen. In all quantifications cells are considered positive if they have three or more foci. Student's t-test was used for statistical analysis (*$p<0.05$).

In both *atmin*$^{\Delta/\Delta}$ and *atmin*$^{+/+}$ MEFs cultured at 20% 0_2 DNA damage increased from P2 to P4 (as measured by pH2AX foci). However, *atmin*$^{\Delta/\Delta}$ cells exhibit a greater proportional increase in DNA damage than their *atmin*$^{+/+}$ counterparts; a 62% increase in pH2AX positive cells compared to the 37% increase of the wildtype population (Figure 18d). Moreover, after four passages *atmin*$^{\Delta/\Delta}$ MEFs cultured at high (20%) oxygen had accumulated more pH2AX positive cells than *atmin*$^{\Delta/\Delta}$ MEFs cultured at low (3%) oxygen. This suggests that *atmin* loss sensitises cells to oxidative stress induced DNA damage.

The two simplest models for the elevated DNA damage in *atmin*$^{\Delta/\Delta}$ cells are either increased DNA damage incidence, or reduced DNA repair. To distinguish between these two possibilities I immunofluorescently co-stained P4 *atmin*$^{+/+}$and *atmin*$^{\Delta/\Delta}$ MEFs for pS1987-ATM and pH2AX (Figure 19a). Although there is no significant difference between the average number of pS1987-ATM foci per cell (Figure 19b), *atmin*$^{\Delta/\Delta}$ MEFs have an average of 4.1 pH2AX foci per cell, significantly higher that the *atmin*$^{\Delta/\Delta}$ average of 1.18 pS1987-ATM foci per cell (Figure 19c). The disparity between pH2AX and pS1987-ATM foci number in *atmin*$^{\Delta/\Delta}$ cells is explained by the observation pS1987-ATM was not recruited to pH2AX in 35% of cells (Figure 19d). The same phenotype - pH2AX foci that do not co-localise with pS1987-ATM - is also observed in *atmin*$^{f/f}$ MEFs after Adeno-Cre mediated *atmin* deletion (Figure 19e). Given pS1987-ATM foci number is unaltered in *atmin*$^{\Delta/\Delta}$ cells, this suggests compromised ATM recruitment, or retention, to sites of DNA damage in ATMIN deficient cells. This implies that loss of ATMIN is detrimental to DNA repair, and *atmin*$^{\Delta/\Delta}$ cells have a reduced rate of DNA repair.

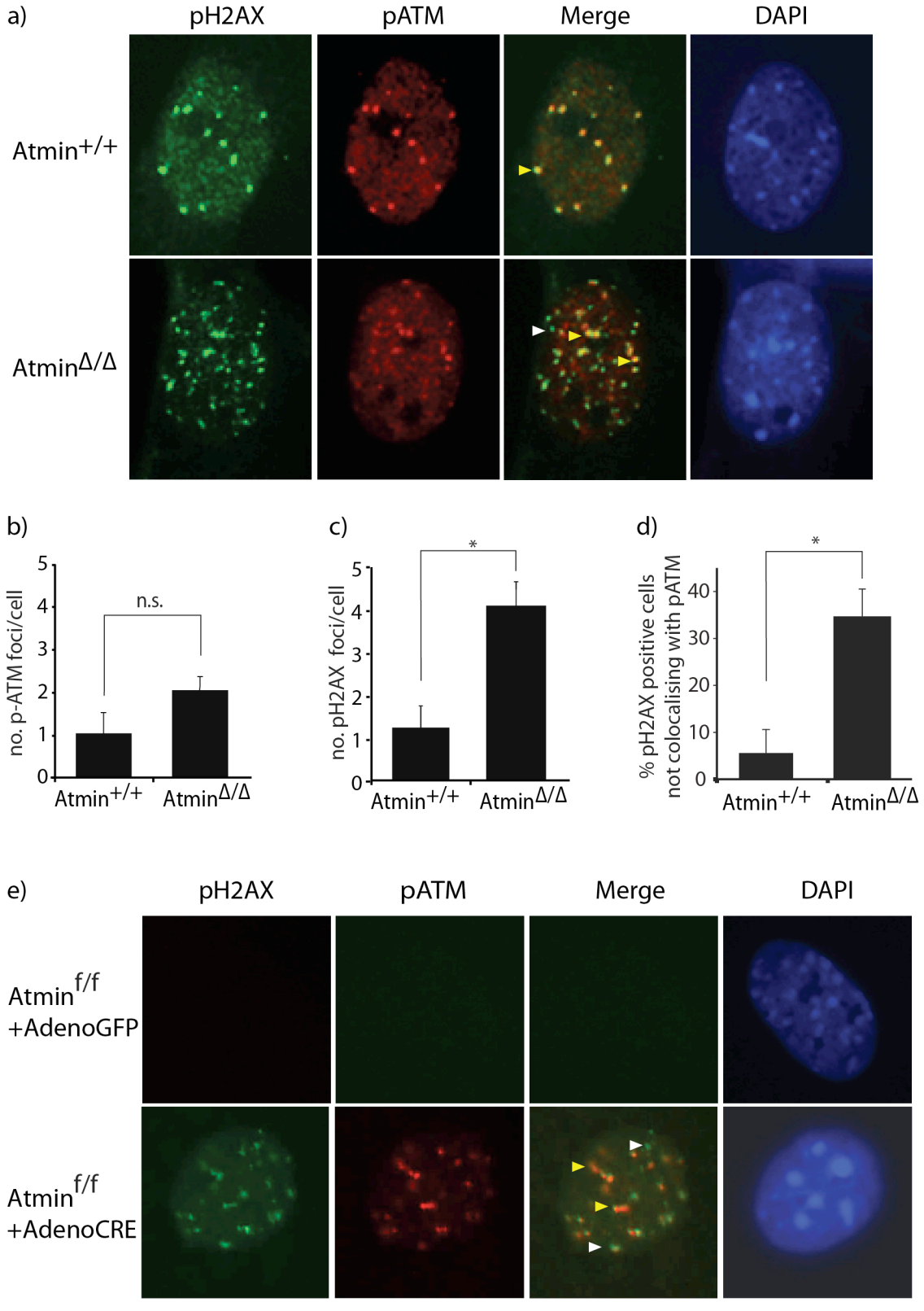

Figure 19: Reduced pS1987-ATM and pH2AX co-localisation in *atmin*$^{\Delta/\Delta}$ MEFs

a) Representative images of *atmin*$^{+/+}$ and *atmin*$^{\Delta/\Delta}$ MEFs cultured at 20% oxygen for four passages then immunofluorescently co-stained for pH2AX and p1987-ATM.

Yellow arrows indicate co-localisation between pH2AX and p1987-ATM. White arrows indicate pH2AX foci that do not co-localise with p1987-ATM. Quantification of the number of (b) p1987-ATM and (c) pH2AX foci per cell. d) Quantification of the percentage of cells with pH2AX foci that do not co-localise with p1987-ATM. e) *atmin*$^{f/f}$ MEFs cultured at 20% oxygen were infected with Adeno-GFP or Adeno-Cre (yielding *atmin*$^{\Delta/\Delta}$ cells) at passage two, then stained for pH2AX and p1987-ATM at passage four. A minimum of 100 cells was counted per experiment and three independent experiments were performed. Student's t-test was used for statistical analysis (*$p<0.05$).

3.1.2 *atmin*$^{\Delta/\Delta}$ MEFs undergo oxidative stress dependent premature senescence

Given ATMIN deletion correlates with increased endogenous DNA damage, I wanted to investigate if its loss impaired cellular proliferation. In collaboration with Dr Nnennaya Kanu *atmin*$^{\Delta/\Delta}$ and *atmin*$^{+/+}$ proliferation potentials were assessed by growth curve analysis. There is no significant difference between *atmin*$^{\Delta/\Delta}$ and *atmin*$^{+/+}$MEFs proliferation at early passage (P2), irrespective of oxygen concentration (Figure 20a). However, at later passage (P4) *atmin*$^{\Delta/\Delta}$ MEFs have reduced proliferation compared to *atmin*$^{+/+}$ MEFs (Figure 20b). Thus as well as increasing endogenous DNA damage, ATMIN deletion hinders proliferation.

Persistent DNA damage can activate senescence programmes. Given *atmin*$^{\Delta/\Delta}$ MEFs display sensitivity to oxidative stress and accumulate endogenous DNA damage, one would predict a higher senescence incidence in *atmin*$^{\Delta/\Delta}$ compared to *atmin*$^{+/+}$MEFs. To test this, in collaboration in Dr Nnennaya Kanu early (P1) and late (P4) passage MEFs were stained for senescence associated β-galactosidase activity (Figure 20c, d). At early passage (P1) *atmin*$^{\Delta/\Delta}$ cells do not have a significantly higher percentage of senescent cells compared to *atmin*$^{+/+}$ MEFs, whether grown at high (20%) or low (3%) oxygen culture conditions (Figure 20e). Conversely, 48% of high oxygen late passage *atmin*$^{\Delta/\Delta}$ MEFs are senescent - significantly higher than the 14% senescent *atmin*$^{+/+}$cells (Figure 20d). Thus senescence induction in *atmin*$^{\Delta/\Delta}$ MEFs can be rescued by either low (3%) oxygen conditions or by addition of the free radical scavenger N-acetyl-cysteine (NAC) (Dr Nnennaya Kanu, personal communication). Consequently, the premature senescence of *atmin*$^{\Delta/\Delta}$ MEFs is at least partially due to oxidative stress.

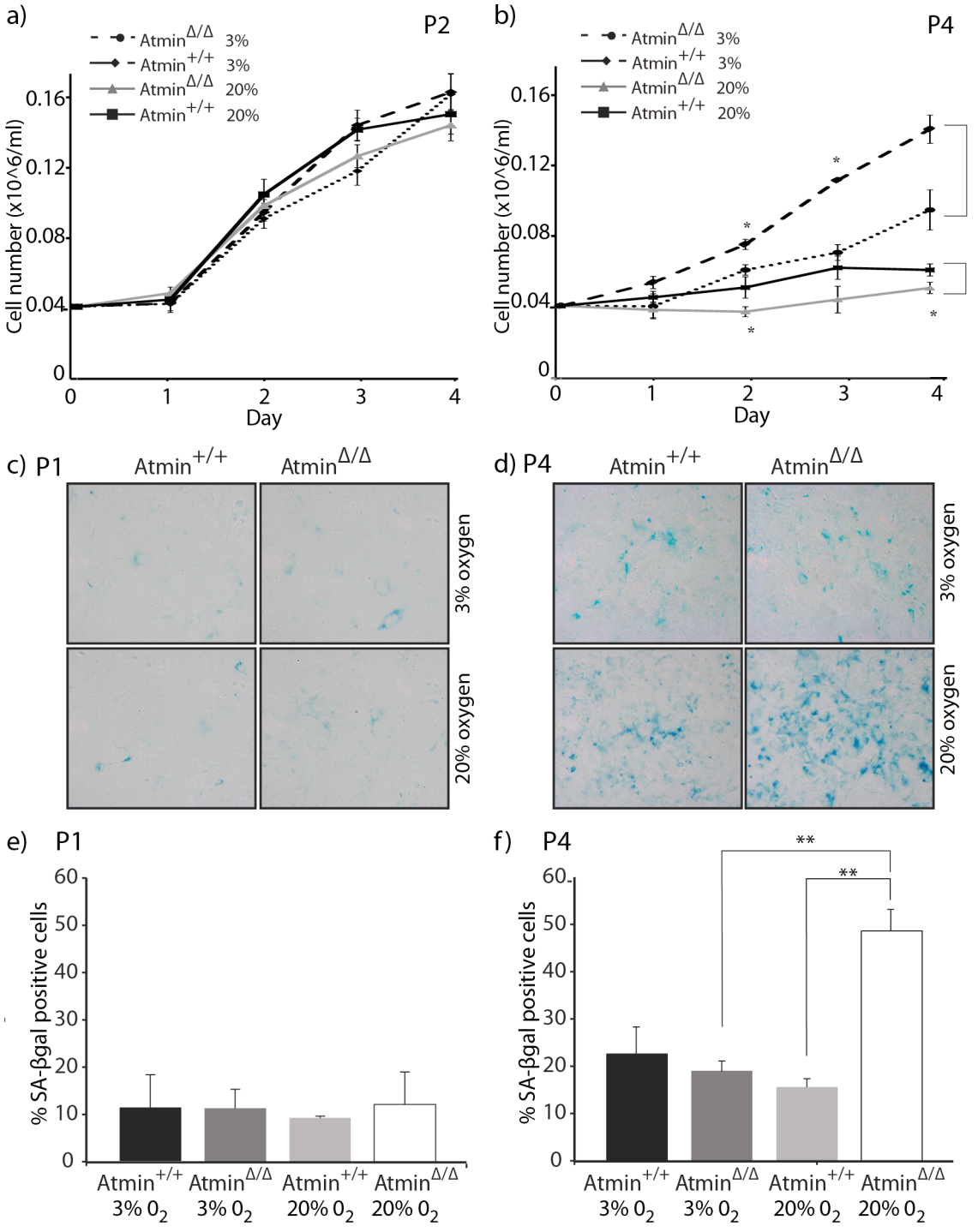

Figure 20: ATMIN deficient cells undergo premature senescence upon oxidative stress

$0.04x10^6$ a) passage two and b) passage four *atmin*$^{+/+}$ and *atmin*$^{\Delta/\Delta}$ cells were plated and viable cell number counted in triplicate each day for four days. Representative photos of *atmin*$^{+/+}$ and *atmin*$^{\Delta/\Delta}$ cells cultured at 3% or 20% oxygen, then stained for senescence associated β-galactosidase activity at c) passage one and d) passage four. e) Quantification of (c). f) Quantification of (d). Student's t-test was used for statistical analysis (*$p<0.05$, **$p<0.01$). Experiments were performed in collaboration with Nnennaya Kanu.

3.2 ATMIN is required for telomere maintenance

The increased incidence of pH2AX foci without co-localised pS1987-ATM observed in *atmin*$^{\Delta/\Delta}$ MEFs is reminiscent of damaged telomeres. As ATM is recruited to damaged telomeres, it was reasonable to assume ATM's co-factor ATMIN may also have a role at the telomere. To study a potential function for ATMIN at the telomere, we first wanted to examine the telomeres in ATMIN deficient cells.

3.2.1 ATMIN is required to suppress DNA damage at the telomere

Telomeres consist of thousands of 'TTAGGG' nucleotide repeats at the ends of chromosomes. A telomeric FISH probe against this sequence can be used to detect the location of telomeres, on either interphase cells or metaphase spreads. If performed in parallel with immunofluorescent staining for pH2AX, it is possible to determine if pH2AX foci are located at telomeric or intra-chromosomal regions. To elucidate a possible function for ATMIN at the telomere, I acutely inactivated ATMIN function by Adenoviral mediated infection of early passage *atmin*$^{f/f}$ primary MEFs with Adeno-*Cre* virus, yielding *atmin*$^{\Delta/\Delta}$ MEFs (see page 163).

In collaboration with Tony Cesare and Jan Karlseder (Salk Institute, U.S.A.) IF-FISH for pH2AX and telomeric DNA was performed on interphase spreads from *atmin*$^{\Delta/\Delta}$ and control *atmin*$^{f/f}$ passage 4 primary MEFs (Figure 21a, b). Cells were maintained at low (3%) oxygen to minimise oxidative damage. Excitingly, this revealed an increase in the percentage chromosome ends co-localising with pH2AX (Figure 21c). Accordingly, the number of pH2AX positive telomeres per cell was significantly increased (Figure 21d). To exclude the possibility this was because loss of ATMIN increased chromosomal copy number, and thus the number of chromosome ends, the number of pH2AX positive telomeres was normalised to chromosome number (Figure 21e). Deletion of *atmin* increases the proportion of telomeres that co-localise with pH2AX, suggesting ATMIN is required to suppress DNA damage at telomeres.

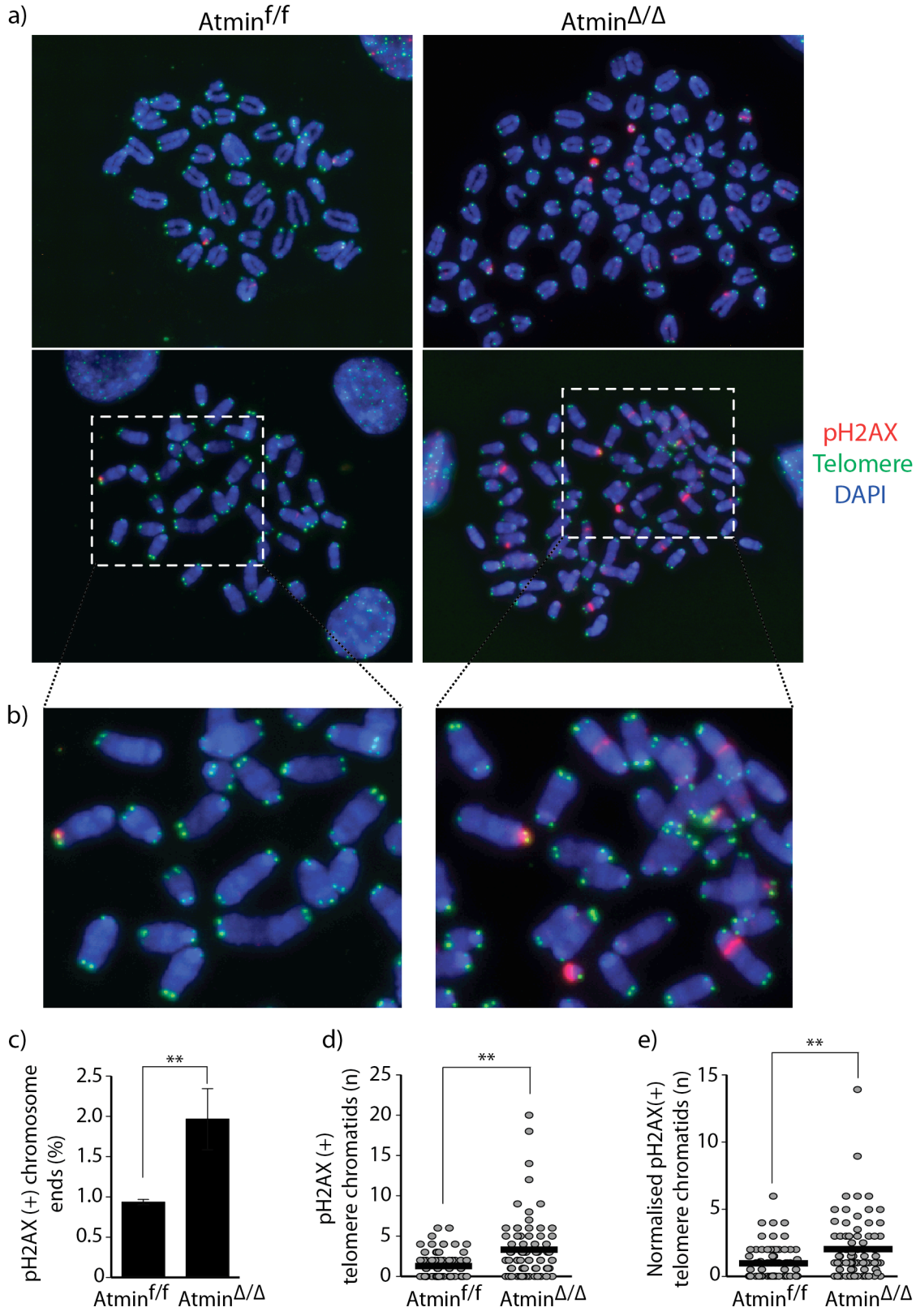

Figure 21: **ATMIN deficient cells have increased telomeric DNA damage**

a, b) Passage one *atmin*$^{f/f}$ primary MEFS were infected with either Adeno-GFP or AdenoCre-GFP yielding *atmin*$^{f/f}$ and *atmin*$^{\Delta/\Delta}$ MEFS. Metaphase spreads were prepared

from P4 MEFs cultured at 3% 0_2 and IF-FISH for telomeric repeats (green) and pH2AX (red) was performed. Representative images are shown. c) The percentage of chromosome ends co-localising with pH2AX. d) Average number of telomeric ends co-localising with pH2AX per metaphase spread, each dot represents a single metaphase. e) Average number of telomeric ends co-localising with pH2AX per metaphase spread, normalised to total chromosome number. Each dot represents a single metaphase. Three independent experiments were performed and a minimum of 25 metaphases quantified per experiment. Student's t-test was used for statistical analysis (**$p<0.01$). Metaphase spreads were performed and quantitated by Dr Tony Cesare.

3.2.2 Telomere dysfunction and ATMIN deficiency compromise neural stem cell function

Each round of chromosome replication leads to telomere shortening. Telomeres can be extended by the enzyme telomerase. Unless the shorter chromosome ends are 'filled-in' multiple rounds of cell replication leads to critically short telomeres, activation of the DNA damage response and premature senescence and proliferation arrest. Telomerase deficient mice (*terc*$^{-/-}$) are characterised by premature ageing, shorter telomeres and genomic instability (Rudolph et al., 1999).

Late generation *atm*$^{-/-}$; *terc*$^{-/-}$ compound mutants exhibit a more deleterious phenotype than the *terc*$^{-/-}$ mutant, including an impaired neural stem cell (NSC) compartment (Wong et al., 2003). Therefore interplay between ATMIN and telomerase *in vivo* was studied in the neuronal lineage. I generated cohorts of *atmin*$^{f/f}$; *terc*$^{-/-}$; *Nestin-Cre* mice. *Nestin-Cre* is expressed in neural stem cells, thus *atmin* is specifically deleted in the neural lineage yielding *atmin*$^{\Delta N/\Delta N}$; *terc*$^{-/-}$ animals. Neuronal *atmin* deletion in *atmin*$^{f/f}$; *Nestin-Cre* mice was confirmed by *atmin* ISH in three month old mice (Figure 22a). Murine telomeres are up to 20kB long, far longer than human telomeres. Consequently, *terc*$^{-/-}$ mice show a severity of phenotype that correlates with generation number. For this study starting generation (G0; *atmin*$^{f/f}$; *terc*$^{+/-}$; *Nestin-Cre*), first generation (G1; *atmin*$^{f/f}$; *terc*$^{-/-}$; *Nestin-Cre*) and third generation (G3; *atmin*$^{f/f}$; *terc*$^{-/-}$; *Nestin-Cre*) animals were primarily studied.

The original description of the *terc*$^{-/-}$ mouse characterised reduced fertility and reduced lifespan in late generation mutants (Rudolph et al., 1999). Accordingly, the litter sizes from *atmin*$^{\Delta N/\Delta N}$; *terc*$^{-/-}$ correlated inversely with generation number (Figure 22b). The survival of G3 *atmin*$^{\Delta N/\Delta N}$ *terc*$^{-/-}$ and G3 *atmin*$^{f/f}$ *terc*$^{-/-}$ littermates was monitored to establish if *atmin* deletion further reduced the lifespan of G3 *terc*$^{-/-}$ mutants. Although neuronal *atmin* deletion also reduces average lifespan (Kanu et al., 2010), there was no difference in age of death of the compound mutant (Figure 22b). Thus there is no combinational effect of *atmin* and *telomerase* deletion on lifespan.

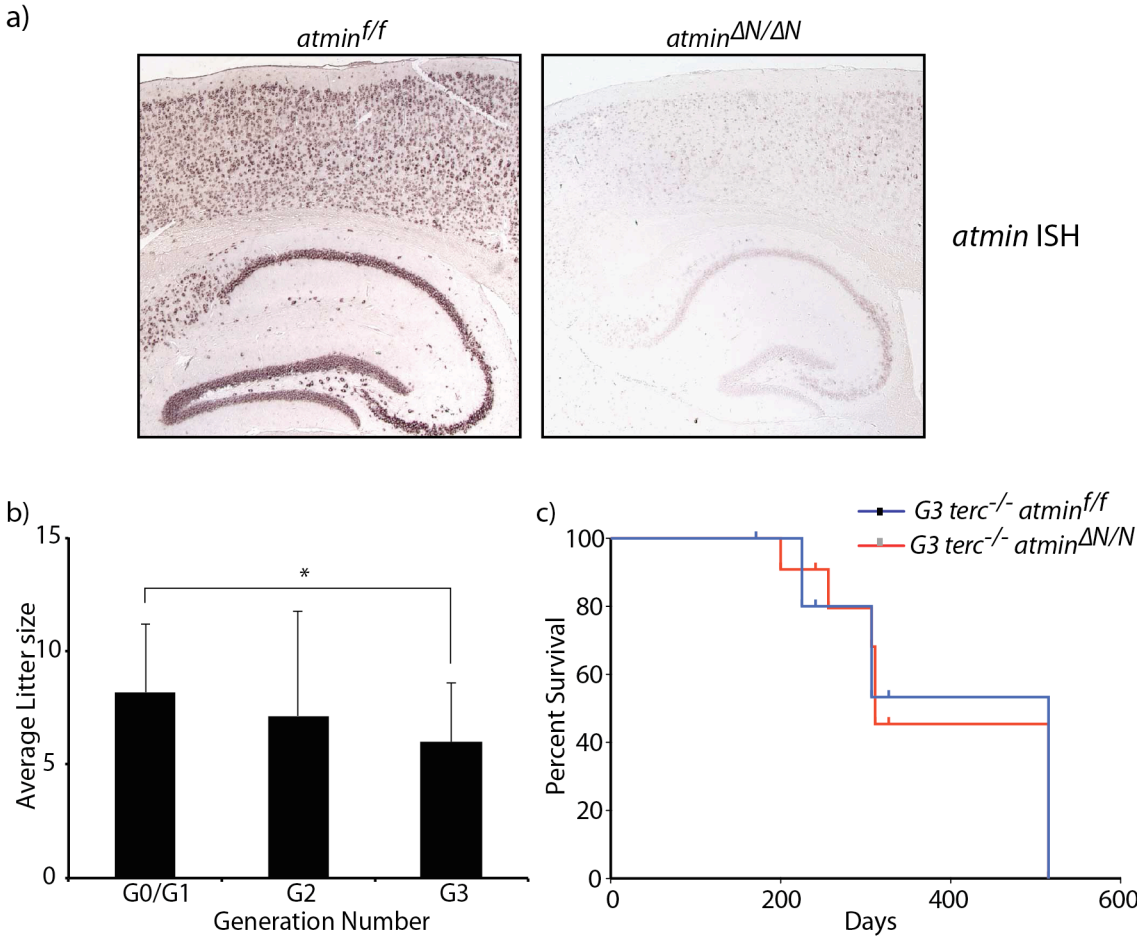

Figure 22: Telomerase loss does not alter the lifespan of *atmin*$^{\Delta N/\Delta N}$ mice

a) Representative images of ISH for *atmin* in the brains of three month old mice. b) Average litter size from *atmin*$^{f/f}$ *terc*$^{-/-}$ and *atmin*$^{f/f}$ *terc*$^{-/-}$ *Nestin-Cre* breeding pairs of the indicated generation (n>10). Note G0/G1 offspring arise from breeding *atmin*$^{f/f}$ *terc*$^{+/-}$ to *atmin*$^{f/f}$ *terc*$^{+/-}$ *Nestin-Cre* mice. c) Survival analysis of G3 and *atmin*$^{f/f}$ *terc*$^{-/-}$(n=14) and *atmin*$^{f/f}$ *terc*$^{-/-}$ *Nestin-Cre* (n=8) animals. Student's t-test was used for statistical analysis (*p<0.05).

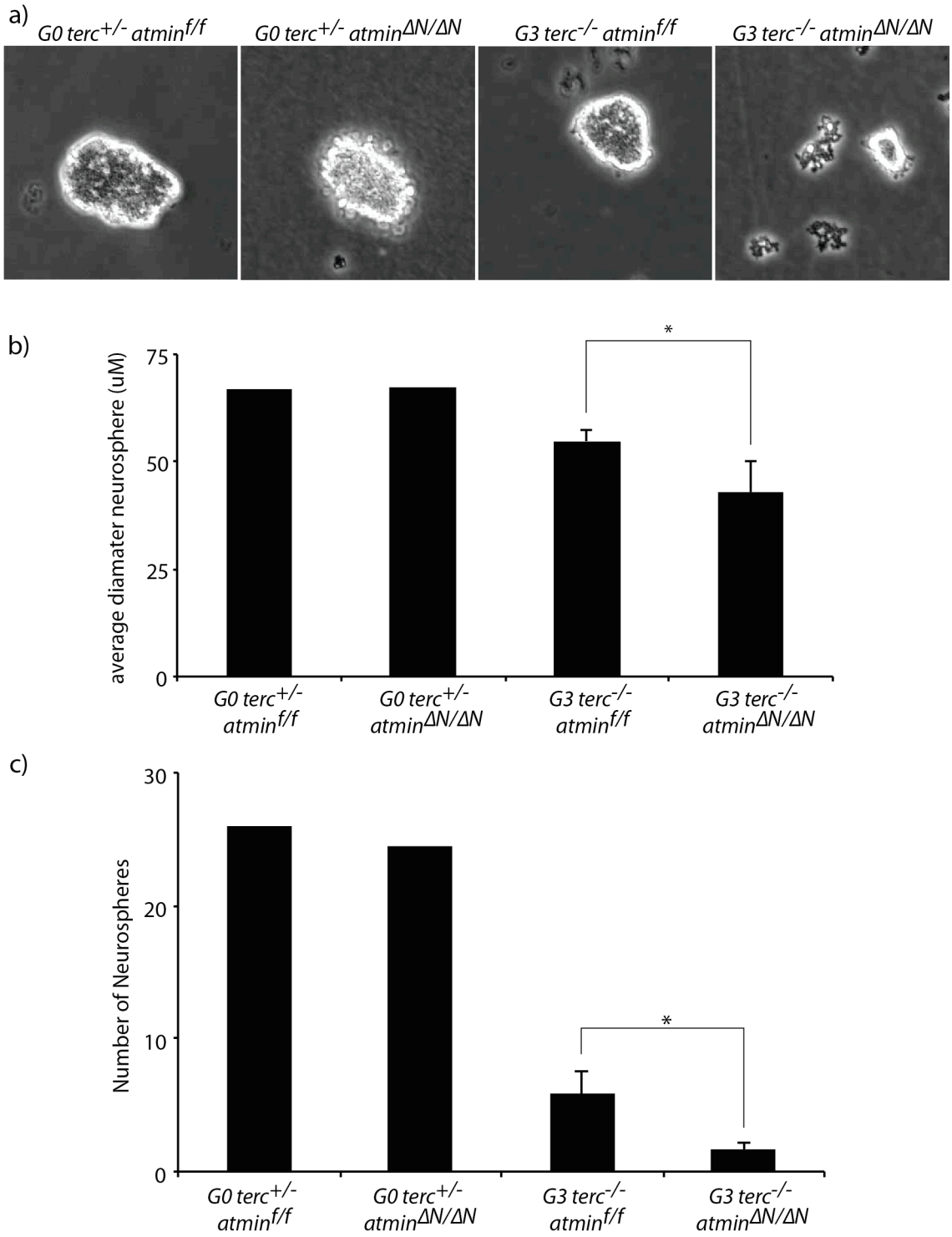

Figure 23: ATMIN deficiency impairs the self-renewal and growth of telomerase null NSCs

a) Representative images of NSCs ten days after isolation, prior to passaging. b) Quantification of neurosphere diameter, as shown in (a). At least 50 neurospheres were counted per culture per experiment. c) Number of neurosphere formed one week after plating 100 cells. Student's t-test was used for statistical analysis (*$p<0.05$).

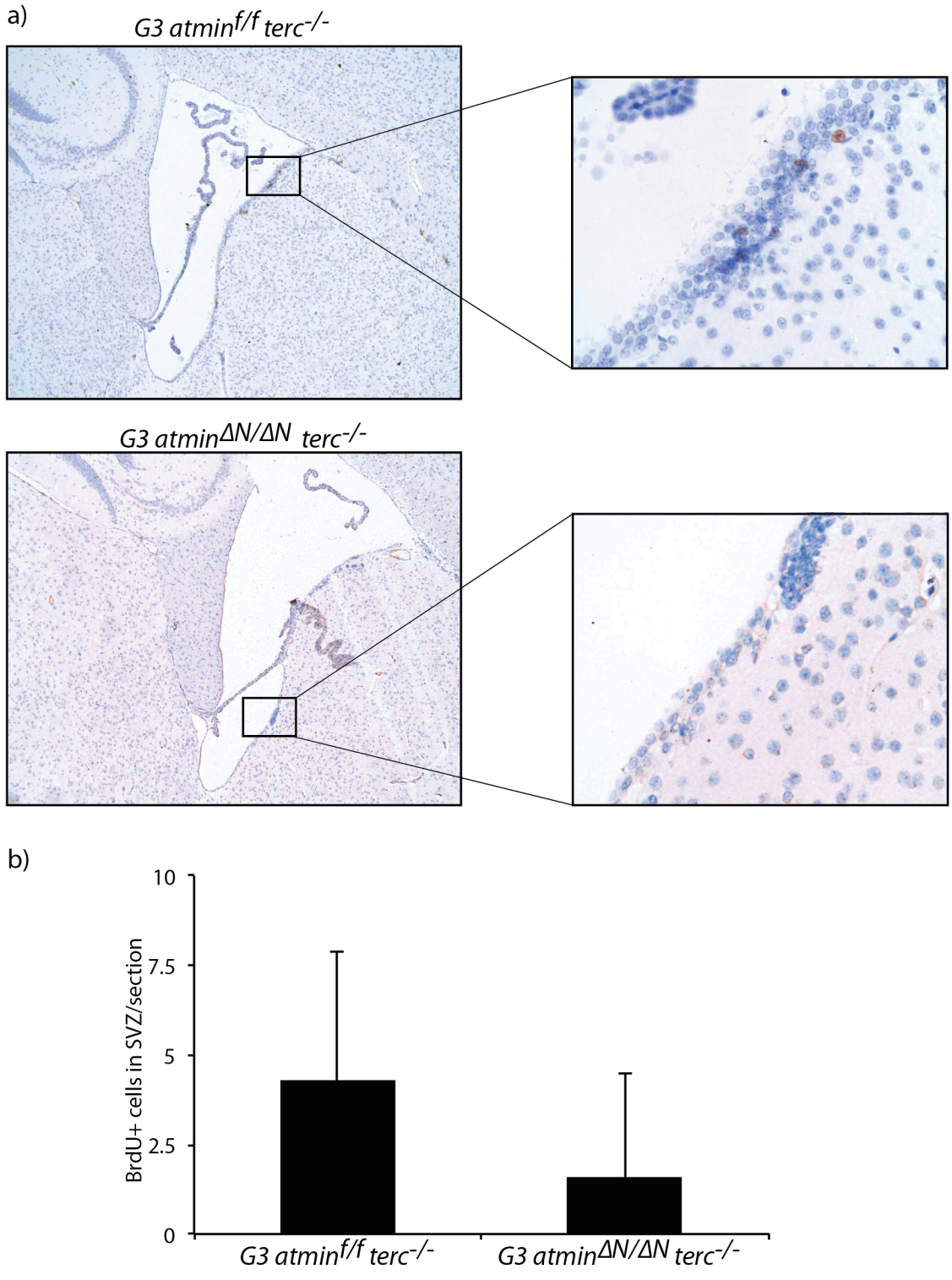

Figure 24: Reduced NSC number in the brains of *atmin*$^{\Delta N/\Delta N}$ *terc*$^{-/-}$ mice

a) Representative images of BrdU immunohistochemistry in the SVZ of mice injected with BrdU 90 minutes prior to cull. b) Quantification of the number of BrdU positive cells per section in the SVZ. At least 15 slides were counted per mouse; two mice per genotype.

To study the role of *atmin* at critically short telomeres I isolated adult neural stem cells from the subventricular zone (SVZ) of aged *atmin*$^{f/f}$ *terc*$^{-/-}$ and *atmin*$^{\Delta N/\Delta N}$ *terc*$^{-/-}$ littermates. It was immediately apparent from the adult neurosphere cultures that dual *atmin* and *telomerase* ablation led to reduced proliferation potential. Indeed, very few G3 *atmin*$^{\Delta N/\Delta N}$ *terc*$^{-/-}$ neurospheres formed after the first passage and virtually none after the second passage. To characterise this defect, I measured the size of primary neurospheres ten days after neural stem cell isolation. As expected, neurospheres from G3 *atmin*$^{f/f}$ *terc*$^{-/-}$ mice were smaller that those from G0 (Figure 23a, b). Additionally, G3 *atmin*$^{\Delta N/\Delta N}$ *terc*$^{-/-}$ neurospheres were significantly smaller their G3 *atmin*$^{f/f}$ *terc*$^{-/-}$ counterparts (Figure 23a, b). To assess self-renewal capacity, neurospheres were dissociated into single cells, counted and plated by serial dilution. The late generation genotypes formed significantly fewer secondary neurospheres that the G0 cultures (Figure 23c). Again, the defect was exacerbated in the G3 *atmin*$^{\Delta N/\Delta N}$ *terc*$^{-/-}$ mutants compared to G3 *atmin*$^{f/f}$ *terc*$^{-/-}$, with the double mutant cells forming significantly fewer secondary spheres. This demonstrates *atmin* loss reduces the self-renewal capacity and proliferative potential of late generation *terc*$^{-/-}$ mutants.

The majority of cells in the adult brain are post-mitotic. As they are not proliferative, they do not experience replication-dependent telomere shortening. In contrast, adult neural stem cells undergo cell division and thus can be specifically labelled by a short BrdU pulse. Quantification of the BrdU^{+} stem cells in the SVZ of adult mice revealed a reduction in the stem cell pool of G3 *atmin*$^{\Delta N/\Delta N}$ *terc*$^{-/-}$ compared to G3 *atmin*$^{f/f}$ *terc*$^{-/-}$ littermate controls (Figure 24a, b). Together, this suggests ATMIN and telomerase co-operate in telomere maintenance, and loss of ATMIN in the context of shortened telomeres is deleterious for the cell

3.3 ATMIN is not part of the oncogene induced senescence barrier in intestinal serrated hyperplasia

Intestinal epithelial cell specific expression of the oncogene *KRas*^{G12D} induces colonic serrated hyperplasia, characterised by senescence induction (Bennecke et al., 2010). However, there is an extremely low frequency of progression to carcinoma. Conversely, if *KRas*^{G12D} is expressed in animals with compromised senescence pathways, such as the *INK4a/Arf*$^{-/-}$ model, 50% of animals develop adenomas of the colon within 12 weeks (Bennecke et al., 2010). As ATM has been shown to be part of the OIS barrier (Bartkova et al., 2005; Bartkova et al., 2006), it was interesting to investigate if loss of ATMIN or ATM impacted on *KRas*^{G12D} induced intestinal tumourigenesis.

3.3.1 Intestinal *KRas*^{G12D} expression promotes hyperplasia, DNA damage and senescence

The initial strategy to investigate ATMIN's role in OIS was to generate *atmin*$^{f/f}$*; LSL-KRas*^{G12D}*; Villin-Cre* animals. Villin-Cre mice express *Cre* recombinase from the *villin* promoter, active in intestinal tissues from E12.5 onwards (Madison et al., 2002). The *LSL-KRas*^{G12D} locus has a transcriptional stop site flanked by two loxP sites (LSL), so *KRas*^{G12D} is only transcribed after *Cre* recombinase mediated excision of the LSL cassette. An advantage of the system is after recombination *KRas*^{G12D} is under the control of its endogenous promoter. The use of *atmin*$^{f/f}$ ensured concomitant *atmin* deletion and *KRas*^{G12D} expression. ATMIN deletion was confirmed by genotyping PCR from villi and crypts isolated from the small bowel and colon (Figure 25a). *KRas*^{G12D} expression was confirmed by analysing protein lysates isolated from murine colon for the phosphorylation of ERK (pT202/pY204-ERK), a downstream substrate of *KRas* (Figure 25b). Phosphorylation of ERK along the length of the villi and crypt was also assessed by immunohistochemical staining for pT202/pY204-ERK (Figure 25c). Thus *Villin-Cre* is an effective system for achieving simultaneous intestinal *atmin* deletion and *KRas*^{G12D} expression.

Mice deleted for *atmin* in the intestine (*atmin*$^{\Delta G/\Delta G}$) have normal intestinal architecture (Figure 26b), and animals aged to one year have no overt phenotype. Mice were culled at seven weeks for initial analysis of *KRas*^{G12D} expression. H&E staining confirmed intestinal KRas^{G12D} expression induced hyperplasia, and the colons of mice expressing *KRas*^{G12D} contained serrated hyperplastic villi of a characteristic '*Christmas-tree structure*' (Figure 26c, d).

To assess the effect of *KRas*^{G12D} on proliferation in the colon, mice were injected with BrdU 90 minutes prior to cull (Figure 27a). The percentage of BrdU positive cells per crypt was counted, and there was no significant difference between the proliferation of *atmin*$^{f/f}$, *atmin*$^{\Delta G/\Delta G}$, *KRas*^{G12D} and *atmin*$^{\Delta G/\Delta G}$; *KRas*^{G12D} colonic crypts. Wildtype proliferation rates in the colons of *KRas*^{G12D} mice recapitulates observations in the original paper (Bennecke et al., 2010). The BrdU analysis demonstrated ATMIN deletion does not affect proliferation of *KRas*^{G12D} expressing cells in the colon.

One prediction of the OIS model is aberrant oncogene expression increases cellular DNA damage (Bartkova et al., 2005). I therefore assessed by the levels of the DNA damage marker pH2AX in the intestines of seven week old *wildtype*, *atmin*$^{\Delta G/\Delta G}$, *KRas*^{G12D} and *atmin*$^{\Delta G/\Delta G}$ *KRas*^{G12D} mice (Figure 27c). As expected, *KRas*^{G12D} expression correlates with increased pH2AX (Figure 27d). However, ATMIN deletion did not further increase the extent of DNA damage in *KRas*^{G12D} expressing cells.

The aim of this tumour model was to establish if ATMIN is required for senescence induction in oncogene expressing cells, so it was important to assess senescence *in vivo.* The senescence marker p21 is frequently upregulated in senescent cells. Indeed, by western blot analysis of intestinal tissue it is evident p21 protein levels increase upon *KRas*^{G12D} expression (Figure 27e, lane 3). However, *KRas*^{G12D} mediated upregulation of p21 was abrogated in *atmin* deficient cells (Figure 27e, lane 4). Interestingly, p21 protein levels are decreased in *atmin*$^{\Delta G/\Delta G}$ cells, compared to *atmin*$^{f/f}$, littermate controls. High p21 protein levels are associated with, but not sufficient to conclude, senescence. Therefore I also looked at the transcriptional levels of the senescence marker Dec1 (Collado et al., 2005), (Qian et al., 2008). As seen previously (Bennecke et al., 2010), intestinal *KRas*^{G12D} expression results in an approximately two fold increase in Dec1

expression (Figure 27f). Dec1 transcriptional upregulation upon *KRas*^{G12D} expression also occurs in the absence of ATMIN (Figure 27f). Thus although p21 is not upregulated in *atmin*$^{\Delta G/\Delta G}$*; KRas*^{G12D} cells, one cannot conclude senescence induction is abolished in *atmin* deficient cells.

The *KRas*^{G12D}*; Villin-Cre* model was also used to analyse the function of ATM in oncogene induced senescence. Cohorts of wildtype, *atm*$^{-/-}$, *KRas*^{G12D}*; Villin-Cre* and *atm*$^{-/-}$*; KRas*^{G12D}*; Villin-Cre* mice were analysed at seven weeks for proliferation, DNA damage and senescence markers. H&E staining of the colon demonstrated serrated hyperplasia in both *KRas*^{G12D} and *atm*$^{-/-}$*; KRas*^{G12D} animals (Figure 28a). In agreement with observations in the *atmin* cohorts, *KRas*^{G12D} expression did not significantly increase proliferation in the colon Figure 28b, c). Recapitulating observations in the *atmin* cohorts, *KRas*^{G12D} expression increased pH2AX foci in both *atm*$^{+/+}$ and *atm*$^{-/-}$ mice (data not shown). Moreover, there was no significant difference in expression of the senescence marker *dec1* when *KRas*^{G12D} and *atm*$^{-/-}$*; KRas*^{G12D} cohorts were compared (Figure 28d). Thus, it appears ATM is not required for the senescence programme activated by colonic *KRas*^{G12D} expression.

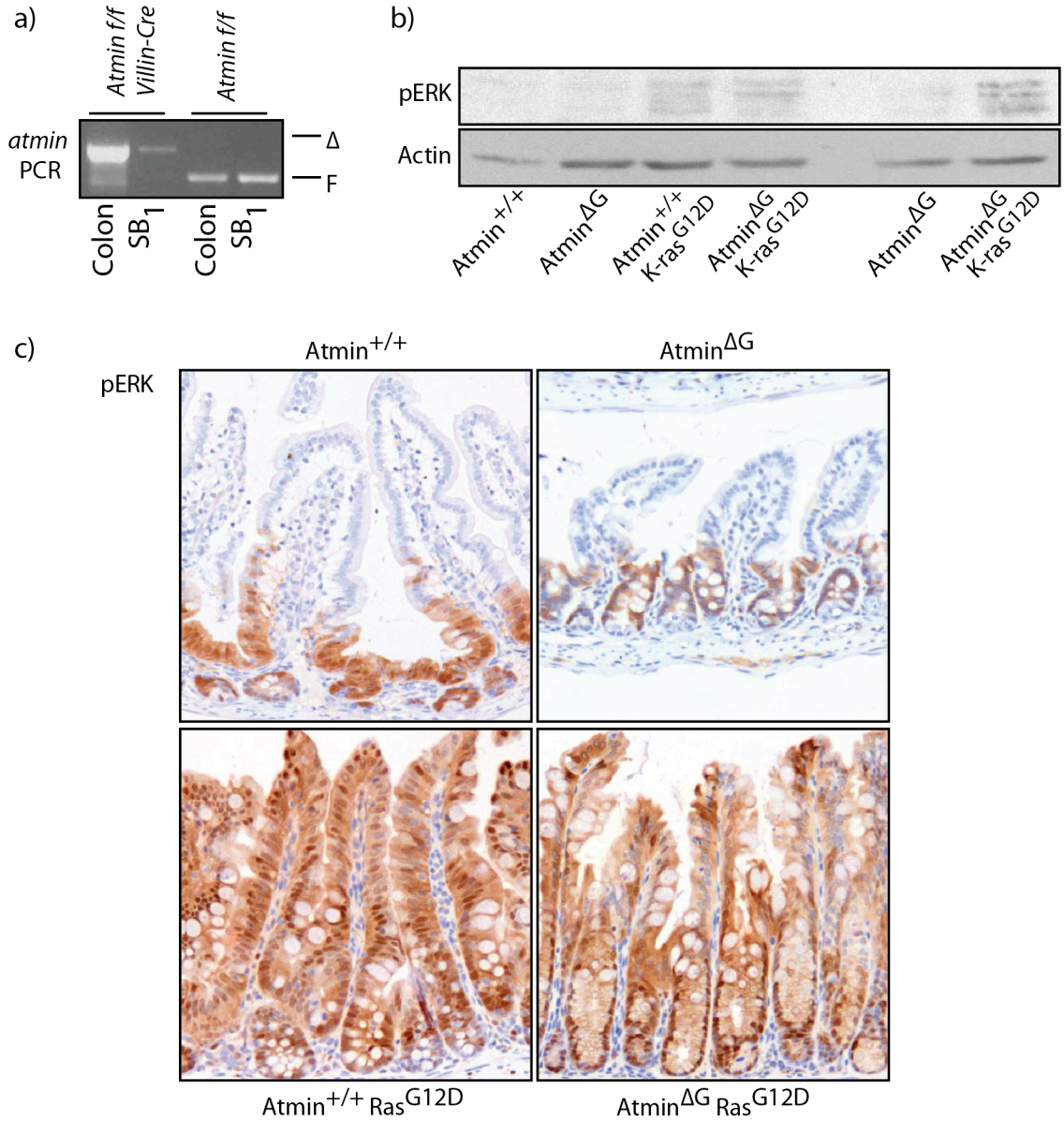

Figure 25: Villin-Cre mediates intestinal RasG12D expression

a) Genotyping PCR of DNA isolated from the intestines of the colon and small intestines of six week old *atmin*$^{f/f}$ and *atmin*$^{f/f}$*; VillinCre* mice. b) Intestinal tissue from six week old mice of the indicated genotypes was isolated and cell lysates separated by 10% SDS-PAGE. Membranes were probed with antibodies against actin and pT202/pY204ERK. c) Representative pT202/pY204-ERK immunohistochemistry from intestinal sections from six week old mice.

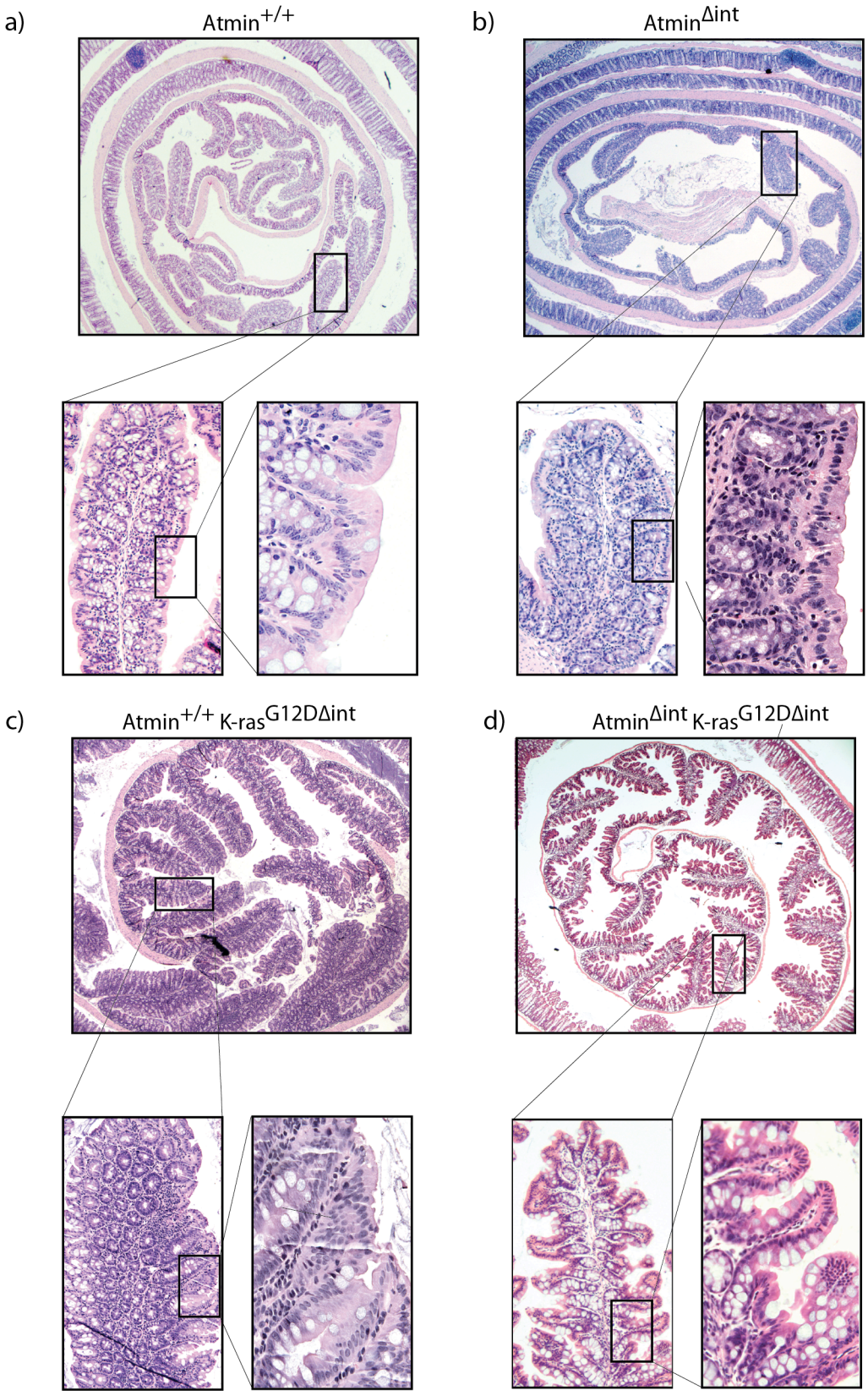

Figure 26: Intestinal KRas^{G2D} expression induced colonic serrated hyperplasia

Representative H&E stained sections from the colons of seven week old mice of the indicated genotypes.

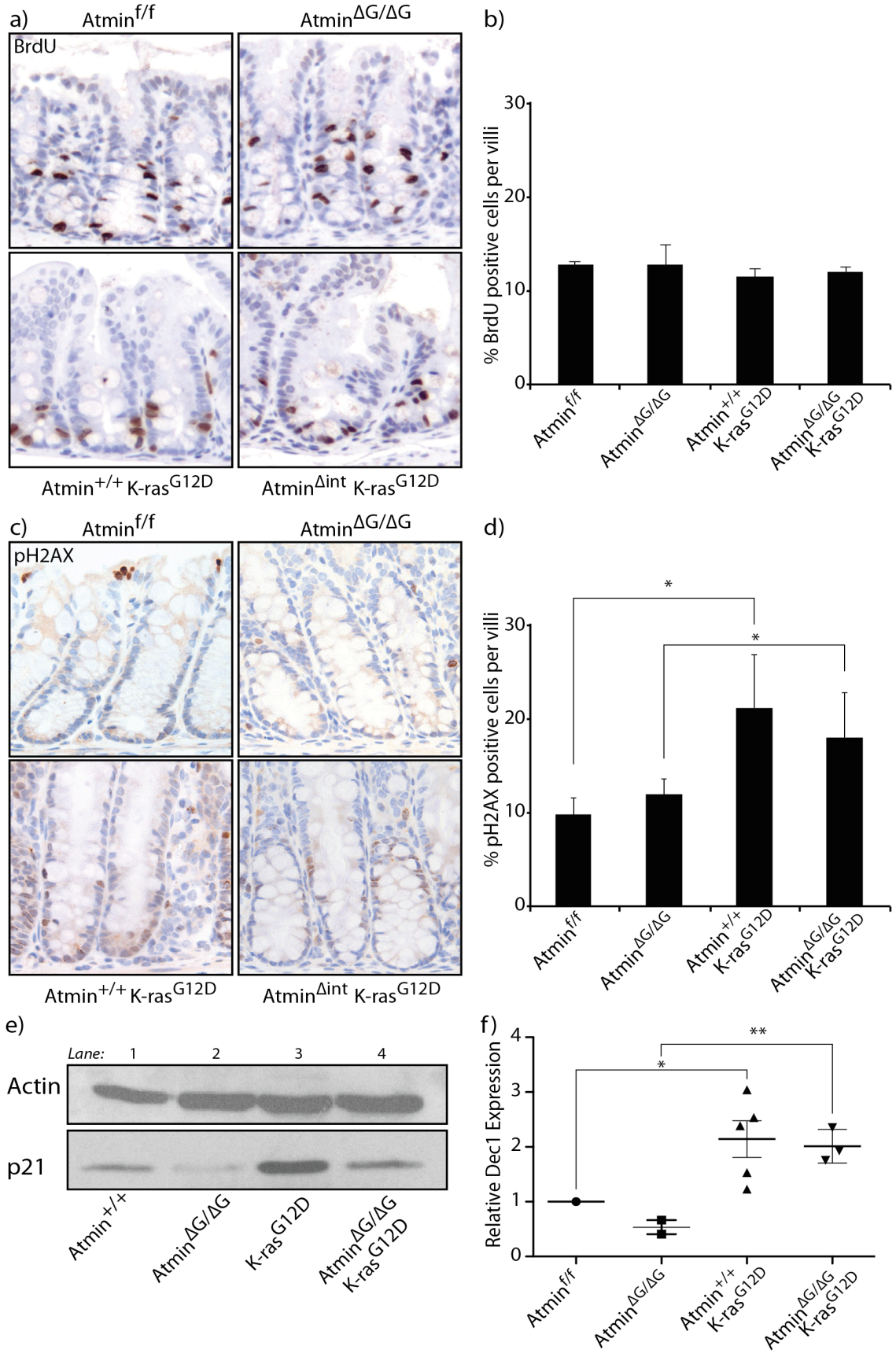

Figure 27: ATMIN is not part of the OIS barrier induced by intestinal *KRas^{G12D}* expression

a) Representative images of the colons of mice injected with BrdU 90 minutes prior to cull. b) Quantification of the percentage of BrdU positive cells per villi, as shown in (a). c) Representative images of pH2AX immunohistochemistry. d) Quantification of the percentage of cells per villi with three or more pH2AX foci. e) Cellular lysates from the colons of seven week old mice, separated by 12% SDS-PAGE and immunostained for p21 and actin. f) mRNA was isolated from the colons of seven week old mice, and qPCR analysis performed for *dec1* mRNA. mRNA levels were normalised to *GAPDH*. In all experiments, a minimum of three mice per genotype were analysed. Students t-test was used for statistical analysis, (*$p<0.05$, **$p<0.01$).

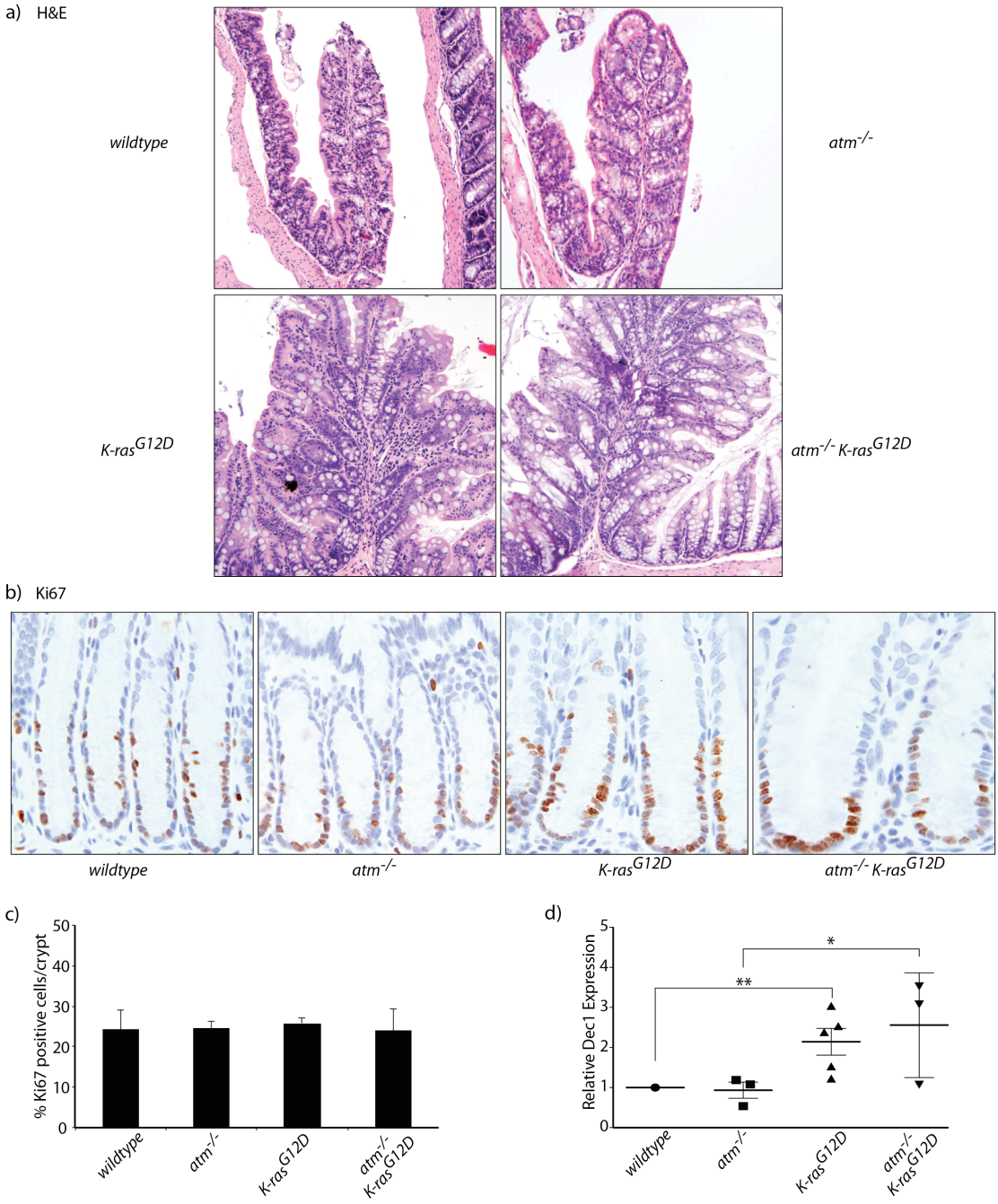

Figure 28: Senescence occurs in *KRas^{G12D}* intestinal cells regardless of *atm* status

a) Representative images of H&E stained villi, in the colons of seven week old mice with the indicated genotype. b) Representative Ki67 immunohistochemistry in the colons of seven week old mice. c) Quantification of the percentage of Ki67 positive cells per villus, as depicted in (b). d) mRNA was extracted from the colons of seven week old mice. *dec1* expression is shown relative to *gapdh* mRNA levels. A minimum

of three mice were genotype were used in all analyses. Student's t-test was used for statistical analysis (*p<0.05, **p<0.01).

3.3.2 Non-intestinal *KRas^{G12D}* expression is lethal

To address whether ATMIN loss co-operates with *KRas^{G12D}* expression to promote the progression to adenoma cohorts of *atmin$^{f/f}$;Villin-Cre*, *atmin$^{f/f}$*; *LSL-KRas^{G12D}*; *Villin-Cre* and *LSL-KRas^{G12D}*; *Villin-Cre* mice, along with Cre negative controls, were generated for a tumour study. The initial aim was to allow the animals to age and monitor for symptoms of intestinal cancer.

Unexpectedly, all animals with *LSL-KRas^{G12D}*; *Villin-Cre* positive genotypes, regardless of ATMIN status, became sick at approximately eight weeks of age. All had to be culled sick by twelve weeks (Figure 29a). There was no significant difference between the median survival of the different genotypes (Figure 29b). Similar survival was observed with *atm$^{-/-}$ KRas^{G12D}* cohorts (data not shown). However, histological analysis of the intestine revealed no progression beyond the serrated hyperplasia stage. Thus the morbidity was not due to intestinal *KRas^{G12D}* expression. Indeed, further analysis of the cohorts revealed lesions and hyperplasia in multiple other organs, especially in the pancreas (Figure 29c). Indeed, GFP staining of *Villin-Cre; ROSA26-LSL-YFP* animals revealed significant activation of Villin-Cre in non-intestinal tissues such as pancreas (Dr Rocio Sancho, personal communication).

The lethality of the *LSL-KRas^{G12D}; Villin-Cre* mice and non-intestinal *Cre* expression was surprising as it is in contrast to previous reports (Bennecke et al., 2010). The difference in phenotype is most likely due to the two different *Villin-Cre* lines used. The previously published intestinal *LSL-KRas^{G12D}* study used a differently designed *Villin-Cre* construct (Madison et al., 2002); to the *Villin-Cre* line used for my study (el Marjou et al., 2004). It is highly likely the *Villin-Cre* line used in my study has significantly more non-intestinal, 'leaky', expression than the *Villin-Cre* line by Bennecke and colleagues.

3.3.3 *atmin* loss does not lead to intestinal adenoma in *KRas^{G12D}* mice

The average survival of any *LSL-KRas^{G12D}*; *Villin-Cre* mice, irrespective of ATM or ATMIN status, was approximately 7-8 weeks. This premature lethality excluded the possibility of a long-term tumour study. To circumvent the lethality in the long-term tumour study I used the *Villin-CreERT* line, in which tamoxifen activatable *Cre* is driven by the villin promoter. Cohorts of mice (*atmin$^{f/f}$*, *atmin$^{f/f}$*; *Villin-CreERT*, *Villin-CreERT; LSL-KRas^{G12D}* and *atmin$^{f/f}$*; *Villin-CreERT*; *LSL-KRas^{G12D}*) were injected with 100μg tamoxifen per gram bodyweight for three consecutive days. Comparable cohorts were set up to investigate ATM's role in tumour protection; *atm$^{-/-}$* and *atm$^{-/-}$; Villin-CreERT; LSL-KRas^{G12D}*. Recombination efficiency was assessed by histological staining of GFP in *LSL-Rosa-YFP Villin-CreERT* mice injected in concert with the experimental cohorts (Figure 30a).

Cohorts were monitored for up to a year for any tumour symptoms. As expected, *atm$^{-/-}$* mice developed T-cell lymphoma at approximately three months (Figure 30b). Indeed, all of the *atm$^{-/-}$; Villin-CreERT; LSL-KRas^{G12D}* mice died of T-cell lymphoma at comparable ages to the *atm$^{-/-}$* controls. Histological analysis of the intestines of these mice revealed although serrated hyperplasia was present in the colon, this had not progressed to adenoma (data not shown). This precluded longer-term analysis of a pro-senescence role for ATM in *KRas^{G12D}* intestines.

On the contrary, neither *atmin$^{\Delta G/\Delta G}$* nor *atmin$^{\Delta G/\Delta G}$; KRas^{G12D}* animals developed any sign of tumours when aged for one year. In agreement with published observations, no tumours were observed in the *KRas^{G12D}* cohort (Bennecke et al., 2010). There was no significant different in their survival compared to tamoxifen-injected, Cre-negative littermate controls. This suggests *atmin* is not part of the oncogene induced senescence barrier induced by intestinal *KRas^{G12D}* expression.

3.4 Concluding Remarks

It is clear ATMIN has an important role in endogenous DNA damage repair; *atmin* deficient cells exhibit increased DNA damage levels (Figure 17, Figure 18), reduced pS1987-ATM recruitment to sites of damage (Figure 19), premature senescence and sensitivity to oxidative stress (Figure 20). Moreover, ATMIN is specifically required for telomere maintenance, $atmin^{\Delta/\Delta}$ cells display increased damage at the telomere (Figure 21) and *atmin* loss co-operates with telomerase deficiency to exacerbate neural stem cell dysfunction (Figure 23). However, the data presented in this chapter does not support a role for ATMIN in the OIS response (Figure 27, Figure 30).

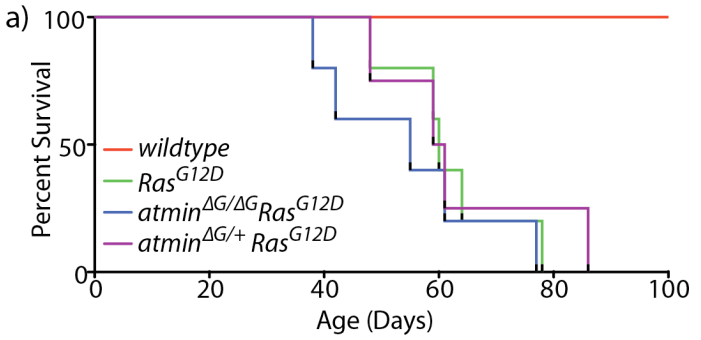

b)

Genotype	Median Survival
wildtype	n/d
Ras^{G12D}	60 days
atmin$^{\Delta G/\Delta G}$*Ras*^{G12D}	55 days
atmin$^{\Delta G/+}$ *Ras*^{G12D}	60 days

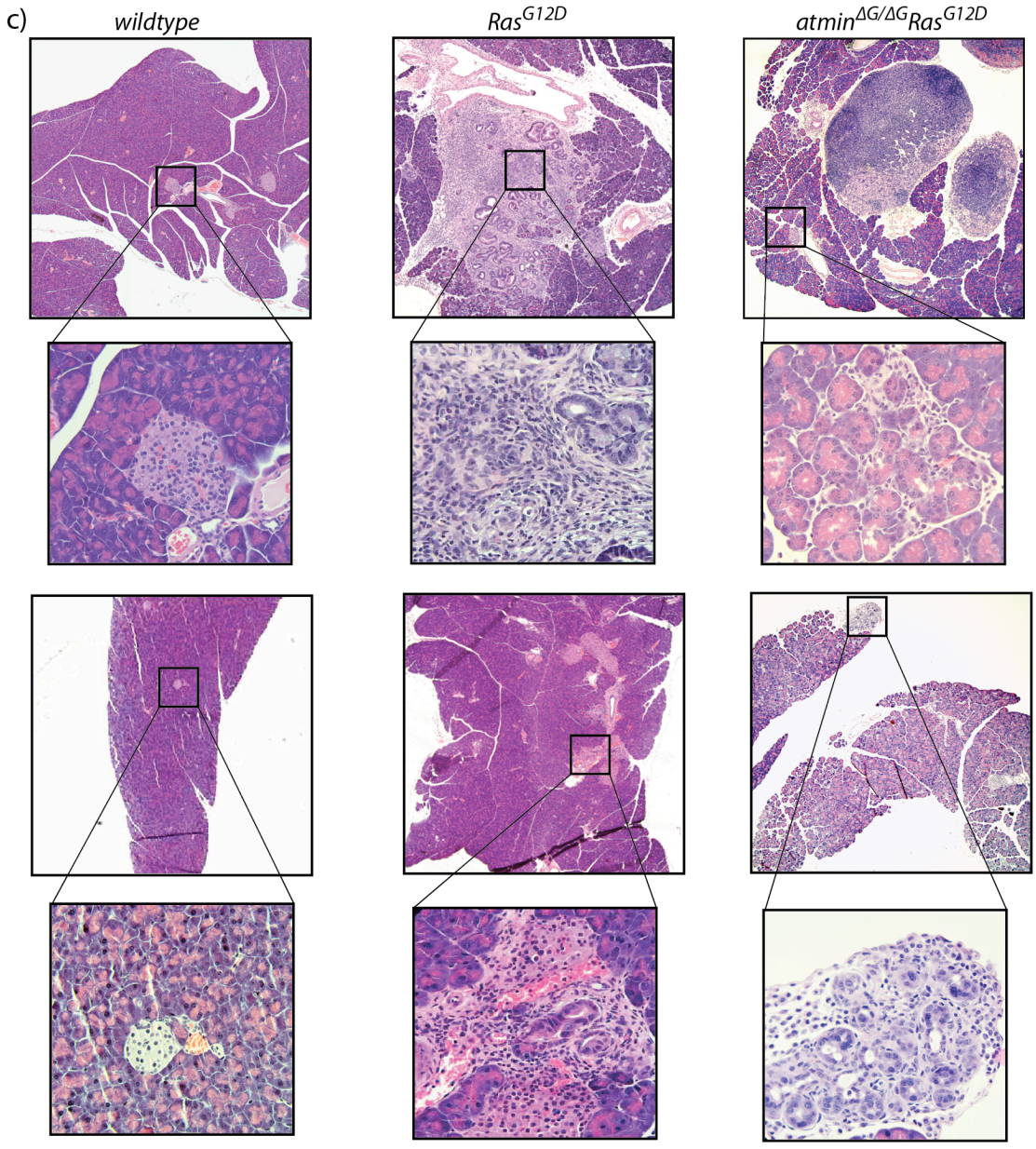

Figure 29: Non-intestinal *KRas*^{G12D} expression is lethal

a) Survival curve of the indicated genotypes, at least five mice per genotype are shown. b) Median survival of the indicated genotypes. c) Representative H&E stained pancreas sections of seven week old mice. Two mice per genotype are shown.

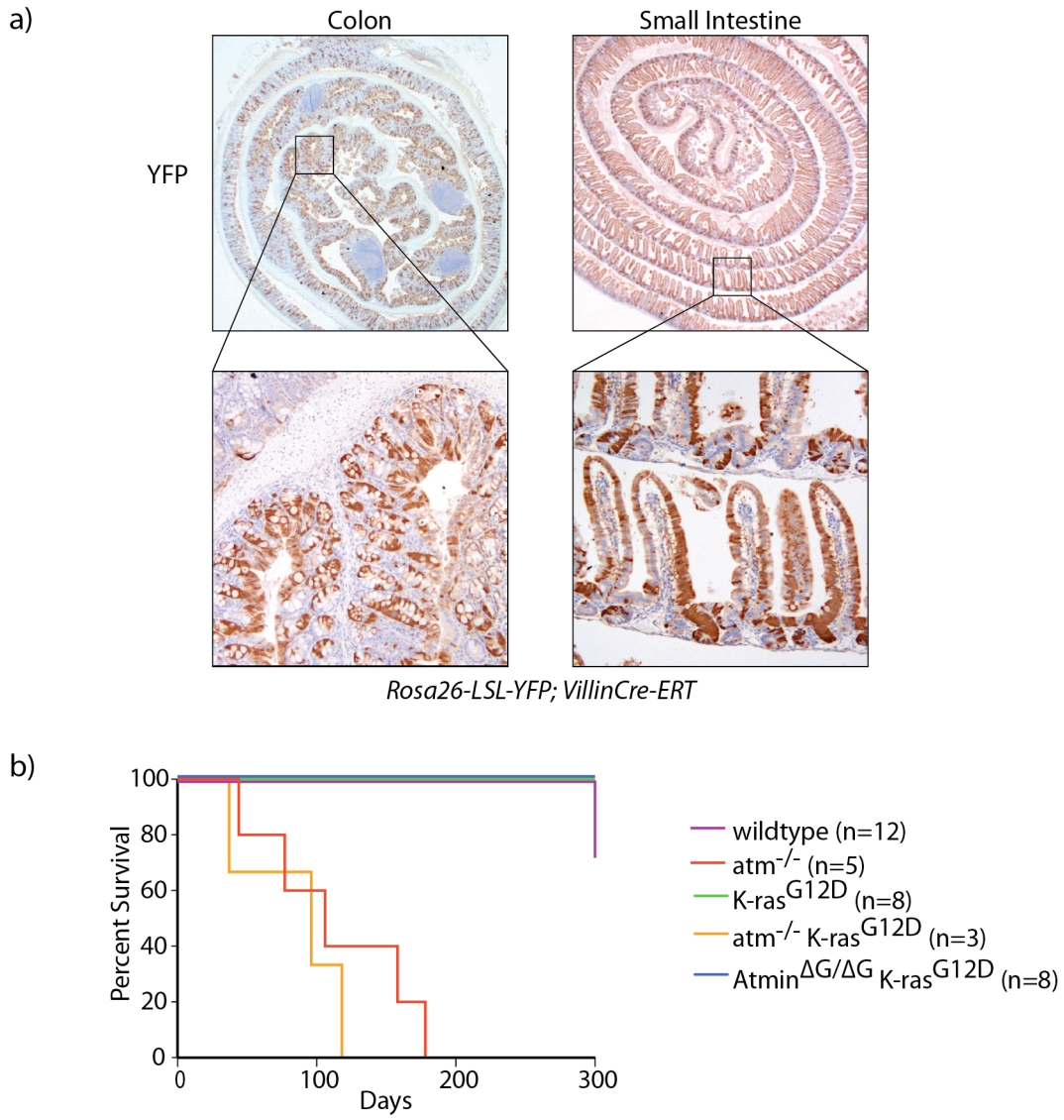

Figure 30: ATMIN and ATM do not contribute to adenoma protection in KRas^{G12D} mice

a) Representative images of GFP immunostains performed on the intestines of *LSL-Rosa-YFP; Villin-CreERT* mice. Animals were injected with three 100 µg/gram bodyweight tamoxifen injections over three consecutive days and culled five days after the final injection. b) Kaplan-Meier curve for mice of the indicated genotypes. All mice were injected with tamoxifen at six weeks old.

Chapter 4. ATMIN and p53 Interplay in B cell Lymphoma

Mutation in DNA damage response proteins, including ATM and NBS1, specifically predispose patients to lymphomas compared to other cancer types. Yet, all cells contain the same DNA damage machinery and presumably experience similar levels of spontaneous DNA damage. This discrepancy is reconciled by consideration of programmed DNA damage. The programmed DNA breaks induced of the immune system presumably elevate the total DNA damage experienced by these cells and thus the likelihood of genomic instability and cancer. Great advances in the DNA damage response field have been made by studying the cellular response to exogenous DNA damage, but studying the function of DNA damage response proteins in cells experiencing programmed DNA damage is an invaluable model for a plethora of cancers and DNA damage syndromes. One aim of my PhD was to examine the consequences of ATMIN and p53 deletion in B cells.

4.1 CD19-Cre enables B cell specific *atmin* and *p53* deletion

DNA double strand breaks are induced in B cells during V(D)J recombination and CSR. ATMIN is important for DNA repair in B cells; ATMIN deletion in B cells results in increased genomic instability and predisposition to B cell lymphoma (Loizou et al., 2011). Conversely, $NBS1^{657\Delta5}$ mice only develop B cell lymphoma in a $p53^{-/-}$ background (Reina-San-Martin et al., 2005). We were interested to see the effect of co-deletion of p53 and ATMIN, so I generated cohorts of $atmin^{f/f}$*; p53*$^{f/f}$*; CD19-Cre,* $atmin^{f/f}$*; CD19-Cre* and $p53^{f/f}$*; CD19-Cre* mice.

CD19-Cre mice carry a copy of *Cre* recombinase inserted into one copy of the CD19 locus, so as expression of *Cre* recombinase is under the control of the endogenous CD19 promoter (Rickert et al., 1997). CD19 is specifically expressed in the B cell lineage from the pro-B stage onwards, and thus genes flanked by loxP sites are deleted

at the pro-B stage (Figure 31a). To confirm *atmin* deletion, I extracted DNA from the B cells of *atmin*$^{f/f}$*; p53*$^{f/f}$*; CD19-Cre* mice and performed ATMIN genotyping PCR. The presence of the delta, and absence of the floxed, PCR band confirmed *atmin* deletion (Figure 31b). p53 deletion was examined by western blot. As expected, B cells from *atmin*$^{f/f}$*; p53*$^{f/f}$*; CD19-Cre* (*atmin*$^{\Delta B/\Delta B}$*; p53*$^{\Delta B/\Delta B}$) do not express p53 protein (Figure 31c). Therefore CD19-Cre is a suitable system in which to study the consequence B cell specific *atmin* and *p53* deletion.

4.2 B cell development in young *atmin*$^{\Delta B/\Delta B}$*; p53*$^{\Delta B/\Delta B}$ and *p53*$^{\Delta B/\Delta B}$ Mice

The consequence of ATMIN and p53 co-deletion on B cell development had not previously been studied. It is plausible *atmin*$^{\Delta B/\Delta B}$*; p53*$^{\Delta B/\Delta B}$ B cell maturation is impaired, generating fewer B cells and thus a reduced pool of cells with the propensity to be transformed. Therefore I analysed B cell development in six week old *atmin*$^{\Delta B/\Delta B}$*; p53*$^{\Delta B/\Delta B}$ mice. Cells from the bone marrow of *atmin*$^{\Delta B/\Delta B}$*; p53*$^{\Delta B/\Delta B}$ and *atmin*$^{f/f}$*; p53*$^{f/f}$ littermate controls were analysed in parallel by FACS for B220, CD43 and IgM marker expression. Three mice of each genotype were analysed.

To gain a comprehensive picture of B cell development, I determined the percentage of B cells at the pro-B, pre-B, immature-B and mature re-circulating B cell stages (Figure 31). There was no difference in the pro-B ($CD43^+$ $B220^+$) population of *atmin*$^{\Delta B/\Delta B}$*; p53*$^{\Delta B/\Delta B}$ mice (Figure 32a,b). The pre-B cell population ($B220^+$ $CD43^-$ IgM^-) was also unaltered in the compound mutants (p=0.294) (Figure 32c,d). Although the percentage of immature B cells ($B220^+$ $CD43^-$ IgM^+) was reduced from 25.5% to 21.6% in *atmin*$^{\Delta B/\Delta B}$*; p53*$^{\Delta B/\Delta B}$ bone marrow (Figure 32c,e), this reduction did not reach statistical significance (p=0.172). There was also no alteration in the percentage of re-circulating mature B cells ($B220^{hi}$ $CD43^-$ IgM^+) the bone marrow of *atmin*$^{\Delta B/\Delta B}$*; p53*$^{\Delta B/\Delta B}$ mice (Figure 32c,f). Taken together, this indicates that there is no significant impairment in the B cell development in bone marrow of *atmin*$^{\Delta B/\Delta B}$*; p53*$^{\Delta B/\Delta B}$ mice.

Mature peripheral B cells reside in the germinal centres of the spleen. To address whether B cell specific loss of ATMIN and p53 affects the frequency of peripheral splenic mature B cells ($B220^+ IgM^+$), I performed FACS analysis of the spleens of six week old *atmin*$^{\Delta B/\Delta B}$*; p53*$^{\Delta B/\Delta B}$ and *atmin*$^{f/f}$*; p53*$^{f/f}$ littermate controls in parallel. There was no significant difference between the percentage of mature splenic B cells ($B220^+ IgM^+$) (Figure 33a, b). Thus B cell specific ATMIN and p53 co-deletion does not impair B cell maturation.

CD19-Cre mediated p53 deletion is not a previously published model. It was therefore necessary to validate B cell development in *p53*$^{f/f}$*; CD19-Cre* mice. Bone marrow FACS analysis was performed on six week old *p53*$^{\Delta B/\Delta B}$ and *p53*$^{f/f}$ littermate controls in parallel. Comparison of the pro-B ($CD43^+ B220^+$) pool showed p53 loss does not alter the percentage of pre-B cells in the bone marrow (Figure 34a, b). Similarly, there was no difference in the percentage of pre-B cells in *p53*$^{\Delta B/\Delta B}$ bone marrow (Figure 34c, d). Loss of p53 does not alter immature B cell number ($B220^+ CD43^- IgM^+$) (Figure 34c, e). Finally, analysis of the re-circulating mature B cell population ($B220^{hi} CD43^- IgM^+$) confirmed no difference between *p53*$^{\Delta B/\Delta B}$ and *p53*$^{f/f}$ controls (Figure 34a, f). Taken together, these data suggests *p53* deletion does not alter B cell development in the bone marrow.

To gain a complete picture of B cell development in *p53*$^{\Delta B/\Delta B}$ animals, I also performed FACS analysis on the spleens of six week old *p53*$^{\Delta B/\Delta B}$ and *p53*$^{f/f}$ mice. Comparison of mature B cell populations ($B220^+ IgM^+$) demonstrated p53 deletion does not effect the percentage of mature B cells in the spleen (Figure 35,b). Thus, CD19-Cre mediated *p53* deletion does not impair B cell maturation.

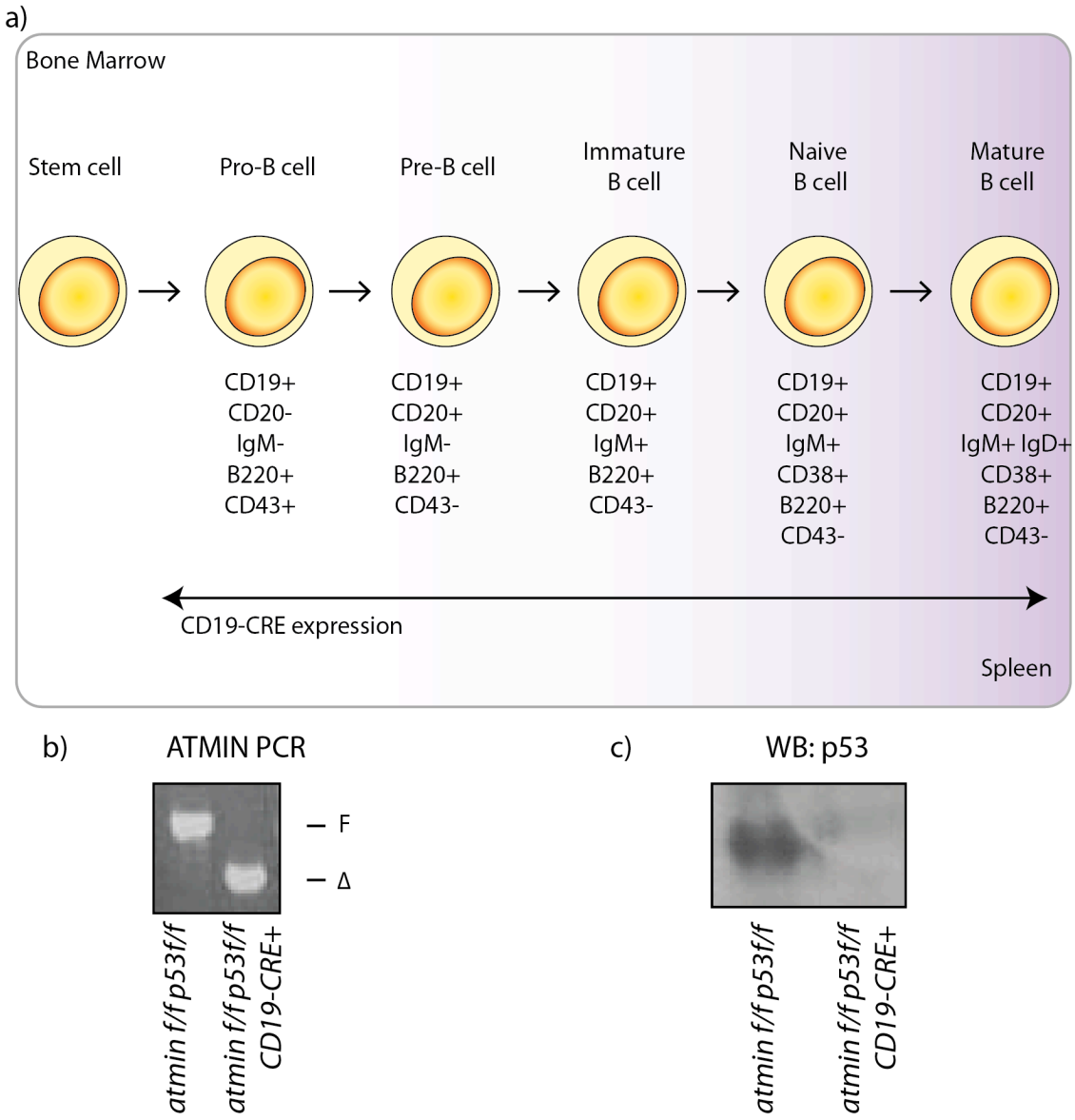

Figure 31: B cell specific deletion of *atmin* and *p53*

a) Cartoon schematic of B cell development from the haematopoietic stem cell in the bone marrow to the mature B cell in the spleen. The expression pattern of B cell markers, including CD19, is indicated. b) ATMIN genotyping PCR of B cells isolated by negative selection from six week old mice of the indicated genotypes. 'F' refers to the floxed allele, 'Δ' to the deleted allele. c) B cells were isolated from six week old mice by negative selection, and protein extracts immunoblotted for p53.

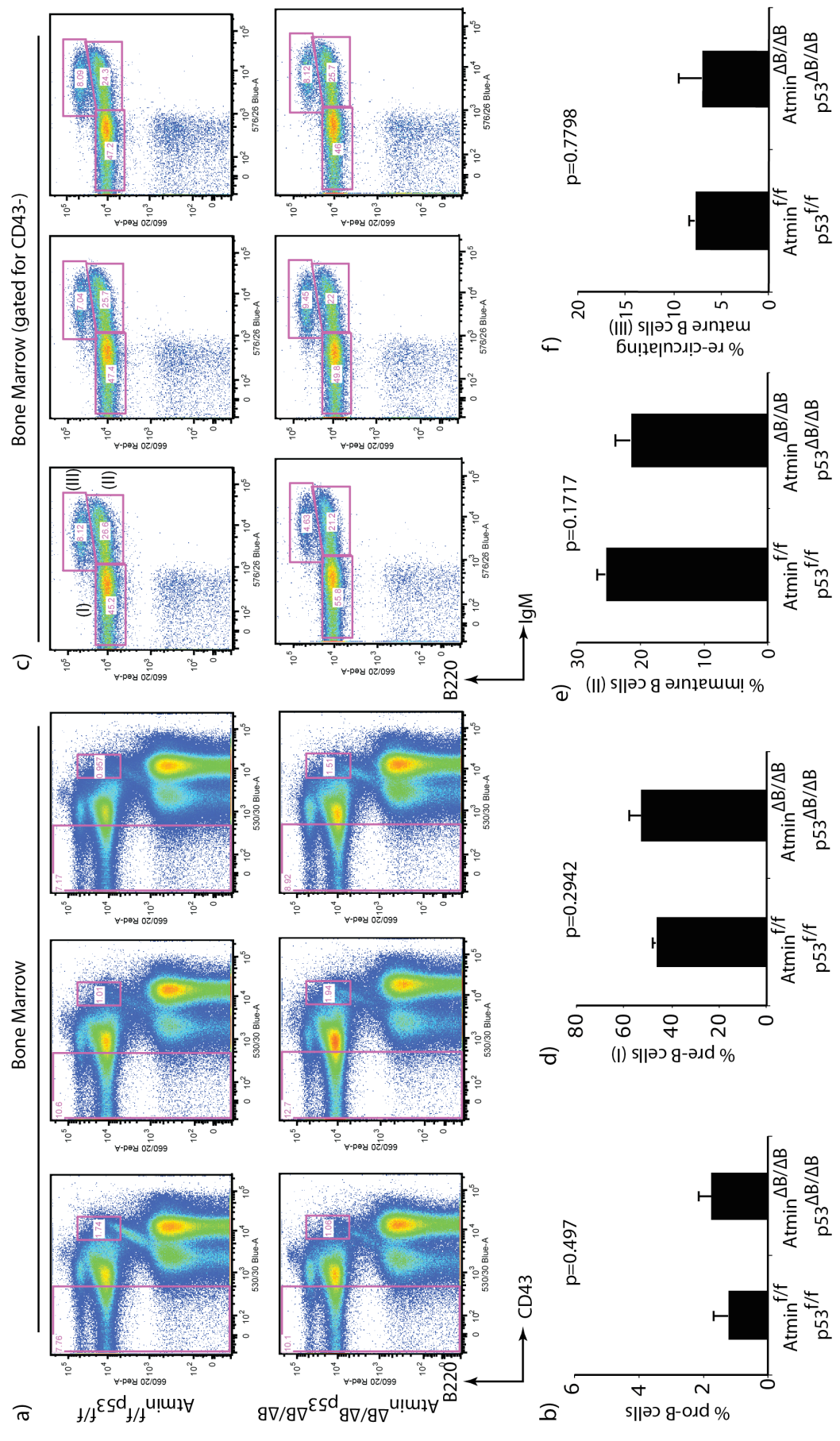
a)
Bone Marrow
Atmin f/f p53 f/f
Atmin ΔB/ΔB p53 ΔB/ΔB
B220
CD43
c)
Bone Marrow (gated for CD43-)
(I)
(II)
(III)
B220
IgM
b)
% pro-B cells
p=0.497
Atmin f/f p53 f/f
Atmin ΔB/ΔB p53 ΔB/ΔB
d)
% pre-B cells (I)
p=0.2942
e)
% immature B cells (II)
p=0.1717
f)
% re-circulating mature B cells (III)
p=0.7798

Figure 32: No striking B cell maturation defect in *atmin*$^{\Delta B/\Delta B}$; *p53*$^{\Delta B/\Delta B}$ mice

a) FACS analysis for B220 and CD43 on bone marrow cells from three mice per genotype. b) Quantification of ($B220^{+}$ $CD43^{+}$) pro-B cells. c) Analysis of the CD43- bone marrow population of three mice. d) Quantification of pre-B cells($B220^{+}$ $CD43^{-}$ IgM^{-}), denoted 'I' in (c). e) Quantification of immature B cells ($B220^{+}$ $CD43^{-}$ IgM^{+}), denoted 'II' in (c). f) Quantification of ($B220^{hi}$ $CD43^{-}$ IgM^{+}) re-circulating mature B cells, denoted 'III' in (c). Student's t-test was used for statistical analysis, n=3 mice per genotype.

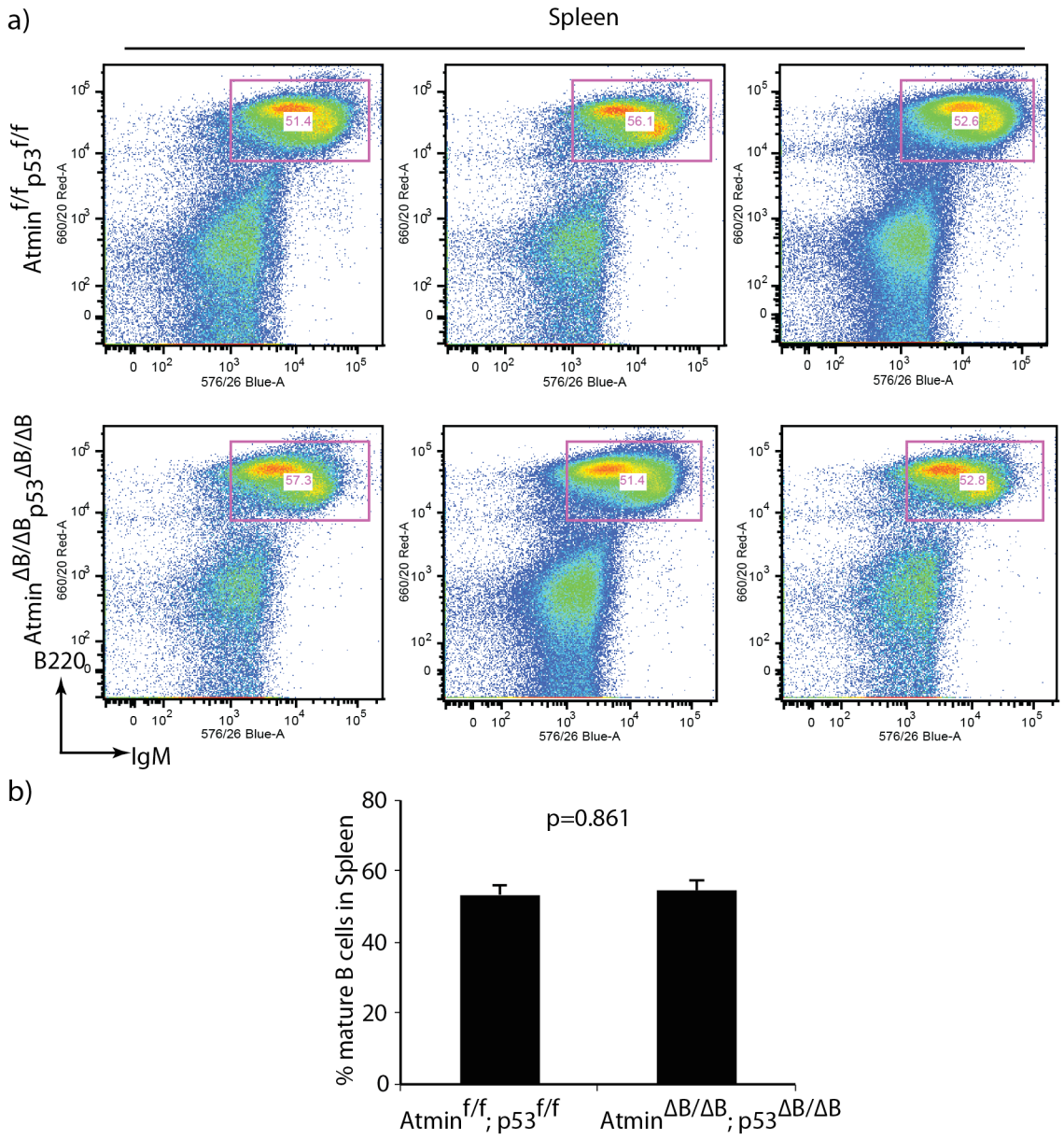

Figure 33: Normal mature B cell number in the spleens of young *atmin*$^{\Delta B/\Delta B}$; *p53*$^{\Delta B/\Delta B}$ mice

a) FACS analysis performed upon the spleens of six week old mice. Three mice per genotype were analysed. b) Quantification of ($B220^+$ IgM^+) mature B cells, as shown in (a). Student's t-test was used for statistical analysis, n=3 mice per genotype.

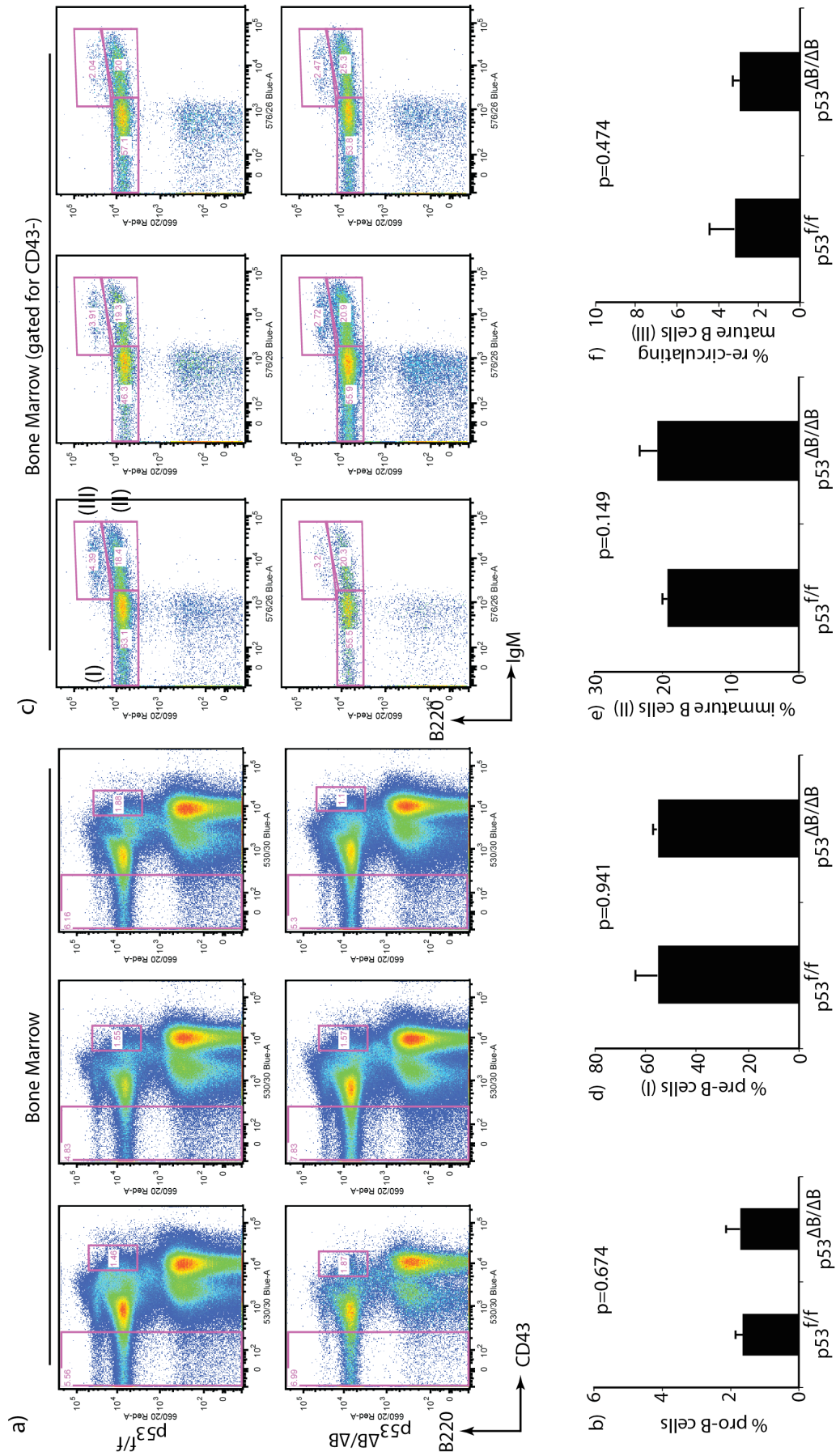
a)
Bone Marrow
p53f/f
p53ΔB/ΔB
B220
CD43
c)
Bone Marrow (gated for CD43-)
(I)
(II)
(III)
B220
IgM
b)
% pro-B cells
p=0.674
p53f/f
p53ΔB/ΔB
d)
% pre-B cells (I)
p=0.941
p53f/f
p53ΔB/ΔB
e)
% immature B cells (II)
p=0.149
p53f/f
p53ΔB/ΔB
f)
% re-circulating mature B cells (III)
p=0.474
p53f/f
p53ΔB/ΔB

Figure 34: p53 deletion does not impair B cell development

a) Bone marrow FACS analysis for B220 and CD43. Three mice per genotype are shown. b) Quantification of ($B220^{+}$ $CD43^{+}$) pro-B cells. c) Analysis of the $CD43^{-}$ bone marrow population of three mice. d) Quantification of pre-B cells ($B220^{+}$ $CD43^{-}$ IgM^{-}), denoted 'I' in (c). e) Quantification of immature B cells ($B220^{+}$ $CD43^{-}$ IgM^{+}), denoted 'II' in (c). f) Quantification of ($B220^{hi}$ $CD43^{-}$ IgM^{+}) re-circulating mature B cells, denoted 'III' in (c). Student's t-test was used for statistical analysis, n=3 mice per genotype.

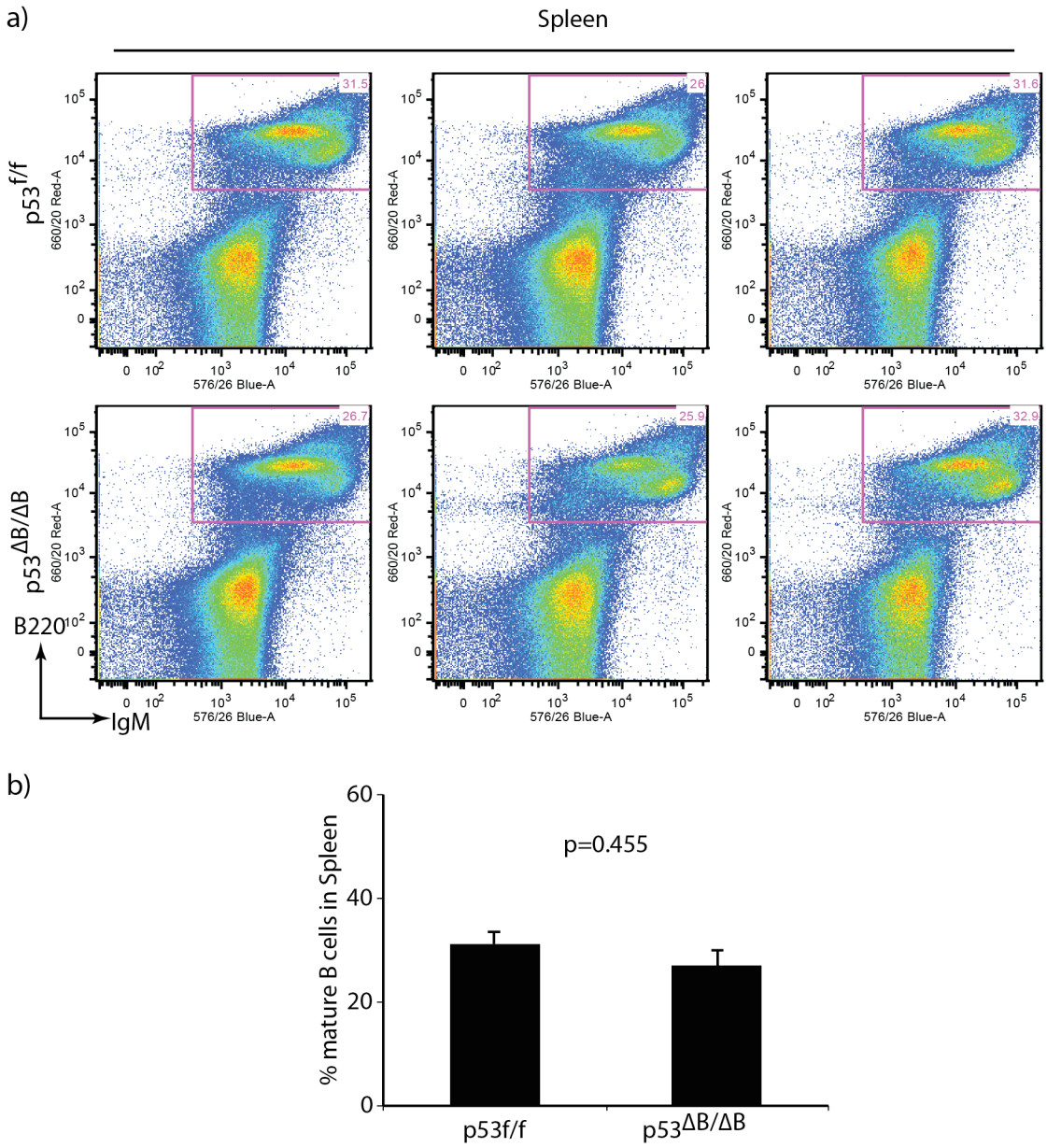

Figure 35: Normal mature B cell number in the spleens of young *p53*$^{\Delta B/\Delta B}$ mice

a) FACS analysis of six week old mice spleens. Three mice of each genotype were analysed. b) Quantification of ($B220^{+}$ IgM^{+}) mature B cells, as shown in (a). Student's t-test was used for statistical analysis, n=3 mice per genotype.

4.3 p53 is required to suppress B cell lymphoma development

p53 deletion resulted in onset of B cell lymphoma in approximately 60% of the $p53^{\Delta B/\Delta B}$ cohort, with an average onset of approximately seven months of age (Figure 36a). The B cell lymphomas in $p53^{\Delta B/\Delta B}$ animals are characterised by a dramatic increase in spleen size, as compared to $p53^{f/f}$ littermates (Figure 36b). H&E and B220 staining of the spleens from $p53^{\Delta B/\Delta B}$ mice with B cell lymphoma illustrated the disorganisation of the spleen, with the germinal centres almost indistinguishable from the red pulp regions (Figure 36c, d).

The development of B cell lymphoma in $p53^{\Delta B/\Delta B}$ animals with enlarged, disorganised spleens was confirmed by the infiltration of B cells into multiple organs. The B cell lymphomas were highly metastatic, and typically spread to several organs including the lung, kidney and pancreas (Figure 37). In some cases solid, abdominal B cell masses formed. It is clear p53 functions to suppress the onset of B cell lymphoma.

4.4 ATMIN deletion rescues B cell lymphoma onset in $p53^{\Delta B}$ mice

To assess any combinatorial effect of *atmin* and *p53* deletion of B cell lymphoma onset I monitored ageing cohorts of $atmin^{f/f}; p53^{f/f}; CD19\text{-}Cre$ and *Cre*-negative littermates for B cell lymphoma. Unexpectedly, $atmin^{\Delta B/\Delta B}; p53^{\Delta B/\Delta B}$ had the same survival as *Cre*-negative controls (Figure 38a). Only one $atmin^{\Delta B/\Delta B}; p53^{\Delta B/\Delta B}$ animal developed B cell lymphoma, at 15 months of age. The survival curve shown only goes as far as 400 days, as at later timepoints many mice were culled for non-lymphoma illness, such as fighting wounds or skin disorders. The lymphoma-free status of any $atmin^{\Delta B/\Delta B}; p53^{\Delta B/\Delta B}$ mice culled for other reasons was confirmed by a histopathologist. The spleens of 400 day old $atmin^{\Delta B/\Delta B}; p53^{\Delta B/\Delta B}$ do not exhibit the loss of architecture characteristic of B cell lymphoma, and appear macroscopically by H&E very similar to $atmin^{f/f}; p53^{f/f}$ littermate controls (Figure 38b). There was no significant difference between the spleen size of one year old $atmin^{\Delta B/\Delta B}; p53^{\Delta B/\Delta B}$ and $atmin^{f/f}; p53^{f/f}$ littermate controls (Figure 38c).

B220 staining indicates the germinal centres of 400 day old *atmin*$^{\Delta B/\Delta B}$*; p53*$^{\Delta B/\Delta B}$ mice maintained a distinct architecture (Figure 38d, e). Together, these observations suggest ablation of ATMIN function rescues the B cell lymphoma observed in *p53*$^{\Delta B/\Delta B}$ mice.

Although it is evident co-deletion of *atmin* and *p53* rescues the B cell lymphoma observed in the single *atmin*$^{\Delta B/\Delta B}$ and *p53*$^{\Delta B/\Delta B}$ mutants, the compound mutants do not have a wildtype phenotype. Quantification of B220 positive cells in 400 day old *atmin*$^{\Delta B/\Delta B}$*; p53*$^{\Delta B/\Delta B}$ spleens revealed reduced B cell numbers in the germinal centres (Figure 39a, b). This suggests that although B cell development is largely normal in young mice, old *atmin*$^{\Delta B/\Delta B}$ and *p53*$^{\Delta B/\Delta B}$ mutants have impaired B cell viability.

4.5 Concluding Remarks

The lymphoma-free survival of *atmin*$^{\Delta B/\Delta B}$ and *p53*$^{\Delta B/\Delta B}$ mutants (Figure 38) is highly surprising given solo deletion of either ATMIN (Loizou et al., 2011) or p53 (Figure 36) in B-cells predisposes to lymphoma. A subsequent study by a colleague, Dr Sophia Blake, demonstrated *p53*$^{f/f}$ *Nestin-Cre*, but not *atmin*$^{f/f}$; *p53*$^{f/f}$ *Nestin-Cre* mice, develop gliomas. This suggests the cancer protection afforded by *atmin* deletion from a p53-null cell is not restricted to B cells. Observations by Dr Sophia Blake in MEFs suggest loss of ATMIN reduces the proliferation of *p53*$^{\Delta/\Delta}$ cells. As further work by the Behrens group increases our understanding of the interplay between ATMIN and p53, it will be exciting to explore the therapeutic applications of inactivating ATMIN in a mutant *p53* cancer cell.

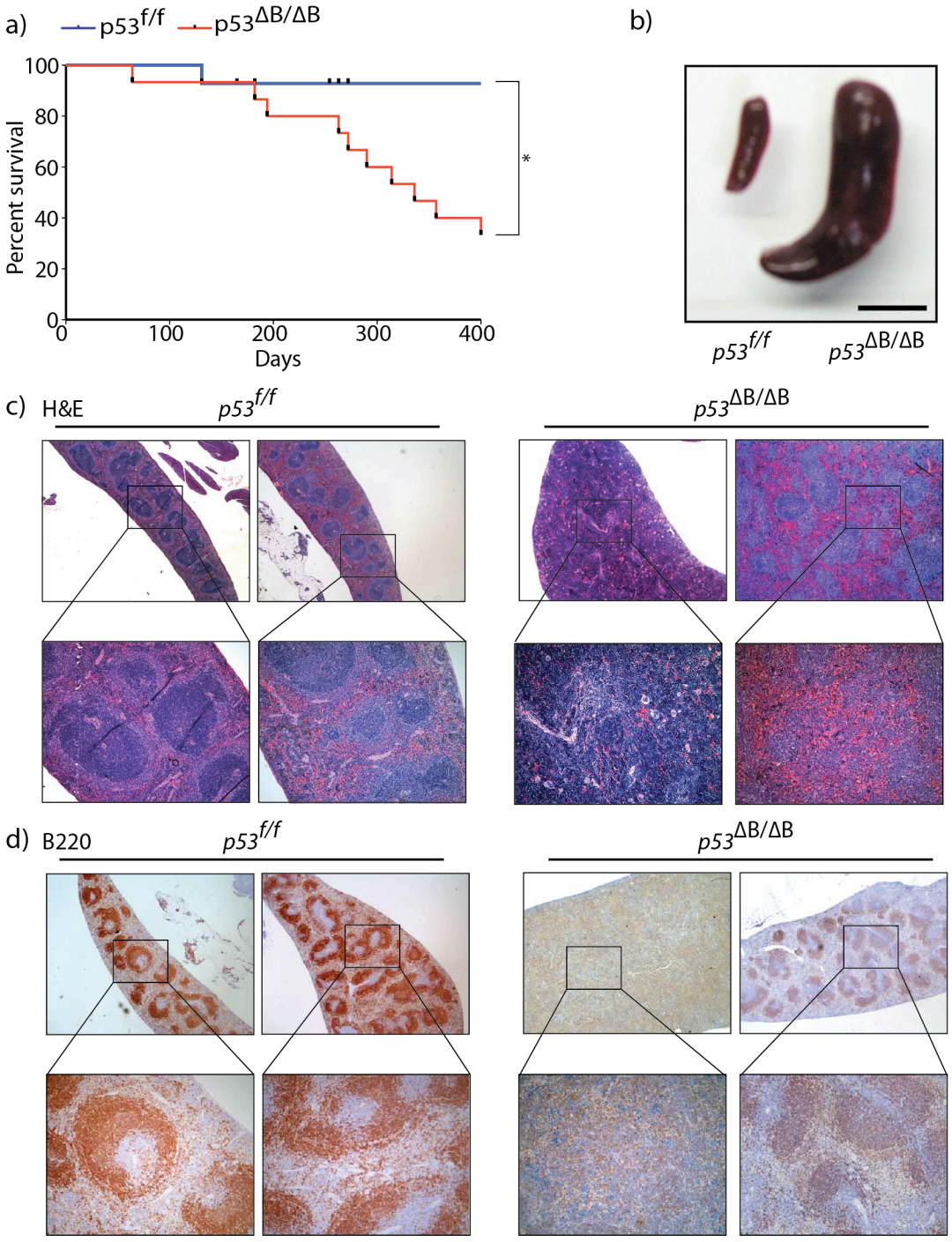

Figure 36: p53 is required to suppress B cell lymphoma

a) Kaplan-Meier curve of $p53^{f/f}$ (n=14) and $p53^{\Delta B/\Delta B}$ (n=15) survival. b) Photographs of the spleens from 38 week old $p53^{f/f}$ and $p53^{\Delta B/\Delta B}$ mice. Scale bar 1 cm. Representative c) H&E and d) B220 staining of two $p53^{\Delta B/\Delta B}$ spleens and littermate control $p53^{f/f}$ spleens. The Log Rank Mann Whitney test was used for statistical analysis (*p<0.05).

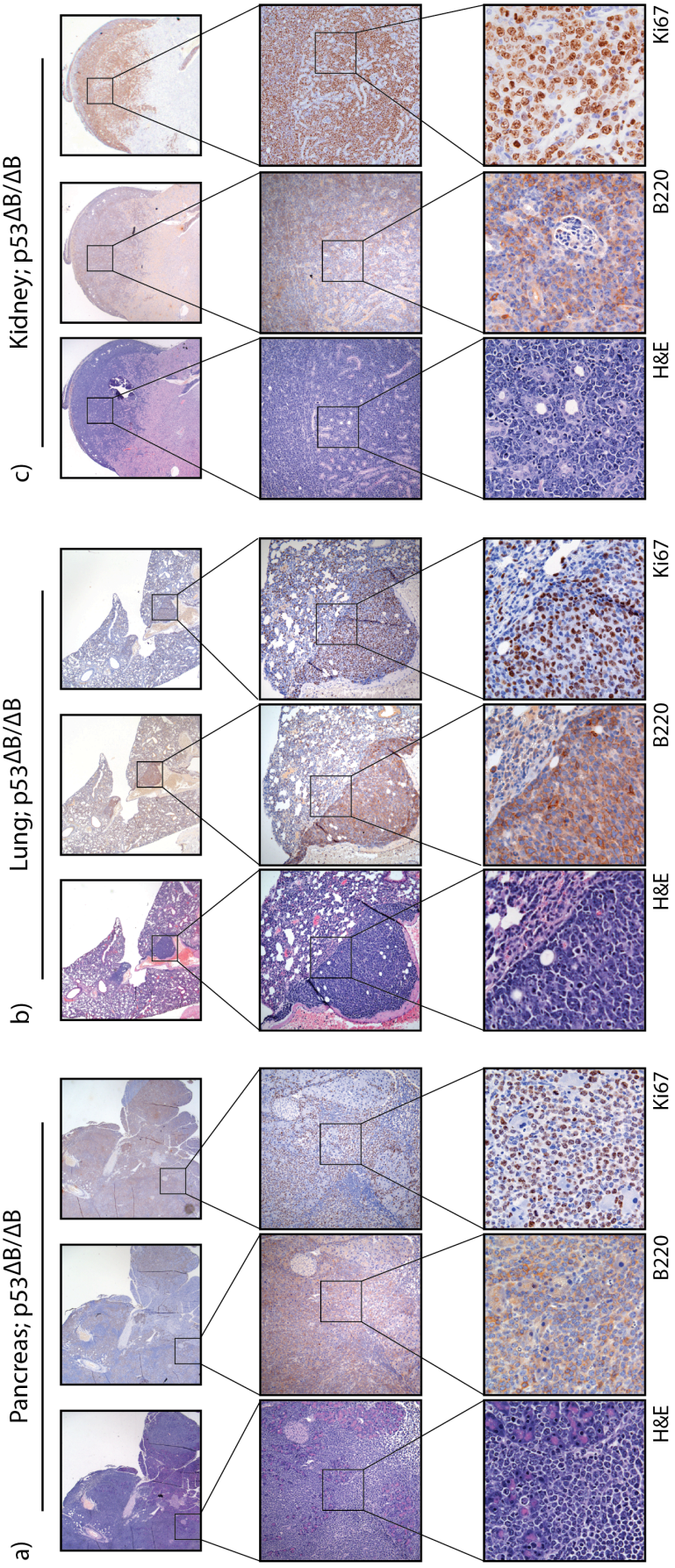
a)
Pancreas; p53ΔB/ΔB
b)
Lung; p53ΔB/ΔB
c)
Kidney; p53ΔB/ΔB
H&E
B220
Ki67

Figure 37: Multiple metastasis of *p53*$^{\Delta B/\Delta B}$ B cell lymphoma

Histological analysis of a metastatic B cell lymphoma in a forty week old *p53*$^{\Delta B/\Delta B}$ animal. Representative H&E, B220 and Ki67 staining in the a) pancreas, b) lung and c) kidney are shown.

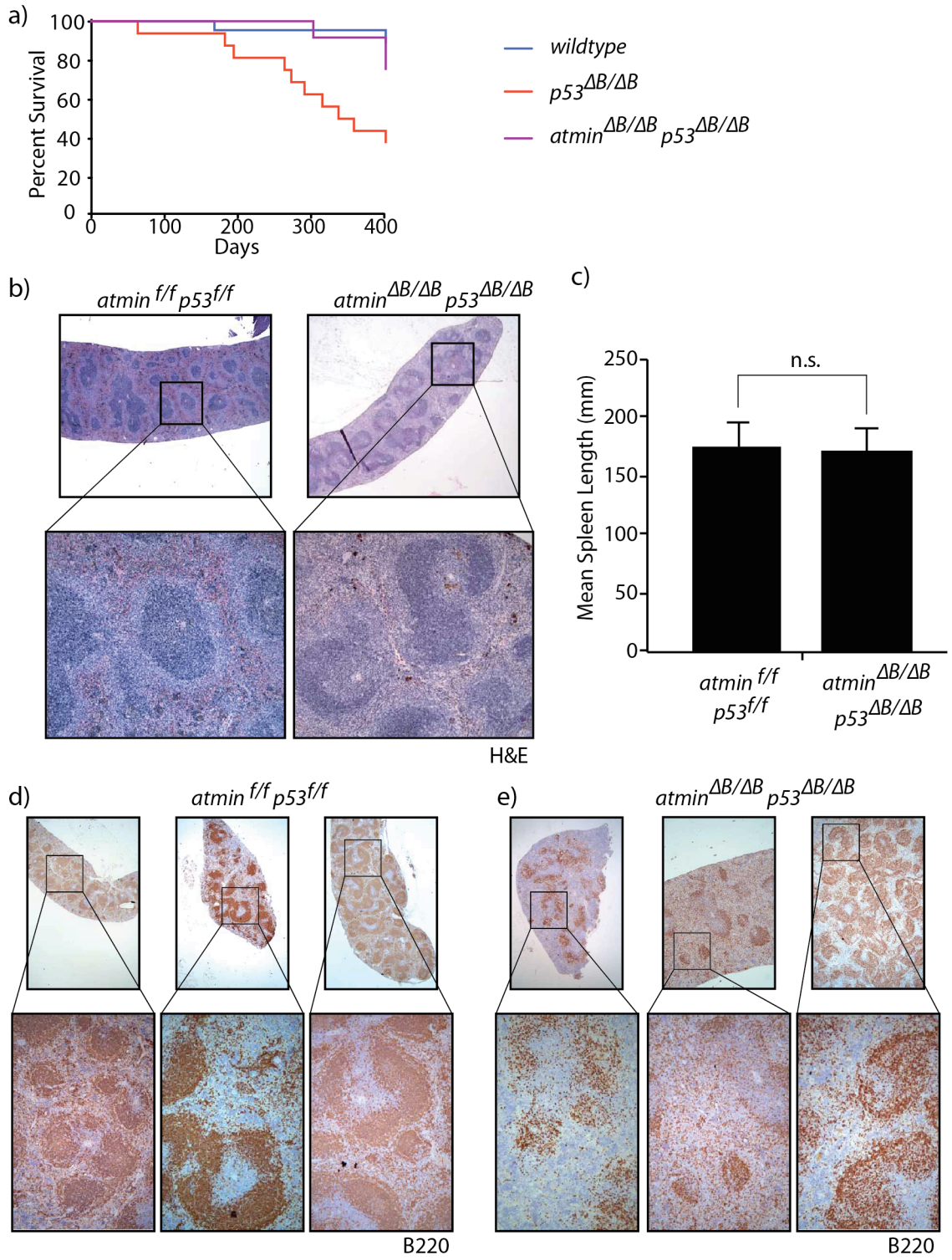

Figure 38: *atmin* deletion protects against B cell lymphoma in $p53^{\Delta B/\Delta B}$ mice

a) Kaplan-Meier curve of $atmin^{f/f}$; $p53^{f/f}$ (n=12) and $atmin^{\Delta B/\Delta B}$; $p53^{\Delta B/\Delta B}$ (n=12) survival. b) Representative H&E sections from the spleens of 400 day old mice. c) Average spleen length of one year old mice, n=4 mice per genotype. Representative B220 immunostains on 400 day old spleens from (d) $atmin^{f/f}$; $p53^{f/f}$ and (e) $atmin^{\Delta B/\Delta B}$; $p53^{\Delta B/\Delta B}$ mice. Three mice per genotype are shown. Student's t-test was used for statistical analysis (n.s. not-significant).

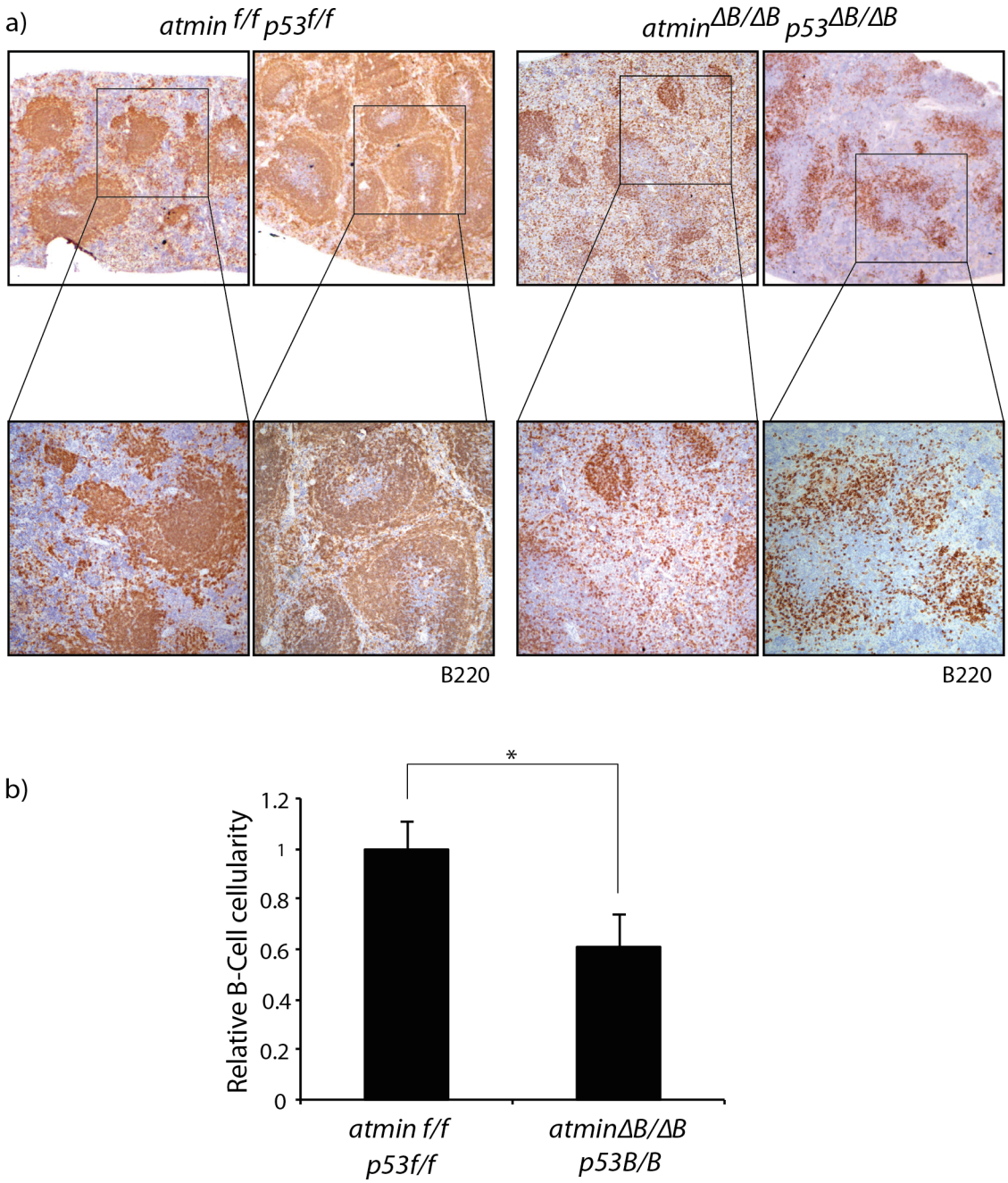

Figure 39: Reduced B cell cellularity in the spleens of old *atmin*$^{\Delta B/\Delta B}$; *p53*$^{\Delta B/\Delta B}$ mice

a) Representative B220 immunostains of 400 day old spleens. Two mice of each genotype are shown. b) Relative B cell cellularity in 400 day old mice. The number of B cells in 0.5mm^2 sections of germinal centres was counted and normalised to wildtype. Student's t-test was used for statistical analysis (*$p<0.05$), n=3 mice per genotype.

Chapter 5. Competition between ATMIN and NBS1 regulates ATM signalling

ATM's two known co-factors, ATMIN and NBS1, both interact with ATM through a conserved C-terminal ATM interaction motif. ATM signalling proceeds via interaction with NBS1 after DSB induction and ATMIN after changes to chromatin structure (Kanu and Behrens, 2008). Although ATM deletion results in viable mice, loss of either ATMIN or NBS1 is embryonically lethal. The aim of my project was to investigate the mechanistic basis of ATM co-factor choice and the discrepancy between NBS1 and ATM null phenotypes.

5.1 ATMIN deficiency rescues the proliferation arrest and senescence induction of NBS1 deleted MEFs

To study ATMIN and NBS1 function I generated *atmin*$^{f/f}$, *nbs1*$^{f/f}$ and compound mutant *nbs1*$^{f/f}$; *atmin*$^{f/f}$ primary MEFs at E12.5. The early embryonic lethality of *nbs1*$^{\Delta/\Delta}$ embryos at approximately E8.5 precluded the use of the straight knockout. Instead, I acutely inactivated *nbs1* and *atmin* gene function by adenoviral mediated expression of *Cre* recombinase (Figure 40a). Floxed MEFs were infected with either Adeno-Cre or Adeno-GFP control virus for 48 hours, yielding the single mutant *atmin*$^{\Delta/\Delta}$, *nbs1*$^{\Delta/\Delta}$ and compound mutant *nbs1*$^{\Delta/\Delta}$; *atmin*$^{\Delta/\Delta}$ MEFs. Cells cultures were left for a further 48 hours to recover. DNA was then extracted from the infected cells and recombination efficiency assessed by genotyping PCR (Figure 40b). The presence of the 'Δ' band, and absence of the 'floxed' band exclusively in the Adeno-Cre infected samples confirms adenoviral infection with *Cre* recombinase achieves efficient recombination of the *atmin* and *nbs1* floxed alleles.

Before embarking on a thorough analysis of the phenotype of recombined cells, I wanted to ensure that infection with Adeno-Cre did not significantly alter the cell cycle profile or genome copy number. FACS analysis for DNA content was performed on

Adeno-Cre and Adeno-GFP infected cells at the end of the 48 hour recovery period. Representative FACS plots are shown (Figure 40c, d). Expression of *Cre* recombinase does not alter cell cycle distribution (Figure 40e). Moreover, genome copy number, as measured by '4N' content, is unaffected (Figure 40f). Thus, adenoviral mediated recombination of floxed MEFs is a good model system to analyse the effects of *atmin* and *nbs1* deletion.

Deletion of *nbs1* from MEFs is reported to result in proliferation arrest (Yang et al., 2006). As expected, deletion of *nbs1* resulted in a rapid cessation of proliferation. Given low oxygen conditions are known to prolong the proliferative lifespan of primary MEFs (Parrinello et al., 2003), it is noteworthy that arrest of $nbs1^{\Delta/\Delta}$ occurs even at low (3%) oxygen culture conditions. Surprisingly, after passaging *wildtype*, $atmin^{\Delta/\Delta}$, and $nbs1^{\Delta/\Delta}$; $atmin^{\Delta/\Delta}$ cell cultures reached confluent densities, whereas proliferation arrest at subconfluent densities occurred in the $nbs1^{\Delta/\Delta}$ mutants (Figure 41a). Growth curves expanded this observation; $nbs1^{\Delta/\Delta}$; $atmin^{\Delta/\Delta}$ compound mutant cells achieved a higher cumulative cell number than the $nbs1^{\Delta/\Delta}$ mutants (Figure 41b). The deletion of *atmin* alone from early passage MEFs at 3% oxygen did not alter cumulative cell number (Figure 41b). This is in agreement with independent growth curves performed on $atmin^{\Delta/\Delta}$ MEFs (Figure 20a). This growth curve analysis suggests $atmin^{\Delta/\Delta}$, $nbs1^{\Delta/\Delta}$; $atmin^{\Delta/\Delta}$ and $nbs1^{\Delta/\Delta}$ mutants have different proliferation potentials.

To further characterise the defects of $nbs1^{\Delta/\Delta}$ cells, proliferation was measured by quantifying BrdU incorporation. NBS1-deficiency reduced by half the number of BrdU positive cells, as measured by FACS analysis (Figure 41c). This proliferation defect was partially rescued in the $nbs1^{\Delta/\Delta}$; $atmin^{\Delta/\Delta}$ double mutant. A proliferation defect was not observed in $atmin^{\Delta/\Delta}$ MEFs. The percentage of BrdU positive cells was also measured by immunofluorescent staining for BrdU (Figure 41d, e). In contrast to the 5.9% BrdU positive cells observed in the wildtype population, 3.3% $nbs1^{\Delta/\Delta}$ cells were BrdU positive. Recapitulating the FACS data, the proliferation defect of $nbs1^{\Delta/\Delta}$ cells was somewhat rescued in the double mutant, where 4.6% of cells were BrdU positive. Taken together, these BrdU analysis and growth curve demonstrate the cellular proliferation defect observed upon *nbs1* deletion is partially rescued by concomitant loss of *atmin*.

The flattened, enlarged morphology and sub-confluent proliferation arrest observed in *nbs1*$^{\Delta/\Delta}$ MEFs strongly suggests senescence. To confirm this, senescence associated β-galactosidase staining was performed ten days after gene deletion (Figure 42a). Quantification of the percentage of positively staining (blue) cells confirmed increased senescence induction in *nbs1*$^{\Delta/\Delta}$ MEFs; with 29.2% of cells senescent compared to 5.4% of wildtype cells (Figure 42b). Senescence induction was significantly reduced, to 12.3%, in *nbs1*$^{\Delta/\Delta}$*; atmin*$^{\Delta/\Delta}$ mutants. It is noteworthy that at later passages, at 3% oxygen conditions, *nbs1*$^{\Delta/\Delta}$; *atmin*$^{\Delta/\Delta}$ MEFs still enter premature senescence (data not shown) - a similar phenotype to *atm*$^{-/-}$ primary MEFs (Xu and Baltimore, 1996).

The reduced cumulative cell number observed in *nbs1*$^{\Delta/\Delta}$; *atmin*$^{\Delta/\Delta}$ mutant MEFs (Figure 41b) could be contributed to by increased apoptosis. I quantified the percentage of trypan blue positive cells in wildtype, *nbs1*$^{\Delta/\Delta}$, *atmin*$^{\Delta/\Delta}$ and *nbs1*$^{\Delta/\Delta}$; *atmin*$^{\Delta/\Delta}$ MEFs at days seven to ten after gene deletion. There was no significant reduction in the percentage of viable cells in either *nbs1*$^{\Delta/\Delta}$ or *nbs1*$^{\Delta/\Delta}$; *atmin*$^{\Delta/\Delta}$ mutants (Figure 42c). Accordingly, the main phenotype of *nbs1* deletion in primary MEFs is proliferation arrest and premature senescence, not increased cell death.

Taking together these results, we can surmise that concomitant *atmin* and *nbs1* deletion significantly ameliorates the proliferation defects and senescence induction observed in the *nbs1*$^{\Delta/\Delta}$ primary MEFs.

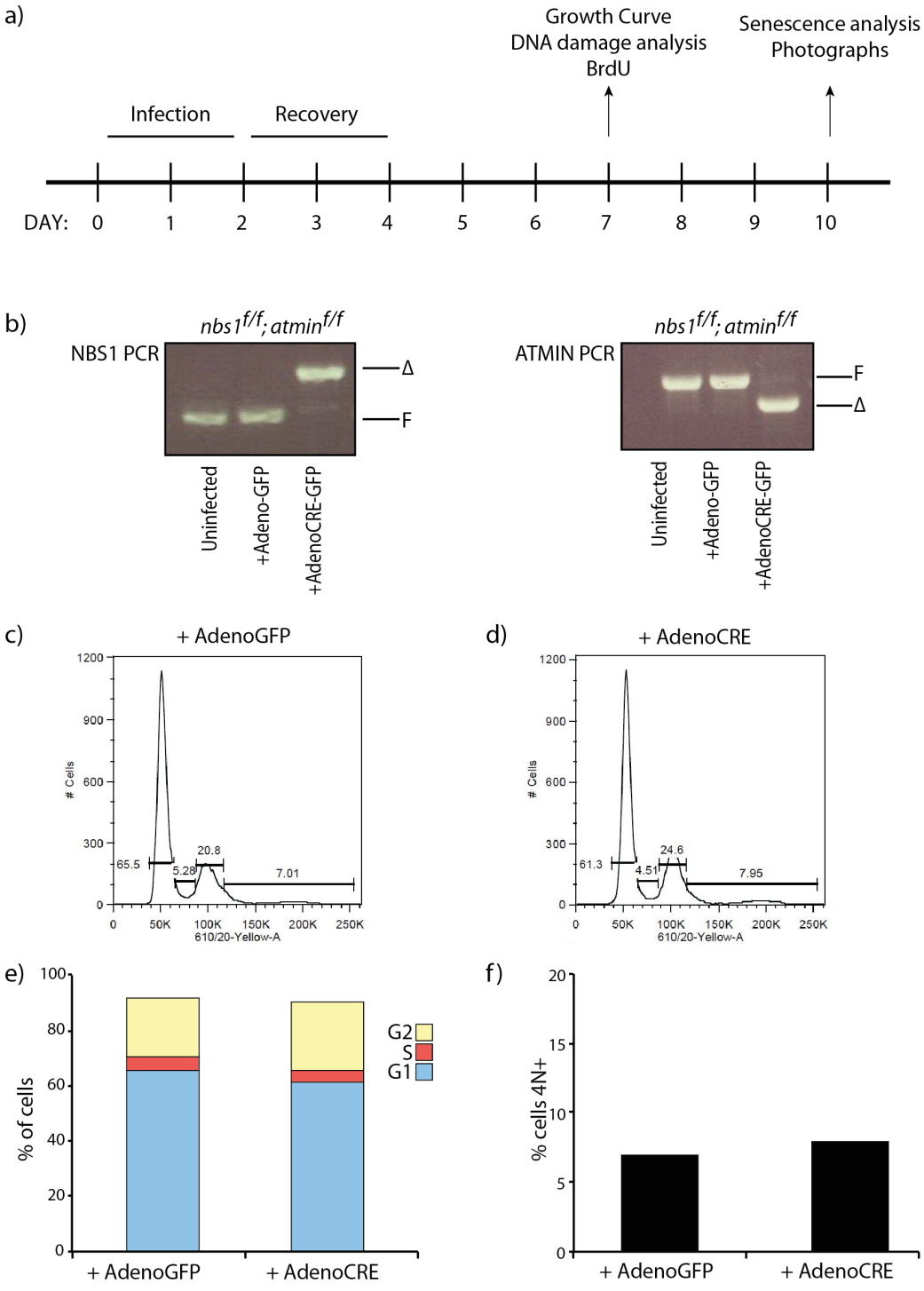

Figure 40: An inducible system for *atmin* and *nbs1* deletion in primary MEFS

a) Timeline of Adenovirus infection of primary MEFs at passage two, and the timepoints of subsequent analyses performed. b) *nbs1*$^{f/f}$*; atmin*$^{f/f}$ MEFs were infected with either AdenoCre-GFP or Adeno-GFP virus. Seven days later ATMIN and NBS1 genotyping PCR was performed to confirm gene deletion. FACS analysis for cell cycle distribution of sub-confluent *atmin*$^{+/+}$ primary MEFs seven days after (c) Adeno-GFP or (d) AdenoCre-GFP infection. e) Quantification of cell cycle phases depicted in (c, d). Percentage of cells with a DNA content of 4N or greater, as analysed in (c,d).

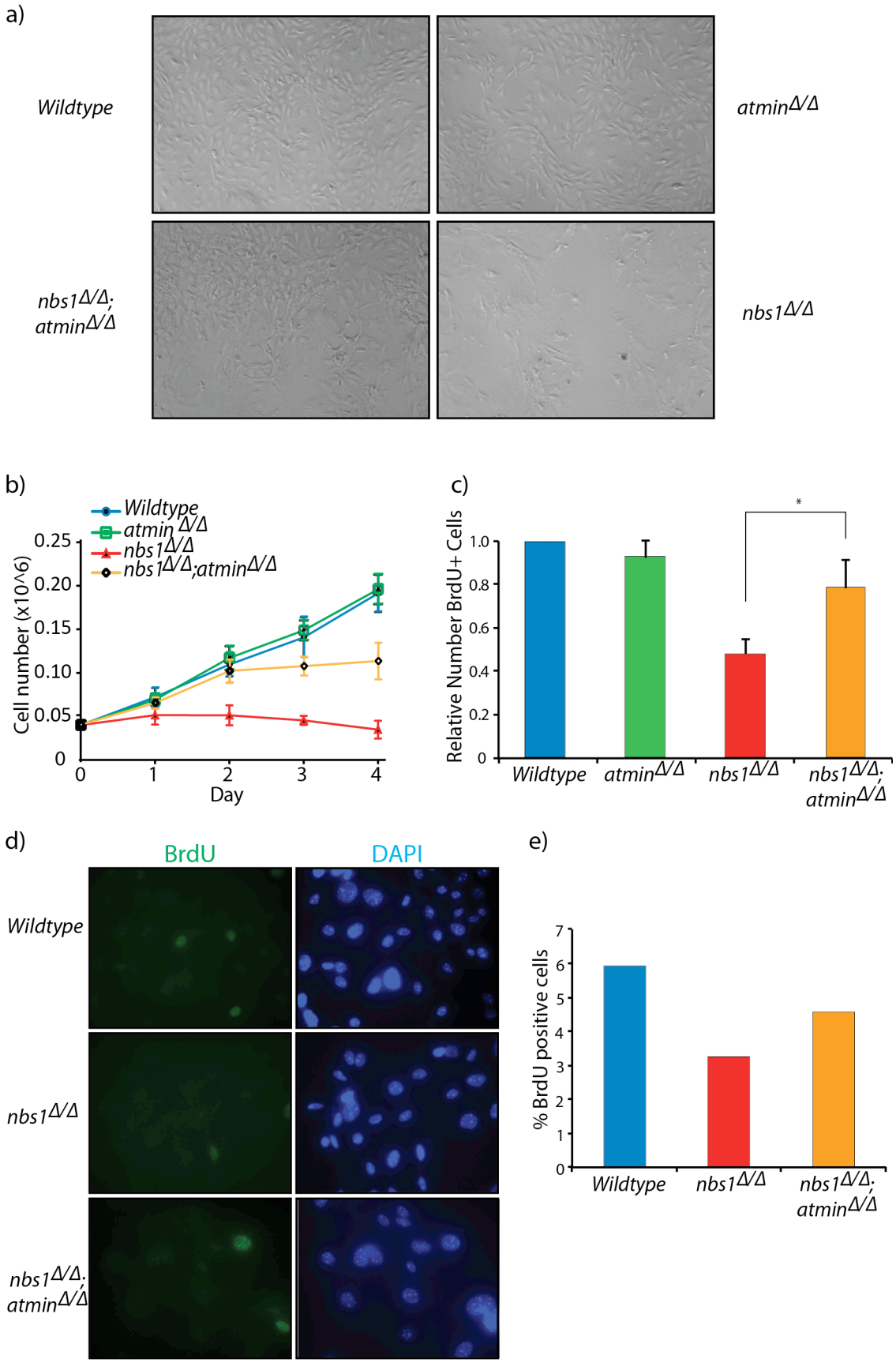

Figure 41: ATMIN co-deletion rescues the proliferation arrest of NBS1 deficient cells

a) Photographs of primary MEFs ten days after infection with either Adeno-GFP (*atmin*$^{f/f}$, *nbs1*$^{f/f}$ and *nbs1*$^{f/f}$*; atmin*$^{f/f}$) or AdenoCre-GFP (*atmin*$^{\Delta/\Delta}$, *nbs1*$^{\Delta/\Delta}$ and *nbs1*$^{\Delta/\Delta}$*;atmin*$^{\Delta/\Delta}$). b) Seven days after Adenovirus infection 0.04x10^6 cells per well of the indicated genotypes were plated. Total cell number was counted in triplicate each day for the following four days. MEFs were cultured in medium containing 10μM BrdU for 30min, and the percentage of cells that had incorporated BrdU was analysed by c) flow cytometry or (d, e) IF staining for BrdU. The percentage of BrdU positive cells is expressed relative to wildtype. Student's t-test was used for statistical analysis (*$p<0.05$).

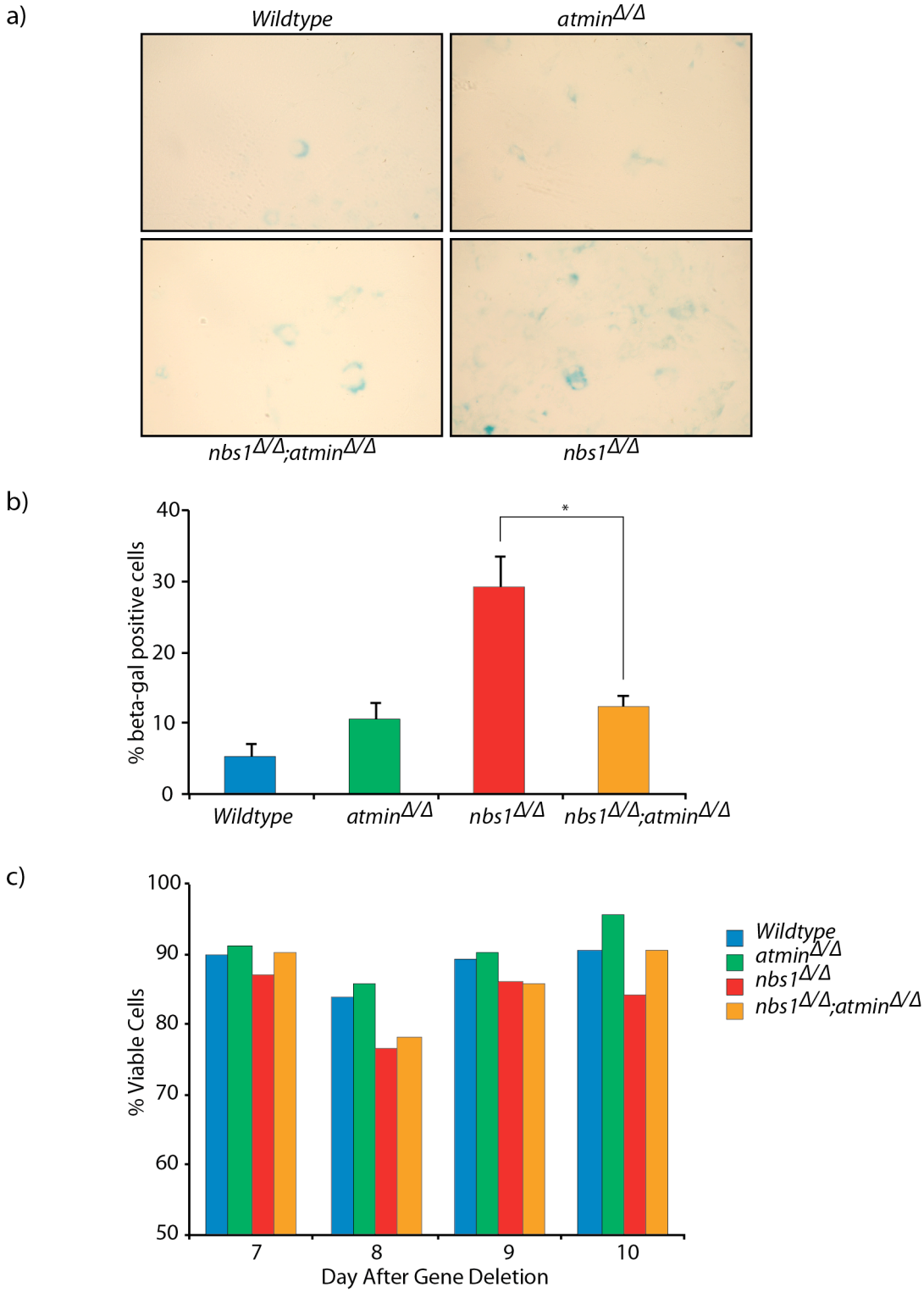

Figure 42: ATMIN deficiency rescues the premature senescence of *nbs1*$^{\Delta/\Delta}$ MEFs

a) Ten days after infection the percentage of senescent cells was analysed by β-galactosidase staining, (b) Quantification of (a). c) Percentage of viable cells, as assessed by trypan blue exclusion, at days seven to ten after gene deletion in primary MEFs. Student's t-test was used for statistical analysis, n=3 independent experiments (*$p<0.05$).

5.2 ATMIN inactivation prevents the intestinal progenitor cell loss induced by NBS1 deficiency

To investigate the phenotype of cells doubly deficient for ATMIN and NBS1 in more detail, the intestine was used as a model system. An inducible Villin-CreERT system was used to specifically induce gene deletion in adult intestinal epithelial cells. Cohorts of *atmin*$^{f/f}$; *Villin-CreERT*, *nbs1*$^{f/f}$*; Villin-CreERT, nbs1*$^{f/f}$*; atmin*$^{f/f}$*; Villin-CreERT* and Cre-negative controls were generated. To activate *Cre* recombinase expression and achieve deletion of the floxed alleles three consecutive daily injections of tamoxifen were administrated, yielding *atmin*$^{\Delta G/\Delta G}$, *nbs1*$^{\Delta G/\Delta G}$ or *nbs1*$^{\Delta G/\Delta G}$*; atmin*$^{\Delta G/\Delta G}$ mice. Five days after the final injection animals were sacrificed and DNA isolated from the villi and crypts of intestine. Genotyping PCR for the *atmin* and *nbs1* loci confirmed efficient gene deletion in the intestines of *nbs1*$^{f/f}$*; atmin*$^{f/f}$*; Villin-CreERT* animals (Figure 43a). Moreover, GFP intestinal staining for LSL-Rosa-YFP; *Villin-CreERT* mice subjected to the same tamoxifen injection regime demonstrated a high efficiency of recombination (Figure 43b). Thus, the Villin-CreERT model is a suitable system to study the consequences of *atmin* and *nbs1* loss *in vivo*.

Five days after intestinal *nbs1* deletion H&E staining demonstrated structural disintegration of the intestinal mucosa (Figure 43c). The loss of integrity of the regular villi structure and reduced cell occupancy in the crypt is particularly evident at higher magnification (Figure 43d). In contract, the intestinal architecture of *nbs1*$^{\Delta G/\Delta G}$; *atmin*$^{\Delta G/\Delta G}$ animals is largely intact (Figure 43c, d).

I next wanted to investigate if *nbs1* deletion influenced stem-cell commitment into different intestinal lineages. Fast Red staining highlighted the loss of villi integrity in *nbs1*$^{\Delta G/\Delta G}$ intestines, and the rescue in *nbs1*$^{\Delta G/\Delta G}$; *atmin*$^{\Delta G/\Delta G}$ animals (Figure 44a). P.A.S. staining for goblet cells demonstrated a mild reduction, from 10.1 to 8.9, in the number of goblet cells per villi in the *nbs1*$^{\Delta G/\Delta G}$ intestine (Figure 44b, e). However this was not statistically significant (n=3, p=0.12). Chromogranin staining to detect endocrine cells demonstrated a mild reduction in the percentage of chromogranin-positive villi, from 35.0% to 31.4% (Figure 44c, f). Sections were stained with lysozyme to detect Paneth

cells, which were still present in all four genotypes (Figure 44d). Taken together, this examination of the different intestinal lineages suggests neither *nbs1* nor *atmin* deletion strongly effects intestinal stem cell lineage commitment.

The intestine is a highly proliferative organ, and differentiated cells are rapidly replenished from the stem cell pool that resides at the base of the crypt. MCM6 is a marker of undifferentiated intestinal cells at the base of the crypt (Haigis et al., 2006). Five days after *atmin* and *nbs1* gene deletion the total number of MCM6 positive cells per crypts had not significantly decreased (Figure 45a, c). However, only MCM6 positive cells at the bottom of the crypts are part of the undifferentiated pool, not cells in higher positions. Examination of MCM6 positive cells at the base of $nbs1^{\Delta G/\Delta G}$ crypts revealed a marked reduction from 55.7% to 22.9% (p=0.0093) in progenitor cells (Figure 45b, d). Conversely, quantification of $nbs1^{\Delta G/\Delta G}$; $atmin^{\Delta G/\Delta G}$ animals demonstrated a rescue of the $nbs1^{\Delta G/\Delta G}$ phenotype; compound mutants had 52.7% MCM6 positive cells in the base of their crypts, similar to wildtype levels (Figure 45b, d). Therefore loss of ATMIN prevents the progenitor cell deficiency induced by NBS1 inactivation.

The observation intestinal *nbs1* deletion leads to progenitor cell loss suggests *nbs1* deletion may required for intestinal stem cell maintenance. To characterise this, ISH for the intestinal stem cell marker *olfm4* was performed on intestines 24 hours and five days after gene deletion. 24 hours after *nbs1* deletion the number of *olfm4* positive cells per crypt had reduced from 5.0 to 3.5 (Figure 45e, f). The reduction in *olfm4* positive cells is rescued in $nbs1^{\Delta G/\Delta G}$; $atmin^{\Delta G/\Delta G}$ mice. However, five days after gene deletion *olfm4* positive stem cells number per crypt was dramatically reduced in both $nbs1^{\Delta G/\Delta G}$ and $nbs1^{\Delta G/\Delta G}$; $atmin^{\Delta G/\Delta G}$ mice (Figure 45g, h). There was a slight rescue in the number of crypts containing at least one *olfm4* positive cell in the compound mutants compared to $nbs1^{\Delta G/\Delta G}$ deletion alone - 39.1% compared to 15.8% (Figure 45g, i). Nevertheless, it is evident that co-deletion of *atmin* and *nbs1* does not fully rescue the intestinal stem cell loss induced by intestinal *nbs1* deletion.

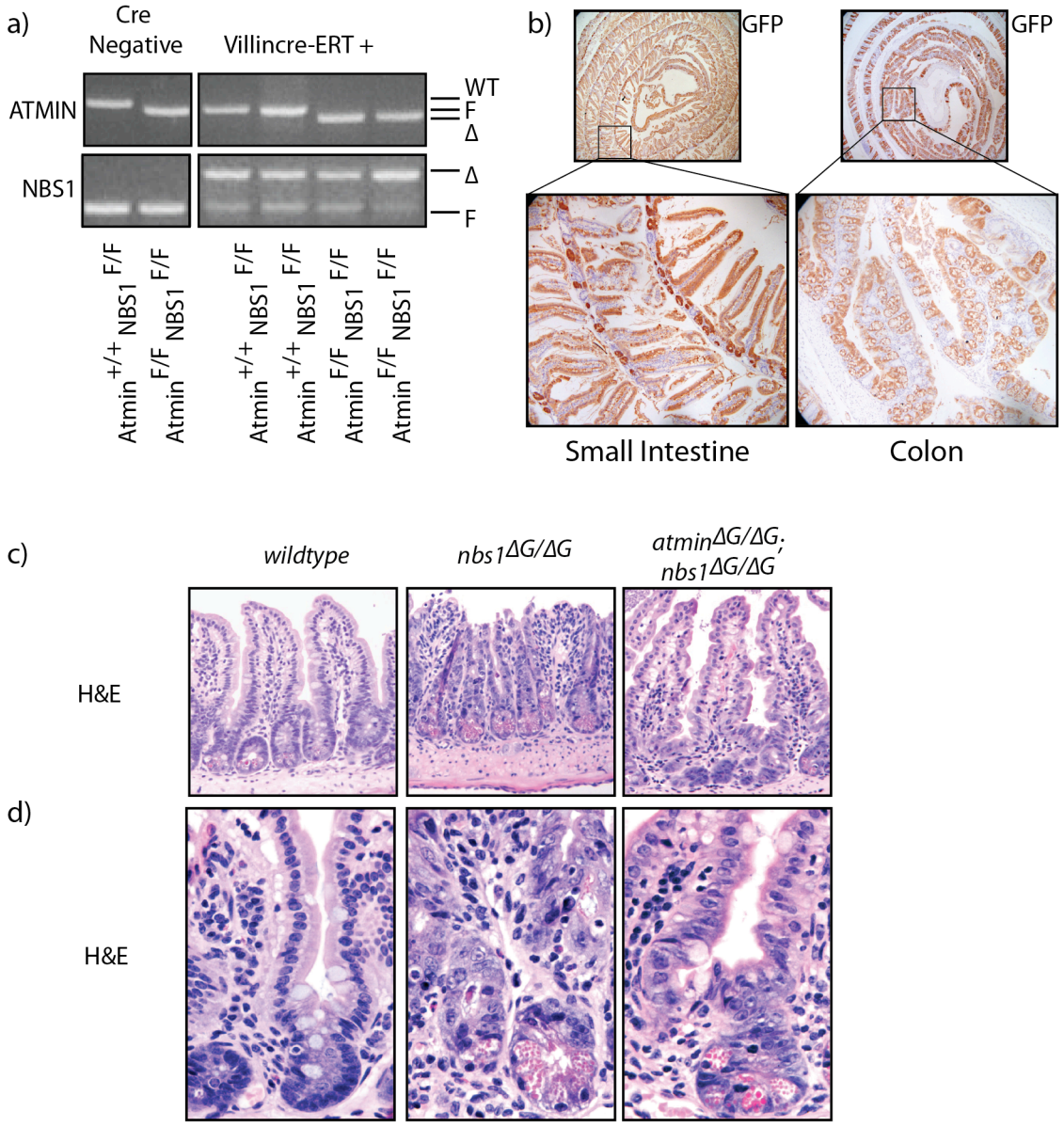

Figure 43: Loss of ATMIN partially rescues the loss of intestinal architecture induced by abrogation of NBS1

a) *atmin* and *nbs1* genotyping PCRs performed on intestinal DNA extracted from mice of the indicated genotypes five days after tamoxifen injection. b) Representative images of GFP stained tamoxifen-injected *Villin-CreERT; LSL-RosaYFP* intestines five days after gene deletion. Representative (c) low and (d) high magnification small intestine H&E sections of the indicated genotypes, five days after gene deletion.

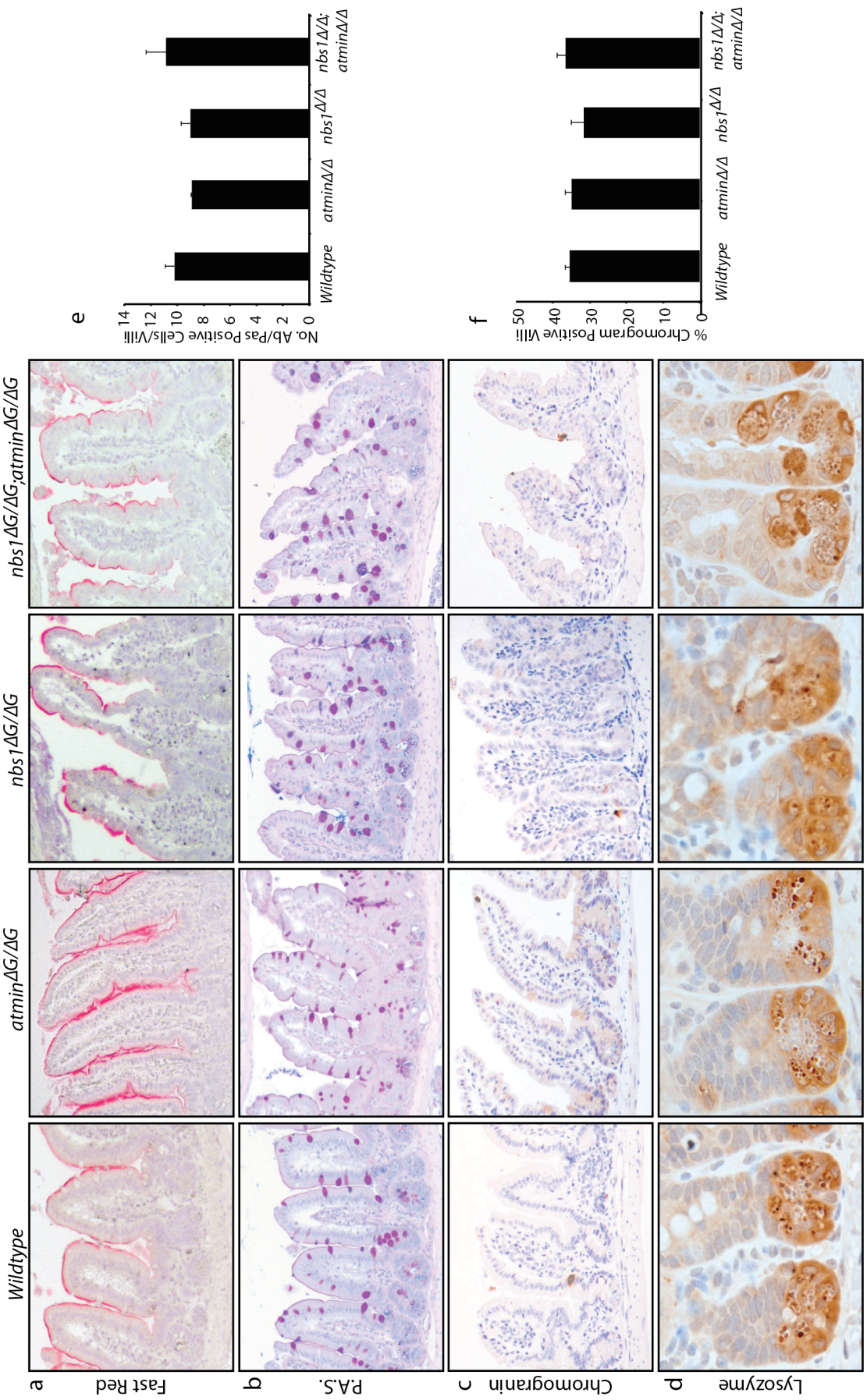
Wildtype
atminΔG/ΔG
nbs1ΔG/ΔG
nbs1ΔG/ΔG;atminΔG/ΔG
a Fast Red
b P.A.S.
c Chromogranin
d Lysozyme
e
No. Ab/Pas Positive Cells/Villi
0
2
4
6
8
10
12
14
Wildtype
atminΔ/Δ
nbs1Δ/Δ
nbs1Δ/Δ; atminΔ/Δ
f
% Chromogram Positive Villi
0
10
20
30
40
50
Wildtype
atminΔ/Δ
nbs1Δ/Δ
nbs1Δ/Δ; atminΔ/Δ

Figure 44: Intestinal architecture of *atmin*$^{\Delta G/\Delta G}$, *nbs1*$^{\Delta G/\Delta G}$, and *nbs1*$^{\Delta G/\Delta G}$*; atmin*$^{\Delta G/\Delta G}$ mice

Representative (a) Fast-red, (b) AB/PAS, (c) chromogranin and (d) lysozyme stainings on the genotypes indicated in untreated conditions, five days after gene deletion. e) Quantification of Ab/Pas positive cells per villus in the SB2 region. f) Quantification of the percentage of villi in the SB2 region with at least one chromogranin positive cells. At least three mice per genotype were analysed.

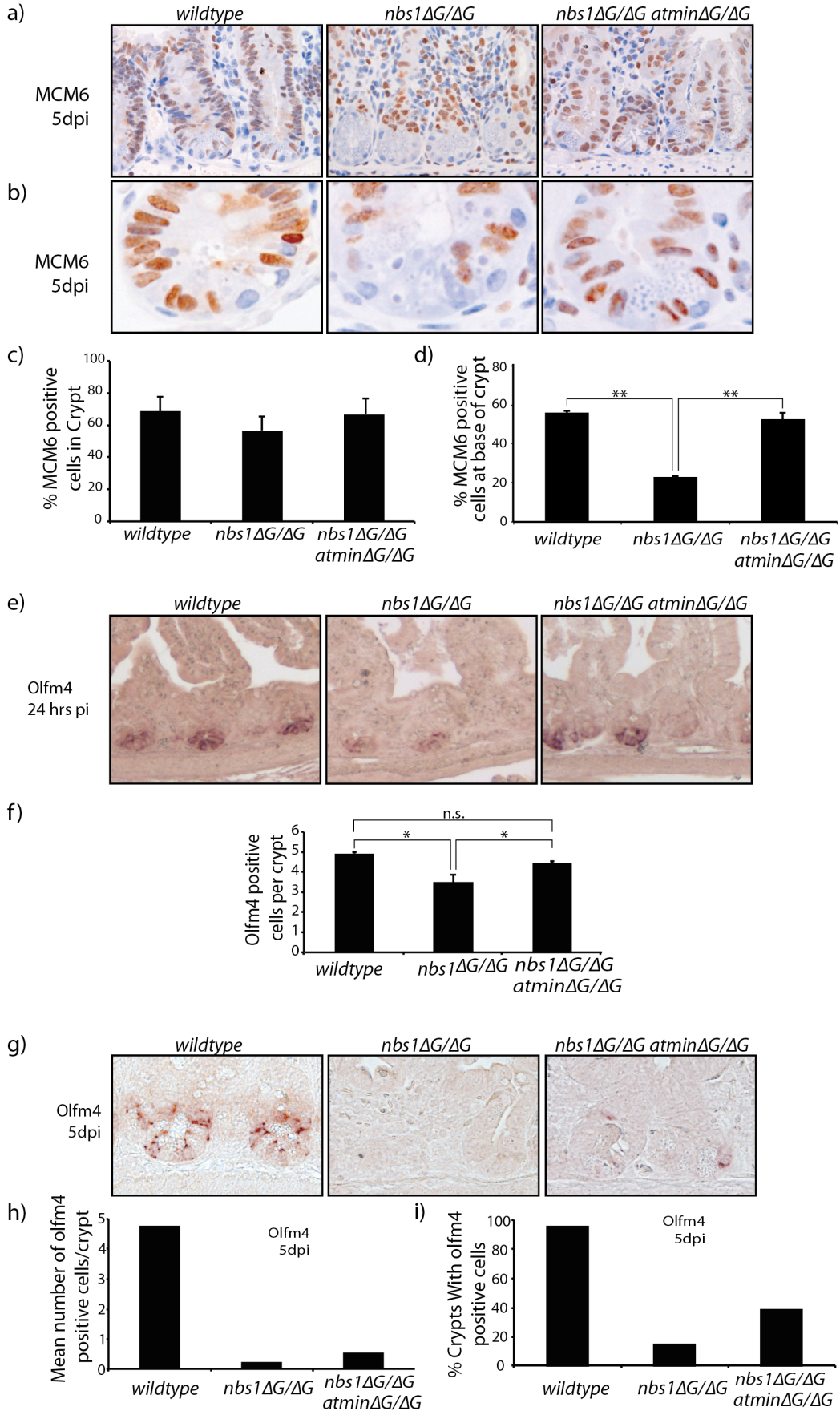
a)
wildtype
nbs1ΔG/ΔG
nbs1ΔG/ΔG atminΔG/ΔG
MCM6
5dpi
b)
MCM6
5dpi
c)
% MCM6 positive cells in Crypt
100
80
60
40
20
0
wildtype
nbs1ΔG/ΔG
nbs1ΔG/ΔG atminΔG/ΔG
d)
% MCM6 positive cells at base of crypt
80
60
40
20
0
**
**
wildtype
nbs1ΔG/ΔG
nbs1ΔG/ΔG atminΔG/ΔG
e)
wildtype
nbs1ΔG/ΔG
nbs1ΔG/ΔG atminΔG/ΔG
Olfm4
24 hrs pi
f)
Olfm4 positive cells per crypt
6
5
4
3
2
1
0
n.s.
*
*
wildtype
nbs1ΔG/ΔG
nbs1ΔG/ΔG atminΔG/ΔG
g)
wildtype
nbs1ΔG/ΔG
nbs1ΔG/ΔG atminΔG/ΔG
Olfm4
5dpi
h)
Mean number of olfm4 positive cells/crypt
5
4
3
2
1
0
Olfm4
5dpi
wildtype
nbs1ΔG/ΔG
nbs1ΔG/ΔG atminΔG/ΔG
i)
% Crypts With olfm4 positive cells
100
80
60
40
20
0
Olfm4
5dpi
wildtype
nbs1ΔG/ΔG
nbs1ΔG/ΔG atminΔG/ΔG

Figure 45: ATMIN loss partially rescues the intestinal stem cell defect induced by NBS1 deletion

a) Immunohistochemistry for MCM6-positive cells on representative small intestine sections of mice with the indicated genotypes, five days after VillinCre-ERT mediated deletion of *atmin* and *nbs1*. b) High magnification of MCM6 immunostained crypts, five days after gene deletion. c) Percentage of MCM6-positive cells in the crypts of the indicated genotypes, as shown in (a). d) Percentage of MCM6-positive cells in the base of the crypts, as shown in (b). e) Representative *olfm4* ISH on small intestine sections of the indicated genotypes, 24 hours after gene deletion. f) Quantification of the number of *olfm4* positive cells per crypt. g) Representative images of *olfm4* ISH on the small intestines five days after gene deletion. h) Quantification of *olfm4* positive cells per crypt, as shown in (g). i) Percentage of crypts with one or more *olfm4* positive cell. Student's t-test was used for statistical analysis (**p<0.01; *p<0.05). At least three mice per genotype were analysed.

5.3 Competition between NBS1 and ATMIN dictates pathway choice of ATM signalling

Depending on the DNA damage stimuli, ATM signalling proceeds via either ATMIN or NBS1. Both ATMIN and NBS1 contain a consensus ATM interaction motif at their C-terminus (Kanu and Behrens, 2007). This indicates ATMIN and NBS1 interact with the same region of ATM and the binding of one precludes the binding of the other, i.e. ATMIN and NBS1 compete for ATM binding. This hypothesis is supported by observation of reduced co-immunoprecipitation, after IR, between ATM and NBS1 upon Flag-ATMIN overexpression (T. Zhang, personal communication). This led to the 'ATM Competition Model' - that competition between NBS1 and ATMIN for ATM binding regulates ATM pathway choice.

One prediction of the 'ATM Competition Model' is increased interaction between ATM-NBS1 should augment irradiation induced ATM signalling. To test this hypothesis, I irradiated $atmin^{\Delta/\Delta}$ MEFs and analysed ATM pathway activation by western blot. $atmin^{\Delta/\Delta}$ MEFs exhibited increased irradiation-induced phosphorylation of pS1987-ATM, pS957-SMC1 and pS824-KAP1 (Figure 46a). Therefore, the absence of ATMIN increases the flux through the NBS1-dependent ATM pathway.

In collaboration with Christopher Bruhn and Zhao-Qi Wang (Fritz-Lipmann Institute, Germany) the reverse experiment was performed. Namely, *nbs1*$^{\Delta/\Delta}$ MEFs were treated with hypotonic shock; an ATMIN dependent ATM stimulus. Western blot analysis demonstrated a mild increase in pS15-p53 and pS1987-ATM levels in *nbs1* deleted cells (Figure 46b). Thus, the lack of NBS1 appears to increase ATMIN-dependent ATM signalling.

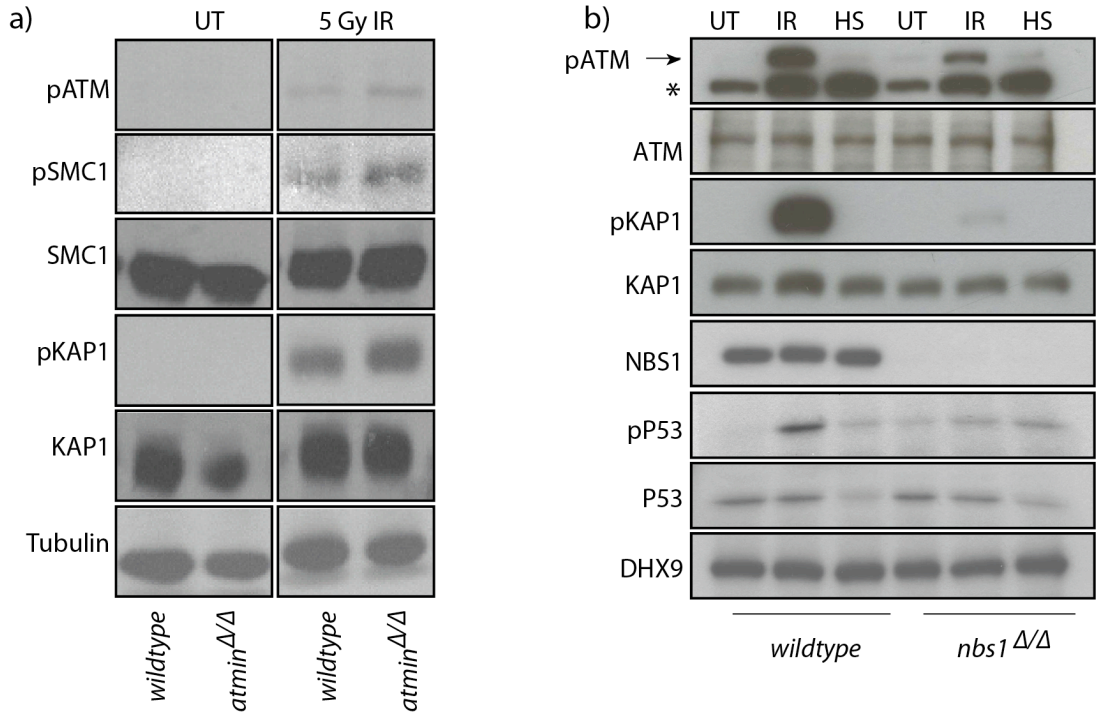

Figure 46: The ATMIN and NBS1 dependent ATM signalling pathways inhibit each other

a) *atmin*$^{f/f}$ primary MEFs were treated with 5 Gy IR five days after infection with Adeno-GFP (wildtype) or AdenoCre-GFP (*atmin*$^{\Delta/\Delta}$). Cells were harvested 60 minutes after IR and immunoblotted for the indicated antibodies. b) *nbs1*$^{f/f}$ *Rosa-CreERT* primary MEFs were spontaneously immortalised by the 3T3 method, then treated with tamoxifen to generate *nbs1*$^{\Delta/\Delta}$ MEFs. Cells were harvested untreated (UT), one hour after 135mOsm hypotonic shock treatment (HS), or 15 minutes after 2 Gy IR (IR). Cell lysates were probed with the indicated antibodies. DHX9 is used as a loading control. The experiment shown in (b) was performed by a collaborator, Christopher Bruhn, at the Leibniz Institute for Age Research, Jena, Germany. * indicates an unspecific band.

5.4 Increased DNA damage and radiosensitivity of *nbs1*$^{\Delta/\Delta}$; *atmin*$^{\Delta/\Delta}$ cells and *nbs1*$^{\Delta G/\Delta G}$; *atmin*$^{\Delta G/\Delta G}$ mice

A hallmark of ATM deficient cells is elevated DNA damage levels under basal conditions. To elucidate the relative contributions of ATMIN and NBS1 to endogenous DNA damage repair I quantified DNA damage in untreated *atmin*$^{\Delta/\Delta}$, *nbs1*$^{\Delta/\Delta}$, and *nbs1*$^{\Delta/\Delta}$; *atmin*$^{\Delta/\Delta}$ MEFs. Cells were grown at low (3%) oxygen for seven days after Adeno-cre mediated gene deletion, then fixed and immunofluorescently stained for the DNA damage markers pH2AX and pS1897-ATM. Compared to wildtype cells, both *atmin*$^{\Delta/\Delta}$ and *nbs1*$^{\Delta/\Delta}$ mutants had increased number of cells with pH2AX foci. Strikingly, compound mutant nbs1$^{\Delta/\Delta}$; *atmin*$^{\Delta/\Delta}$ MEFs had a substantially higher number of cells with pH2AX foci (Figure 47a, b). Moreover, western blot analysis indicated increased pS15-p53 in *atmin*$^{\Delta/\Delta}$ MEFs, indicative of DNA damage (Figure 47c).

The phosphorylation of variant histone H2AX (pH2AX) is a marker for DNA damage, but does not necessarily indicate activation of the ATM signalling pathway. Quantification of cells with pS1987-ATM foci revealed background levels of ATM activation in wildtype, *atmin*$^{\Delta/\Delta}$ and *nbs1*$^{\Delta/\Delta}$ MEFs. All these three genotypes had approximately 10% of cells positive with pS1987-ATM, consistent with endogenous DNA damage levels (Figure 47a, b). Conversely, there were no detectable pATM foci in *nbs1*$^{\Delta/\Delta}$*; atmin*$^{\Delta/\Delta}$ double mutant cells (Figure 47a, b). This indicates either ATMIN or NBS1 is required for ATM activation; there is no other protein that can substitute for the dual deletion of the two ATM co-factors.

Although unlikely, given the rescue of proliferation and senescence observed in *nbs1*$^{\Delta/\Delta}$; *atmin*$^{\Delta/\Delta}$ cells compared to *nbs1*$^{\Delta/\Delta}$, it is formally possible co-deletion of *atmin* and *nbs1* rescues IR signalling defect of *nbs1* deficient cells. To exclude this possibility I examined pS1987-ATM and pH2AX foci formation after IR. As expected, deletion of *atmin*, *nbs1* or both did not hinder the pH2AX foci formation after irradiation. Irradiated wildtype and *atmin*$^{\Delta/\Delta}$ MEFs activated pS1987-ATM (Figure 48a, b). In contrast, *nbs1* deletion led to a substantial decrease to the formation of pATM foci.

However, the *nbs1*$^{\Delta/\Delta}$*; atmin*$^{\Delta/\Delta}$ double mutants did not form any pS1987-ATM foci after irradiation, despite inducing pH2AX foci formation (Figure 48a, b). Thus, co-deletion of *atmin* and *nbs1* abolishes ATM recruitment to sites of irradiation induced DNA damage, but H2AX phosphorylation still occurs.

Given p1987-ATM foci do not form after IR in *nbs1*$^{\Delta/\Delta}$*; atmin*$^{\Delta/\Delta}$ MEFs, one would expect ATM and its downstream substrates are not phosphorylated. To confirm this, I performed a western blot analysis for pS1987-ATM, pS957-SMC1 and pS824-KAP1 phosphorylation in irradiated mutant cells. As seen previously, *atmin* deletion augments the phosphorylation of these ATM substrates (Figure 48c). Furthermore, neither *nbs1*$^{\Delta/\Delta}$ nor *nbs1*$^{\Delta/\Delta}$*; atmin*$^{\Delta/\Delta}$ MEFs show any detectable ATM substrate phosphorylation in irradiated cells (Figure 48). Indeed, even at very high radiation doses, 10 Gy and 20 Gy, there is no phosphorylation of pS284-KAP1 in *nbs1*$^{\Delta/\Delta}$*; atmin*$^{\Delta/\Delta}$ and *nbs1*$^{\Delta/\Delta}$ cells (Figure 48d). Thus, *atmin* deletion does not recuse the DSB signalling defect of *nbs1*$^{\Delta/\Delta}$ MEFs.

Given *nbs1*$^{\Delta/\Delta}$*; atmin*$^{\Delta/\Delta}$ MEFs have total abrogation of IR-induced ATM signalling, it followed to assess the functionality of IR-induced DNA repair. Radiosensitivity was measured as the percentage of apoptotic (sub-G1) cells over 36 hours after 10 Gy irradiation (Figure 49a). *nbs1*$^{\Delta/\Delta}$*; atmin*$^{\Delta/\Delta}$ MEFs undergo increased apoptosis compared to wildtype cells. In line with published data, *atmin*$^{\Delta/\Delta}$ deficient MEFs demonstrated mild radioresistance (Kanu and Behrens, 2007). To more clearly analyse the radiosensitivity of *nbs1*$^{\Delta/\Delta}$; *atmin*$^{\Delta/\Delta}$ MEFs, the radiosensitivity assay was repeated at 20 Gy IR. At every timepoint after IR, *nbs1*$^{\Delta/\Delta}$*; atmin*$^{\Delta/\Delta}$ MEFs had a higher percentage of sub-G1 cells than observed in the wildtype population (Figure 49b). Representative FACS plots are shown (Figure 49c). The deletion of *atmin* renders MEFs mildly radioresistant; co-deletion of *nbs1*$^{\Delta/\Delta}$ and *atmin*$^{\Delta/\Delta}$ renders MEFs severely radiosensitive.

The *in vivo*, as well as *in vitro,* functionality of DNA repair after IR was investigated. Whole-body irradiation of *nbs1*$^{f/f}$*; atmin*$^{f/f}$ and *nbs1*$^{\Delta G/\Delta G}$*; atmin*$^{\Delta G/\Delta G}$ mice at the sub-lethal doses 7 Gy and 10 Gy resulted in the dose-dependent lethality of *nbs1*$^{\Delta G/\Delta G}$*; atmin*$^{\Delta G/\Delta G}$ mice (Figure 50a). Histological analysis of *nbs1*$^{\Delta G/\Delta G}$*; atmin*$^{\Delta G/\Delta G}$ mice 24

hours after irradiation showed cell loss and extensive radiation injury (Figure 50b). Although pH2AX foci were observed in IR treated *nbs1*$^{\Delta G/\Delta G}$*; atmin*$^{\Delta G/\Delta G}$ intestines (Figure 50c), no 53BP1 focus formation was observed (Figure 50d). To confirm the abrogation of ATM pathway activation in irradiated *nbs1*$^{\Delta G/\Delta G}$*; atmin*$^{\Delta G/\Delta G}$ animals, intestinal cells were isolated and cell lysates prepared. Western blotting revealed a complete absence of pS1987-ATM, pS957-SMC1, pS824-KAP1 and pS15-p53 - i.e. no ATM pathway activation (Figure 50e). In summary, both *in vivo* and in *vitro* doubly deficient *nbs1; atmin* cells are radiosensitive and are unable to activate the IR-induced ATM signalling pathway.

5.5 Concluding Remarks

ATM activation proceeds by interaction with either ATMIN or NBS1. To investigate co-factor choice I studied *nbs1*$^{\Delta/\Delta}$, *atmin*$^{\Delta/\Delta}$*;* and compound mutant *nbs1*$^{\Delta/\Delta}$*; atmin*$^{\Delta/\Delta}$ MEFs and murine intestines. Unexpectedly, *atmin* deletion from *nbs1*$^{\Delta/\Delta}$ cells partially rescues the premature senescence and proliferation defect of *nbs1*$^{\Delta/\Delta}$ MEFs (Figure 41, Figure 42), and the progenitor pool loss of *nbs1*$^{\Delta G/\Delta G}$ intestines (Figure 45). There is competition between ATMIN and NBS1 for ATM. Loss of ATMIN increases IR-induced, NBS1-dependent ATM signalling and loss of NBS1 increases hypotonic shock-induced, ATMIN-dependent ATM signalling (Figure 46). *nbs1*$^{\Delta/\Delta}$*; atmin*$^{\Delta/\Delta}$ compound mutant MEFs exhibit greater endogenous DNA damage than either of the single mutants (Figure 47), are radiosensitive (Figure 49) and display and no pS1987-ATM autophosphorylation after IR (Figure 48). Hence ATMIN and NBS1 mediate all pS1981-ATM foci formation, and increased ATMIN-dependent ATM signalling explains the different phenotypes of nbs1- and atm-mutant cells. Thus antagonism between ATMIN and NBS1 is a crucial regulatory mechanism of ATM signalling and function.

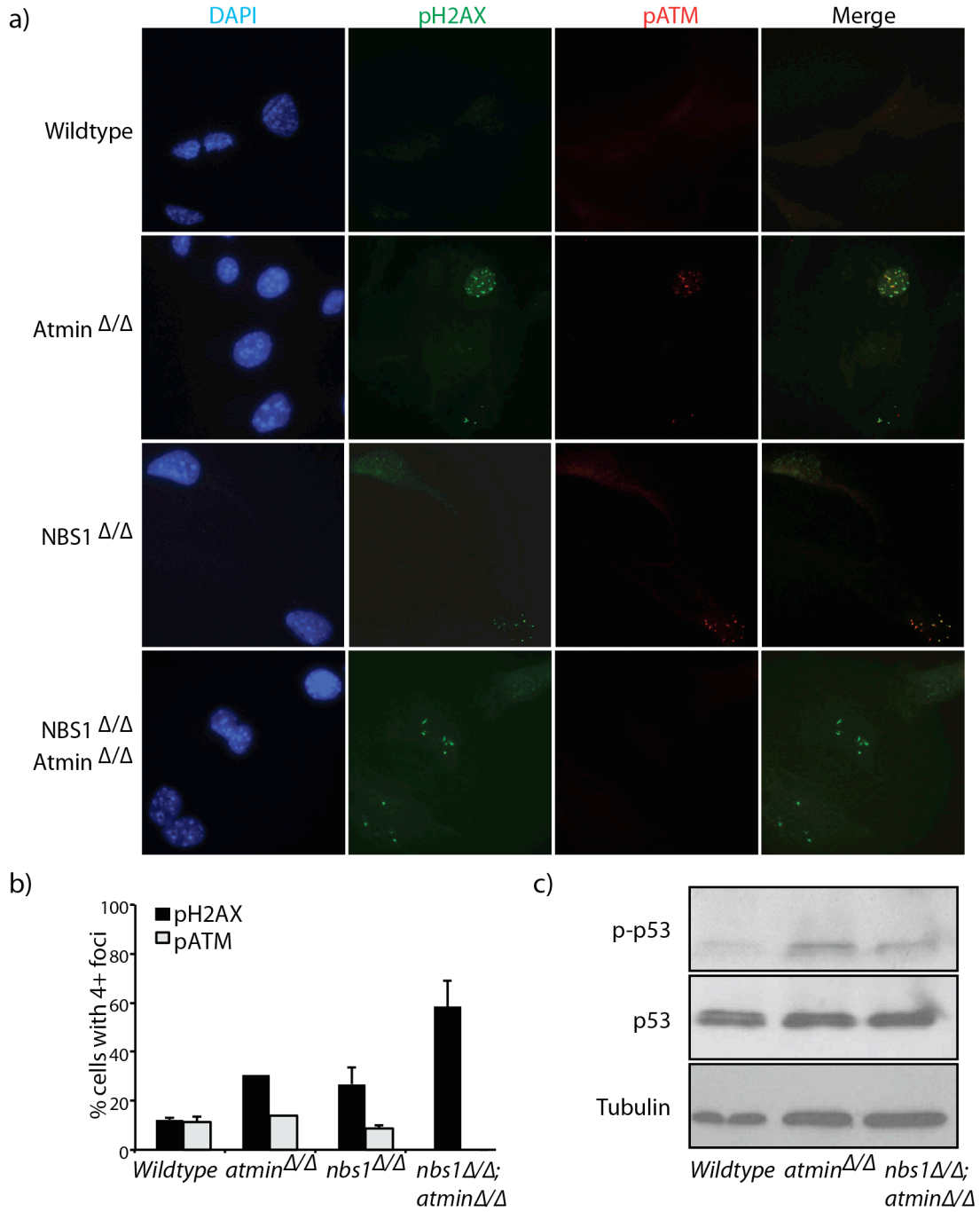

Figure 47: *nbs1*$^{\Delta/\Delta}$;*atmin*$^{\Delta/\Delta}$ MEFs have high levels of endogenous DNA damage

a) MEFs were infected with either Adeno-GFP (*atmin*$^{f/f}$, *nbs1*$^{f/f}$ and *nbs1*$^{f/f}$;*atmin*$^{f/f}$) or AdenoCre-GFP (*atmin*$^{\Delta/\Delta}$, *nbs1*$^{\Delta/\Delta}$ and *nbs1*$^{\Delta/\Delta}$;*atmin*$^{\Delta/\Delta}$), cultured for seven days, then fixed without treatment and stained for pS1981-ATM and p139-γH2AX. b) Quantification of (a), cells containing four or more foci were counted as positive. c) Cells were harvested seven days after gene deletion and cell lysates separated by SDS-PAGE and membranes probed for p53, pS15-p53 and tubulin.

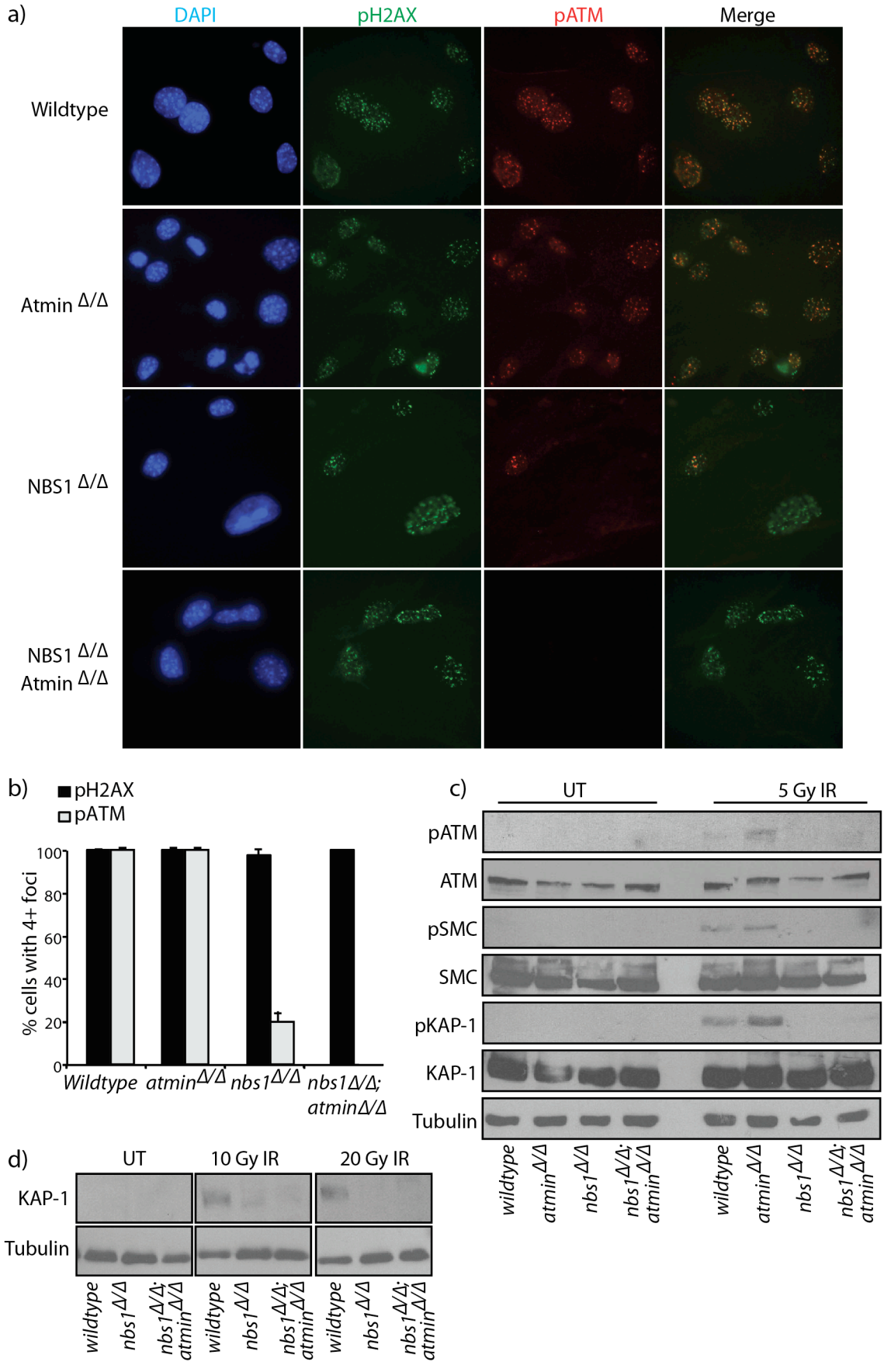
a)
DAPI
pH2AX
pATM
Merge
Wildtype
Atmin Δ/Δ
NBS1 Δ/Δ
NBS1 Δ/Δ
Atmin Δ/Δ
b)
pH2AX
pATM
% cells with 4+ foci
100
80
60
40
20
0
Wildtype
atminΔ/Δ
nbs1Δ/Δ
nbs1Δ/Δ; atminΔ/Δ
c)
UT
5 Gy IR
pATM
ATM
pSMC
SMC
pKAP-1
KAP-1
Tubulin
wildtype
atminΔ/Δ
nbs1Δ/Δ
nbs1Δ/Δ; atminΔ/Δ
d)
UT
10 Gy IR
20 Gy IR
KAP-1
Tubulin
wildtype
nbs1Δ/Δ
nbs1Δ/Δ; atminΔ/Δ

Figure 48: *nbs1*$^{\Delta/\Delta}$*; atmin*$^{\Delta/\Delta}$ MEFs do not activate ATM signalling after IR

MEFs were infected with either Adeno-GFP (*atmin*$^{f/f}$, *nbs1*$^{f/f}$ and *nbs1*$^{f/f}$*;atmin*$^{f/f}$) or AdenoCre-GFP (*atmin*$^{\Delta/\Delta}$, *nbs1*$^{\Delta/\Delta}$ and *nbs1*$^{\Delta/\Delta}$*;atmin*$^{\Delta/\Delta}$), cultured for seven days then a) fixed 60 minutes after treatment with 5 Gy IR and stained for pS1981-ATM and p139-γH2AX. b) Quantification of (a), cells containing four or more foci were counted as positive. Three independent experiments were performed. c) MEFs were treated with 5 Gy IR and lysed after 60 minutes. Whole cell lysates were resolved on a 6% SDS-PAGE gel and immunostained with the indicated antibodies. d) As for (c), except cells were harvested 60 minutes after treatment with either 10 or 20 Gy IR.

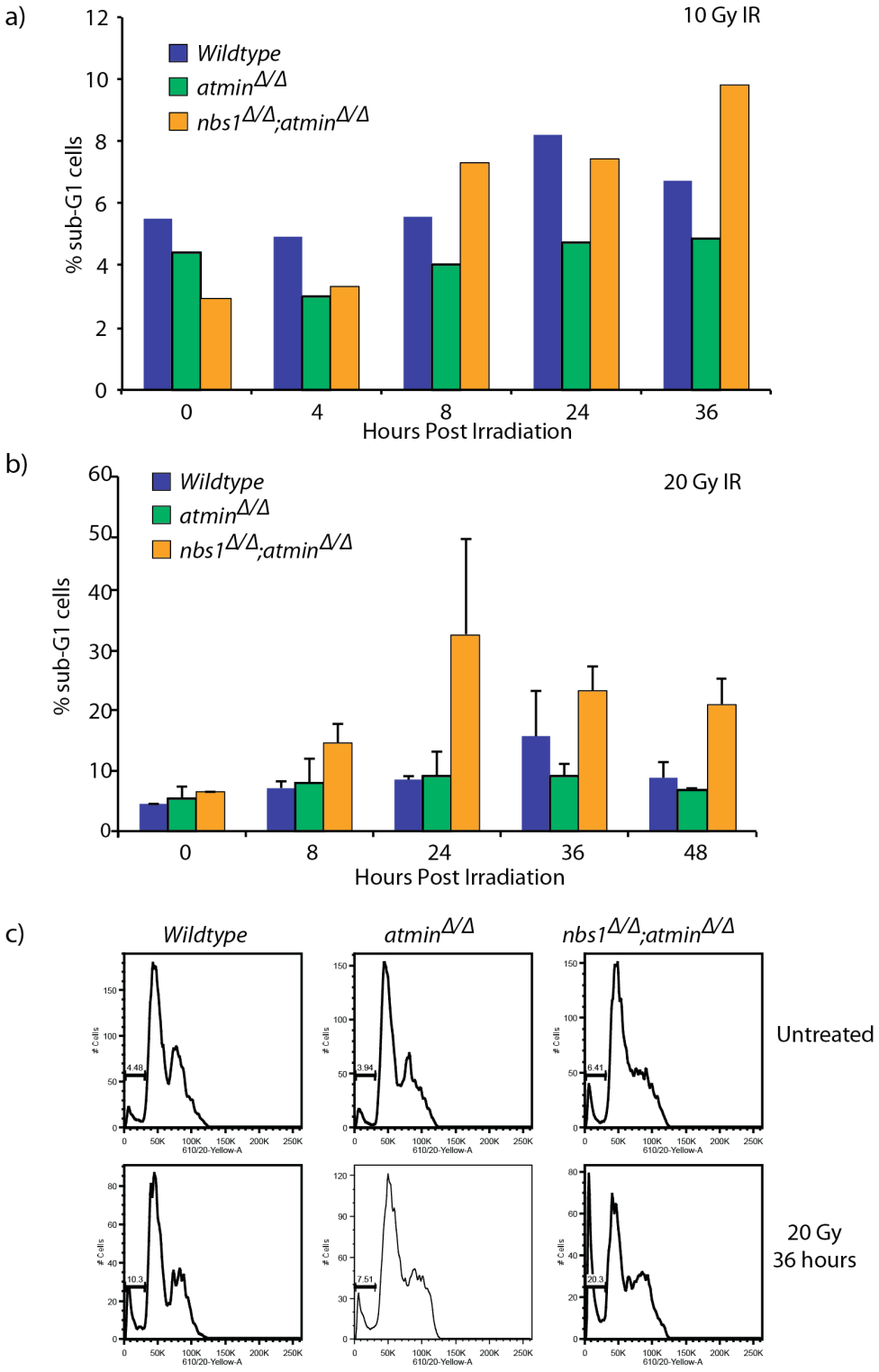

Figure 49: *nbs1*$^{\Delta/\Delta}$*;atmin*$^{\Delta/\Delta}$ cells are radiosensitive

Cells were treated with a) 10 Gy or b) 20 Gy irradiation, and fixed at the indicated timepoints post-treatment. The percentage of subG1 cells was determined by flow cytometry analysis. c) Representative FACS plots for the experiment quantified in (b), which is an average of three independent experiments performed on independent MEF lines.

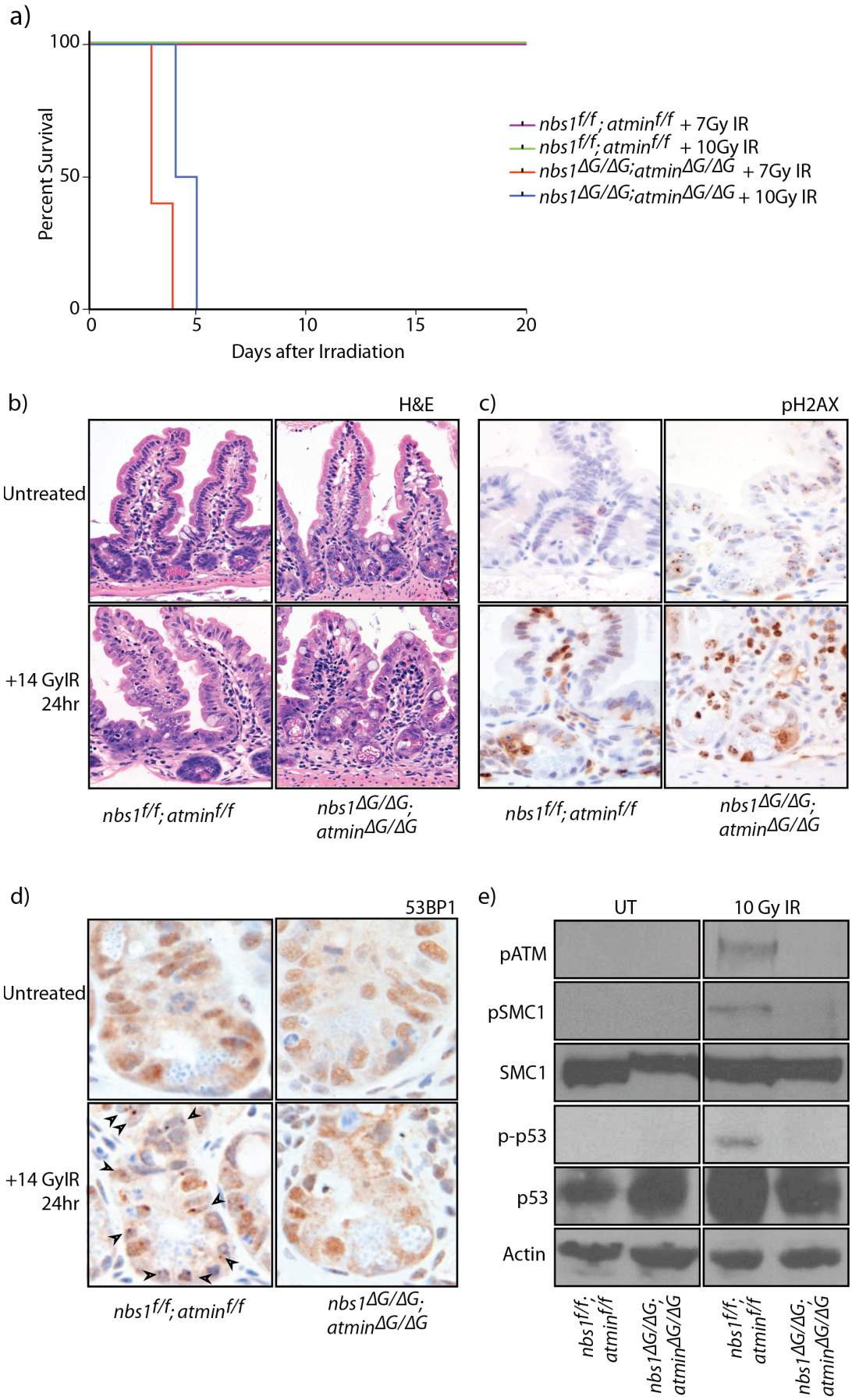
a)
100
50
0
Percent Survival
0
5
10
15
20
Days after Irradiation
nbs1f/f; atminf/f + 7Gy IR
nbs1f/f; atminf/f + 10Gy IR
nbs1ΔG/ΔG;atminΔG/ΔG + 7Gy IR
nbs1ΔG/ΔG;atminΔG/ΔG + 10Gy IR
b)
H&E
Untreated
+14 GyIR 24hr
nbs1f/f; atminf/f
nbs1ΔG/ΔG; atminΔG/ΔG
c)
pH2AX
nbs1f/f; atminf/f
nbs1ΔG/ΔG; atminΔG/ΔG
d)
53BP1
Untreated
+14 GyIR 24hr
nbs1f/f; atminf/f
nbs1ΔG/ΔG; atminΔG/ΔG
e)
UT
10 Gy IR
pATM
pSMC1
SMC1
p-p53
p53
Actin
nbs1f/f; atminf/f
nbs1ΔG/ΔG; atminΔG/ΔG
nbs1f/f; atminf/f
nbs1ΔG/ΔG; atminΔG/ΔG

Figure 50: *nbs1*$^{\Delta G/\Delta G}$*;atmin*$^{\Delta G/\Delta G}$ are radiosensitive

a) Four days after VillinCre-ERT mediated deletion of *atmin* and *nbs1*, mice were treated with the indicated doses of irradiation (n=5 per genotype per dose). b) H&E, c) pH2AX and d) 53BP1 staining on representative intestines of mice with the indicated genotypes, untreated or 24 hours after treatment with 14Gy irradiation. e) Mice were culled two hours after 10 Gy IR, and protein lysates prepared from intestinal tissue. Lysates were resolved on a 6% SDS-PAGE gel and the membrane probed for pS1987-ATM, pS957-SMC1, SMC1 and pS824-KAP1

Chapter 6. DMAP1 is a novel regulator of ATM function

6.1 An shRNA screen for novel ATM regulatory proteins

ATM's two known co-factors, NBS1 and ATMIN, both contain consensus ATM interaction motifs towards their C-termini. Many PI3-K interacting proteins, including Ku80 and ATRIP, share this conserved motif (Falck et al., 2005). It is therefore a reasonable assumption that other, as yet unidentified, proteins involved in DNA repair also contain the conserved ATM interaction motif. One aim of my PhD thesis was to identify novel ATM regulatory proteins in an shRNA based screen. Rather than a genome wide approach, the ATM interaction motif was the basis of a candidate based shRNA screen (Figure 51a).

Firstly, Prosite was used to search the UniProtKB/Swiss-Prot database for proteins containing the sequence (A-X-[DE]-X-[IL]-X-X[DE]-[IL]). This retrieved approximately 40 proteins, including ATMIN and NBS1. The inclusion of ATM's known co-factors in the search results is a positive control for the search criteria. A literature search was performed on the candidate proteins to determine those selected for further screening. The criteria employed for candidate selection were subcellular localisation (if known), the presence of other conserved protein domains and whether the ATM interaction motif was highly conserved. The species conservation of each potential ATM interaction motif was established using the UCSC genome browser. Fifteen proteins were selected for the biochemical phase of the screen.

The second, biochemical, phase of the screen was the design and cloning of two shRNA's for each candidate protein (see page 105). HCT-116 cells transfected with a pool of the two shRNAs were treated with 5 Gy IR or 5 μM aphidicolin. The magnitude of ATM pathway activation was assessed by western blot for the ATM substrate pS957-SMC1. To ensure the SMC1 phosphorylation was ATM specific, cells were also pre-treated with a small molecule ATM kinase inhibitor prior to IR treatment.

Representative results from two candidates, AlkBH7 and Znf507, are shown (Figure 51b).

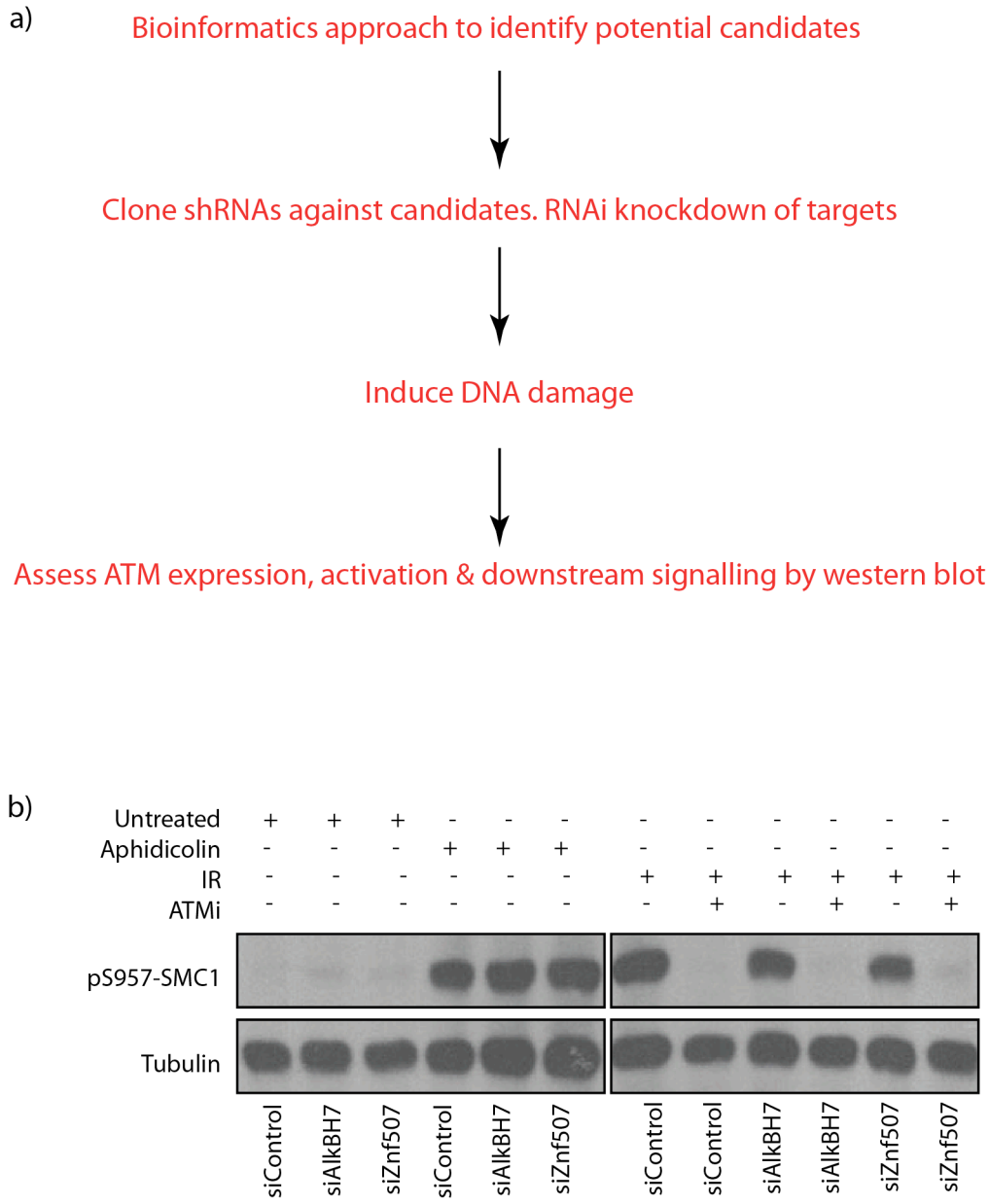

Figure 51: An shRNA screen for novel ATM regulators

a) Schematic overview of the screen for novel ATM regulatory proteins. b) Sample results from two 'negative hits'. Cells were transfected with the indicated shRNAs, then after 48 hours were harvested one hour after 5 Gy IR, or after incubation in 5 μM aphidicolin for two hours. A subset of cells were pre-treated with ATM inhibitor one hour before irradiation. Whole cell lysates were resolved on a 6%SDS-PAGE gel and immunostained with the indicated antibodies.

6.2 DMAP1 is required for ATM signalling and function after IR

A positive hit from the initial biochemical screen was DNMT1-associated protein 1 (DMAP1). DMAP1's conserved ATM interaction motif is shown schematically (Figure 52a). To ensure the phenotype observed was not due to off-target shRNA effects, two further shRNAs targeted against *dmap1* were cloned. *dmap1* mRNA levels were significantly downregulated by each of the four individual shRNAs (Figure 52b). Loss of DMAP1 caused a substantial decrease to the extent of phosphorylation of the ATM substrates pS957-SMC1 and pS824-KAP1 after IR (Figure 52c). However, total ATM, KAP1 and SMC1 protein levels were unaltered. This suggests that DMAP1 is required for ATM signalling in response to DSBs.

To investigate the role of DMAP1 in ATM recruitment to DSBs, the percentage of cells with pS1987-ATM foci at short time points after IR was assessed. Five minutes after IR, significantly fewer DMAP1 deficient cells had formed p1981-ATM foci compared to wildtype cells. This suggests that DMAP1 is required for the efficient formation of irradiation-induced foci. Conversely, 45 minutes after IR no difference in the percentage of cells with p1981-ATM foci was observed. This delay could reflect the shRNA mediated reduction, but not elimination, of DMAP1. Alternatively, it could be due to redundancy in the cellular DNA damage pathways. Interestingly, delayed DNA damage foci formation is also observed in NBS1 hypomorphic cells (Difilippantonio et al., 2007).

To rule out cell cycle defects underlie the impaired DNA damage signalling in DMAP1 depleted cells, siDMAP1 and siControl treated cells were assessed by FACS for their cell cycle profile (**Figure 54**). There was no significant difference between the cell cycle distribution of control and DMAP1 depleted cells. Thus, DMAP1 does not appear to regulate the cell cycle.

In response to IR, ATM signals to arrest proliferating cells at the G2/M checkpoint. I performed a G2 Trap experiment on DMAP1 depleted cells to assess if DMAP1 is required for G2/M checkpoint activation after DNA damage. The G2 Trap experiment

uses the mitotic inhibitor nocodazole to arrest cells that pass through the G2/M checkpoint in mitosis. The proportion of cells in mitosis is determined by the FACS analysis for phosphorylated histone H3, pS10-H3. The percentage of pS10-H3 positive cells is a measure of those cells that have passed through the ATM dependent G2/M checkpoint.

In line with the observation DMAP1 depleted cells have a normal cell cycle profile (**Figure 54**) in the presence of nocodazole untreated HCT-116 cells transfected with either siDMAP1 or siControl arrested in mitosis to the same extent (Figure 55a, b). In the absence of nocodazole, the loss of DMAP1 had no effect on the proportion of cells in mitosis. As expected five, ten, and 20 Gy irradiation decreased mitotic entry in a dose dependent manner, in both siControl and siDMAP1 treated cells. However, DMAP1 depletion resulted in a higher proportion of cells entering mitosis at 10 and 20 Gy IR (Figure 55a, b). This indicates that DMAP1 is required for proper activation of the ATM-regulated G2/M checkpoint.

Having established impaired checkpoint activation in DMAP1 depleted cells, I next wanted to investigate whether the impaired signalling had any impact on cell viability. I performed clonogenic survival assays. At each irradiation dose assayed, DMAP1 depleted cells formed fewer colonies compared to control cells (Figure 55c). As a positive control for the importance of ATM signalling after irradiation, siControl transfected cells were pre-treated with a small molecule ATM kinase inhibitor before irradiation. Interestingly, the colony formation defect observed in DMAP1 deficient cells is of a similar magnitude to the defect in cells lacking ATM kinase activity (Figure 55c). It is worth noting colony forming ability was assessed over seven days, over which the DMAP1 protein levels in siDMAP1 transfected cells presumably return to normal and the potency of the ATM inhibitor is reduced. Therefore this experiment directly assays the role of DMAP1, and ATM's kinase activity, in the immediate cellular response to IR. The temporary nature of the ATM kinase inhibition very likely accounts for the increased clonogenic survival of ATM kinase inhibitor treated cells, compared to published observations of a more severe colony formation defect in *atm*$^{-/-}$ cells (Cox et al., 1978).

a)

DMAP1	A	E	E	E	Y	L	L	Q	E	L
NBS1	A	K	E	E	S	L	A	D	D	L
ATMIN	A	M	D	D	F	L	L	A	D	L

b)

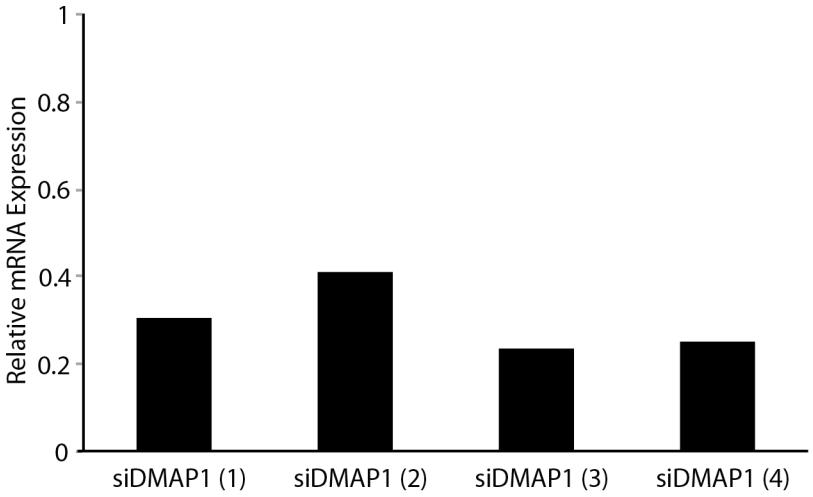

c)

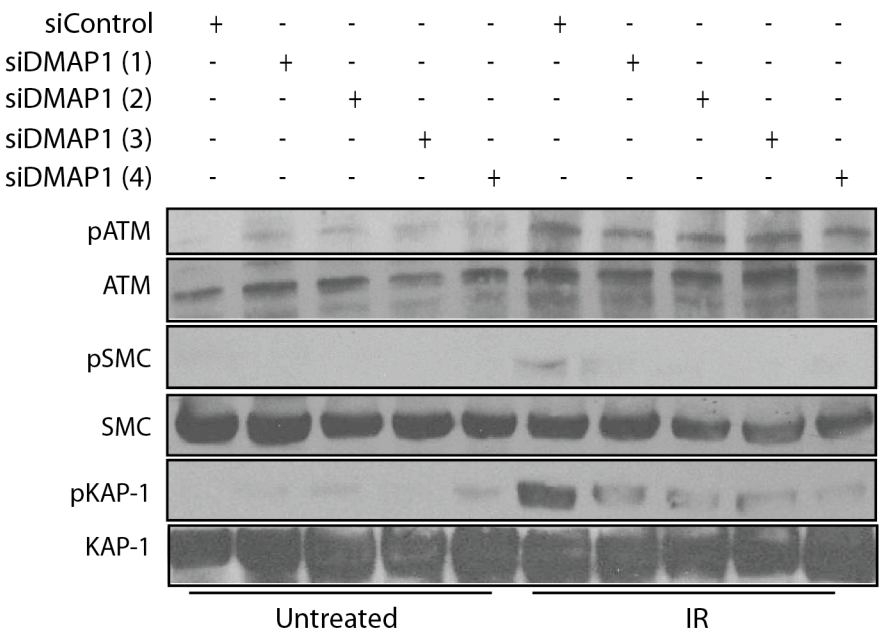

Figure 52: DMAP1 is required for ATM substrate phosphorylation after IR

a) Sequence of the consensus ATM interaction motifs present upon human DMAP1, NBS1 and ATMIN. b) RT-PCR for *dmap1* mRNA in HCT-116 cells 48 hours after transfection with one of four shRNAs targeted against *dmap1*. mRNA levels are normalised to shRNA control transfected cells. c) HCT-116 cells were transfected with control shRNA or one of four different shRNA's against DMAP1. 48hr later cells were treated with 5.0 Gy IR, harvested after one hour and whole cell lysates immunostained for pS1981-ATM, ATM, pS957-SMC1, SMC1 pS824-KAP1 and KAP1.

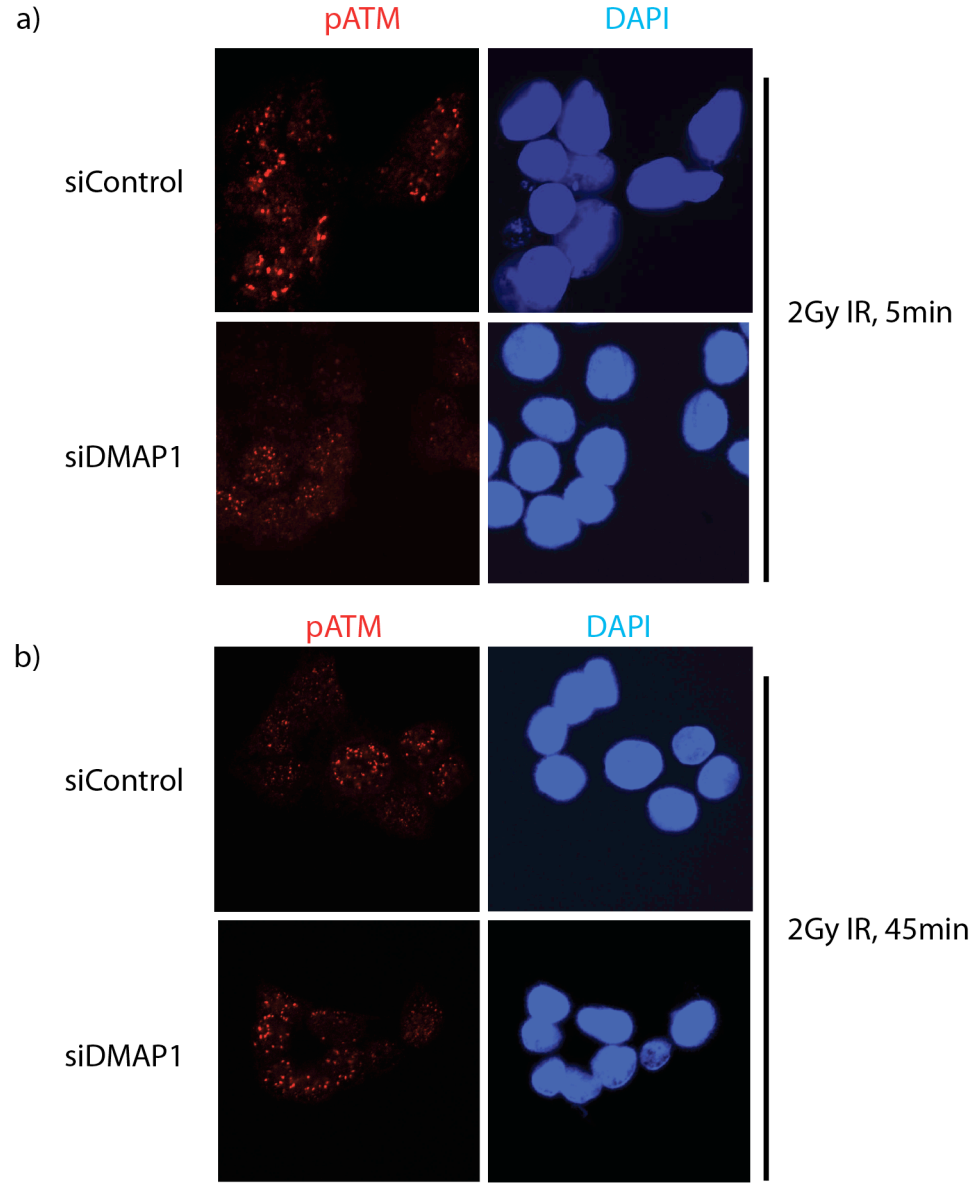
a)
pATM
DAPI
siControl
siDMAP1
2Gy IR, 5min
b)
pATM
DAPI
siControl
siDMAP1
2Gy IR, 45min

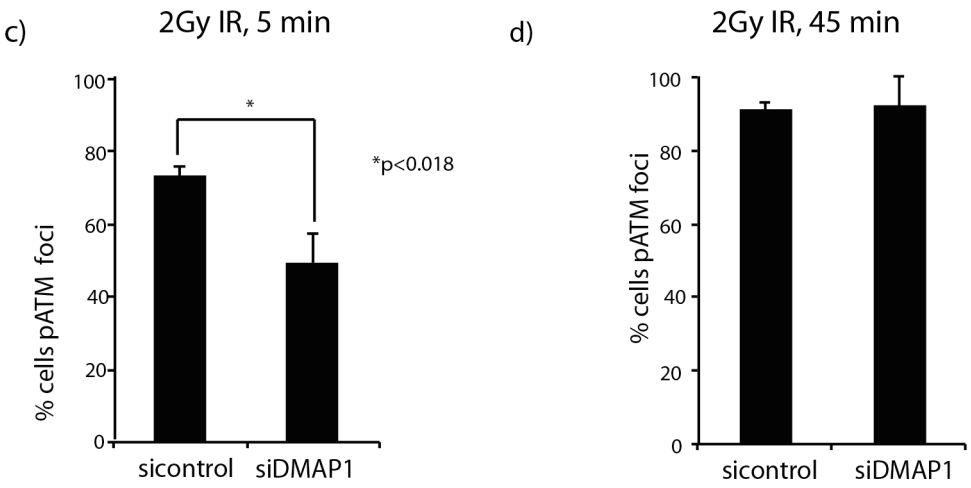
c)
2Gy IR, 5 min
% cells pATM foci
100
80
60
40
20
0
*
*p<0.018
sicontrol
siDMAP1
d)
2Gy IR, 45 min
% cells pATM foci
100
80
60
40
20
0
sicontrol
siDMAP1

Figure 53: Delayed IR-induced pATM focus formation in *dmap1* deficient cells

HCT-116 cells were treated with a pool of DMAP1 shRNAs and 48 hours later treated with 2.0 Gy IR. Cells were fixed at (a) five minutes and (b) 45 minutes after irradiation and immunofluorescently stained for pS1981-ATM. Quantification of cells with four or more pATM foci at (c) five minutes and (d) 45 minutes after irradiation. The p-value of three independent experiments was calculated using the student's t-test (*p<0.05).

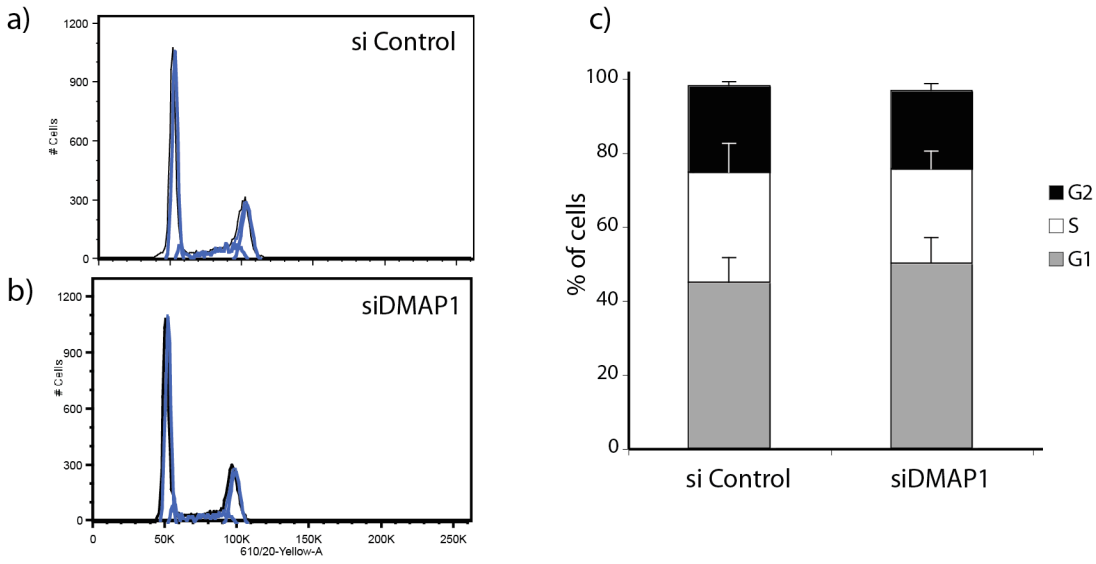

Figure 54: Knockdown of *dmap1* does not alter cell cycle progression

FACS analysis of the cell cycle profile of a) siControl and b) siDMAP1 treated HCT-116 cells 48 hours after transfection. c) Quantification of (b). Error bars represent the standard deviation of three independent experiments.

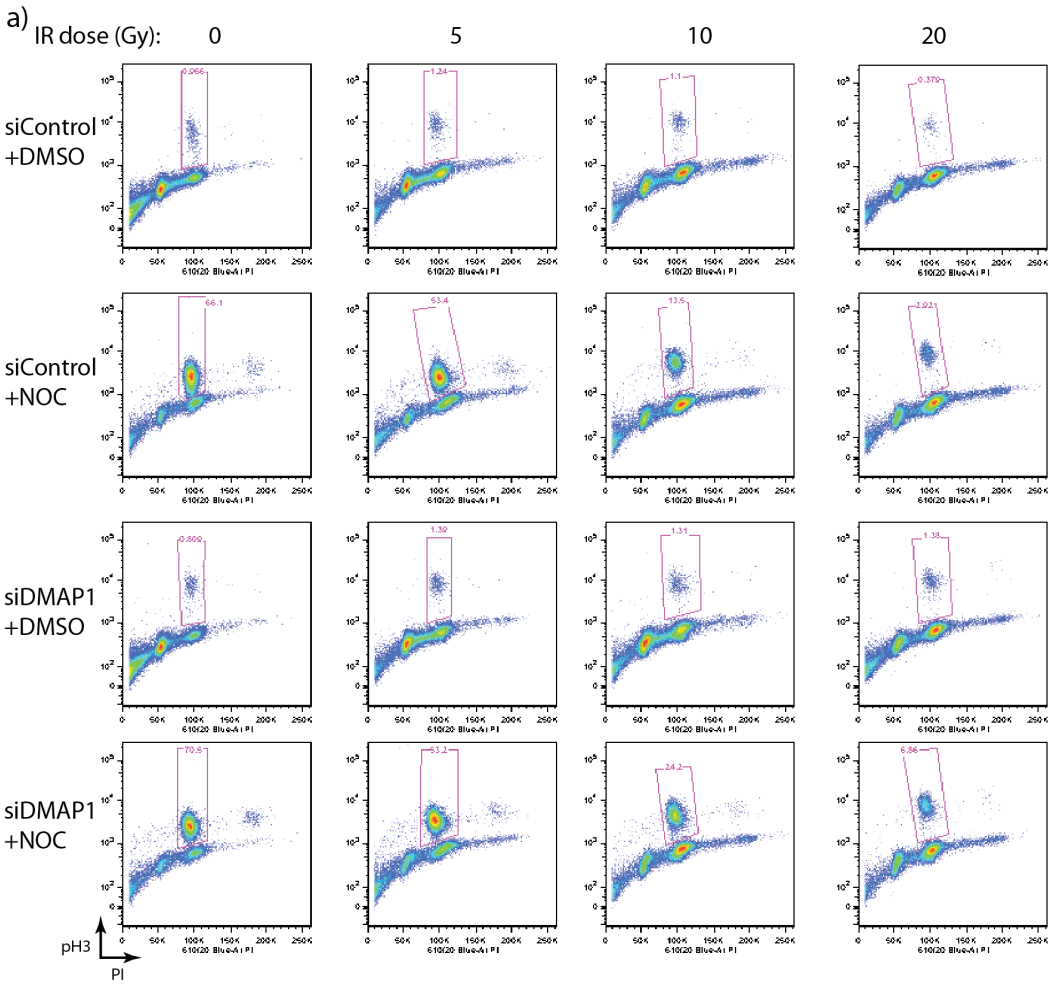
a)
IR dose (Gy): 0
5
10
20
siControl +DMSO
siControl +NOC
siDMAP1 +DMSO
siDMAP1 +NOC
pH3
PI

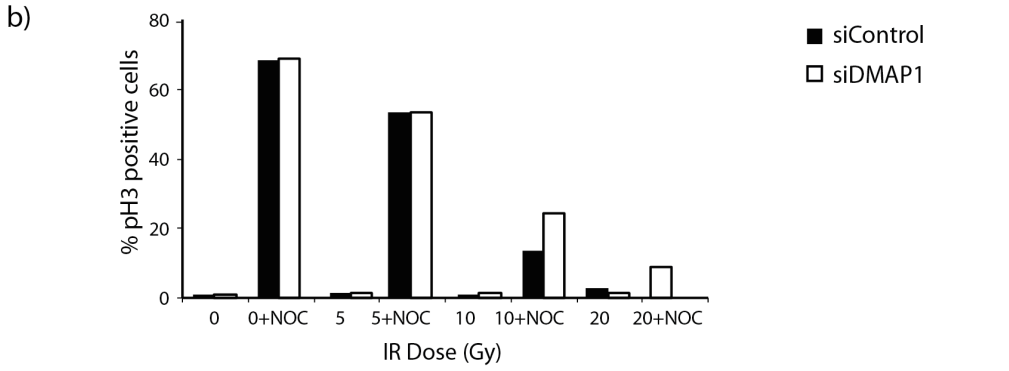
b)
% pH3 positive cells
0
20
40
60
80
0
0+NOC
5
5+NOC
10
10+NOC
20
20+NOC
IR Dose (Gy)
siControl
siDMAP1

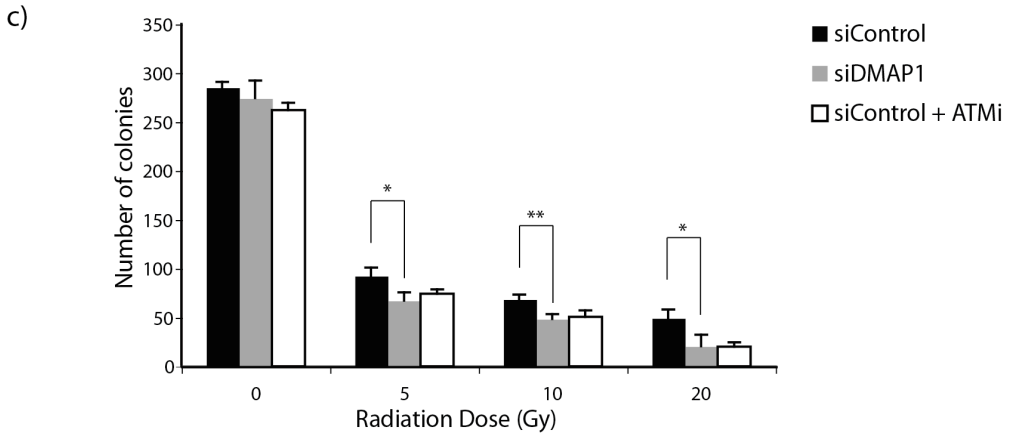
c)
Number of colonies
0
50
100
150
200
250
300
350
*
**
*
0
5
10
20
Radiation Dose (Gy)
siControl
siDMAP1
siControl + ATMi

Figure 55: DMAP1 deficient cells are radiosensitive

HCT-116 cells were transfected with DMAP1 or control shRNA, and after 48 hours were irradiated at the indicated doses. Cells were immediately incubated in the presence of either nocodazole or DMSO, and after 18 hours fixed and analysed for pS10-H3 by FACS analysis. Representative FACS plots are shown in (a), and quantification in (b). c) HCT-116 cells were transfected with siDMAP1 or control shRNA. 48 hours later DMSO or ATM inhibitor was added for one hour then cells were treated with the indicated radiation doses and counted. 250 cells were plated per condition and the number of colonies formed was counted seven days later. At least three independent experiments were performed and p values calculated using the student's t-test, (*$p<0.05$; **$p<0.01$).

6.3 DMAP1 is required for non-canonical ATM signalling

Having established DMAP1 is important for irradiation induced ATM signalling, it was interesting to ascertain if DMAP1's function was limited to DSB signalling. It was recently shown that ATM is activated by oxidative stress (Guo et al., 2010b). To investigate which ATM substrates are phosphorylated in response to oxidative stress, I performed a timecourse on H_20_2 treated HCT-116 cells (Figure 56a). To elucidate a possible role of DMAP1 in oxidative stress signalling, DMAP1 depleted cells were subjected to H_20_2 treatment. DMAP1 depleted cells exhibited markedly reduced levels of pS1981-ATM, pS957-SMC1 and pS824-KAP1 compared to control cells. (Figure 56b). This suggests that DMAP1 contributes to ATM activation by oxidative stress.

To address if DMAP1 is required for non-canonical ATM signalling, HCT-116 cells were exposed to hypotonic stress. Compared to control cells, DMAP1 depleted cells displayed reduced levels of pS1981-ATM and pS957-SMC1 (Figure 56b), suggesting DMAP1 is required for full ATM activation after both canonical and non-canonical ATM stimuli.

As DMAP1 was originally identified in a screen for proteins containing P13-K interaction motifs, I wanted to determine if DMAP1 was required for ATR signalling. I treated cells with ultraviolent radiation (UV), which induces single strand DNA breaks, activating ATR. DMAP1 depletion did not alter the extent of pS957-SMC1 or pS317-Chk1 phosphorylation after UV (Figure 56c). Inhibition of ATM's kinase activity with

a small molecule kinase inhibitor had negligible effect on the induction of pS957-SMC1 and pS317-Chk1 phosphorylation after UV. Thus it is clear that these are ATR, not ATM, dependent phosphorylation events and DMAP1 is dispensable for ATR signalling.

Given DMAP1 is required for both canonical and non-canonical ATM signalling, it is conceivable DMAP1 overexpression is sufficient to trigger ATM substrate phosphorylation in the absence of DNA damage. Expression of a Myc tagged DMAP1 construct (Myc-DMAP1) did not elevate basal phosphorylation of the ATM substrates pS957-SMC1 and pS824-KAP1 (Figure 57a). Conversely, DMAP1overexpression resulted in increased ATM substrate phosphorylation after both IR and hypotonic stress (Figure 57a). The overexpression of Myc-DMAP1 and GFP-DMAP1 (Figure 57b) was able to augment ATM substrate phosphorylation after oxidative stress. Thus DMAP1 appears to be a rate-limiting factor in both DSB induced and non-canonical ATM signalling.

The increased ATM substrate phosphorylation observed with DMAP1 overexpression (Figure 57a) led to the possibility that cells with higher DMAP1 levels repair DNA damage faster. To address this, Myc-DMAP1 overexpressing cells were fixed twenty-four hours after treatment with 2.0 Gy irradiation and immunostained for pH2AX or pS1987-ATM (Figure 57c, d). There was no significant difference in the percentage of cells with either or pH2AX (Figure 57e) pATM (Figure 57f) foci. There was also no difference in the pATM foci intensity (Figure 57g). Therefore, although DMAP1 overexpression increases the magnitude of ATM substrate phosphorylation at short time points after induction of DNA damage, it does not alter the persistence of DNA damage foci.

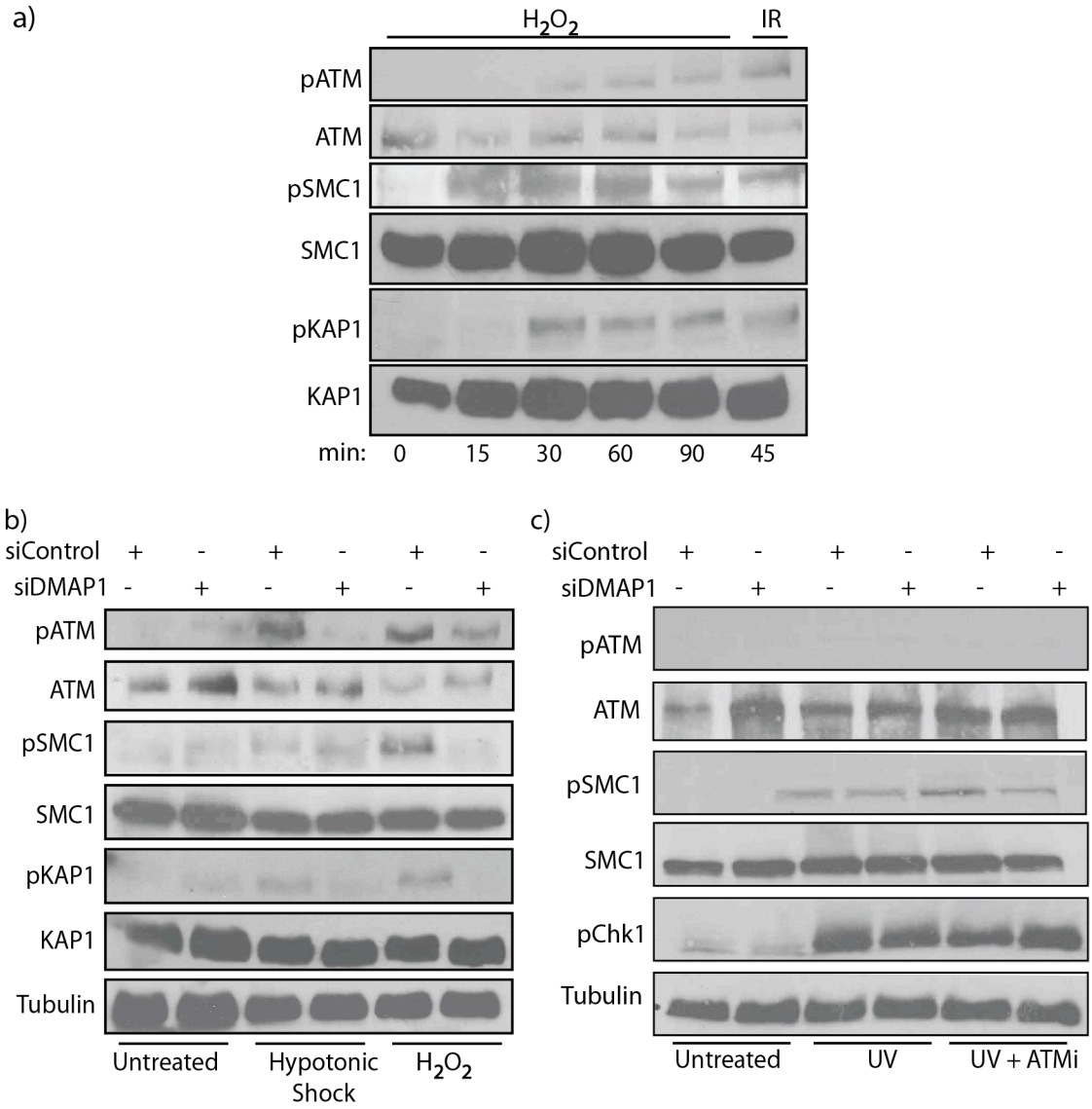

Figure 56: DMAP1 is required for non-canonical ATM signalling, but not for ATR signalling

a) HCT-116 cells were treated with 250 μM H_20_2 and harvested after the indicated timepoints. As a control some cells were harvested 45 minutes after 5 Gy IR. b) HCT-116 cells were transfected with a pool of shRNAs against DMAP1 or shRNA control, then 48hr later were treated with 135 mOsm NaCl or 250 μM H_20_2 for one hour. c) Cells were pre-treated for one hour with ATM inhibitor or DMSO then treated with 50 J m^2 UV and harvested after 60 minutes. Whole cell lysates were resolved on a 6% SDS-PAGE gel and membranes immunoblotted for pS1981-ATM, ATM, pS957-SMC1, SMC1, pS824-KAP1, KAP1, pS317-Chk1 and tubulin.

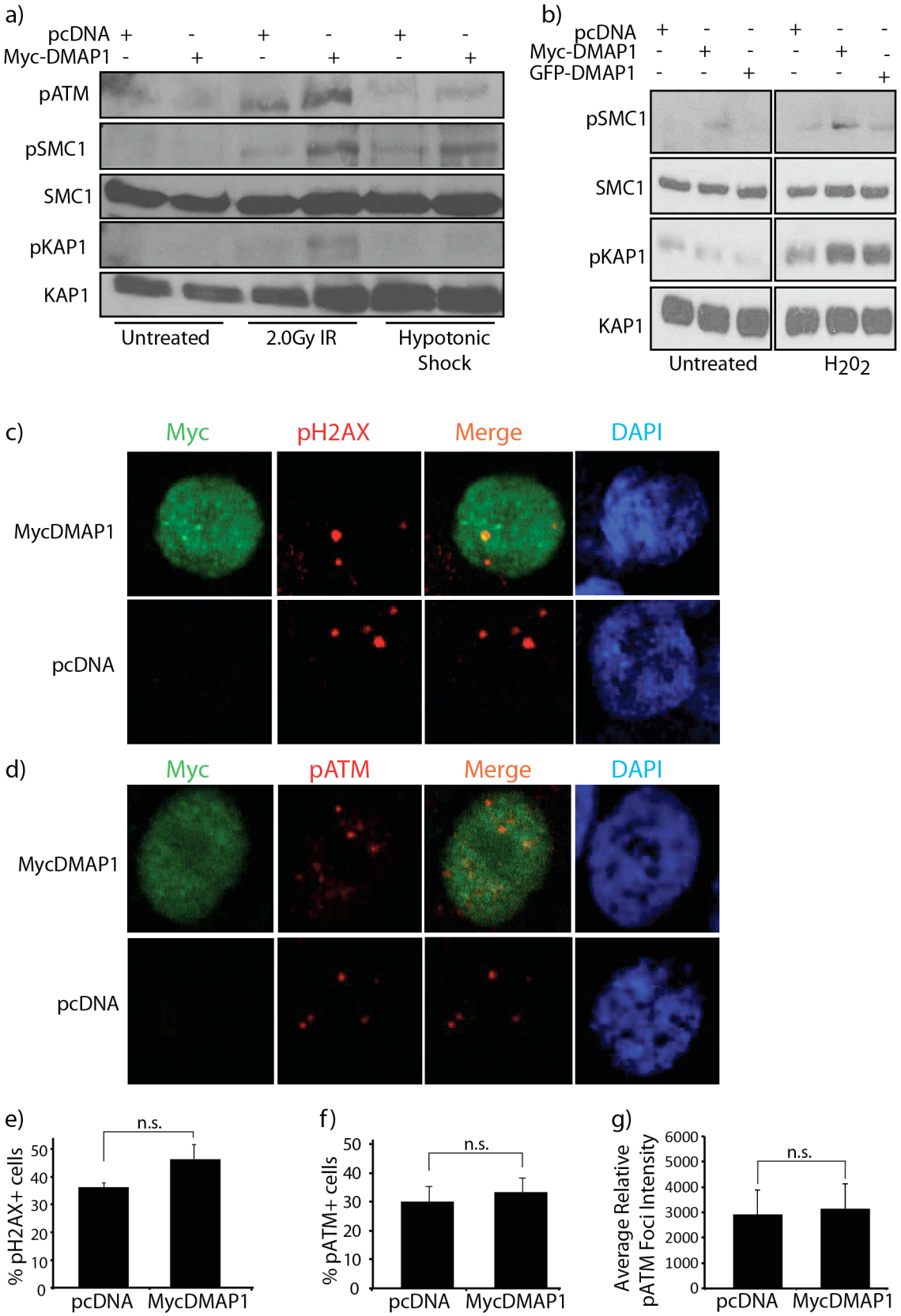

Figure 57: DMAP1 overexpression increase the magnitude of ATM signalling

HCT-116 cells were transfected with a, b) pcDNA, Myc-DMAP1 and c) GFP-DMAP1, and 48 hours later treated with 2.0 Gy IR, 135 mOsm NaCl, or 250 μM H_20_2 then harvested after one hour. Whole cell lysates were resolved on a 6% SDS-PAGE gel and membranes immunoblotted for pS1981-ATM, pS957-SMC1, SMC1, pS824-KAP1 and KAP1. c, d) 293A cells were transfected with pcDNA or Myc-DMAP1 then irradiated at 2 Gy after 48 hours. Cells were left to recover for a further 24 hours before fixation and immunofluorescent staining for pH2AX, pATM and Myc. e) Percentage of cells containing three or more pH2AX foci 24 hours after IR, as shown in (c). f) Percentage of cells containing three or more pS1981-ATM foci, as shown in (d). g) Relative pATM foci intensity 24 hours after IR in cells transfected with the indicated constructs. At least 100 cells per experiment were quantified per experiment. The p-value of three independent experiments was calculated using the student's t-test.

6.4 DMAP1 does not detectably interact with ATM

The identification of DMAP1 in a screen for proteins containing an ATM interaction motif strongly suggested that DMAP1 and ATM would interact. I initially investigated a possible endogenous ATM-DMAP1 interaction by performing reciprocal co-immunoprecipitations in untreated HCT-116 cells. However, despite a reproducible immunoprecipitation of Myc-DMAP1 and ATM, I could not detect the reciprocal protein (Figure 58a). In case an ATM-DMAP1 interaction does not occur in HCT-116 cells for cell-line specific reasons I performed immunoprecipitations in a range of other cell lines, including 293A, 293T and Hela Ohio (data not shown). I could not detect co-immunoprecipitation between ATM and DMAP1 under basal conditions in any cell line.

ATM exists in undamaged cells as a dimer, and thus it is feasible DMAP1's potential interaction motif binds a region of ATM shielded in the dimer conformation. To address this I immunoprecipitated Myc-DMAP1 and endogenous ATM one hour after 5 Gy irradiation, when ATM is in its monomeric form. However, there was no detectable co-immunoprecipitation (Figure 58b). I also performed immunoprecipitations at five minutes, 20 minutes and six hours after irradiation but did not detect an interaction between ATM and MycDMAP1 (data not shown).

To exclude the possibility that I could not detect an interaction due to the technical difficulties in immunoprecipiating an endogenous protein of ATM's large size

(~350kDa) I overexpressed Flag-ATM in 293A cells. I performed Flag IP's in both control and Myc-DMAP1 expressing cells. Despite a reproducible ATM enrichment, I did not detect any Myc-DMAP1 in the Flag IP (Figure 58c). To address a model in which DMAP1 and ATM only interact after DNA damage I used irradiated cells, but did not see an interaction (Figure 58d). As in the endogenous ATM IP's, I could not detect an interaction between DMAP1 and ATM at five minutes, 20 minutes, one hour and six hours after irradiation (data not shown). Hence, interaction between DMAP1 and ATM does not appear to be DNA damage dependent.

It is possible DMAP1 has a very transitory interaction with ATM during the initial phase of ATM activation. Often, inhibitors can trap proteins in conformations they normally only briefly adopt during a catalytic step. DMAP1 could interact with ATM before it autophosphorylates. I therefore irradiated cells pre-treated with an ATM kinase inhibitor, and harvested the cells at five and 60 minutes after IR. However, immunoprecipitation of Myc-DMAP1 did not yield ATM (Figure 58e, f).

ATM activation by oxidative stress proceeds via a cysteine-linked dimer (Guo et al., 2010b). To determine if DMAP1 interacts with this ATM conformation, I immunoprecipitated Myc-DMAP1 from cells after one hour of H_20_2 treatment. However, ATM was not co-immunoprecipitated (Figure 58g). As histone acetylation is important for ATM activation (Li et al., 2010), I postulated a histone deacetylase inhibitor might prompt ATM to adopt conformation that interacts with DMAP1. I immunoprecipitated Myc-DMAP1 from cells pre-treated with the histone deacetylase inhibitor TSA, but did not co-immunoprecipitate ATM (Figure 58h). Therefore neither oxidative stress or histone deacetylation inhibition leads to detectable ATM-DMAP1 interaction.

In summary, despite an extensive effort to co-immunoprecipitate ATM and DMAP1 from several cell lines under a wide range of conditions, I was unable to detect an interaction between the two proteins. I was also unable to detect ATM binding to a peptide containing DMAP1's putative ATM interaction motif (data not shown). Although this could be due to technical limitations, these results are consistent with a model in which ATM and DMAP1 do not directly interact. With 'no interaction' as a

working model, I next wanted to understand the role of DMAP1's ATM interaction motif.

To establish if DMAP1's putative ATM interaction motif is required for its function in the DNA damage response, I generated a C-terminal truncation mutant, DMAP1ΔC, which lacks the putative ATM interaction motif (Figure 59a). As overexpression of full length DMAP1 augments ATM substrate phosphorylation after DNA damage, I assessed if DMAP1ΔC was also able to do this. Unexpectedly, despite lacking an ATM interaction motif DMAP1ΔC overexpression was sufficient to increase the phosphorylation levels of the ATM substrates pS957-SMC1 and pS824-KAP1 after oxidative stress treatment (Figure 59b). and irradiation (Figure 59c). This, taken together with the lack of a detectable interaction between DMAP1 and ATM, suggests that an interaction between DMAP1 and ATM is not required for DMAP1's role in ATM biology.

Many of the proteins involved in the DNA damage response become localised into foci at the sites of DNA damage. These foci are readily detected by confocal microscopy, so I assessed if DMAP1 became recruited to DNA damage foci by immunofluorescence staining. In untreated cells, GFP-DMAP1 localises to the nucleus in a pan-nuclear distribution (Figure 60a). However, one hour after 5 Gy IR GFP-DMAP1 was still in a pan-nuclear distribution and did not co-localise with the DNA damage marker pH2AX (Figure 60b). To rule out the possibility the relatively large, 27kDa GFP tag impedes recruitment I also assessed if Myc-DMAP1, containing the smaller 11 amino acid Myc tag, co-localised pATM or pH2AX foci. Nevertheless, Myc-DMAP1 remained in a pan-nuclear distribution after DNA damage (Figure 60c).

It is plausible only a subset of the total cellular pool of DMAP1 localises to DNA damage foci, and the remaining pan-nuclear DMAP1 masks the foci-localised DMAP1. I generated Z-stacks covering the entire cell to thoroughly examine if GFP-DMAP1 co-localised with pATM at short (one hour) or longer (24 hour) times after IR. However, although some GFP-DMAP1 foci were sometimes visible, these showed no significant degree of overlap with pATM (Figure 61a, b). These GFP-DMAP1 foci were also seen

at the same frequency in untreated cells (data not shown). I also performed the same set of experiments using Myc-DMAP1, with very similar results (data not shown).

Nevertheless, I could not rule out the possibility DMAP1 is transiently recruited to damage sites immediately after IR treatment, at timepoints shorter than it is technically possible to observe. Therefore, I used NCS to induce DNA damage. NCS is a radiomimetic that binds the minor groove of the DNA double helix, promoting the thiol activation of NCS to a radical form that induces single and double strand DNA breaks. Firstly, I optimised a timecourse of NCS treatment and determined that pH2AX foci first start appearing at five minutes after drug addition, and continue to accumulate over time (Figure 62a). However, I was unable to see co-localisation of GFP-DMAP1 to pH2AX or 53BP1 at five or 30 minutes after addition of NCS. Therefore, it appears that DMAP1 is not recruited into DNA damage foci (Figure 62b).

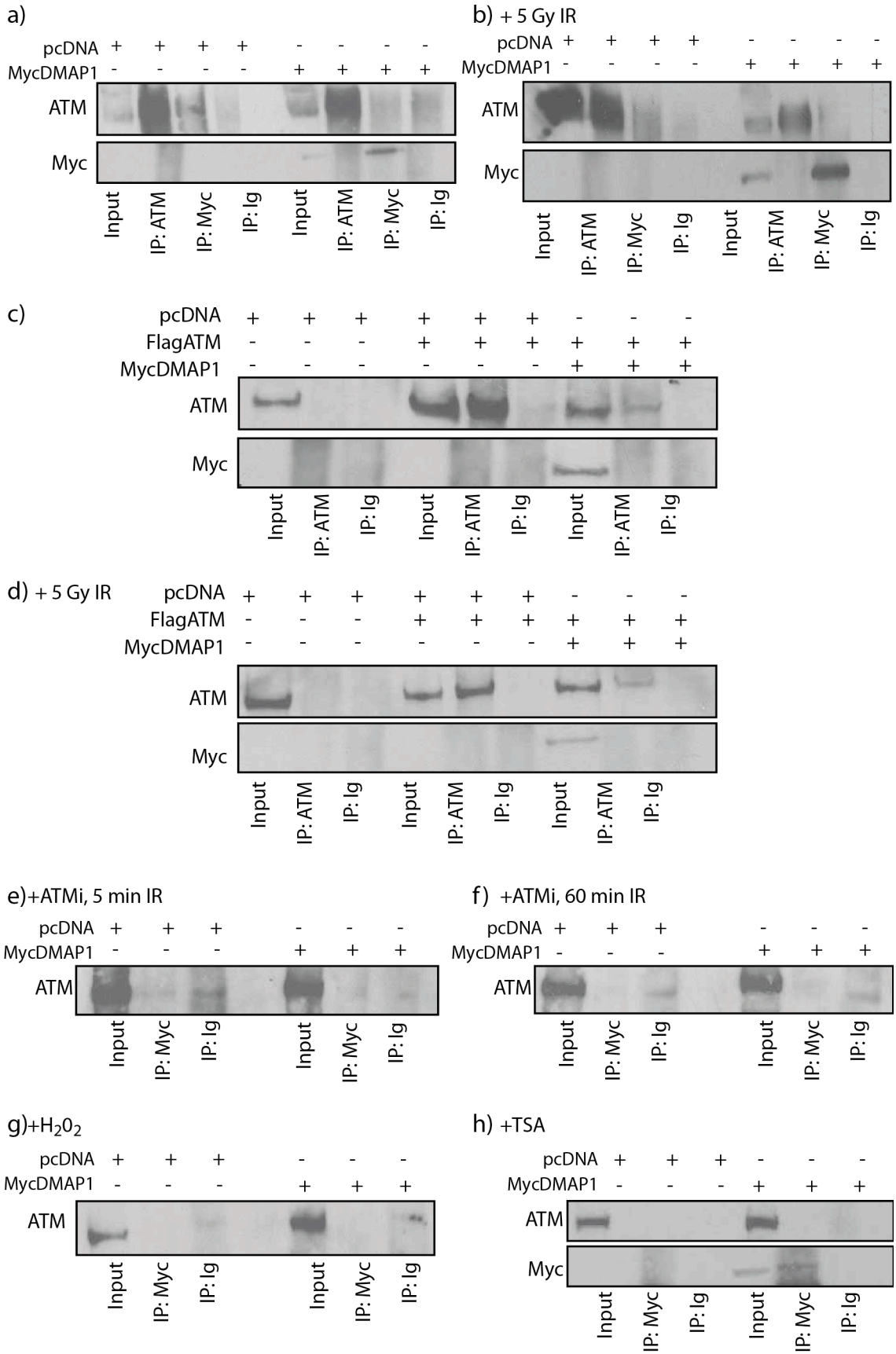

Figure 58: DMAP1 and ATM do not appear to co-immunoprecipitate

a) HCT-116 cells were transfected with pcDNA or Myc-DMAP1 and harvested after 48 hours. Cell lysates were immunoprecipitated with antibodies against ATM, Myc or IgG control. b) As for (a), except cells were treated with 5 Gy IR one hour before harvesting. c) 293A cells were transfected with combinations of pcDNA, Flag-ATM and Myc-DMAP1, harvested after 48 hours, and immunoprecipitated with antibodies against Flag, Myc or IgG control. d) As for (c), except cells one hour before harvesting cells were treated with 5 Gy IR. (e, f, g, h). 293A cells were transfected with pcDNA or MycDMAP1, harvested 48 hours after transfection, and immunoprecipitated with anti-Myc antibody or IgG control. (e, f,) Cells were incubated with ATM inhibitor one hour prior to 5 Gy irradiation, and harvested after (e) five minutes or (f) one hour. Cells were treated with (g) 250 µM H_20_2 for one hour or (h) 5 µM TSA for six hours before cell lysis. IP's and the corresponding inputs (10%) were resolved by 6% SDS-PAGE and membranes immunoblotted for Myc and ATM.

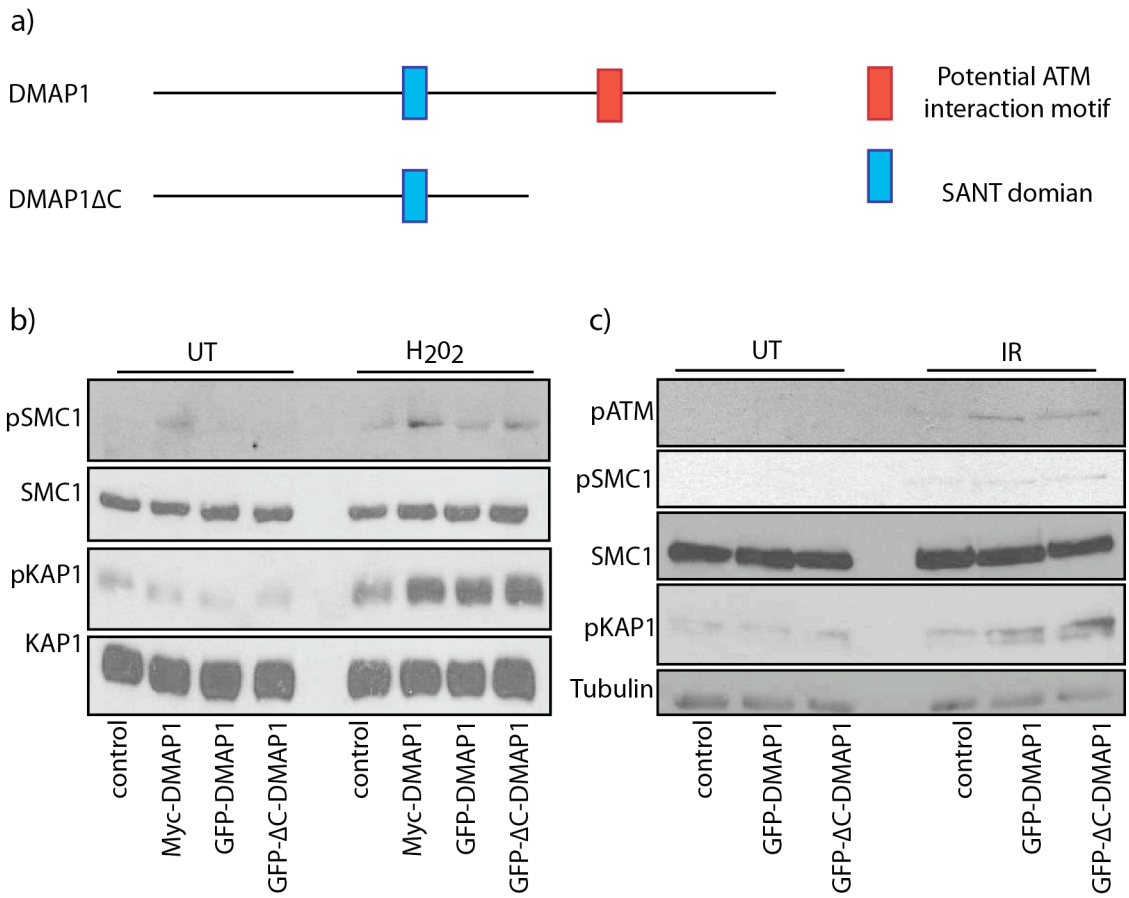

Figure 59: DMAP1's C-terminus is not required for augmentation of ATM signalling

a) Schematic of full length DMAP1 and the DMAP1ΔC truncation mutation; the SANT domain and potential ATM interaction motif are indicated. HCT-116 cells transfected with the indicated constructs were treated (b) with 250 µM H_20_2 or (c) 5 Gy IR and harvested one hour later. Whole cell lysates were separated by 6% SDS-PAGE and membranes probed with pS957-SMC1, SMC1, pS824-KAP1 and KAP1.

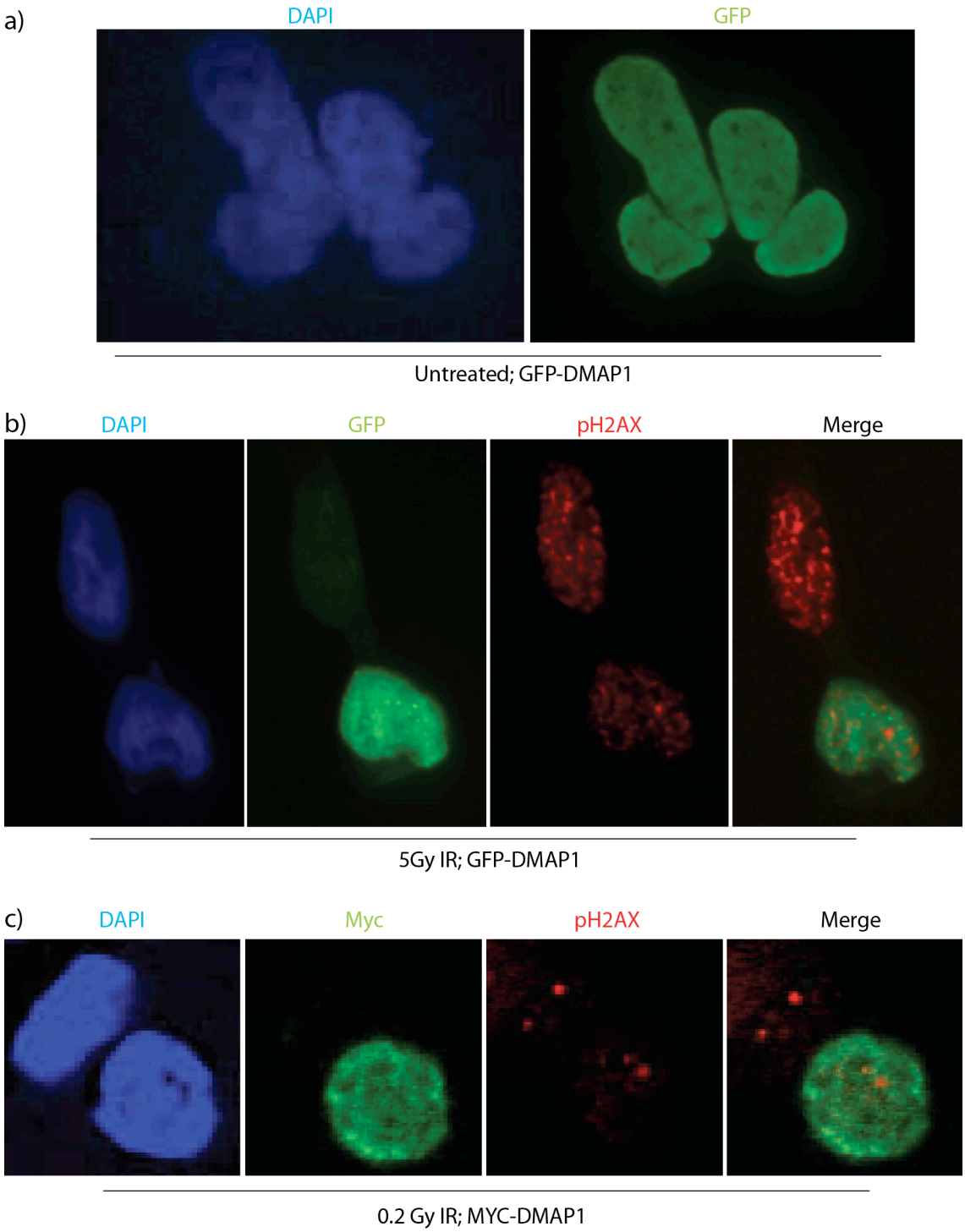

Figure 60: DMAP1 does not localise to DNA damage foci one hour after IR

Representative images of HCT-116 cells transfected with GFP-DMAP1 (a) fixed without treatment or (b) one hour after 5 Gy IR and immunofluorescently stained for pH2AX. c) Cells transiently transfected with Myc-DMAP1 were fixed one hour after 0.2 Gy irradiation and stained with antibodies against Myc and pH2AX.

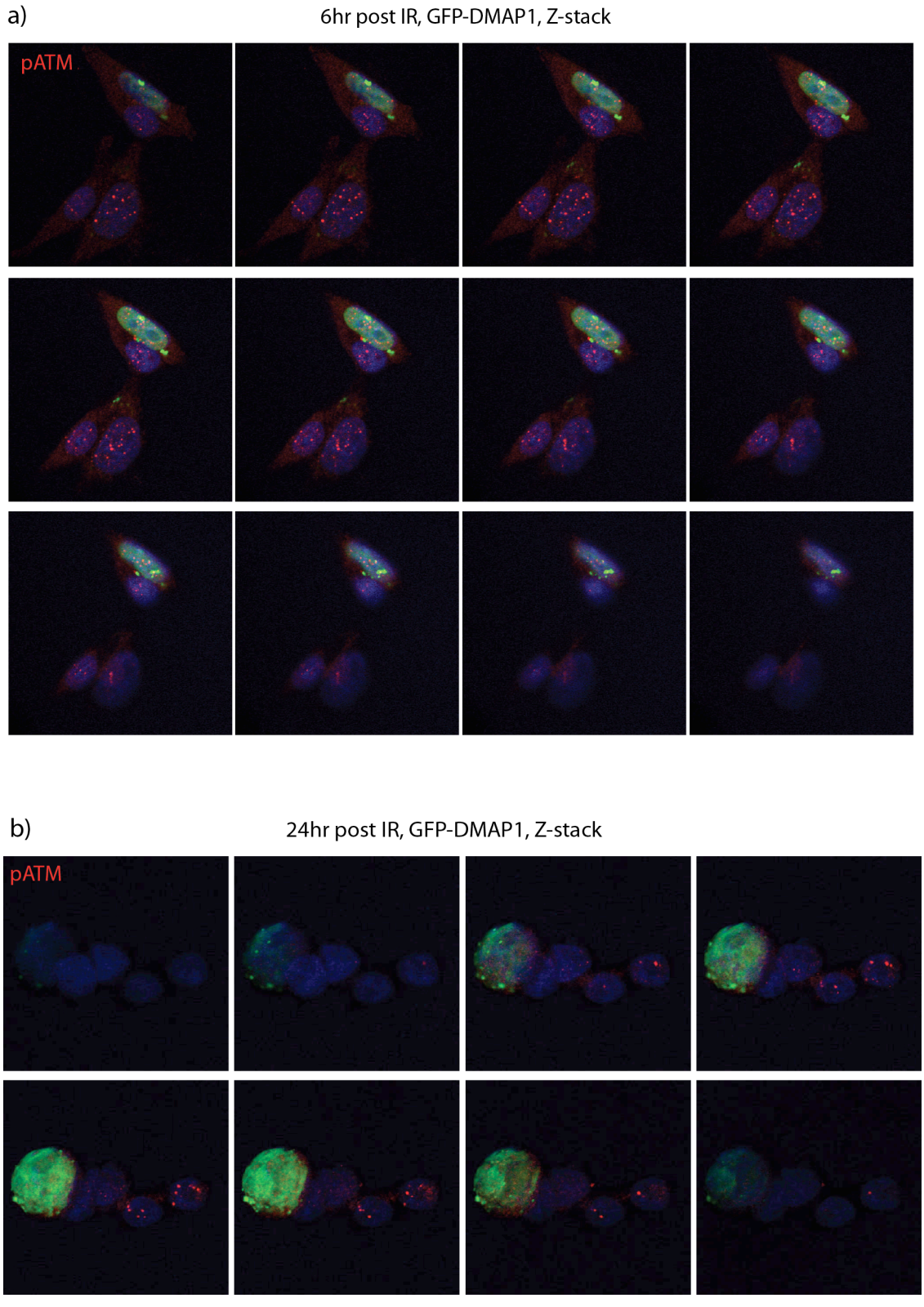

Figure 61 DMAP1 does not localise to DNA damage foci at later timepoints after IR

Consecutive Z-stack images for 293A cells transiently transfected with GFP-DMAP1 at (a) six hours and (b) 24 hours after 2 Gy IR. Fixed cells were stained with anti-pS1981-ATM antibody.

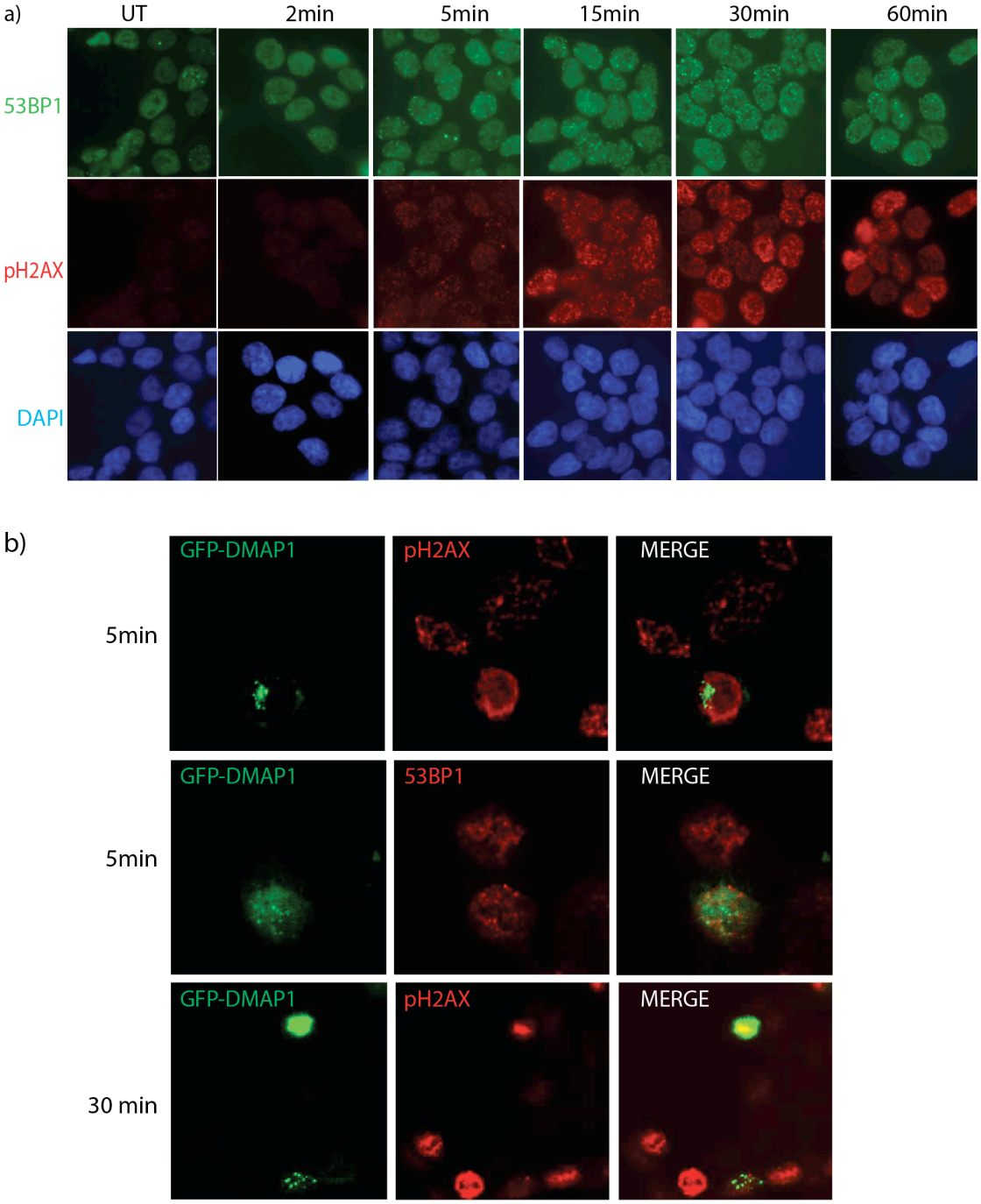

Figure 62 DMAP1 does not localise to DNA damage foci at short timepoints after DSB induction

a) HCT-116 cells were treated with 200 ng/ml NCS and fixed at the indicated times. Cells were immunofluorescently stained for pH2AX and 53BP1. b) Representative images of GFP-DMAP1 transfected cells treated with NCS for the indicated length of time. Cells were stained for pH2AX or 53BP1.

6.5 DMAP1 is required for histone H4 acetylation by Tip60

DMAP1 has previously been identified as a subunit of the human NuA4 complex (Cai et al., 2003; Doyon et al., 2004). Another component of the NuA4 complex is the histone acetyltransferase Tip60, which has been shown to modulate its activity in response to DNA damage and acetylate a range of targets including histone H4 on lysine16 (H4K16Ac) (Wu et al., 2011). However, the relevance of DMAP1 activity for Tip60 function had not yet been analysed.

I first wanted to determine if I could reproduce the published interaction between DMAP1 and Tip60, which used a mass spectrophotometry approach (Cai et al., 2003). I performed immunoprecipitations for GFP-DMAP1 and HA-Tip60 on 293A cells. HA immunoprecipitation from cells without transfected HA-Tip60 does not enrich for DMAP1. However, HA immunoprecipitation from HA-Tip60 expressing cells also enriched for GFP-DMAP1 (Figure 63a). Thus, Tip60 and DMAP1 interact.

Having confirmed the DMAP1-Tip60 interaction in my system, I wanted to establish if DMAP1 played a role in regulating Tip60's histone acetyltransferase (HAT) activity. I overexpressed HA-Tip60 in 293A cells, and performed an anti-HA immunoprecipitation. The washed immunoprecipitates were incubated with an artificial colourimetric substrate and the HAT activity determined using spectrophotometry. As expected, Tip60 immunoprecipitates had significant HAT activity (Figure 63b). The same assay was also performed on washed anti-GFP immunoprecipitates from GFP-DMAP1 expressing cells. These immunoprecipitates also contained significant amounts of HAT activity (Figure 63c), suggesting DMAP1 associates with HAT activity.

To establish if a DMAP1-Tip60 complex was responsible for the HAT activity associated with DMAP1, I performed the HAT assay on Myc-DMAP1 immunoprecipitates from cells transfected with shRNA against Tip60. Knock-down of Tip60 significantly reduced the HAT activity associated with DMAP1 (Figure 63d). Tip60 depletion also reduced pS957-SMC1 phosphorylation to a similar extent as

DMAP1 depletion (Figure 63e). The extent of Tip60 knockdown by the shRNA Tip60 hairpins was validated by qPCR (Figure 63f).

H4K16 acetylation is mainly catalysed by the histone acetyltransferases MOF and Tip60 (Rea et al., 2007), (Kusch et al., 2004). Moreover, H4K16 acetylation has recently been shown to be necessary for efficient ATM activation and signalling (Wu et al., 2011). It therefore follows DMAP1 deficiency may affect ATM signalling by reducing the extent of H4K16 acetylation. To test this hypothesis, HCT-116 cells were treated with the radiomimetic drug bleomycin, which induces DSBs. Control cells displayed an increase in H4K16 acetylation after DNA damage. However, this increase was not observed in DMAP1 depleted cells (Figure 64a).

The reduced H4K16Ac in DMAP1 depleted cells after DNA damage suggests artificially increasing histone acetylation levels could circumvent DMAP1's function in the DNA damage response pathway. The organic compound Trichostatin A (TSA) selectively inhibits mammalian class I and II histone deacetylases (HDACs), increasing histone acetylation levels (Sharma et al., 2010), (Miller et al., 2010). DMAP1 depleted HCT-116 cells were incubated with TSA for six hours then treated with either 250 μM H_20_2 or 5 Gy IR. This partially rescued the requirement for DMAP1 in H4K16 acetylation (Figure 64b). Crucially, HDAC inhibition also rescued pS957-SMC1 and pS824-KAP1 levels after IR in both Tip60 and DMAP1 depleted cells (Figure 64c).

DMAP1 depleted cells have delayed DNA damage repair foci formation at short time points after irradiation. Only 47% of siDMAP1 transfected cells had four or more 53BP1 foci, compared to 93% of siControl transfected cells, five minutes after 2 Gy IR (Figure 65a, b). However, 87% of DMAP1 depleted cells pre-incubated with TSA had 53BP1 foci formation five minutes after IR (Figure 65a, b). Thus treatment with histone deacetylase inhibitors rescues the delay in DNA damage foci formation observed in DMAP1 depleted cells. Depletion of DMAP1 had no affect on 53BP1 foci formation 45 minutes after IR (Figure 65c). As TSA did not increase foci formation in untreated cells (Figure 65d), we can rule out the possibility TSA rescues the delayed foci formation by

increasing basal DNA damage. A DMAP1-Tip60 complex acetylates H4K16 after DNA damage - which is required for ATM signalling and DNA damage foci formation.

6.6 Concluding Remarks

Having established a role for DMAP1 in ATM signalling, I next wanted to generate a DMAP1 knockout mouse (*dmap1*$^{-/-}$). One would expect the *dmap1*$^{-/-}$ mouse to be radiosensitive and cancer prone. It would be interesting to cross *dmap1*$^{-/-}$ into the Eu-Myc lymphoma model, in which Tip60 is a haplo-insufficient tumour suppressor. Three independent clones of *dmap1*$^{-/-}$ ES cells were obtained from the KOMP consortium (Figure 66a) and injected at the blastocyst stage. However, despite extensive validation that the ES cells were *dmap1*$^{-/-}$ cells, no germline transmission was ever observed (Figure 66b). Three chimeras produced 86 offspring between them, none of which contained the DMAP knockout allele. The failure to achieve *dmap1*$^{-/-}$ germline is in agreement with a recently published paper describing the pre-implantation lethality of *dmap1*$^{-/-}$mice (Mohan et al., 2011).

Nonetheless, although it was not possible to address DMAP1's function as a potential tumour suppressor gene *in vivo*, it is clear DMAP1 is an important component of the DNA damage response. DMAP1 deficient cells exhibit reduced ATM substrate phosphorylation after DSB induction (Figure 52) and oxidative stress (Figure 56); radiosensitivity and impaired checkpoint activation after IR (Figure 55). DMAP1 interacts with the histone acetyltransferase Tip60 (Figure 63). Histone deacetylase inhibitors rescues ATM signalling in si*dmap1* cells (Figure 65), suggesting DMAP1 is required for the acetylation of Tip60 targets, including H4K16, after DNA damage (Figure 64). DMAP1 is therefore a novel regulator of ATM signalling.

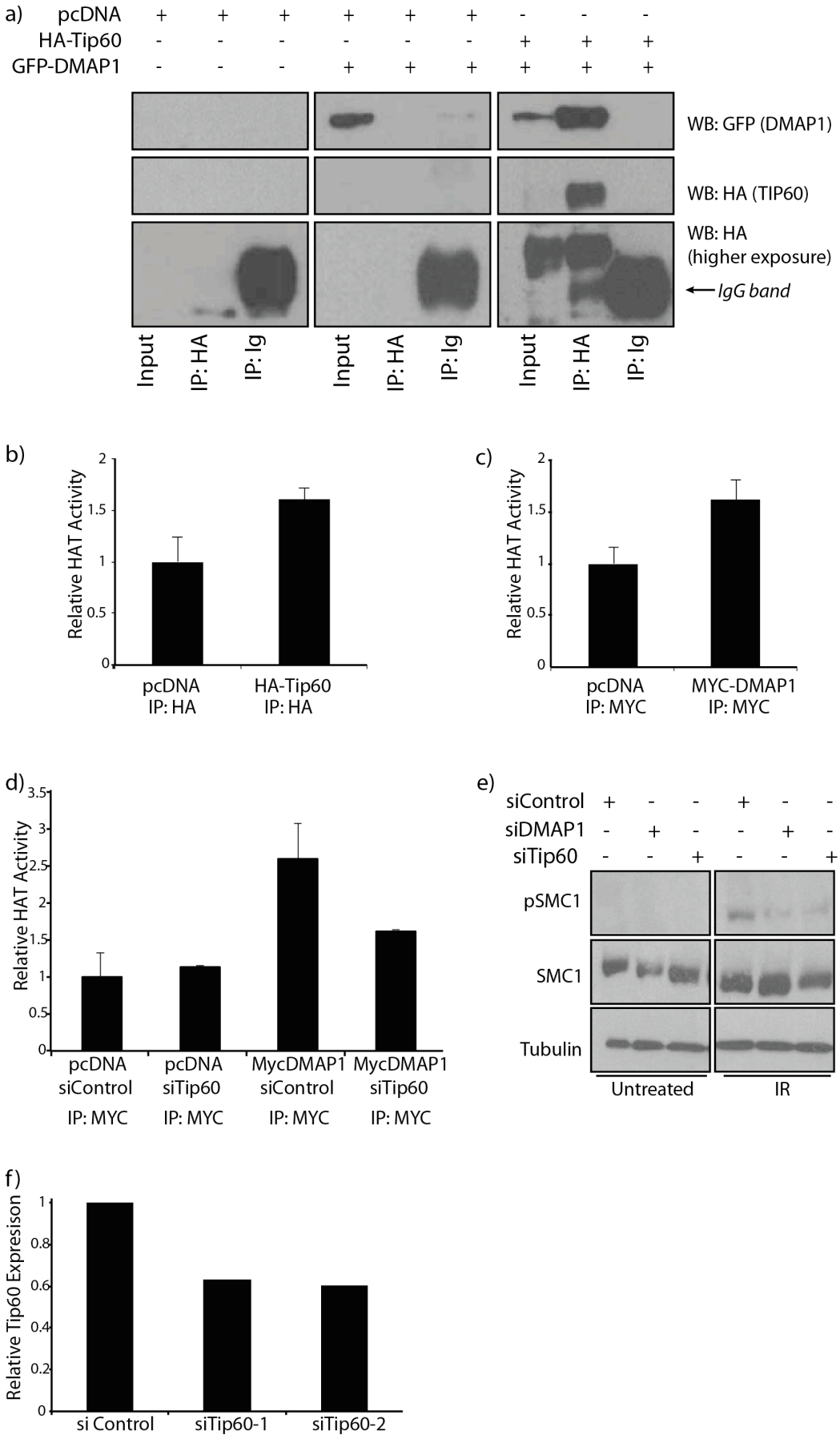
a)
pcDNA + + + + + + - - -
HA-Tip60 - - - - - - + + +
GFP-DMAP1 - - - + + + + + +
WB: GFP (DMAP1)
WB: HA (TIP60)
WB: HA
(higher exposure)
IgG band
Input
IP: HA
IP: Ig
Input
IP: HA
IP: Ig
Input
IP: HA
IP: Ig
b)
Relative HAT Activity
0
0.5
1
1.5
2
pcDNA
IP: HA
HA-Tip60
IP: HA
c)
Relative HAT Activity
0
0.5
1
1.5
2
pcDNA
IP: MYC
MYC-DMAP1
IP: MYC
d)
Relative HAT Activity
0
0.5
1
1.5
2
2.5
3
3.5
pcDNA
siControl
IP: MYC
pcDNA
siTip60
IP: MYC
MycDMAP1
siControl
IP: MYC
MycDMAP1
siTip60
IP: MYC
e)
siControl + - - + - -
siDMAP1 - + - - + -
siTip60 - - + - - +
pSMC1
SMC1
Tubulin
Untreated
IR
f)
Relative Tip60 Expresison
0
0.2
0.4
0.6
0.8
1
si Control
siTip60-1
siTip60-2

Figure 63: DMAP1 interacts with the histone acetyltransferase Tip60

a) 293A cells were transfected with the indicated combination of pcDNA, HA-Tip60 and GFP-DMAP1. 48 hours later cells were harvested and immunoprecipitated using either HA antibody or IgG control. Inputs (10%) and IP's were immunoblotted for HA and GFP. Two different exposures of the HA immunoblot are indicated. b, c, d) 239A cells were transfected with the indicated combination of pcDNA, Myc-DMAP1, HA-Tip60, siControl and siTip60. After 48 hours cells were immunoprecipitated with either HA antibody, Myc antibody or Ig control. Washed IPs were incubated with a colourimetric histone substrate, and HAT activity determined by spectrophotometer. Values were normalised to a reaction containing no IP. e) 293A cells were transfected with control, siDMAP1 or siTip60 shRNA then after 48 hours treated with 5 Gy IR and harvested one hour later. Whole cell lysates were resolved by 6% SDS-PAGE and membranes probed with pS1981-ATM, pS957-SMC1, SMC1 and tubulin. f) HCT-116 cells were transfected with control shRNA or one of two different shRNA's targeting Tip60. 48 hours later RNA was isolated and analysed for *tip60* mRNA by RT-PCR.

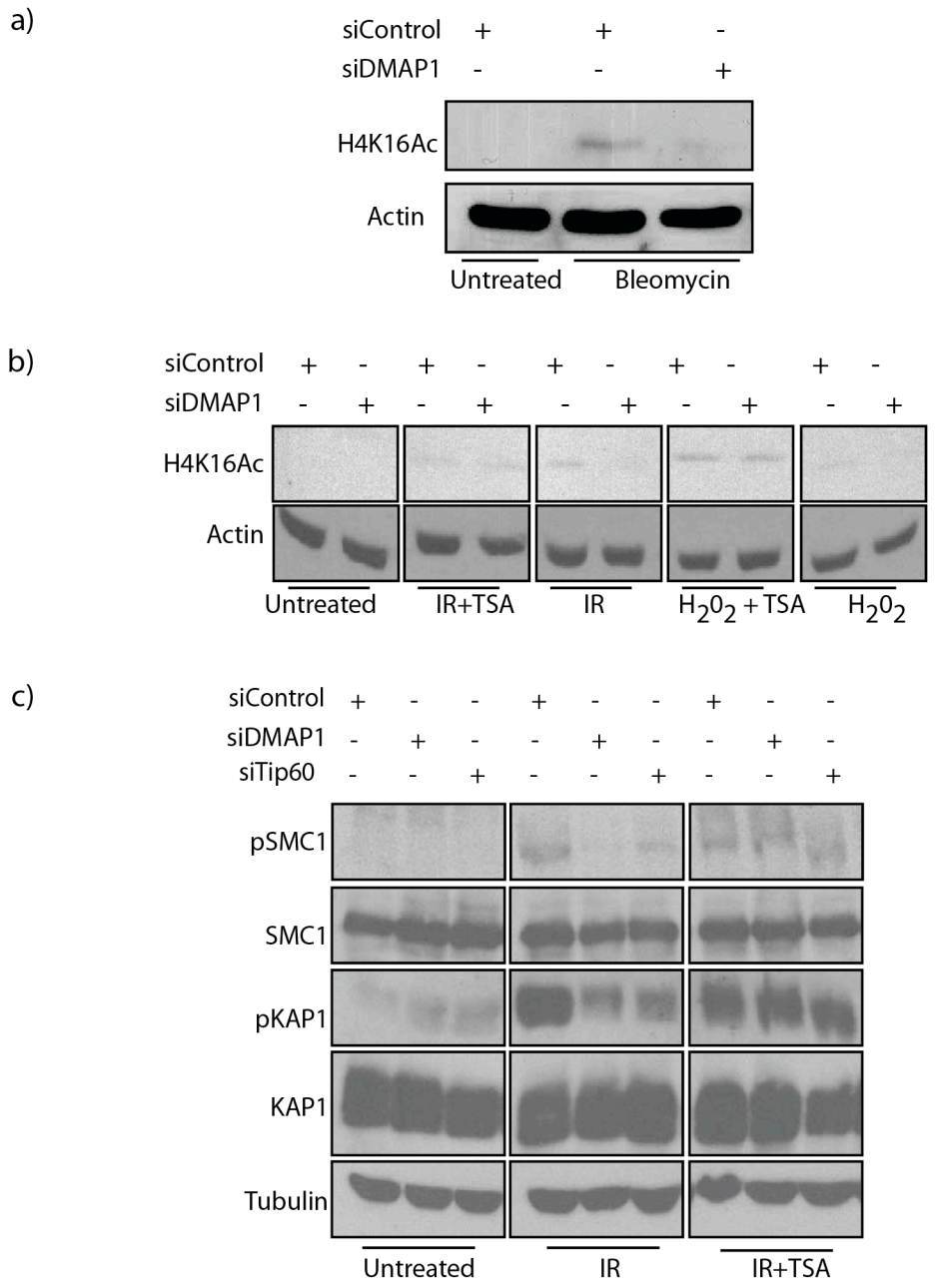

Figure 64: DMAP1 is required for H4K16 acetylation after IR

a) After 48 hours HCT-116 cells transfected with control or DMAP1 shRNA were treated with 5 μM bleomycin for 30 minutes. b, c) Cells transfected with the indicated shRNAs pre-treated with 5 μM TSA or DMSO for six hours, then treated with 5 Gy IR or 250 μM H_20_2 and harvested after one hour. Whole cell lysates were separated by (a, b) 15% or (c) 6% SDS-PAGE and immunoblotted for pS957-SMC1, SMC1, pS824-KAP1, KAP1, tubulin, actin and H4K16Ac.

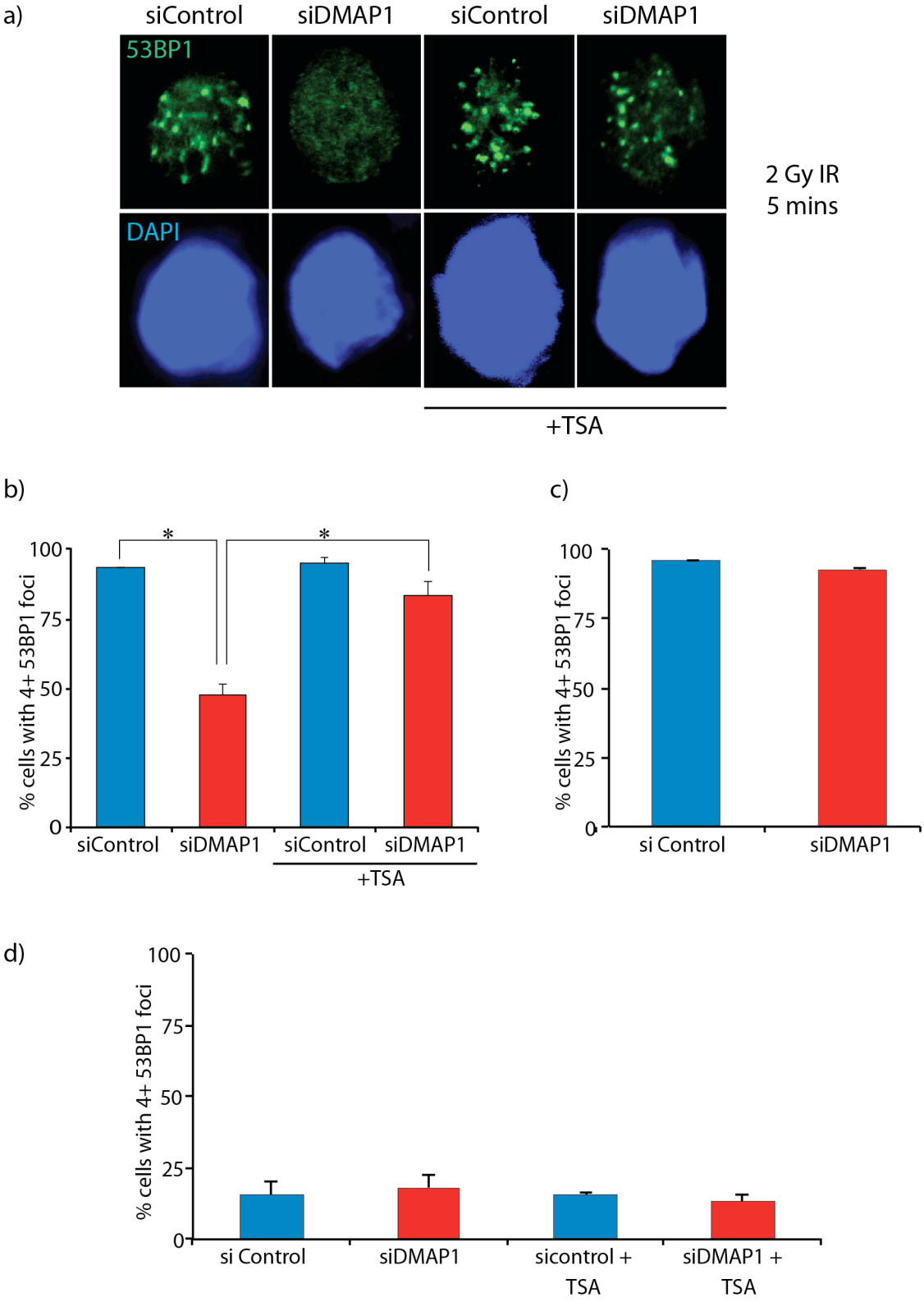

Figure 65: HDAC inhibitors rescue DNA damage foci formation in siDMAP1 cells

a) HCT-116 transfected with control or *dmap1* shRNA were cultured in the presence of either DMSO or TSA for six hours. Cells were treated with 2 Gy IR and fixed after five minutes. Cells were stained for 53BP1, representative images are shown. b)

Quantification of cells with four or more 53BP1 foci five minutes after 2 Gy IR, as shown in (b). c) HCT-116 transfected with control or *dmap1* shRNA were irradiated with 2 Gy IR and fixed after 45 minutes. Cells were stained for 53BP1 and the percentage of cells with four or more 53BP1 foci quantified. d) HCT-116 transfected with control or *dmap1* shRNA were cultured in the presence of either DMSO or TSA for six hours. Cells were fixed without treatment, stained for 53BP1 and the number of cells with four or more 53BP1 foci counted. The student's t-test was used for statistical analysis (*p<0.05).

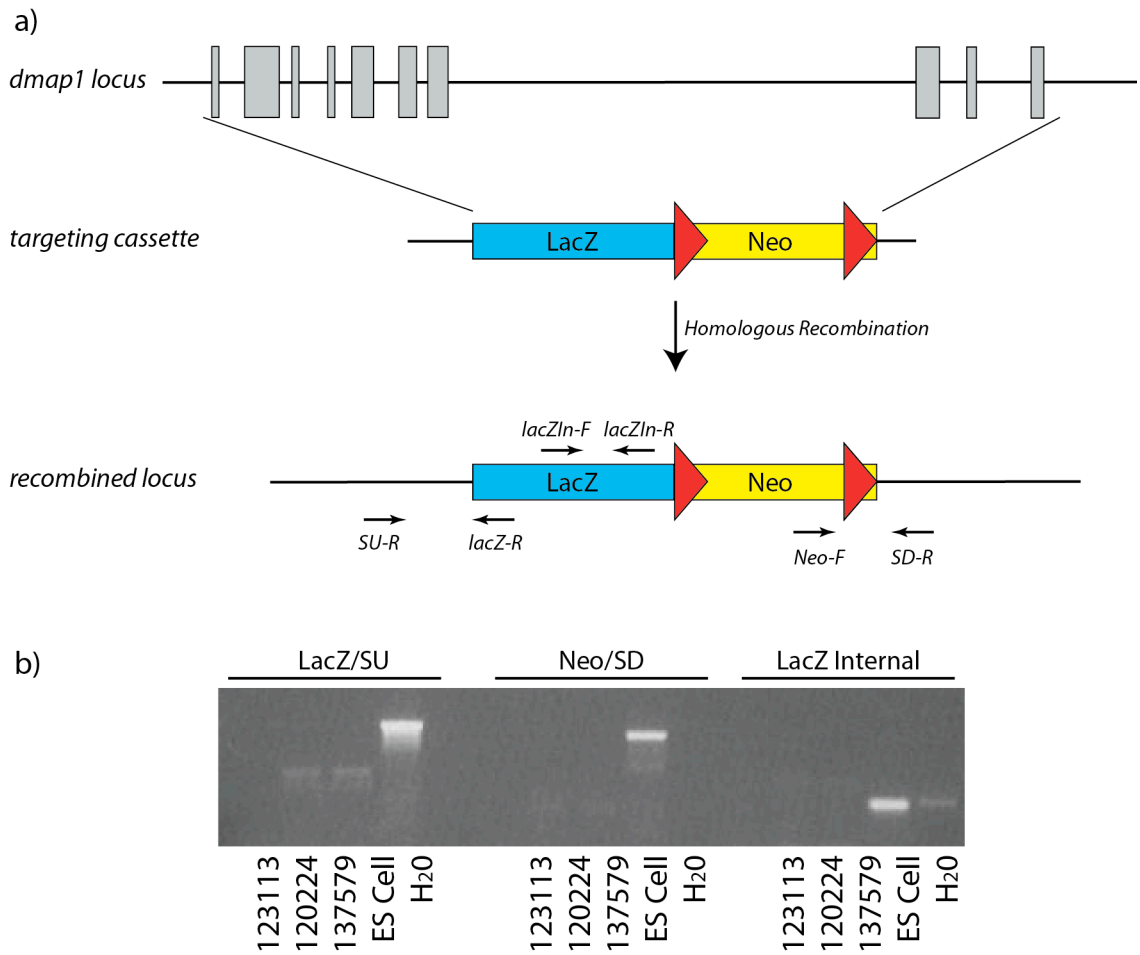

Figure 66: The *dmap1*$^{-/-}$ mouse is pre-implantation lethal

a) Schematic of the targeted *dmap1* locus indicating location of genotyping primer pairs b) Genotyping PCR performed upon three representative chimera offspring, and DNA from the original ES cells. Two sets of primer detect correctly targeted *dmap1* loci (LacZ/SU, Neo/SD) and one primer pair detects the presence of the targeting cassette (LacZ Internal).

Chapter 7. Discussion

7.1 ATMIN and telomeres

A key function of the shelterin complex is to shield telomeres from DSB recognition by the cellular DNA repair machinery. Paradoxically DDR components, including ATM, are required for telomere maintenance and are recruited to telomeres (Rudolph et al., 1999; Karlseder et al., 2004). We therefore investigated ATMIN function at the telomere. Excitingly, we observed increased pH2AX at the telomeres of *atmin*$^{\Delta/\Delta}$ MEFs (Figure 21) and impaired self-renewal and maintenance of late generation *terc*$^{-/-}$*; atmin*$^{\Delta N/\Delta N}$ NSCs both *in vivo* and *in vitro* (Figure 23*,* Figure 24). Thus, we propose ATMIN is required for telomere maintenance.

It was recently demonstrated that telomeric DNA damage is refractory to repair, and induces a long-term proliferation arrest (Fumagalli et al., 2012). ATMIN deficient cells have elevated DNA damage at the telomere and exhibit premature senescence (Figure 20, Figure 21). Therefore it is tempting to speculate the premature senescence of *atmin*$^{\Delta/\Delta}$ MEFs is at least partially due to increased telomeric damage.

7.1.1 Model: ATMIN is required for efficient telomere replication

It is unlikely ATMIN is required for protection of the telomere termini per se; *atmin*$^{\Delta/\Delta}$ MEFs do not exhibit the extreme phenotypes of cells deficient for essential telomere protection proteins, such as end to end chromosome fusions of *trf2*$^{\Delta/\Delta}$ MEFs (Sfeir and de Lange, 2012). Rather, the increased telomeric pH2AX foci in *atmin*$^{\Delta/\Delta}$ MEFs suggests replicative stress at the telomere and is reminiscent of the *trf1*$^{-/-}$ phenotype (Sfeir et al., 2009). Telomeres are considered fragile sites because repetitive (TTAGGG) telomeric repeats pose a problem to the DNA replication machinery. Replication forks can stall upon very repetitive sequences, potentially resulting in loss of telomeric DNA distal to the fork and DDR activation. It has been shown that specific factors, including TRF1 (Sfeir et al., 2009) and WRN (Crabbe et al., 2004), are required

for efficient telomere replication. Our working model is that ATMIN is required for efficient telomere replication (Figure 67).

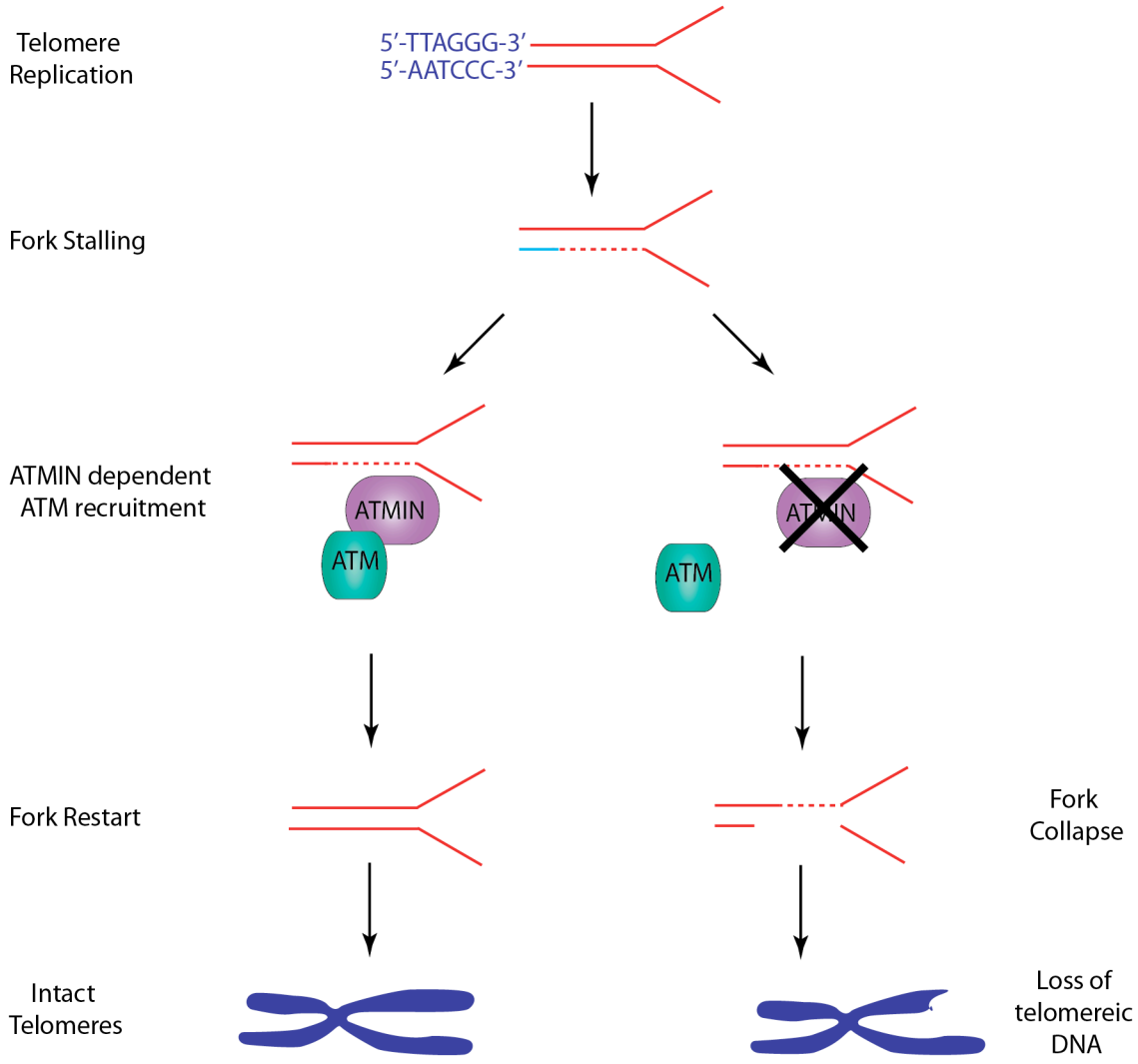

Figure 67: ATMIN is required for telomere replication

The repetitive sequences of telomeres can cause replication fork stalling. ATMIN is recruited to stalled replication forks, and recruits ATM. ATM signalling can promote repair of stalled forks and fork restart, ensuring telomeres are correctly replicated. However, in the absence of ATMIN stalled replication forks can collapse, forming a DSB and loss of all telomeric DNA distal to fork collapse.

7.1.2 ATMIN and telomeres: Open Questions and Future Plans

ATMIN's potential role in telomere replication could be further examined by directly establishing replicative stress at the telomeres of *atmin*$^{\Delta/\Delta}$ cells. One approach is to perform Single Molecule Analysis of Replicated DNA (SMARD) on *atmin*$^{+/+}$ and *atmin*$^{\Delta/\Delta}$ MEFs. After sequential incubations in dNTP analogues, for example IdU and CldU, denatured telomeric DNA is isolated and linearly stretched onto glass sides (DNA combing). The pattern of IdU and CldU incorporation reveals the progression of replication forks along telomeric DNA. We predict *atmin*$^{\Delta/\Delta}$ cells have increased replication fork stalling and a reduced rate of dNTP incorporation compared to *atmin*$^{+/+}$ cells. Although informative, this experiment will not establish the molecular detail by which ATMIN aids telomeric replication.

It is important to establish if ATMIN localises to the telomere. The lack of a good IF antibody against ATMIN precludes using IF-FISH to directly visualise ATMIN's potential telomeric binding. Chromatin-IP for ATMIN, followed by Southern Blot for telomeric repeats, would establish if ATMIN binds telomeric DNA. It is known that an ATMIN/Rad18/WRNIP complex recruits ATM to stalled replication forks (Kanu et al, submitted). Thus, one could perform IF-FISH for WRNIP, Rad18 and pS1987-ATM in *atmin*$^{+/+}$ and *atmin*$^{\Delta/\Delta}$ MEFs to establish if these repair factors - especially ATM - are recruited to telomeres in an ATMIN-dependent mechanism. This model is in agreement with the reduced pS1987-ATM localisation to pH2AX sites observed in *atmin*$^{\Delta/\Delta}$ MEFs (Figure 19). As it is likely a similar mechanism for ATMIN function will prevail at both telomeric and non-telomeric fragile sites, this is a good first approach to understand the mechanism behind ATMIN's repression of telomeric DNA damage.

One prediction of our model is the neurons of late generation *terc*$^{-/-}$*; atmin*$^{\Delta N/\Delta N}$ mice exhibit shorter telomeres than age-matched *terc*$^{-/-}$*; atmin*$^{+/+}$ controls. We propose the pH2AX foci at *atmin*$^{\Delta N/\Delta N}$ telomeres mark single and double strand breaks arising through replication stress. This damage leads to loss of all telomeric DNA distal to the break site, and thus telomere shortening. We plan to address this in collaboration with the Leonard Rudolph group (Ulm, Germany). Quantitative FISH will be performed on late generation *terc*$^{-/-}$*; atmin*$^{\Delta N/\Delta N}$ mice and littermate *terc*$^{-/-}$*; atmin*$^{+/+}$ controls. We

predict *terc*$^{-/-}$*; atmin*$^{\Delta N/\Delta N}$ mice will exhibit significantly shorter telomeres. We do not think telomerase deficiency is absolutely required for telomere shortening in *atmin*-deficient cells. Rather, telomerase loss will exacerbate the phenotype and make the difference in telomere length easier to detect *in vivo.*

All ATM activity at the telomere is unlikely to proceed via ATMIN; the MRN complex is also recruited to telomeres (Verdun et al., 2005). pS1987-ATM foci formation upon siRNA mediated *trf2* depletion is reduced in *mre11*$^{\Delta/\Delta}$ MEFs, but not in Mre11 nuclease-dead mutants (*mre11*^{H129N}) (Deng et al., 2009). This indicates the MRN complex, but not its end-processing activities, is important for telomere maintenance. It will be interesting to elucidate ATMIN and NBS1 dependent ATM function at the telomere. One speculates that ATMIN's role lies largely in protecting against replication stress, whereas NBS1 signals the presence of uncapped, DSB-resembling, telomeres.

7.2 ATMIN is not part of the OIS barrier induced by intestinal *KRas*^{G12D} expression

ATM has been shown to be required for oncogene induced senescence (OIS) in xenograft experiments (Bartkova et al., 2006). We investigated a role for ATMIN and ATM in the OIS barrier in a transgenic mouse model for *KRas*^{G12D} induced colorectal serrated hyperplasia (Bennecke et al., 2010).

7.2.1 Senescence induction in *atmin*$^{\Delta G/\Delta G}$*; KRas*^{G12D} mice

The senescence marker Dec1 was upregulated in both *atmin*$^{\Delta G/\Delta G}$*; KRas*^{G12D} and *KRas*^{G12D} intestines, suggesting OIS pathways do not require ATMIN (Figure 27f). Unexpectedly, intestinal protein levels of the senescence marker p21 were lower in *atmin*$^{\Delta G/\Delta G}$*; KRas*^{G12D} compared to *KRas*^{G12D} mice (Figure 27e). However, it would be premature to interpret this as a failure to induce senescence. Basal p21 levels were lower in the intestines of *atmin*$^{\Delta G/\Delta G}$ mice. Therefore there is still an increase in p21 levels upon *KRas*^{G12D} expression in *atmin*$^{\Delta G/\Delta G}$ mice. Together with *dec1* upregulation,

this suggests *atmin* deficient cells are still able to activate senescence programmes after $KRas^{G12D}$ expression. Further work is required to determine if reduced p21 levels in $atmin^{\Delta G/\Delta G}$ cells is a tissue-specific phenomena or reflects a regulatory loop between ATMIN and p21. ATMIN is part of the PCNA-interacting ATMIN-WRNIP-Rad18 complex (Kanu et al, submitted). Perhaps loss of ATMIN increases binding between p21 and PCNA, leading to increased ubiquitination and degradation of PCNA-bound p21 (Abbas et al., 2008). A reduced level of tumour-protective p21 in ATMIN-deficient cells is in keeping with ATMIN's role as a tumour suppressor (Loizou et al., 2011).

In agreement with the biochemical observations, there was no difference in the survival of $atmin^{\Delta G/\Delta G}$; $KRas^{G12D}$ and $KRas^{G12D}$ animals (Figure 30). ATMIN loss did not lead to progression from serrated hyperplasia to adenoma. Therefore we conclude ATMIN does not have an important function in senescence induced by intestinal $KRas^{G12D}$ expression.

One cannot draw the same conclusion for ATM as $atm^{-/-}$; $KRas^{G12D}$ animals succumbed to T-cell lymphoma at approximately three months, precluding a longer-term tumour study (Figure 30). However, *dec1* upregulation in $atm^{-/-}$; $KRas^{G12D}$ intestines strongly suggests that *atm* deficient cells are able to induce senescence upon oncogene expression (Figure 28d). It is noteworthy that $p53^{\Delta G/\Delta G}$; $KRas^{G12D}$ animals do not develop adenoma (Bennecke et al., 2010). Thus, given $Ink4a/Arf^{-/-}$; $KRas^{G12D}$ animals do develop adenomas of the colon, Ink4a/Arf rather than ATM-p53 signalling is predominantly responsible for senescence induction upon intestinal $KRas^{G12D}$ expression.

7.2.2 ATMIN, ATM and OIS: Open Questions and Future Directions

This study does not suggest ATM is dispensable for OIS in every context. For example, although early onset T-cell lymphoma precluded long-term tumour study, Efeyan and colleagues observed higher tumour grades in the lungs of $atm^{-/-}$; $KRas^{G12D}$ compared to $atm^{+/+}$; $KRas^{G12D}$ controls (Efeyan et al., 2009). However, one cannot necessarily attribute this to breached OIS in $atm^{-/-}$ cells as senescent cells were not quantified. The

increased genomic instability of *atm*$^{-/-}$ cells could underlie the accelerated lung tumour development of *atm*$^{-/-}$*; KRas*^{G12D} mice.

Senescence induction in response to oncogenic stress is subject to many tissue and oncogene-specific influences. For example, Skp2 inactivation in *pten*$^{+/-}$ mice induces senescence and protects against tumour progression in a p53-independent mechanism (Lin et al., 2010). Conversely, p53-dependent senescence induction protects against tumour progression in a *pten*$^{-/-}$ prostate cancer model (Chen et al., 2005). It is tempting to speculate ATM, and perhaps ATMIN, are required for senescence induction only in tumour models with *p53*- dependent, as oppose to *Ink4a/Arf*- dependent, senescence.

7.3 ATMIN/NBS1: The Competition Model

7.3.1 Doubly deficient *nbs1*$^{\Delta/\Delta}$*; atmin*$^{\Delta/\Delta}$ cells resemble an *atm*$^{-/-}$ phenotype

Loss of ATMIN partially rescues the proliferation arrest and senescence induction of *nbs1*$^{\Delta/\Delta}$ MEFs (Figure 41, Figure 42). Importantly, this rescue occurs despite greatly increased DNA damage in the *nbs1*$^{\Delta/\Delta}$*; atmin*$^{\Delta/\Delta}$ double mutant cells (Figure 47), excluding the possibility that DNA damage per se is solely responsible for the *nbs1*$^{\Delta/\Delta}$ phenotype.

It should be noted that co-deletion of ATMIN from *nbs1*$^{\Delta/\Delta}$ cells does not wholly rescue the *nbs1*$^{\Delta/\Delta}$ phenotype. Compound mutant *nbs1*$^{\Delta/\Delta}$*; atmin*$^{\Delta/\Delta}$ MEFs exhibit increased senescence and reduced proliferation potential compared to wildtype cells, with greatly increased DNA damage (Figure 41, Figure 42, Figure 47). Rather, these doubly deficient cells behave like *atm*$^{-/-}$ cells. The elevated pH2AX level in the compound mutants indicates ATMIN and NBS1 co-operate to maintain genomic integrity and are unable to substitute for each other. The complete absence of pS1987-ATM foci in the *nbs1*$^{\Delta/\Delta}$*; atmin*$^{\Delta/\Delta}$ compound mutants argues against the existence of a third ATM co-factor.

Whereas *atm*$^{-/-}$ mice are viable, albeit infertile and tumour prone (Barlow et al., 1996), *nbs1*$^{-/-}$ mice die at approximately E3.5 (Zhu et al., 2001). The phenotypic differences between *atm*$^{-/-}$ and *nbs1*$^{-/-}$ mice has long-suggested ATM-independent functions for NBS1. For example, NBS1 is required for the nuclear localisation of Mre11 and Rad50 (Williams et al., 2009). Defects resulting from NBS1's ATM-independent functions will persist in *nbs1*$^{\Delta/\Delta}$ cells regardless of ATMIN status. Accordingly, *nbs1*$^{\Delta/\Delta}$*; atmin*$^{\Delta/\Delta}$ MEFs and *nbs1*$^{\Delta G/\Delta G}$*; atmin*$^{\Delta G/\Delta G}$ mice are radiosensitive and do not activate ATM after DSB induction (Figure 50).

7.3.2 ATMIN and NBS1 compete for ATM interaction

Difilippantonio and colleagues have previously shown increased pS1981-ATM after osmotic stress in *nbs1*$^{\Delta/\Delta}$ B cells (Figure 5c, Difilippantonio et al., 2005). We also observed increased ATM activation after hypotonic shock in *nbs1*$^{\Delta/\Delta}$ MEFs (Figure 46b) Similarly, *atmin*$^{\Delta/\Delta}$ MEFs display increased ATM signalling after irradiation (Figure 46a).

In parallel to my *in vivo* and *in vitro* observations, my colleague Tianyi Zhang analysed ATM co-factor choice on a biochemical level. She observed increasing concentrations of ATMIN inhibited NBS1-dependent ATM substrate phosphorylation and 53BP1 foci formation after IR. However, overexpression of an ATMIN mutant lacking the ATM interaction motif did not inhibit IR-dependent ATM signalling. Crucially, ATMIN overexpression reduced the amount of NBS1 co-immunoprecipitated with ATM.

7.3.3 NBS1 in the intestine

Using the intestine as a model system, we were able to confirm *in vivo* a partial rescue of the *nbs1*$^{\Delta G/\Delta G}$ phenotype upon *atmin* deletion. In comparison to single mutant *nbs1*$^{\Delta G/\Delta G}$ mice, *nbs1*$^{\Delta G/\Delta G}$*; atmin*$^{\Delta G/\Delta G}$ animals exhibit reduced degeneration of the intestinal mucosa (Figure 43).

Depletion of *MCM6*$^{+}$ intestinal progenitors in *nbs1*-deficient intestines is partially rescued by ablation of ATMIN function (Figure 45d). However, the abundance of *olfm4*$^{+}$ intestinal stem cells was drastically reduced five days after gene deletion in both *nbs1*$^{\Delta G/\Delta G}$*; atmin*$^{\Delta G/\Delta G}$ and *nbs1*$^{\Delta G/\Delta G}$ intestines (Figure 45h). As MCM6 marks a wider progenitor pool than just *olfm4*$^{+}$ stem cells, perhaps at longer timepoints after deletion the *MCM6*$^{+}$ pool would also be depleted in *nbs1*$^{\Delta G/\Delta G}$*; atmin*$^{\Delta G/\Delta G}$ crypts as the depleted stem cell pool is unable to replenish the progenitor pool. Interestingly, a higher percentage of *nbs1*$^{\Delta G/\Delta G}$*; atmin*$^{\Delta G/\Delta G}$ crypts contained at least one *olfm4*$^{+}$ cell compared to *nbs1*$^{\Delta G/\Delta G}$ single mutants (Figure 45i). This suggests that although *atmin* loss does not completely rescue the stem cell pool depletion of *nbs1*$^{\Delta G/\Delta G}$ intestines, *atmin* loss does increase the propensity of an NBS1 deficient crypt to maintain at least one stem cell.

In summary, although ablation of ATMIN function from *nbs1* deficient cells does somewhat rescue cellular function, ultimately these doubly deficient cells do not behave as wildtype and thus it is not a complete rescue of function.

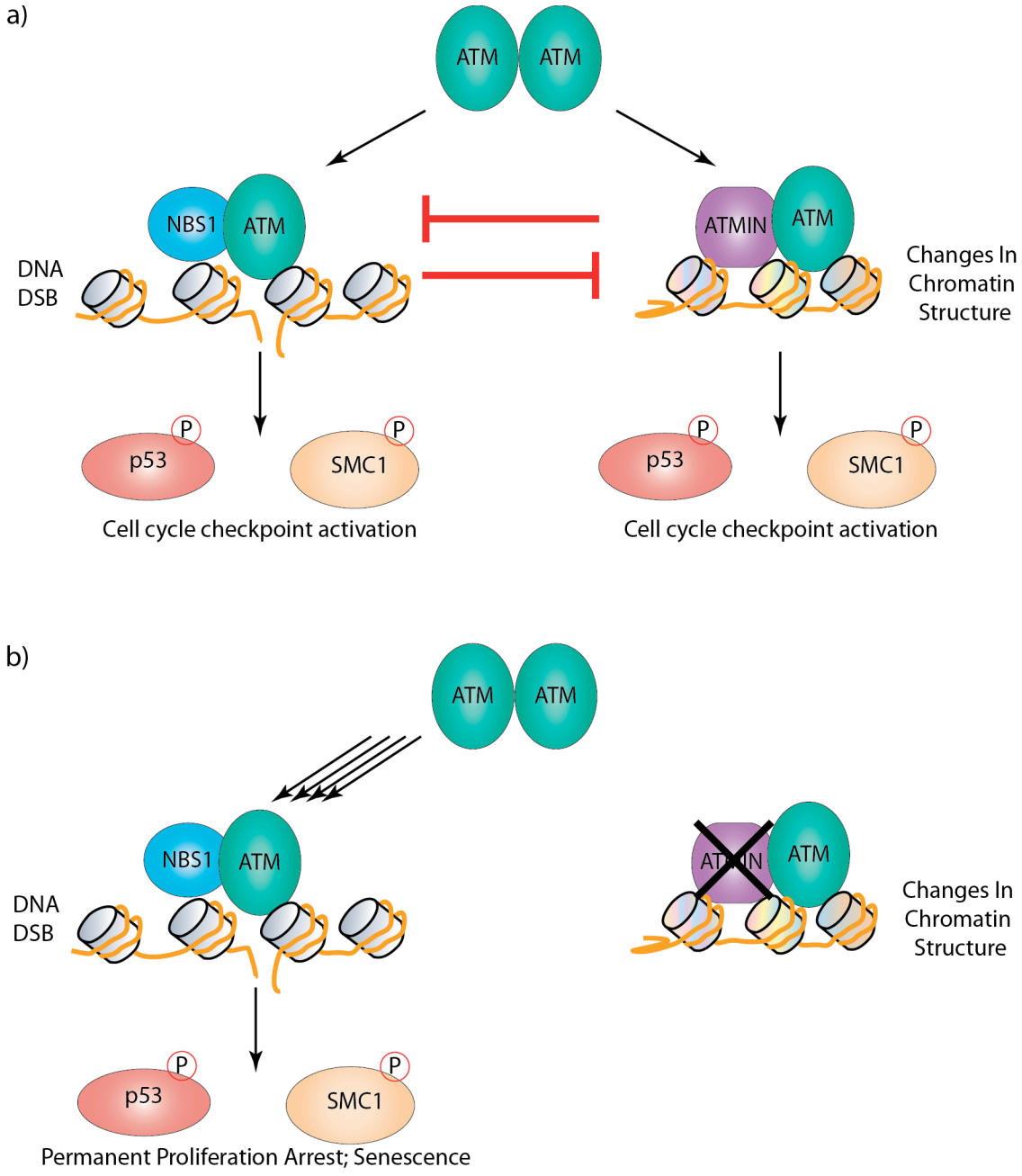

Figure 68: The ATMIN/NBS1 Competition Model

a) ATMIN and NBS1 compete for ATM binding. ATM signalling proceeds via either ATMIN or NBS1 in a stimulus dependent manner. b) In *atmin* deficient cells, increased NBS1-dependent ATM signalling contributes to premature senescence and proliferation arrest.

7.3.4 The Competition Model: Open Questions and Future Directions

We propose the consequences of *nbs1* deficiency extend beyond defective DSB-signalling, and increased ATMIN-dependent ATM signalling in $nbs1^{\Delta/\Delta}$ cells contributes to the defects observed in $nbs1^{\Delta/\Delta}$ cells. Thus *atmin* ablation recues the cellular defects of $nbs1^{\Delta/\Delta}$ cells caused by increased non-canonical, ATMIN-dependent ATM signalling (Figure 68). For example, p53 activation by the ATMIN-ATM pathway in $nbs1^{\Delta/\Delta}$ cells could activate cell-cycle checkpoints and induce senescence. The competition of NBS1 and ATMIN for ATM interaction is a fundamental mechanism of ATM signalling, and disruption of this balance is deleterious to cells.

The next step of this study would be to determine the molecular mechanism by which ATMIN and NBS1 compete for ATM binding. Both could bind ATM with comparable affinity and the proportion of ATM bound to either co-factor is simply determined by the stoichiometry between ATMIN and NBS1. Thus, we observe increased IR-induced ATM signaling in $nbs1^{\Delta/\Delta}$ cells as a larger percentage of ATM molecules are bound to NBS1, and vice versa. Secondly, NBS1 and/or ATMIN could undergo posttranslational modification upon DSB induction. For example IR-regulated monoubiquitination of ATMIN could reduce its affinity for ATM, increasing NBS1-dependent ATM signalling.

It would be interesting to elucidate other components of the non-canonical ATM pathway contributing to the defects of $nbs1^{\Delta/\Delta}$ cells. For example, increased ATMIN-dependent ATM activation of p53 could promote proliferation arrest. Both $nbs1^{f/f}$ and $nbs1^{f/f}$; $atmin^{f/f}$ MEFs could be infected with lenti-sh*p53* prior to gene deletion. We predict p53 loss will partially rescue proliferation arrest in the *nbs1*-null MEFs

Given $atmin^{\Delta/\Delta}$ cells are radioresistant, the 'Competition Model' has some interesting therapeutic implications. For example, increasing ATMIN levels in non-cancerous tissues prior to radiation therapy should reduce their propensity undergo apoptosis, and hence reduce the detrimental side-effects and enable a higher dose of radiation to be tolerated by the patient.

7.4 ATMIN loss protects against lymphoma in *p53*$^{\Delta B/\Delta B}$ mice

7.4.1 ATMIN deletion rescues B cell lymphoma onset in *p53*$^{\Delta B/\Delta B}$ mice

Approximately 40% of *atmin*$^{\Delta B/\Delta B}$ mice develop B cell lymphoma at a mean age of six months (Loizou et al., 2011). We monitored cohorts of *p53*$^{\Delta B/\Delta B}$ and *atmin*$^{\Delta B/\Delta B}$*; p53*$^{\Delta B/\Delta B}$ mice for cancer onset. B cell specific p53 deletion led to B cell lymphoma in 60% of the cohort, at a mean age of 7 months (Figure 36). Surprisingly, no B cell lymphoma was observed in a cohort of *atmin*$^{\Delta B/\Delta B}$*; p53*$^{\Delta B/\Delta B}$ mice monitored for over a year (Figure 38). Thus, ablation of *atmin* function rescues the B cell lymphoma onset of *p53*-deficient mice.

The simplest model for the lymphoma-free survival of *atmin*$^{\Delta B/\Delta B}$*; p53*$^{\Delta B/\Delta B}$ mice is that loss of both p53 and ATMIN is detrimental to B cell development. If so, *atmin*$^{\Delta B/\Delta B}$*; p53*$^{\Delta B/\Delta B}$ mice would have substantially fewer B cells and thus a reduced chance of a B cell accumulating sufficient cancer-promoting mutations. However, FACS analysis of the different stages of B cell development revealed no significant B cell development defect in either *p53*$^{\Delta B/\Delta B}$ or *atmin*$^{\Delta B/\Delta B}$*; p53*$^{\Delta B/\Delta B}$ mice (Figure 32, Figure 33). The *atmin*$^{\Delta B/\Delta B}$ mouse is published to have a mild reduction in the immature B cell population (Loizou et al., 2011) recapitulating the *atm*$^{-/-}$ phenotype (Xu et al., 1996). Although *atmin*$^{\Delta B/\Delta B}$*; p53*$^{\Delta B/\Delta B}$ mice demonstrated a reduced pre-B population compared to littermate *atmin*$^{\Delta B/\Delta B}$*; p53*$^{\Delta B/\Delta B}$ controls, this difference did not reach statistical significance (p=0.172). However, the individual percentages were lower in *atmin*$^{\Delta B/\Delta B}$*; p53*$^{\Delta B/\Delta B}$ mice, and I predict that increasing the number of mice analysed would lead to the mild defect reaching statistical significance. Notwithstanding, it is evident that *atmin*$^{\Delta B/\Delta B}$*; p53*$^{\Delta B/\Delta B}$ mice do not display overt B cell maturation defects.

7.4.2 ATMIN and p53 interplay in other tissues

Consideration of my B cell lymphoma study alone does not permit a conclusion on whether the phenomenon of tumour-free doubly deficient *atmin*$^{\Delta/\Delta}$*; p53*$^{\Delta/\Delta}$ tissues is limited to the B cell lineage. Two colleagues, Nnennaya Kanu and Sophia Blake, have subsequently performed a similar brain-tumour study in cohorts of *atmin*$^{\Delta N/\Delta N}$*, p53*$^{\Delta N/\Delta N}$

and *atmin*$^{\Delta N/\Delta N}$*; p53*$^{\Delta N/\Delta N}$ mice. Preliminary data suggests that whilst approximately a quarter of *p53*$^{\Delta N/\Delta N}$ mice develop glioblastoma, no cases were observed in either *atmin*$^{\Delta N/\Delta N}$ or *atmin*$^{\Delta N/\Delta N}$*; p53*$^{\Delta N/\Delta N}$ cohorts. This study allows us to draw two important conclusions. Firstly, the cancer-free survival of *atmin*$^{\Delta/\Delta}$*; p53*$^{\Delta/\Delta}$ compound mutants is not restricted to B cells. Secondly, no cancer was observed in *atmin*$^{\Delta N/\Delta N}$ animals (Kanu et al., 2010). Thus we can infer ablation of *atmin* function from a *p53*-deficient cells protects against cancer development. Based only on the B cell data, one could have concluded loss of p53 protected against *atmin*$^{\Delta/\Delta}$-driven lymphoma.

Importantly, this does not appear to be a universal mechanism. Co-deletion of *atmin* and *p53* from a *KRas*^{G12D} lung cancer model did not prevent or slow tumour development (Sophia Blake, unpublished observations). I have also observed β-cell specific *atmin* deletion did not affect pancreatic cancer development in the Rip-TAg model, in which the large T antigen is expressed in β-cells (data not shown). Elucidation of the underlying mechanism by which *atmin* deletion rescues cancer onset in *p53* deficient cells should shed light on the tissue specificities.

7.4.3 ATMIN and p53: Open Questions and Future Directions

There are two working models for the lymphoma free survival of *atmin*$^{\Delta B/\Delta B}$*; p53*$^{\Delta B/\Delta B}$ mice. Both ATMIN and p53 are transcription factors, thus overlapping transcriptional targets could underlie the unique characteristics of *atmin*$^{\Delta B/\Delta B}$*; p53*$^{\Delta B/\Delta B}$ cells (Figure 69). Whilst this is an attractive model, much experimental investigation is needed to validate it. It is probable that networks of ATMIN and p53 dependent transcription contribute to the lymphoma-free phenotype of *atmin*$^{\Delta B/\Delta B}$*; p53*$^{\Delta B/\Delta B}$ cells. Therefore one future plan is to perform a microarray on B cells from six week old *atmin*$^{\Delta B/\Delta B}$*, p53*$^{\Delta B/\Delta B}$ and *atmin*$^{\Delta B/\Delta B}$*; p53*$^{\Delta B/\Delta B}$ mice. The interesting targets are those upregulated in *p53*$^{\Delta B/\Delta B}$ (and possibly *atmin*$^{\Delta B/\Delta B}$ cells) but that return to wildtype transcription levels in the compound mutant.

An *in vivo* way to test 'The Transcription Model' would be to make use of a transcriptionally-dead ATMIN mutant. Mutations in ATMIN's zinc-fingers abolish its

transcriptional activity. It would be interesting to cross this mutant with *p53$^{f/f}$; CD19-Cre* mice. If ATMIN's transcriptional activity is required for suppression of p53-driven lymphoma, the ATMIN mutant should develop B-cell lymphoma at the same age as the *p53$^{\Delta B/\Delta B}$* cohort. The phenotypic differences between *atmin$^{\Delta/\Delta}$* and *atm$^{-/-}$* mice, especially the embryonic lethality of *atmin$^{\Delta/\Delta}$* but not *atm$^{-/-}$* mice, illustrates that ATMIN has ATM-independent functions. For example, ATM-independent transcriptional regulation by ATMIN may explain its unusual relationship with p53.

Indeed, compound *atm$^{-/-}$; p53$^{-/-}$* mutants develop lymphoma approximately two months prior to earlier than either of the single mutants (Westphal et al., 1997; Xu et al., 1998). This suggests the lymphoma rescue of *atmin$^{\Delta B/\Delta B}$; p53$^{\Delta B/\Delta B}$* mice is either independent of ATM function, or is dependent upon intact ATM signalling.

Both ATMIN and p53 are part of the DNA damage response network. 'The DNA Damage Model' (Figure 70) predicts increased ATM-NBS1 signalling in the *atmin$^{\Delta B/\Delta B}$; p53$^{\Delta B/\Delta B}$* mutants is able to circumvent of p53 loss, and activate sufficient cell-cycle checkpoints after DNA damage to prevent accumulation of deleterious mutations. One would predict over-expression of an ATMIN protein unable to bind ATM would reduce the proliferation of *p53$^{\Delta B/\Delta B}$* MEFs.

It is important to establish the tissue-specificities of the mechanism. Ablation of ATMIN function in some tissues types, including B cells and brain, should protect against cancer development in *p53*-deficient cells. We currently do not know if ATMIN suppresses the initiation or maintenance of cancerous cells. ATMIN function could be acutely inactivated by tamoxifen injection of *p53$^{\Delta/\Delta}$; atmin$^{f/f}$; CD19-CreERT* mice once they show symptoms of lymphoma. Defining whether loss of ATMIN from an established *p53$^{\Delta B/\Delta B}$* cancer promotes tumour regression will establish the therapeutic potential of targeting ATMIN in *p53$^{\Delta/\Delta}$* driven cancers.

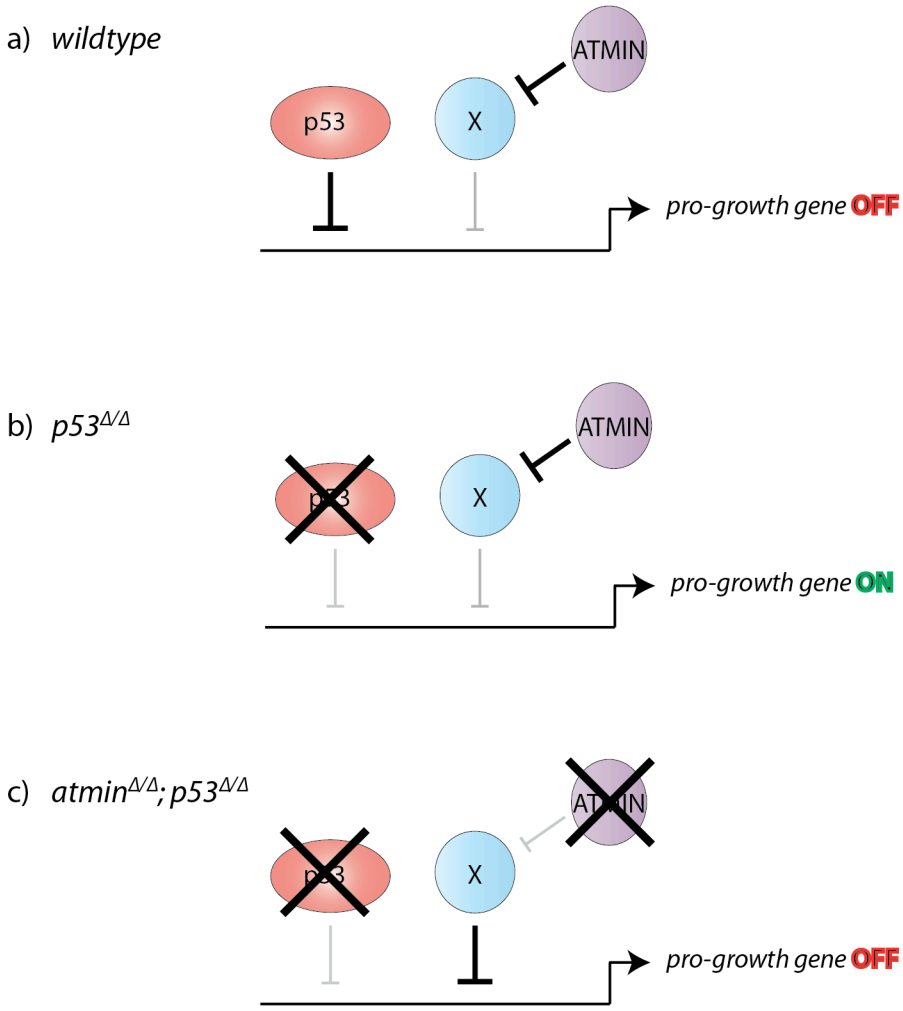

Figure 69: The Transcription Model for ATMIN/p53 cross-talk

a) In wildtype cells p53 represses a 'pro-growth gene', and transcription does not occur. b) In $p53^{\Delta/\Delta}$ cells the repression of the 'pro-growth' gene is lost. ATMIN represses transcription of a second repressor 'X', and the 'pro-growth' gene is activated. c) $atmin^{\Delta/\Delta}$; $p53^{\Delta/\Delta}$ cells have lost the ability to repress 'X', and thus 'X' is now able to repress transcription of the 'pro-growth' gene. Therefore, even though p53-mediated is repression is absent; the loss of ATMIN ensures the 'pro-growth' gene is not expressed.

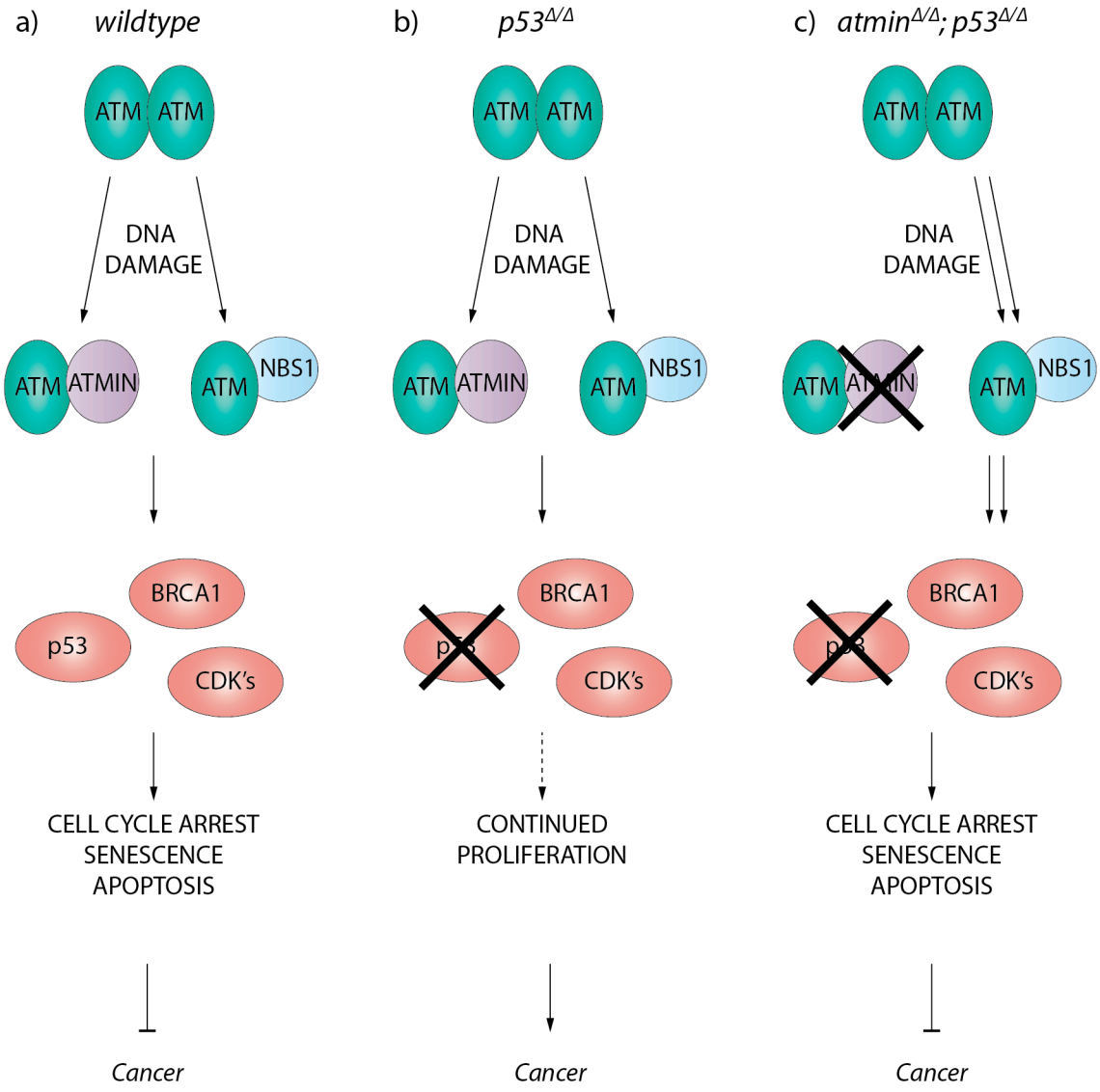

Figure 70: The 'DNA Damage' Model for p53 and ATMIN signalling

a) In wildtype cells, upon DNA damage ATM signals via either ATMIN or NBS1 to activate cell cycle checkpoints, promoting DNA repair or apoptosis. This prevents genomic instability and accumulation of cancer-promoting mutations. b) Loss of p53 impairs checkpoint activation, leading to the continued proliferation of cells harbouring DNA damage. There is the increased likelihood of cancer development. c) In the absence of ATMIN and p53, increased NBS1-dependent ATM signalling increases the propensity of checkpoint activation by p53-independent mechanisms, for example BRCA1 phosphorylation. Thus, pre-malignant cells undergo DNA repair, senescence or apoptosis and probability of cancer development is reduced.

7.5 DMAP1 is a novel regulator of ATM function

We have identified DMAP1 as a novel regulator of ATM function. DMAP1 deficient cells exhibit reduced ATM signalling after IR (Figure 52), hypotonic stress and oxidative stress (Figure 56). Abrogation of DMAP1 function renders cells radiosensitive and defective in DNA-damage induced G2/M cell cycle arrest (Figure 55).

7.5.1 DMAP1's putative PI3-K interaction motif is dispensable for regulation of ATM signalling

DMAP1 was identified in a screen for proteins containing PI3-K interaction motifs (Figure 51). Surprisingly, I was unable to demonstrate interaction between ATM and DMAP1 under a wide range of conditions (Figure 58). It is plausible that DMAP1 and ATM interact but I cannot detect such an interaction due to technical limitations; ATM's large molecular weight makes it difficult immunoprecipitate with high efficiency. I therefore characterised the functional importance of DMAP1's PI3-K interaction motif. Overexpression of both full-length DMAP1 and a truncation mutant lacking the ATM interaction domain augmented ATM signalling (Figure 59). This suggests interaction with ATM is not required for DMAP1 regulation of ATM signalling. DMAP1's putative PI3-K interaction motif could be coincidental, or reflect DMAP1's evolution from an ancestral PI3-K interacting protein.

Moreover, I was unable to detect DMAP1 localisation to the double strand break site (Figure 60, Figure 61, Figure 62). This could be due to a number of technical limitations. For example, DMAP1 could transiently associate with the break site. Alternatively, only a fraction total cellular DMAP1 protein localises to the break site. Detection is masked by the strong IF signal from pan-nuclear, DNMT1-associated DMAP1 (Rountree et al., 2000). However, considering DMAP1 does not detectably interact with ATM, its putative ATM interaction motif is not required for augmentation of ATM signalling, and DMAP1 is not detectably recruited to DNA damage foci it is probable that DMAP1 does not regulate ATM pathway activation through direct interaction with ATM.

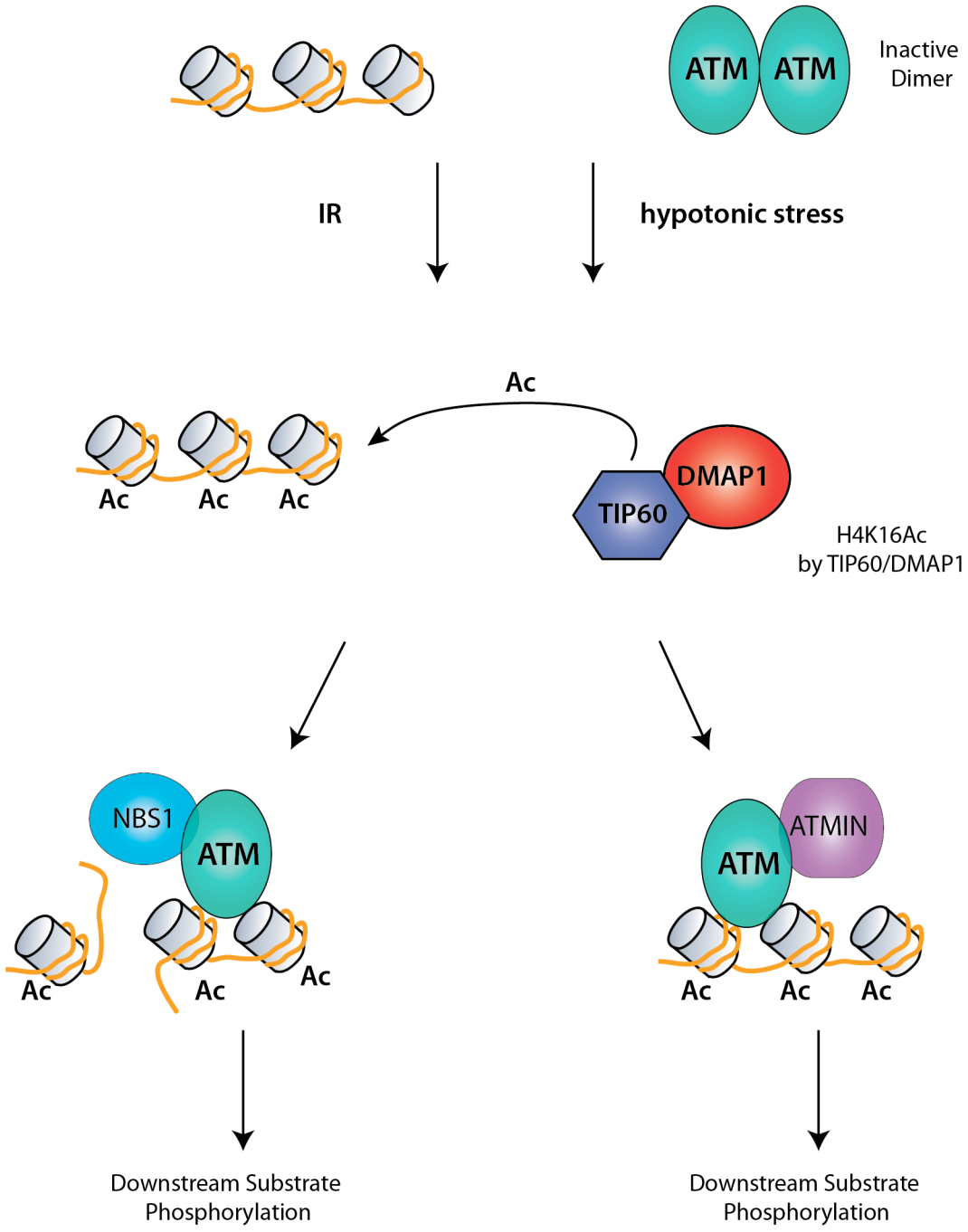

Figure 71: DMAP1-Tip60 H4K16 acetylation regulates ATM signalling

Upon either IR-induced DSBs or hypotonic shock ATM autophosphorylates, monomerises and localises to the damage site. For full activation of ATM signalling, chromatin changes must also occurs. A Tip60-DMAP1 complex acetylates H4K16, facilitating ATM activation.

7.5.2 DMAP1 regulates ATM signalling by H4K16 acetylation

It is known that ATM activation is regulated by changes in chromatin structure (Bakkenist and Kastan, 2003; Kim et al., 2009). For example, H4K16 is acetylated by the histone acetyltransferase Tip60 after DNA damage (Li et al., 2010; Wu et al., 2011). DMAP1 interacts with Tip60, and H4K16Ac is dramatically downregulated in DMAP1 deficient cells. ATM substrate phosphorylation and 53BP1 foci formation is rescued in DMAP1 deficient cells pre-treated with histone deacetylase inhibitors. This suggests a model whereby DMAP1's impact on ATM signalling occurs through its interaction with the histone acetyltransferase Tip60 and modulates chromatin acetylation, including H4K16Ac (Figure 71).

It must be noted that whilst there is clear evidence DMAP1-Tip60 influences ATM signalling via H4K16Ac levels, one cannot rule out a model whereby DMAP1-Tip60 also acetylates non-histone proteins. Crucially, it is postulated Tip60 acetylates ATM after DNA damage (Sun et al., 2009; Sun et al., 2007). However, I was unable to reliably detect ATM acetylation or interaction between Tip60 and ATM, probably due to technical limitations. Alternatively, perhaps Tip60 is capable of acetylating ATM *in vitro*, but this does not reflect Tip60's *in vivo* substrates.

7.5.3 DMAP1, histone acetylation, and oxidative stress

The reduced H_20_2 induced ATM signalling in *dmap1* deficient cells suggests DMAP1-Tip60 dependent H4K16 acetylation is required for ATM signalling after oxidative-stress (Figure 56b). However, these results must be interpreted with caution.

A recent paper by the Tanya Paull group demonstrated pS1987-ATM and pS15-p53, but neither pS824-KAP1 nor pH2AX, phosphorylation after 30 minutes 250μM H_20_2 treatment (Figure 1, Guo et al., 2010b). As pH2AX and pS824-KAP1 are considered to only be phosphorylated at DSB sites, this was interpreted as ATM activation by oxidative stress independently of DSB induction. In contrast to their results, I observe robust pS824-KAP1 after 30 minutes 250μM H_20_2 treatment (Figure 56a). The

observation of pS824-KAP1 in my H_20_2 treatment protocol does alter the interpretation of the experiments. Whilst it is evident DMAP1 is required for ATM pathway activation after oxidative stress, one cannot conclude DMAP1 is required for formation of ATM cysteine linked dimers; as the oxidative stress treatment appears to be inducing DSBs and thus presumably monomeric ATM is present. It is unclear why I observe pS824-KAP1 whilst the Paull group do not. Perhaps differences in cellular sensitivity to oxidative stress, or an increased pS824-KAP1 detection threshold are responsible.

7.5.4 DMAP1: Open Questions and Future Directions

A key outstanding question is the mechanism by which DMAP1 regulates Tip60 activity. Tip60 has a wide range of acetylation targets under basal conditions, so Tip60 catalytic activity per se is unlikely to be regulated by DNA damage (Squatrito et al., 2006).

DMAP1 contains a SANT domain, also present in the yeast homolog Eaf2, which interacts with histone tails (Boyer et al., 2002). It is therefore tempting to conjecture DMAP1 provides Tip60 with positional information. It has been proposed that Tip60 recruitment to DSBs occurs by binding H3K9me3, which is exposed after CK2 phosphorylates HP1-β, prompting HP1-β dissociation from chromatin (Sun et al., 2009). However, several unanswered questions remain from this model. Firstly, the mechanism of CK2 regulation by DNA damage is unknown. Secondly, it is premature to conclude HP1-β dissociation is the only mechanism of Tip60 recruitment to DSBs. Thirdly, the model proposed by Sun and colleagues suggests Tip60 association with H3K9me3 activates its acetyltransferase activity. Given the wide range of Tip60 substrates, this is unlikely to be the only mechanism of Tip60 activation (Squatrito et al., 2006). Thus it is conceivable DMAP1 provides Tip60 with positional information.

To investigate DMAP1 regulation of Tip60, I would initially focus on DMAP1's SANT domain. IP-Mass Spectrometry of DMAP1 could determine the histone modifications bound by the SANT domain. This would provide insight into how DMAP1 confers positional information to Tip60, especially through comparison of DMAP1 histone

binding in untreated and irradiated cells. If successful, mutation of the amino acids proposed to interact directly with histones would reveal if interaction between DMAP1's SANT domain and chromatin regulates ATM signalling.

7.5.5 DMAP1-Tip60 - A therapeutic potential?

Unfortunately, the pre-implantation lethality of *dmap1*$^{-/-}$ mice precluded study of the consequence of *dmap1* loss in murine tumour models (Figure 66). Conversely, Tip60 is an established haploinsufficient tumour suppressor; *Eμ-Myc; tip60*$^{+/-}$ B cells do not activate an oncogene-induced DDR and mice have accelerated lymphoma onset (Gorrini et al., 2007). Moreover, H4K16Ac is downregulated in a range of cancers (Fraga et al., 2005). Taken together, this suggests DMAP1-Tip60 offers an intriguing therapeutic potential. The HDAC inhibitors Vorinostat and Romidepsin are approved for treatment of T-cell lymphoma, with many more currently in clinical trials (Mann et al., 2007; Prince and Dickinson, 2012). Our study suggests treatment of cancers exhibiting abrogated ATM signalling with HDAC inhibitors would have therapeutic benefit.

7.6 Concluding Remarks

In my PhD studies I have identified DMAP1 as a novel regulator of ATM function. DMAP1 interacts with the histone acetyltransferase Tip60. Acetylation of H4K16 by DMAP1-Tip60 facilitates ATM signalling, presumably by creating a permissive chromatin structure for recruitment and phosphorylation of DNA damage proteins.

Furthermore, I have also investigated the *in vivo* functions of the ATM interacting protein ATMIN. Loss of ATMIN in MEFs leads to DNA damage accumulation, premature senescence and reduced recruitment of pS1987-ATM to sites of DNA damage. ATMIN is required for suppression of telomeric DNA damage; we propose ATMIN is required for efficient telomere maintenance. However, I observed that ATMIN is dispensable for OIS in $KRas^{G21D}$ induced colonic serrated hyperplasia. Investigation of ATM signalling in doubly-deficient $nbs1^{\Delta/\Delta}$; $atmin^{\Delta/\Delta}$ MEFs and intestines revealed increased ATMIN-dependent ATM signalling is partly responsible for the proliferation arrest of $nbs1^{\Delta/\Delta}$ cells. Thus, competition between the ATM co-factors ATMIN and NBS1 is a fundamental mechanism of ATM signalling, and disruption of this balance is deleterious to cells.

Moreover, I have characterised the lymphoma-free survival of $atmin^{\Delta B/\Delta B}$; $p53^{\Delta B/\Delta B}$ mice, compared to the B-cell lymphoma predisposition of $p53^{\Delta B/\Delta B}$ mutants. Due to p53's frequent mutation in cancer, ATMIN is therefore an attractive therapeutic target.

Chapter 8. References

Abbas, T., Sivaprasad, U., Terai, K., Amador, V., Pagano, M., and Dutta, A. (2008). PCNA-dependent regulation of p21 ubiquitylation and degradation via the CRL4Cdt2 ubiquitin ligase complex. Genes Dev *22*, 2496-2506.

Abdallah, P., Luciano, P., Runge, K.W., Lisby, M., Geli, V., Gilson, E., and Teixeira, M.T. (2009). A two-step model for senescence triggered by a single critically short telomere. Nat Cell Biol *11*, 988-993.

Adamson, B., Smogorzewska, A., Sigoillot, F.D., King, R.W., and Elledge, S.J. (2012). A genome-wide homologous recombination screen identifies the RNA-binding protein RBMX as a component of the DNA-damage response. Nat Cell Biol *14*, 318-328.

Ayoub, N., Jeyasekharan, A.D., Bernal, J.A., and Venkitaraman, A.R. (2008). HP1-beta mobilization promotes chromatin changes that initiate the DNA damage response. Nature *453*, 682-686.

Badie, S., Escandell, J.M., Bouwman, P., Carlos, A.R., Thanasoula, M., Gallardo, M.M., Suram, A., Jaco, I., Benitez, J., Herbig, U.*, et al.* (2010). BRCA2 acts as a RAD51 loader to facilitate telomere replication and capping. Nat Struct Mol Biol *17*, 1461-1469.

Bakkenist, C.J., and Kastan, M.B. (2003). DNA damage activates ATM through intermolecular autophosphorylation and dimer dissociation. Nature *421*, 499-506.

Banin, S., Moyal, L., Shieh, S., Taya, Y., Anderson, C.W., Chessa, L., Smorodinsky, N.I., Prives, C., Reiss, Y., Shiloh, Y.*, et al.* (1998). Enhanced phosphorylation of p53 by ATM in response to DNA damage. Science *281*, 1674-1677.

Barlow, C., Hirotsune, S., Paylor, R., Liyanage, M., Eckhaus, M., Collins, F., Shiloh, Y., Crawley, J.N., Ried, T., Tagle, D.*, et al.* (1996). Atm-deficient mice: a paradigm of ataxia telangiectasia. Cell *86*, 159-171.

Barlow, C., Liyanage, M., Moens, P.B., Tarsounas, M., Nagashima, K., Brown, K., Rottinghaus, S., Jackson, S.P., Tagle, D., Ried, T.*, et al.* (1998). Atm deficiency results in severe meiotic disruption as early as leptonema of prophase I. Development *125*, 4007-4017.

Barlow, C., Ribaut-Barassin, C., Zwingman, T.A., Pope, A.J., Brown, K.D., Owens, J.W., Larson, D., Harrington, E.A., Haeberle, A.M., Mariani, J.*, et al.* (2000). ATM is a cytoplasmic protein in mouse brain required to prevent lysosomal accumulation. Proc Natl Acad Sci U S A *97*, 871-876.

Bartkova, J., Horejsi, Z., Koed, K., Kramer, A., Tort, F., Zieger, K., Guldberg, P., Sehested, M., Nesland, J.M., Lukas, C.*, et al.* (2005). DNA damage response as a candidate anti-cancer barrier in early human tumorigenesis. Nature *434*, 864-870.

Bartkova, J., Rezaei, N., Liontos, M., Karakaidos, P., Kletsas, D., Issaeva, N., Vassiliou, L.V., Kolettas, E., Niforou, K., Zoumpourlis, V.C.*, et al.* (2006). Oncogene-induced senescence is part of the tumorigenesis barrier imposed by DNA damage checkpoints. Nature *444*, 633-637.

Bassing, C.H., Swat, W., and Alt, F.W. (2002). The mechanism and regulation of chromosomal V(D)J recombination. Cell *109 Suppl*, S45-55.

Baumann, P., and Cech, T.R. (2001). Pot1, the putative telomere end-binding protein in fission yeast and humans. Science *292*, 1171-1175.

Beamish, H., and Lavin, M.F. (1994). Radiosensitivity in ataxia-telangiectasia: anomalies in radiation-induced cell cycle delay. Int J Radiat Biol *65*, 175-184.

Begus-Nahrmann, Y., Lechel, A., Obenauf, A.C., Nalapareddy, K., Peit, E., Hoffmann, E., Schlaudraff, F., Liss, B., Schirmacher, P., Kestler, H.*, et al.* (2009). p53 deletion impairs clearance of chromosomal-instable stem cells in aging telomere-dysfunctional mice. Nat Genet *41*, 1138-1143.

Behrens, A., Sibilia, M., and Wagner, E.F. (1999). Amino-terminal phosphorylation of c-Jun regulates stress-induced apoptosis and cellular proliferation. Nat Genet *21*, 326-329.

Bekker-Jensen, S., Rendtlew Danielsen, J., Fugger, K., Gromova, I., Nerstedt, A., Lukas, C., Bartek, J., Lukas, J., and Mailand, N. (2010). HERC2 coordinates ubiquitin-dependent assembly of DNA repair factors on damaged chromosomes. Nat Cell Biol *12*, 80-86; sup pp 81-12.

Bennecke, M., Kriegl, L., Bajbouj, M., Retzlaff, K., Robine, S., Jung, A., Arkan, M.C., Kirchner, T., and Greten, F.R. (2010). Ink4a/Arf and oncogene-induced senescence prevent tumor progression during alternative colorectal tumorigenesis. Cancer Cell *18*, 135-146.

Berkovich, E., Monnat, R.J., Jr., and Kastan, M.B. (2007). Roles of ATM and NBS1 in chromatin structure modulation and DNA double-strand break repair. Nat Cell Biol *9*, 683-690.

Bianchi, A., Stansel, R.M., Fairall, L., Griffith, J.D., Rhodes, D., and de Lange, T. (1999). TRF1 binds a bipartite telomeric site with extreme spatial flexibility. EMBO J *18*, 5735-5744.

Bilaud, T., Brun, C., Ancelin, K., Koering, C.E., Laroche, T., and Gilson, E. (1997). Telomeric localization of TRF2, a novel human telobox protein. Nat Genet *17*, 236-239.

Bird, A.W., Yu, D.Y., Pray-Grant, M.G., Qiu, Q., Harmon, K.E., Megee, P.C., Grant, P.A., Smith, M.M., and Christman, M.F. (2002). Acetylation of histone H4 by Esa1 is required for DNA double-strand break repair. Nature *419*, 411-415.

Boder, E., and Sedgwick, R.P. (1957). A familial syndrome of progressive cerebellar ataxia, oculocutaneous telangiectasia and frequent pulmonary infection. A preliminary report on 7 children, an autopsy and a case history. Univ S Calif Med Bull *9*, 15-28.

Boehrs, J.K., He, J., Halaby, M.J., and Yang, D.Q. (2007). Constitutive expression and cytoplasmic compartmentalization of ATM protein in differentiated human neuron-like SH-SY5Y cells. J Neurochem *100*, 337-345.

Bosotti, R., Isacchi, A., and Sonnhammer, E.L. (2000). FAT: a novel domain in PIK-related kinases. Trends Biochem Sci *25*, 225-227.

Boyer, L.A., Langer, M.R., Crowley, K.A., Tan, S., Denu, J.M., and Peterson, C.L. (2002). Essential role for the SANT domain in the functioning of multiple chromatin remodeling enzymes. Mol Cell *10*, 935-942.

Braig, M., Lee, S., Loddenkemper, C., Rudolph, C., Peters, A.H., Schlegelberger, B., Stein, H., Dorken, B., Jenuwein, T., and Schmitt, C.A. (2005). Oncogene-induced senescence as an initial barrier in lymphoma development. Nature *436*, 660-665.

Bredemeyer, A.L., Sharma, G.G., Huang, C.Y., Helmink, B.A., Walker, L.M., Khor, K.C., Nuskey, B., Sullivan, K.E., Pandita, T.K., Bassing, C.H.*, et al.* (2006). ATM stabilizes DNA double-strand-break complexes during V(D)J recombination. Nature *442*, 466-470.

Broccoli, D., Smogorzewska, A., Chong, L., and de Lange, T. (1997). Human telomeres contain two distinct Myb-related proteins, TRF1 and TRF2. Nat Genet *17*, 231-235.

Buis, J., Wu, Y., Deng, Y., Leddon, J., Westfield, G., Eckersdorff, M., Sekiguchi, J.M., Chang, S., and Ferguson, D.O. (2008). Mre11 nuclease activity has essential roles in DNA repair and genomic stability distinct from ATM activation. Cell *135*, 85-96.

Cai, Y., Jin, J., Tomomori-Sato, C., Sato, S., Sorokina, I., Parmely, T.J., Conaway, R.C., and Conaway, J.W. (2003). Identification of new subunits of the multiprotein mammalian TRRAP/TIP60-containing histone acetyltransferase complex. J Biol Chem *278*, 42733-42736.

Callen, E., Jankovic, M., Difilippantonio, S., Daniel, J.A., Chen, H.T., Celeste, A., Pellegrini, M., McBride, K., Wangsa, D., Bredemeyer, A.L.*, et al.* (2007). ATM prevents the persistence and propagation of chromosome breaks in lymphocytes. Cell *130*, 63-75.

Canman, C.E., Lim, D.S., Cimprich, K.A., Taya, Y., Tamai, K., Sakaguchi, K., Appella, E., Kastan, M.B., and Siliciano, J.D. (1998). Activation of the ATM kinase by ionizing radiation and phosphorylation of p53. Science *281*, 1677-1679.

Celli, G.B., and de Lange, T. (2005). DNA processing is not required for ATM-mediated telomere damage response after TRF2 deletion. Nat Cell Biol *7*, 712-718.

Cerosaletti, K., and Concannon, P. (2004). Independent roles for nibrin and Mre11-Rad50 in the activation and function of Atm. J Biol Chem *279*, 38813-38819.

Chaudhuri, J., and Alt, F.W. (2004). Class-switch recombination: interplay of transcription, DNA deamination and DNA repair. Nat Rev Immunol *4*, 541-552.

Chen, Z., Trotman, L.C., Shaffer, D., Lin, H.K., Dotan, Z.A., Niki, M., Koutcher, J.A., Scher, H.I., Ludwig, T., Gerald, W.*, et al.* (2005). Crucial role of p53-dependent cellular senescence in suppression of Pten-deficient tumorigenesis. Nature *436*, 725-730.

Chong, L., van Steensel, B., Broccoli, D., Erdjument-Bromage, H., Hanish, J., Tempst, P., and de Lange, T. (1995). A human telomeric protein. Science *270*, 1663-1667.

Collado, M., Gil, J., Efeyan, A., Guerra, C., Schuhmacher, A.J., Barradas, M., Benguria, A., Zaballos, A., Flores, J.M., Barbacid, M.*, et al.* (2005). Tumour biology: senescence in premalignant tumours. Nature *436*, 642.

Collado, M., and Serrano, M. (2006). The power and the promise of oncogene-induced senescence markers. Nat Rev Cancer *6*, 472-476.

Cook, P.J., Ju, B.G., Telese, F., Wang, X., Glass, C.K., and Rosenfeld, M.G. (2009). Tyrosine dephosphorylation of H2AX modulates apoptosis and survival decisions. Nature *458*, 591-596.

Cox, R., Hosking, G.P., and Wilson, J. (1978). Ataxia Talangeictasia: Evaluatoin of radiosensitivity in cultured skin fibroblasts as a diagnostic test. Archieves of Disease in Childhood *53*, 386-390.

Crabbe, L., Verdun, R.E., Haggblom, C.I., and Karlseder, J. (2004). Defective telomere lagging strand synthesis in cells lacking WRN helicase activity. Science *306*, 1951-1953.

Daniel, J.A., Pellegrini, M., Lee, J.H., Paull, T.T., Feigenbaum, L., and Nussenzweig, A. (2008). Multiple autophosphorylation sites are dispensable for murine ATM activation in vivo. J Cell Biol *183*, 777-783.

Dar, I., Yosha, G., Elfassy, R., Galron, R., Wang, Z.Q., Shiloh, Y., and Barzilai, A. (2011). Investigation of the functional link between ATM and NBS1 in the DNA damage response in the mouse cerebellum. J Biol Chem *286*, 15361-15376.

de Jager, M., van Noort, J., van Gent, D.C., Dekker, C., Kanaar, R., and Wyman, C. (2001). Human Rad50/Mre11 is a flexible complex that can tether DNA ends. Mol Cell *8*, 1129-1135.

de Klein, A., Muijtjens, M., van Os, R., Verhoeven, Y., Smit, B., Carr, A.M., Lehmann, A.R., and Hoeijmakers, J.H. (2000). Targeted disruption of the cell-cycle checkpoint gene ATR leads to early embryonic lethality in mice. Curr Biol *10*, 479-482.

Deckbar, D., Birraux, J., Krempler, A., Tchouandong, L., Beucher, A., Walker, S., Stiff, T., Jeggo, P., and Lobrich, M. (2007). Chromosome breakage after G2 checkpoint release. J Cell Biol *176*, 749-755.

Dejardin, J., and Kingston, R.E. (2009). Purification of proteins associated with specific genomic Loci. Cell *136*, 175-186.

Denchi, E.L., and de Lange, T. (2007). Protection of telomeres through independent control of ATM and ATR by TRF2 and POT1. Nature *448*, 1068-1071.

Deng, Y., Guo, X., Ferguson, D.O., and Chang, S. (2009). Multiple roles for MRE11 at uncapped telomeres. Nature *460*, 914-918.

Desai-Mehta, A., Cerosaletti, K.M., and Concannon, P. (2001). Distinct functional domains of nibrin mediate Mre11 binding, focus formation, and nuclear localization. Mol Cell Biol *21*, 2184-2191.

Di Micco, R., Fumagalli, M., Cicalese, A., Piccinin, S., Gasparini, P., Luise, C., Schurra, C., Garre, M., Nuciforo, P.G., Bensimon, A.*, et al.* (2006). Oncogene-induced senescence is a DNA damage response triggered by DNA hyper-replication. Nature *444*, 638-642.

Difilippantonio, S., Celeste, A., Fernandez-Capetillo, O., Chen, H.T., Reina San Martin, B., Van Laethem, F., Yang, Y.P., Petukhova, G.V., Eckhaus, M., Feigenbaum, L.*, et al.* (2005). Role of Nbs1 in the activation of the Atm kinase revealed in humanized mouse models. Nat Cell Biol *7*, 675-685.

Difilippantonio, S., Celeste, A., Kruhlak, M.J., Lee, Y., Difilippantonio, M.J., Feigenbaum, L., Jackson, S.P., McKinnon, P.J., and Nussenzweig, A. (2007). Distinct domains in Nbs1 regulate irradiation-induced checkpoints and apoptosis. J Exp Med *204*, 1003-1011.

Dimitrova, N., Chen, Y.C., Spector, D.L., and de Lange, T. (2008). 53BP1 promotes non-homologous end joining of telomeres by increasing chromatin mobility. Nature *456*, 524-528.

Doil, C., Mailand, N., Bekker-Jensen, S., Menard, P., Larsen, D.H., Pepperkok, R., Ellenberg, J., Panier, S., Durocher, D., Bartek, J.*, et al.* (2009). RNF168 binds and amplifies ubiquitin conjugates on damaged chromosomes to allow accumulation of repair proteins. Cell *136*, 435-446.

Donehower, L.A., Harvey, M., Slagle, B.L., McArthur, M.J., Montgomery, C.A., Jr., Butel, J.S., and Bradley, A. (1992). Mice deficient for p53 are developmentally normal but susceptible to spontaneous tumours. Nature *356*, 215-221.

Downs, J.A., Allard, S., Jobin-Robitaille, O., Javaheri, A., Auger, A., Bouchard, N., Kron, S.J., Jackson, S.P., and Cote, J. (2004). Binding of chromatin-modifying activities to phosphorylated histone H2A at DNA damage sites. Mol Cell *16*, 979-990.

Downs, J.A., Lowndes, N.F., and Jackson, S.P. (2000). A role for Saccharomyces cerevisiae histone H2A in DNA repair. Nature *408*, 1001-1004.

Doyon, Y., Selleck, W., Lane, W.S., Tan, S., and Cote, J. (2004). Structural and functional conservation of the NuA4 histone acetyltransferase complex from yeast to humans. Mol Cell Biol *24*, 1884-1896.

Efeyan, A., Murga, M., Martinez-Pastor, B., Ortega-Molina, A., Soria, R., Collado, M., Fernandez-Capetillo, O., and Serrano, M. (2009). Limited role of murine ATM in oncogene-induced senescence and p53-dependent tumor suppression. PLoS One *4*, e5475.

el Marjou, F., Janssen, K.P., Chang, B.H., Li, M., Hindie, V., Chan, L., Louvard, D., Chambon, P., Metzger, D., and Robine, S. (2004). Tissue-specific and inducible Cre-mediated recombination in the gut epithelium. Genesis *39*, 186-193.

Elson, A., Wang, Y., Daugherty, C.J., Morton, C.C., Zhou, F., Campos-Torres, J., and Leder, P. (1996). Pleiotropic defects in ataxia-telangiectasia protein-deficient mice. Proc Natl Acad Sci U S A *93*, 13084-13089.

Erdmann, N., Liu, Y., and Harrington, L. (2004). Distinct dosage requirements for the maintenance of long and short telomeres in mTert heterozygous mice. Proc Natl Acad Sci U S A *101*, 6080-6085.

Esashi, F., Christ, N., Gannon, J., Liu, Y., Hunt, T., Jasin, M., and West, S.C. (2005). CDK-dependent phosphorylation of BRCA2 as a regulatory mechanism for recombinational repair. Nature *434*, 598-604.

Falck, J., Coates, J., and Jackson, S.P. (2005). Conserved modes of recruitment of ATM, ATR and DNA-PKcs to sites of DNA damage. Nature *434*, 605-611.

Falck, J., Mailand, N., Syljuasen, R.G., Bartek, J., and Lukas, J. (2001). The ATM-Chk2-Cdc25A checkpoint pathway guards against radioresistant DNA synthesis. Nature *410*, 842-847.

Fan, Q., Zhang, F., Barrett, B., Ren, K., and Andreassen, P.R. (2009). A role for monoubiquitinated FANCD2 at telomeres in ALT cells. Nucleic Acids Res *37*, 1740-1754.

Fokkema, I.F., Taschner, P.E., Schaafsma, G.C., Celli, J., Laros, J.F., and den Dunnen, J.T. (2011). LOVD v.2.0: the next generation in gene variant databases. Hum Mutat *32*, 557-563.

Fraga, M.F., Ballestar, E., Villar-Garea, A., Boix-Chornet, M., Espada, J., Schotta, G., Bonaldi, T., Haydon, C., Ropero, S., Petrie, K*., et al.* (2005). Loss of acetylation at Lys16 and trimethylation at Lys20 of histone H4 is a common hallmark of human cancer. Nat Genet *37*, 391-400.

Frappart, P.O., Tong, W.M., Demuth, I., Radovanovic, I., Herceg, Z., Aguzzi, A., Digweed, M., and Wang, Z.Q. (2005). An essential function for NBS1 in the prevention of ataxia and cerebellar defects. Nat Med *11*, 538-544.

Fumagalli, M., Rossiello, F., Clerici, M., Barozzi, S., Cittaro, D., Kaplunov, J.M., Bucci, G., Dobreva, M., Matti, V., Beausejour, C.M.*, et al.* (2012). Telomeric DNA damage is irreparable and causes persistent DNA-damage-response activation. Nat Cell Biol *14*, 355-365.

Gajjar, M., Candeias, M.M., Malbert-Colas, L., Mazars, A., Fujita, J., Olivares-Illana, V., and Fahraeus, R. (2012). The p53 mRNA-Mdm2 interaction controls Mdm2 nuclear trafficking and is required for p53 activation following DNA damage. Cancer Cell *21*, 25-35.

Gatei, M., Young, D., Cerosaletti, K.M., Desai-Mehta, A., Spring, K., Kozlov, S., Lavin, M.F., Gatti, R.A., Concannon, P., and Khanna, K. (2000). ATM-dependent phosphorylation of nibrin in response to radiation exposure. Nat Genet *25*, 115-119.

Gatti, R.A., Berkel, I., Boder, E., Braedt, G., Charmley, P., Concannon, P., Ersoy, F., Foroud, T., Jaspers, N.G., Lange, K.*, et al.* (1988). Localization of an ataxia-telangiectasia gene to chromosome 11q22-23. Nature *336*, 577-580.

Gil, J., and Peters, G. (2006). Regulation of the INK4b-ARF-INK4a tumour suppressor locus: all for one or one for all. Nat Rev Mol Cell Biol *7*, 667-677.

Goodarzi, A.A., Noon, A.T., Deckbar, D., Ziv, Y., Shiloh, Y., Lobrich, M., and Jeggo, P.A. (2008). ATM signaling facilitates repair of DNA double-strand breaks associated with heterochromatin. Mol Cell *31*, 167-177.

Gorgoulis, V.G., Vassiliou, L.V., Karakaidos, P., Zacharatos, P., Kotsinas, A., Liloglou, T., Venere, M., Ditullio, R.A., Jr., Kastrinakis, N.G., Levy, B.*, et al.* (2005). Activation of the DNA damage checkpoint and genomic instability in human precancerous lesions. Nature *434*, 907-913.

Gorrini, C., Squatrito, M., Luise, C., Syed, N., Perna, D., Wark, L., Martinato, F., Sardella, D., Verrecchia, A., Bennett, S.*, et al.* (2007). Tip60 is a haplo-insufficient tumour suppressor required for an oncogene-induced DNA damage response. Nature *448*, 1063-1067.

Greider, C.W., and Blackburn, E.H. (1985). Identification of a specific telomere terminal transferase activity in Tetrahymena extracts. Cell *43*, 405-413.

Greider, C.W., and Blackburn, E.H. (1987). The telomere terminal transferase of Tetrahymena is a ribonucleoprotein enzyme with two kinds of primer specificity. Cell *51*, 887-898.

Greider, C.W., and Blackburn, E.H. (1989). A telomeric sequence in the RNA of Tetrahymena telomerase required for telomere repeat synthesis. Nature *337*, 331-337.

Griffith, J., Bianchi, A., and de Lange, T. (1998). TRF1 promotes parallel pairing of telomeric tracts in vitro. J Mol Biol *278*, 79-88.

Griffith, J.D., Comeau, L., Rosenfield, S., Stansel, R.M., Bianchi, A., Moss, H., and de Lange, T. (1999). Mammalian telomeres end in a large duplex loop. Cell *97*, 503-514.

Guo, Z., Deshpande, R., and Paull, T.T. (2010a). ATM activation in the presence of oxidative stress. Cell Cycle *9*, 4805-4811.

Guo, Z., Kozlov, S., Lavin, M.F., Person, M.D., and Paull, T.T. (2010b). ATM activation by oxidative stress. Science *330*, 517-521.

Haigis, K., Sage, J., Glickman, J., Shafer, S., and Jacks, T. (2006). The related retinoblastoma (pRb) and p130 proteins cooperate to regulate homeostasis in the intestinal epithelium. J Biol Chem *281*, 638-647.

Hanahan, D., and Weinberg, R.A. (2011). Hallmarks of cancer: the next generation. Cell *144*, 646-674.

Hanaoka, S., Nagadoi, A., and Nishimura, Y. (2005). Comparison between TRF2 and TRF1 of their telomeric DNA-bound structures and DNA-binding activities. Protein Sci *14*, 119-130.

Hayflick, L., and Moorhead, P.S. (1961). The serial cultivation of human diploid cell strains. Exp Cell Res *25*, 585-621.

Henson, J.D., Cao, Y., Huschtscha, L.I., Chang, A.C., Au, A.Y., Pickett, H.A., and Reddel, R.R. (2009). DNA C-circles are specific and quantifiable markers of alternative-lengthening-of-telomeres activity. Nat Biotechnol *27*, 1181-1185.

Hewitt, G., Jurk, D., Marques, F.D., Correia-Melo, C., Hardy, T., Gackowska, A., Anderson, R., Taschuk, M., Mann, J., and Passos, J.F. (2012). Telomeres are favoured targets of a persistent DNA damage response in ageing and stress-induced senescence. Nat Commun *3*, 708.

Hockemeyer, D., Sfeir, A.J., Shay, J.W., Wright, W.E., and de Lange, T. (2005). POT1 protects telomeres from a transient DNA damage response and determines how human chromosomes end. EMBO J *24*, 2667-2678.

Hopfner, K.P., Craig, L., Moncalian, G., Zinkel, R.A., Usui, T., Owen, B.A., Karcher, A., Henderson, B., Bodmer, J.L., McMurray, C.T.*, et al.* (2002). The Rad50 zinc-hook is a structure joining Mre11 complexes in DNA recombination and repair. Nature *418*, 562-566.

Hopfner, K.P., Karcher, A., Craig, L., Woo, T.T., Carney, J.P., and Tainer, J.A. (2001). Structural biochemistry and interaction architecture of the DNA double-strand break repair Mre11 nuclease and Rad50-ATPase. Cell *105*, 473-485.

Hopfner, K.P., Karcher, A., Shin, D.S., Craig, L., Arthur, L.M., Carney, J.P., and Tainer, J.A. (2000). Structural biology of Rad50 ATPase: ATP-driven conformational control in DNA double-strand break repair and the ABC-ATPase superfamily. Cell *101*, 789-800.

Houldsworth, J., and Lavin, M.F. (1980). Effect of ionizing radiation on DNA synthesis in ataxia telangiectasia cells. Nucleic Acids Res *8*, 3709-3720.

Huen, M.S., Grant, R., Manke, I., Minn, K., Yu, X., Yaffe, M.B., and Chen, J. (2007). RNF8 transduces the DNA-damage signal via histone ubiquitylation and checkpoint protein assembly. Cell *131*, 901-914.

Huertas, P., and Jackson, S.P. (2009). Human CtIP mediates cell cycle control of DNA end resection and double strand break repair. J Biol Chem *284*, 9558-9565.

Iacovoni, J.S., Caron, P., Lassadi, I., Nicolas, E., Massip, L., Trouche, D., and Legube, G. (2010). High-resolution profiling of gammaH2AX around DNA double strand breaks in the mammalian genome. EMBO J *29*, 1446-1457.

Ikura, T., Ogryzko, V.V., Grigoriev, M., Groisman, R., Wang, J., Horikoshi, M., Scully, R., Qin, J., and Nakatani, Y. (2000). Involvement of the TIP60 histone acetylase complex in DNA repair and apoptosis. Cell *102*, 463-473.

Ito, K., Hirao, A., Arai, F., Matsuoka, S., Takubo, K., Hamaguchi, I., Nomiyama, K., Hosokawa, K., Sakurada, K., Nakagata, N*., et al.* (2004). Regulation of oxidative stress by ATM is required for self-renewal of haematopoietic stem cells. Nature *431*, 997-1002.

Jackson, E.L., Willis, N., Mercer, K., Bronson, R.T., Crowley, D., Montoya, R., Jacks, T., and Tuveson, D.A. (2001). Analysis of lung tumor initiation and progression using conditional expression of oncogenic K-ras. Genes Dev *15*, 3243-3248.

Jeggo, P.A., and Lobrich, M. (2005). Artemis links ATM to double strand break rejoining. Cell Cycle *4*, 359-362.

Jiang, W.Q., Zhong, Z.H., Henson, J.D., Neumann, A.A., Chang, A.C., and Reddel, R.R. (2005). Suppression of alternative lengthening of telomeres by Sp100-mediated sequestration of the MRE11/RAD50/NBS1 complex. Mol Cell Biol *25*, 2708-2721.

Jonkers, J., Meuwissen, R., van der Gulden, H., Peterse, H., van der Valk, M., and Berns, A. (2001). Synergistic tumor suppressor activity of BRCA2 and p53 in a conditional mouse model for breast cancer. Nat Genet *29*, 418-425.

Jurado, S., Conlan, L.A., Baker, E.K., Ng, J.L., Tenis, N., Hoch, N.C., Gleeson, K., Smeets, M., Izon, D., and Heierhorst, J. (2012). ATM substrate Chk2-interacting Zn2+ finger (ASCIZ) Is a bi-functional transcriptional activator and feedback sensor in the regulation of dynein light chain (DYNLL1) expression. J Biol Chem *287*, 3156-3164.

Jurado, S., Smyth, I., van Denderen, B., Tenis, N., Hammet, A., Hewitt, K., Ng, J.L., McNees, C.J., Kozlov, S.V., Oka, H*., et al.* (2010). Dual functions of ASCIZ in the DNA base damage response and pulmonary organogenesis. PLoS Genet *6*, e1001170.

Kamsler, A., Daily, D., Hochman, A., Stern, N., Shiloh, Y., Rotman, G., and Barzilai, A. (2001). Increased oxidative stress in ataxia telangiectasia evidenced by alterations in redox state of brains from Atm-deficient mice. Cancer Res *61*, 1849-1854.

Kang, J., Bronson, R.T., and Xu, Y. (2002). Targeted disruption of NBS1 reveals its roles in mouse development and DNA repair. EMBO J *21*, 1447-1455.

Kanu, N., and Behrens, A. (2007). ATMIN defines an NBS1-independent pathway of ATM signalling. EMBO J *26*, 2933-2941.

Kanu, N., and Behrens, A. (2008). ATMINistrating ATM signalling: regulation of ATM by ATMIN. Cell Cycle *7*, 3483-3486.

Kanu, N., Penicud, K., Hristova, M., Wong, B., Irvine, E., Plattner, F., Raivich, G., and Behrens, A. (2010). The ATM cofactor ATMIN protects against oxidative stress and accumulation of DNA damage in the aging brain. J Biol Chem *285*, 38534-38542.

Karlseder, J., Hoke, K., Mirzoeva, O.K., Bakkenist, C., Kastan, M.B., Petrini, J.H., and de Lange, T. (2004). The telomeric protein TRF2 binds the ATM kinase and can inhibit the ATM-dependent DNA damage response. PLoS Biol *2*, E240.

Karlseder, J., Smogorzewska, A., and de Lange, T. (2002). Senescence induced by altered telomere state, not telomere loss. Science *295*, 2446-2449.

Kastan, M.B., Zhan, Q., el-Deiry, W.S., Carrier, F., Jacks, T., Walsh, W.V., Plunkett, B.S., Vogelstein, B., and Fornace, A.J., Jr. (1992). A mammalian cell cycle checkpoint pathway utilizing p53 and GADD45 is defective in ataxia-telangiectasia. Cell *71*, 587-597.

Khanna, K.K., Keating, K.E., Kozlov, S., Scott, S., Gatei, M., Hobson, K., Taya, Y., Gabrielli, B., Chan, D., Lees-Miller, S.P.*, et al.* (1998). ATM associates with and phosphorylates p53: mapping the region of interaction. Nat Genet *20*, 398-400.

Kim, S.H., Kaminker, P., and Campisi, J. (1999). TIN2, a new regulator of telomere length in human cells. Nat Genet *23*, 405-412.

Kim, Y.C., Gerlitz, G., Furusawa, T., Catez, F., Nussenzweig, A., Oh, K.S., Kraemer, K.H., Shiloh, Y., and Bustin, M. (2009). Activation of ATM depends on chromatin interactions occurring before induction of DNA damage. Nat Cell Biol *11*, 92-96.

Kitagawa, R., Bakkenist, C.J., McKinnon, P.J., and Kastan, M.B. (2004). Phosphorylation of SMC1 is a critical downstream event in the ATM-NBS1-BRCA1 pathway. Genes Dev *18*, 1423-1438.

Kolas, N.K., Chapman, J.R., Nakada, S., Ylanko, J., Chahwan, R., Sweeney, F.D., Panier, S., Mendez, M., Wildenhain, J., Thomson, T.M.*, et al.* (2007). Orchestration of the DNA-damage response by the RNF8 ubiquitin ligase. Science *318*, 1637-1640.

Krishnan, N., Jeong, D.G., Jung, S.K., Ryu, S.E., Xiao, A., Allis, C.D., Kim, S.J., and Tonks, N.K. (2009). Dephosphorylation of the C-terminal tyrosyl residue of the DNA damage-related histone H2A.X is mediated by the protein phosphatase eyes absent. J Biol Chem *284*, 16066-16070.

Kusch, T., Florens, L., Macdonald, W.H., Swanson, S.K., Glaser, R.L., Yates, J.R., 3rd, Abmayr, S.M., Washburn, M.P., and Workman, J.L. (2004). Acetylation by Tip60 is required for selective histone variant exchange at DNA lesions. Science *306*, 2084-2087.

Lallemand, Y., Luria, V., Haffner-Krausz, R., and Lonai, P. (1998). Maternally expressed PGK-Cre transgene as a tool for early and uniform activation of the Cre site-specific recombinase. Transgenic Res *7*, 105-112.

Lamarche, B.J., Orazio, N.I., and Weitzman, M.D. (2010). The MRN complex in double-strand break repair and telomere maintenance. FEBS Lett *584*, 3682-3695.

Lee, J.H., and Paull, T.T. (2005). ATM activation by DNA double-strand breaks through the Mre11-Rad50-Nbs1 complex. Science *308*, 551-554.

Li, B., Oestreich, S., and de Lange, T. (2000a). Identification of human Rap1: implications for telomere evolution. Cell *101*, 471-483.

Li, J., Han, Y.R., Plummer, M.R., and Herrup, K. (2009). Cytoplasmic ATM in neurons modulates synaptic function. Curr Biol *19*, 2091-2096.

Li, S., Ting, N.S., Zheng, L., Chen, P.L., Ziv, Y., Shiloh, Y., Lee, E.Y., and Lee, W.H. (2000b). Functional link of BRCA1 and ataxia telangiectasia gene product in DNA damage response. Nature *406*, 210-215.

Li, X., Corsa, C.A., Pan, P.W., Wu, L., Ferguson, D., Yu, X., Min, J., and Dou, Y. (2010). MOF and H4 K16 acetylation play important roles in DNA damage repair by modulating recruitment of DNA damage repair protein Mdc1. Mol Cell Biol *30*, 5335-5347.

Lim, D.S., Kim, S.T., Xu, B., Maser, R.S., Lin, J., Petrini, J.H., and Kastan, M.B. (2000). ATM phosphorylates p95/nbs1 in an S-phase checkpoint pathway. Nature *404*, 613-617.

Lin, H.K., Chen, Z., Wang, G., Nardella, C., Lee, S.W., Chan, C.H., Yang, W.L., Wang, J., Egia, A., Nakayama, K.I*., et al.* (2010). Skp2 targeting suppresses tumorigenesis by Arf-p53-independent cellular senescence. Nature *464*, 374-379.

Liu, D., Safari, A., O'Connor, M.S., Chan, D.W., Laegeler, A., Qin, J., and Songyang, Z. (2004). PTOP interacts with POT1 and regulates its localization to telomeres. Nat Cell Biol *6*, 673-680.

Lloyd, J., Chapman, J.R., Clapperton, J.A., Haire, L.F., Hartsuiker, E., Li, J., Carr, A.M., Jackson, S.P., and Smerdon, S.J. (2009). A supramodular FHA/BRCT-repeat architecture mediates Nbs1 adaptor function in response to DNA damage. Cell *139*, 100-111.

Loayza, D., and De Lange, T. (2003). POT1 as a terminal transducer of TRF1 telomere length control. Nature *423*, 1013-1018.

Loizou, J.I., Sancho, R., Kanu, N., Bolland, D.J., Yang, F., Rada, C., Corcoran, A.E., and Behrens, A. (2011). ATMIN Is Required for Maintenance of Genomic Stability and Suppression of B Cell Lymphoma. Cancer Cell *19*, 587-600.

Lukas, C., Melander, F., Stucki, M., Falck, J., Bekker-Jensen, S., Goldberg, M., Lerenthal, Y., Jackson, S.P., Bartek, J., and Lukas, J. (2004). Mdc1 couples DNA double-strand break recognition by Nbs1 with its H2AX-dependent chromatin retention. EMBO J *23*, 2674-2683.

Lumsden, J.M., McCarty, T., Petiniot, L.K., Shen, R., Barlow, C., Wynn, T.A., Morse, H.C., 3rd, Gearhart, P.J., Wynshaw-Boris, A., Max, E.E.*, et al.* (2004). Immunoglobulin class switch recombination is impaired in Atm-deficient mice. J Exp Med *200*, 1111-1121.

Madison, B.B., Dunbar, L., Qiao, X.T., Braunstein, K., Braunstein, E., and Gumucio, D.L. (2002). Cis elements of the villin gene control expression in restricted domains of the vertical (crypt) and horizontal (duodenum, cecum) axes of the intestine. J Biol Chem *277*, 33275-33283.

Mailand, N., Bekker-Jensen, S., Faustrup, H., Melander, F., Bartek, J., Lukas, C., and Lukas, J. (2007). RNF8 ubiquitylates histones at DNA double-strand breaks and promotes assembly of repair proteins. Cell *131*, 887-900.

Makarov, V.L., Hirose, Y., and Langmore, J.P. (1997). Long G tails at both ends of human chromosomes suggest a C strand degradation mechanism for telomere shortening. Cell *88*, 657-666.

Makinen, M.J. (2007). Colorectal serrated adenocarcinoma. Histopathology *50*, 131-150.

Mann, B.S., Johnson, J.R., Cohen, M.H., Justice, R., and Pazdur, R. (2007). FDA approval summary: vorinostat for treatment of advanced primary cutaneous T-cell lymphoma. Oncologist *12*, 1247-1252.

Maser, R.S., Zinkel, R., and Petrini, J.H. (2001). An alternative mode of translation permits production of a variant NBS1 protein from the common Nijmegen breakage syndrome allele. Nat Genet *27*, 417-421.

Matsuoka, S., Ballif, B.A., Smogorzewska, A., McDonald, E.R., 3rd, Hurov, K.E., Luo, J., Bakalarski, C.E., Zhao, Z., Solimini, N., Lerenthal, Y.*, et al.* (2007). ATM and ATR substrate analysis reveals extensive protein networks responsive to DNA damage. Science *316*, 1160-1166.

Maya, R., Balass, M., Kim, S.T., Shkedy, D., Leal, J.F., Shifman, O., Moas, M., Buschmann, T., Ronai, Z., Shiloh, Y.*, et al.* (2001). ATM-dependent phosphorylation of Mdm2 on serine 395: role in p53 activation by DNA damage. Genes Dev *15*, 1067-1077.

McNees, C.J., Conlan, L.A., Tenis, N., and Heierhorst, J. (2005). ASCIZ regulates lesion-specific Rad51 focus formation and apoptosis after methylating DNA damage. EMBO J *24*, 2447-2457.

McNees, C.J., Tejera, A.M., Martinez, P., Murga, M., Mulero, F., Fernandez-Capetillo, O., and Blasco, M.A. (2010). ATR suppresses telomere fragility and recombination but is dispensable for elongation of short telomeres by telomerase. J Cell Biol *188*, 639-652.

McVey, M., and Lee, S.E. (2008). MMEJ repair of double-strand breaks (director's cut): deleted sequences and alternative endings. Trends Genet *24*, 529-538.

Meyerson, M., Counter, C.M., Eaton, E.N., Ellisen, L.W., Steiner, P., Caddle, S.D., Ziaugra, L., Beijersbergen, R.L., Davidoff, M.J., Liu, Q.*, et al.* (1997). hEST2, the putative human telomerase catalytic subunit gene, is up-regulated in tumor cells and during immortalization. Cell *90*, 785-795.

Michaloglou, C., Vredeveld, L.C., Soengas, M.S., Denoyelle, C., Kuilman, T., van der Horst, C.M., Majoor, D.M., Shay, J.W., Mooi, W.J., and Peeper, D.S. (2005). BRAFE600-associated senescence-like cell cycle arrest of human naevi. Nature *436*, 720-724.

Miller, K.M., Tjeertes, J.V., Coates, J., Legube, G., Polo, S.E., Britton, S., and Jackson, S.P. (2010). Human HDAC1 and HDAC2 function in the DNA-damage response to promote DNA nonhomologous end-joining. Nat Struct Mol Biol *17*, 1144-1151.

Milman, N., Higuchi, E., and Smith, G.R. (2009). Meiotic DNA double-strand break repair requires two nucleases, MRN and Ctp1, to produce a single size class of Rec12 (Spo11)-oligonucleotide complexes. Mol Cell Biol *29*, 5998-6005.

Mirzoeva, O.K., and Petrini, J.H. (2001). DNA damage-dependent nuclear dynamics of the Mre11 complex. Mol Cell Biol *21*, 281-288.

Mitchell, J.R., Cheng, J., and Collins, K. (1999a). A box H/ACA small nucleolar RNA-like domain at the human telomerase RNA 3' end. Mol Cell Biol *19*, 567-576.

Mitchell, J.R., Wood, E., and Collins, K. (1999b). A telomerase component is defective in the human disease dyskeratosis congenita. Nature *402*, 551-555.

Mohan, K.N., Ding, F., and Chaillet, J.R. (2011). Distinct Roles of DMAP1 in Mouse Development. Mol Cell Biol *31*, 1861-1869.

Murga, M., Bunting, S., Montana, M.F., Soria, R., Mulero, F., Canamero, M., Lee, Y., McKinnon, P.J., Nussenzweig, A., and Fernandez-Capetillo, O. (2009). A mouse model of ATR-Seckel shows embryonic replicative stress and accelerated aging. Nat Genet *41*, 891-898.

Murr, R., Loizou, J.I., Yang, Y.G., Cuenin, C., Li, H., Wang, Z.Q., and Herceg, Z. (2006). Histone acetylation by Trrap-Tip60 modulates loading of repair proteins and repair of DNA double-strand breaks. Nat Cell Biol *8*, 91-99.

Nagy, R., Sweet, K., and Eng, C. (2004). Highly penetrant hereditary cancer syndromes. Oncogene *23*, 6445-6470.

Nakada, S., Tai, I., Panier, S., Al-Hakim, A., Iemura, S., Juang, Y.C., O'Donnell, L., Kumakubo, A., Munro, M., Sicheri, F.*, et al.* (2010). Non-canonical inhibition of DNA damage-dependent ubiquitination by OTUB1. Nature *466*, 941-946.

Negishi, M., Chiba, T., Saraya, A., Miyagi, S., and Iwama, A. (2009). Dmap1 plays an essential role in the maintenance of genome integrity through the DNA repair process. Genes Cells *14*, 1347-1357.

Noffsinger, A.E. (2009). Serrated polyps and colorectal cancer: new pathway to malignancy. Annu Rev Pathol *4*, 343-364.

Noon, A.T., Shibata, A., Rief, N., Lobrich, M., Stewart, G.S., Jeggo, P.A., and Goodarzi, A.A. (2010). 53BP1-dependent robust localized KAP-1 phosphorylation is essential for heterochromatic DNA double-strand break repair. Nat Cell Biol *12*, 177-184.

O'Connor, M.S., Safari, A., Liu, D., Qin, J., and Songyang, Z. (2004). The human Rap1 protein complex and modulation of telomere length. J Biol Chem *279*, 28585-28591.

Oka, H., Sakai, W., Sonoda, E., Nakamura, J., Asagoshi, K., Wilson, S.H., Kobayashi, M., Yamamoto, K., Heierhorst, J., Takeda, S.*, et al.* (2008). DNA damage response protein ASCIZ links base excision repair with immunoglobulin gene conversion. Biochem Biophys Res Commun *371*, 225-229.

Painter, R.B., and Young, B.R. (1980). Radiosensitivity in ataxia-telangiectasia: a new explanation. Proc Natl Acad Sci U S A *77*, 7315-7317.

Parrinello S., Samper E., Krtolica A., Goldstein J., Melov S., and Campisi J. (2003). Oxygen sensitivity severely limits the replicative lifespan of murine fibroblasts. Nat. Cell Biol. 5:741-747.

Paull, T.T., and Gellert, M. (1998). The 3' to 5' exonuclease activity of Mre 11 facilitates repair of DNA double-strand breaks. Mol Cell *1*, 969-979.

Paull, T.T., and Gellert, M. (1999). Nbs1 potentiates ATP-driven DNA unwinding and endonuclease cleavage by the Mre11/Rad50 complex. Genes Dev *13*, 1276-1288.

Pellegrini, M., Celeste, A., Difilippantonio, S., Guo, R., Wang, W., Feigenbaum, L., and Nussenzweig, A. (2006). Autophosphorylation at serine 1987 is dispensable for murine Atm activation in vivo. Nature *443*, 222-225.

Perrem, K., Bryan, T.M., Englezou, A., Hackl, T., Moy, E.L., and Reddel, R.R. (1999). Repression of an alternative mechanism for lengthening of telomeres in somatic cell hybrids. Oncogene *18*, 3383-3390.

Petersen-Mahrt, S.K., Harris, R.S., and Neuberger, M.S. (2002). AID mutates E. coli suggesting a DNA deamination mechanism for antibody diversification. Nature *418*, 99-103.

Petrini, J.H., Walsh, M.E., DiMare, C., Chen, X.N., Korenberg, J.R., and Weaver, D.T. (1995). Isolation and characterization of the human MRE11 homologue. Genomics *29*, 80-86.

Prince, H.M., and Dickinson, M. (2012). Romidepsin for Cutaneous T-cell Lymphoma. Clin Cancer Res.

Qian, Y., Zhang, J., Yan, B., and Chen, X. (2008). DEC1, a basic helix-loop-helix transcription factor and a novel target gene of the p53 family, mediates p53-dependent premature senescence. J Biol Chem *283*, 2896-2905.

Raivich, G., Bohatschek, M., Da Costa, C., Iwata, O., Galiano, M., Hristova, M., Nateri, A.S., Makwana, M., Riera-Sans, L., Wolfer, D.P.*, et al.* (2004). The AP-1 transcription factor c-Jun is required for efficient axonal regeneration. Neuron *43*, 57-67.

Ranganathan, V., Heine, W.F., Ciccone, D.N., Rudolph, K.L., Wu, X., Chang, S., Hai, H., Ahearn, I.M., Livingston, D.M., Resnick, I.*, et al.* (2001). Rescue of a telomere length defect of Nijmegen breakage syndrome cells requires NBS and telomerase catalytic subunit. Curr Biol *11*, 962-966.

Rapali, P., Garcia-Mayoral, M.F., Martinez-Moreno, M., Tarnok, K., Schlett, K., Albar, J.P., Bruix, M., Nyitray, L., and Rodriguez-Crespo, I. (2011). LC8 dynein light chain (DYNLL1) binds to the C-terminal domain of ATM-interacting protein (ATMIN/ASCIZ) and regulates its subcellular localization. Biochem Biophys Res Commun *414*, 493-498.

Rea, S., Xouri, G., and Akhtar, A. (2007). Males absent on the first (MOF): from flies to humans. Oncogene *26*, 5385-5394.

Reina-San-Martin, B., Nussenzweig, M.C., Nussenzweig, A., and Difilippantonio, S. (2005). Genomic instability, endoreduplication, and diminished Ig class-switch recombination in B cells lacking Nbs1. Proc Natl Acad Sci U S A *102*, 1590-1595.

Reliene, R., and Schiestl, R.H. (2006). Antioxidant N-acetyl cysteine reduces incidence and multiplicity of lymphoma in Atm deficient mice. DNA Repair (Amst) *5*, 852-859.

Rendtlew Danielsen, J., Povlsen, L.K., Villumsen, B.H., Streicher, W., Nilsson, J., Wikstrom, M., Bekker-Jensen, S., and Mailand, N. (2012). DNA damage-inducible SUMOylation of HERC2 promotes RNF8 binding via a novel SUMO-binding Zinc finger. J Cell Biol *197*, 179-187.

Riballo, E., Kuhne, M., Rief, N., Doherty, A., Smith, G.C., Recio, M.J., Reis, C., Dahm, K., Fricke, A., Krempler, A.*, et al.* (2004). A pathway of double-strand break rejoining dependent upon ATM, Artemis, and proteins locating to gamma-H2AX foci. Mol Cell *16*, 715-724.

Rickert, R.C., Roes, J., and Rajewsky, K. (1997). B lymphocyte-specific, Cre-mediated mutagenesis in mice. Nucleic Acids Res *25*, 1317-1318.

Roberts, S.A., Strande, N., Burkhalter, M.D., Strom, C., Havener, J.M., Hasty, P., and Ramsden, D.A. (2010). Ku is a 5'-dRP/AP lyase that excises nucleotide damage near broken ends. Nature *464*, 1214-1217.

Rogakou, E.P., Pilch, D.R., Orr, A.H., Ivanova, V.S., and Bonner, W.M. (1998). DNA double-stranded breaks induce histone H2AX phosphorylation on serine 139. J Biol Chem *273*, 5858-5868.

Rountree, M.R., Bachman, K.E., and Baylin, S.B. (2000). DNMT1 binds HDAC2 and a new co-repressor, DMAP1, to form a complex at replication foci. Nat Genet *25*, 269-277.

Rudolph, K.L., Chang, S., Lee, H.W., Blasco, M., Gottlieb, G.J., Greider, C., and DePinho, R.A. (1999). Longevity, stress response, and cancer in aging telomerase-deficient mice. Cell *96*, 701-712.

Saidi, A., Li, T., Weih, F., Concannon, P., and Wang, Z.Q. (2010). Dual functions of Nbs1 in the repair of DNA breaks and proliferation ensure proper V(D)J recombination and T-cell development. Mol Cell Biol *30*, 5572-5581.

Sarkisian, C.J., Keister, B.A., Stairs, D.B., Boxer, R.B., Moody, S.E., and Chodosh, L.A. (2007). Dose-dependent oncogene-induced senescence in vivo and its evasion during mammary tumorigenesis. Nat Cell Biol *9*, 493-505.

Sartori, A.A., Lukas, C., Coates, J., Mistrik, M., Fu, S., Bartek, J., Baer, R., Lukas, J., and Jackson, S.P. (2007). Human CtIP promotes DNA end resection. Nature *450*, 509-514.

Savic, V., Yin, B., Maas, N.L., Bredemeyer, A.L., Carpenter, A.C., Helmink, B.A., Yang-Iott, K.S., Sleckman, B.P., and Bassing, C.H. (2009). Formation of dynamic gamma-H2AX domains along broken DNA strands is distinctly regulated by ATM and MDC1 and dependent upon H2AX densities in chromatin. Mol Cell *34*, 298-310.

Savitsky, K., Bar-Shira, A., Gilad, S., Rotman, G., Ziv, Y., Vanagaite, L., Tagle, D.A., Smith, S., Uziel, T., Sfez, S.*, et al.* (1995). A single ataxia telangiectasia gene with a product similar to PI-3 kinase. Science *268*, 1749-1753.

Serrano, M., Lin, A.W., McCurrach, M.E., Beach, D., and Lowe, S.W. (1997). Oncogenic ras provokes premature cell senescence associated with accumulation of p53 and p16INK4a. Cell *88*, 593-602.

Sfeir, A., and de Lange, T. (2012). Removal of shelterin reveals the telomere end-protection problem. Science *336*, 593-597.

Sfeir, A., Kosiyatrakul, S.T., Hockemeyer, D., MacRae, S.L., Karlseder, J., Schildkraut, C.L., and de Lange, T. (2009). Mammalian telomeres resemble fragile sites and require TRF1 for efficient replication. Cell *138*, 90-103.

Sharma, G.G., So, S., Gupta, A., Kumar, R., Cayrou, C., Avvakumov, N., Bhadra, U., Pandita, R.K., Porteus, M.H., Chen, D.J.*, et al.* (2010). MOF and histone H4 acetylation at lysine 16 are critical for DNA damage response and double-strand break repair. Mol Cell Biol *30*, 3582-3595.

Shogren-Knaak, M., Ishii, H., Sun, J.M., Pazin, M.J., Davie, J.R., and Peterson, C.L. (2006). Histone H4-K16 acetylation controls chromatin structure and protein interactions. Science *311*, 844-847.

Shroff, R., Arbel-Eden, A., Pilch, D., Ira, G., Bonner, W.M., Petrini, J.H., Haber, J.E., and Lichten, M. (2004). Distribution and dynamics of chromatin modification induced by a defined DNA double-strand break. Curr Biol *14*, 1703-1711.

Sluss, H.K., Armata, H., Gallant, J., and Jones, S.N. (2004). Phosphorylation of serine 18 regulates distinct p53 functions in mice. Mol Cell Biol *24*, 976-984.

Sorensen, C.S., Hansen, L.T., Dziegielewski, J., Syljuasen, R.G., Lundin, C., Bartek, J., and Helleday, T. (2005). The cell-cycle checkpoint kinase Chk1 is required for mammalian homologous recombination repair. Nat Cell Biol *7*, 195-201.

Soutoglou, E., and Misteli, T. (2008). Activation of the cellular DNA damage response in the absence of DNA lesions. Science *320*, 1507-1510.

Spring, K., Cross, S., Li, C., Watters, D., Ben-Senior, L., Waring, P., Ahangari, F., Lu, S.L., Chen, P., Misko, I.*, et al.* (2001). Atm knock-in mice harboring an in-frame deletion corresponding to the human ATM 7636del9 common mutation exhibit a variant phenotype. Cancer Res *61*, 4561-4568.

Squatrito, M., Gorrini, C., and Amati, B. (2006). Tip60 in DNA damage response and growth control: many tricks in one HAT. Trends Cell Biol *16*, 433-442.

Srinivas, S., Watanabe, T., Lin, C.S., William, C.M., Tanabe, Y., Jessell, T.M., and Costantini, F. (2001). Cre reporter strains produced by targeted insertion of EYFP and ECFP into the ROSA26 locus. BMC Dev Biol *1*, 4.

Stansel, R.M., de Lange, T., and Griffith, J.D. (2001). T-loop assembly in vitro involves binding of TRF2 near the 3' telomeric overhang. EMBO J *20*, 5532-5540.

Stewart, G.S., Panier, S., Townsend, K., Al-Hakim, A.K., Kolas, N.K., Miller, E.S., Nakada, S., Ylanko, J., Olivarius, S., Mendez, M.*, et al.* (2009). The RIDDLE syndrome protein mediates a ubiquitin-dependent signaling cascade at sites of DNA damage. Cell *136*, 420-434.

Stiff, T., O'Driscoll, M., Rief, N., Iwabuchi, K., Lobrich, M., and Jeggo, P.A. (2004). ATM and DNA-PK function redundantly to phosphorylate H2AX after exposure to ionizing radiation. Cancer Res *64*, 2390-2396.

Sun, Y., Jiang, X., Chen, S., Fernandes, N., and Price, B.D. (2005). A role for the Tip60 histone acetyltransferase in the acetylation and activation of ATM. Proc Natl Acad Sci U S A *102*, 13182-13187.

Sun, Y., Jiang, X., Xu, Y., Ayrapetov, M.K., Moreau, L.A., Whetstine, J.R., and Price, B.D. (2009). Histone H3 methylation links DNA damage detection to activation of the tumour suppressor Tip60. Nat Cell Biol *11*, 1376-1382.

Sun, Y., Xu, Y., Roy, K., and Price, B.D. (2007). DNA damage-induced acetylation of lysine 3016 of ATM activates ATM kinase activity. Mol Cell Biol *27*, 8502-8509.

Sung, P., and Klein, H. (2006). Mechanism of homologous recombination: mediators and helicases take on regulatory functions. Nat Rev Mol Cell Biol *7*, 739-750.

Syllaba, L., and Henner, K. (1926). Contribution a l'independance de l'athetose double idiopathique et congenitale. Rev Neurol (Paris) *1*, 514-562.

Taniguchi, T., Garcia-Higuera, I., Xu, B., Andreassen, P.R., Gregory, R.C., Kim, S.T., Lane, W.S., Kastan, M.B., and D'Andrea, A.D. (2002). Convergence of the fanconi anemia and ataxia telangiectasia signaling pathways. Cell *109*, 459-472.

Taubert, S., Gorrini, C., Frank, S.R., Parisi, T., Fuchs, M., Chan, H.M., Livingston, D.M., and Amati, B. (2004). E2F-dependent histone acetylation and recruitment of the Tip60 acetyltransferase complex to chromatin in late G1. Mol Cell Biol *24*, 4546-4556.

Theunissen, J.W., Kaplan, M.I., Hunt, P.A., Williams, B.R., Ferguson, D.O., Alt, F.W., and Petrini, J.H. (2003). Checkpoint failure and chromosomal instability without lymphomagenesis in Mre11(ATLD1/ATLD1) mice. Mol Cell *12*, 1511-1523.

Trujillo, K.M., Yuan, S.S., Lee, E.Y., and Sung, P. (1998). Nuclease activities in a complex of human recombination and DNA repair factors Rad50, Mre11, and p95. J Biol Chem *273*, 21447-21450.

Uziel, T., Lerenthal, Y., Moyal, L., Andegeko, Y., Mittelman, L., and Shiloh, Y. (2003). Requirement of the MRN complex for ATM activation by DNA damage. EMBO J *22*, 5612-5621.

van der Linden, E., Sanchez, H., Kinoshita, E., Kanaar, R., and Wyman, C. (2009). RAD50 and NBS1 form a stable complex functional in DNA binding and tethering. Nucleic Acids Res *37*, 1580-1588.

Varon, R., Vissinga, C., Platzer, M., Cerosaletti, K.M., Chrzanowska, K.H., Saar, K., Beckmann, G., Seemanova, E., Cooper, P.R., Nowak, N.J*., et al.* (1998). Nibrin, a novel DNA double-strand break repair protein, is mutated in Nijmegen breakage syndrome. Cell *93*, 467-476.

Vaziri, H., West, M.D., Allsopp, R.C., Davison, T.S., Wu, Y.S., Arrowsmith, C.H., Poirier, G.G., and Benchimol, S. (1997). ATM-dependent telomere loss in aging human diploid fibroblasts and DNA damage lead to the post-translational activation of p53 protein involving poly(ADP-ribose) polymerase. EMBO J *16*, 6018-6033.

Venteicher, A.S., Meng, Z., Mason, P.J., Veenstra, T.D., and Artandi, S.E. (2008). Identification of ATPases pontin and reptin as telomerase components essential for holoenzyme assembly. Cell *132*, 945-957.

Ventura, A., Kirsch, D.G., McLaughlin, M.E., Tuveson, D.A., Grimm, J., Lintault, L., Newman, J., Reczek, E.E., Weissleder, R., and Jacks, T. (2007). Restoration of p53 function leads to tumour regression in vivo. Nature *445*, 661-665.

Verdun, R.E., Crabbe, L., Haggblom, C., and Karlseder, J. (2005). Functional human telomeres are recognized as DNA damage in G2 of the cell cycle. Mol Cell *20*, 551-561.

Walker, J.R., Corpina, R.A., and Goldberg, J. (2001). Structure of the Ku heterodimer bound to DNA and its implications for double-strand break repair. Nature *412*, 607-614.

Waltes, R., Kalb, R., Gatei, M., Kijas, A.W., Stumm, M., Sobeck, A., Wieland, B., Varon, R., Lerenthal, Y., Lavin, M.F.*, et al.* (2009). Human RAD50 deficiency in a Nijmegen breakage syndrome-like disorder. Am J Hum Genet *84*, 605-616.

Ward, I.M., and Chen, J. (2001). Histone H2AX is phosphorylated in an ATR-dependent manner in response to replicational stress. J Biol Chem *276*, 47759-47762.

Watters, D., Kedar, P., Spring, K., Bjorkman, J., Chen, P., Gatei, M., Birrell, G., Garrone, B., Srinivasa, P., Crane, D.I.*, et al.* (1999). Localization of a portion of extranuclear ATM to peroxisomes. J Biol Chem *274*, 34277-34282.

Weinrich, S.L., Pruzan, R., Ma, L., Ouellette, M., Tesmer, V.M., Holt, S.E., Bodnar, A.G., Lichtsteiner, S., Kim, N.W., Trager, J.B.*, et al.* (1997). Reconstitution of human telomerase with the template RNA component hTR and the catalytic protein subunit hTRT. Nat Genet *17*, 498-502.

Westphal, C.H., Rowan, S., Schmaltz, C., Elson, A., Fisher, D.E., and Leder, P. (1997). atm and p53 cooperate in apoptosis and suppression of tumorigenesis, but not in resistance to acute radiation toxicity. Nat Genet *16*, 397-401.

Williams, B.R., Mirzoeva, O.K., Morgan, W.F., Lin, J., Dunnick, W., and Petrini, J.H. (2002). A murine model of Nijmegen breakage syndrome. Curr Biol *12*, 648-653.

Williams, R.S., Dodson, G.E., Limbo, O., Yamada, Y., Williams, J.S., Guenther, G., Classen, S., Glover, J.N., Iwasaki, H., Russell, P.*, et al.* (2009). Nbs1 flexibly tethers Ctp1 and Mre11-Rad50 to coordinate DNA double-strand break processing and repair. Cell *139*, 87-99.

Williams, R.S., Moncalian, G., Williams, J.S., Yamada, Y., Limbo, O., Shin, D.S., Groocock, L.M., Cahill, D., Hitomi, C., Guenther, G.*, et al.* (2008). Mre11 dimers coordinate DNA end bridging and nuclease processing in double-strand-break repair. Cell *135*, 97-109.

Wong, K.K., Maser, R.S., Bachoo, R.M., Menon, J., Carrasco, D.R., Gu, Y., Alt, F.W., and DePinho, R.A. (2003). Telomere dysfunction and Atm deficiency compromises organ homeostasis and accelerates ageing. Nature *421*, 643-648.

Woodbine, L., Brunton, H., Goodarzi, A.A., Shibata, A., and Jeggo, P.A. (2011). Endogenously induced DNA double strand breaks arise in heterochromatic DNA regions and require ataxia telangiectasia mutated and Artemis for their repair. Nucleic Acids Res *39*, 6986-6997.

Wright, W.E., Piatyszek, M.A., Rainey, W.E., Byrd, W., and Shay, J.W. (1996). Telomerase activity in human germline and embryonic tissues and cells. Dev Genet *18*, 173-179.

Wu, J., Chen, Y., Lu, L.Y., Wu, Y., Paulsen, M.T., Ljungman, M., Ferguson, D.O., and Yu, X. (2011). Chfr and RNF8 synergistically regulate ATM activation. Nat Struct Mol Biol *18*, 761-768.

Wu, X., Ranganathan, V., Weisman, D.S., Heine, W.F., Ciccone, D.N., O'Neill, T.B., Crick, K.E., Pierce, K.A., Lane, W.S., Rathbun, G.*, et al.* (2000). ATM phosphorylation of Nijmegen breakage syndrome protein is required in a DNA damage response. Nature *405*, 477-482.

Wu-Baer, F., and Baer, R. (2001). Effect of DNA damage on a BRCA1 complex. Nature *414*, 36.

Xiao, A., Li, H., Shechter, D., Ahn, S.H., Fabrizio, L.A., Erdjument-Bromage, H., Ishibe-Murakami, S., Wang, B., Tempst, P., Hofmann, K.*, et al.* (2009). WSTF regulates the H2A.X DNA damage response via a novel tyrosine kinase activity. Nature *457*, 57-62.

Xu, X., Qiao, W., Linke, S.P., Cao, L., Li, W.M., Furth, P.A., Harris, C.C., and Deng, C.X. (2001). Genetic interactions between tumor suppressors Brca1 and p53 in apoptosis, cell cycle and tumorigenesis. Nat Genet *28*, 266-271.

Xu, Y., Ashley, T., Brainerd, E.E., Bronson, R.T., Meyn, M.S., and Baltimore, D. (1996). Targeted disruption of ATM leads to growth retardation, chromosomal fragmentation during meiosis, immune defects, and thymic lymphoma. Genes Dev *10*, 2411-2422.

Xu, Y., and Baltimore, D. (1996). Dual roles of ATM in the cellular response to radiation and in cell growth control. Genes Dev *10*, 2401-2410.

Xu, Y., Yang, E.M., Brugarolas, J., Jacks, T., and Baltimore, D. (1998). Involvement of p53 and p21 in cellular defects and tumorigenesis in Atm-/- mice. Mol Cell Biol *18*, 4385-4390.

Xue, W., Zender, L., Miething, C., Dickins, R.A., Hernando, E., Krizhanovsky, V., Cordon-Cardo, C., and Lowe, S.W. (2007). Senescence and tumour clearance is triggered by p53 restoration in murine liver carcinomas. Nature *445*, 656-660.

Yang, Y.G., Saidi, A., Frappart, P.O., Min, W., Barrucand, C., Dumon-Jones, V., Michelon, J., Herceg, Z., and Wang, Z.Q. (2006). Conditional deletion of Nbs1 in murine cells reveals its role in branching repair pathways of DNA double-strand breaks. EMBO J *25*, 5527-5538.

Ye, J.Z., Donigian, J.R., van Overbeek, M., Loayza, D., Luo, Y., Krutchinsky, A.N., Chait, B.T., and de Lange, T. (2004). TIN2 binds TRF1 and TRF2 simultaneously and stabilizes the TRF2 complex on telomeres. J Biol Chem *279*, 47264-47271.

Yi, M., Rosin, M.P., and Anderson, C.K. (1990). Response of fibroblast cultures from ataxia-telangiectasia patients to oxidative stress. Cancer Lett *54*, 43-50.

You, Z., Bailis, J.M., Johnson, S.A., Dilworth, S.M., and Hunter, T. (2007). Rapid activation of ATM on DNA flanking double-strand breaks. Nat Cell Biol *9*, 1311-1318.

You, Z., Chahwan, C., Bailis, J., Hunter, T., and Russell, P. (2005). ATM activation and its recruitment to damaged DNA require binding to the C terminus of Nbs1. Mol Cell Biol *25*, 5363-5379.

Yu, X., and Chen, J. (2004). DNA damage-induced cell cycle checkpoint control requires CtIP, a phosphorylation-dependent binding partner of BRCA1 C-terminal domains. Mol Cell Biol *24*, 9478-9486.

Zhu, J., Petersen, S., Tessarollo, L., and Nussenzweig, A. (2001). Targeted disruption of the Nijmegen breakage syndrome gene NBS1 leads to early embryonic lethality in mice. Curr Biol *11*, 105-109.

Zhu, X.D., Kuster, B., Mann, M., Petrini, J.H., and de Lange, T. (2000). Cell-cycle-regulated association of RAD50/MRE11/NBS1 with TRF2 and human telomeres. Nat Genet *25*, 347-352.

Zhuang, J., Jiang, G., Willers, H., and Xia, F. (2009). Exonuclease function of human Mre11 promotes deletional nonhomologous end joining. J Biol Chem *284*, 30565-30573.